Physiological and Biochemical Mechanisms of Phenazine-Mediated Survival in *Pseudomonas aeruginosa*

Thesis by

Nathaniel Robert Glasser

In Partial Fulfillment of the Requirements for the Degree of
Doctor of Philosophy

California Institute of Technology
Pasadena, California

2017
(Defended April 26, 2017)

© 2017
Nathaniel Robert Glasser
All Rights Reserved

ACKNOWLEDGEMENTS

I owe any accomplishments to my family: to my father, for teaching me a love of math and science; to my mother, for teaching me a love of reading and writing; and to my sister, for grounding me with music and fun.

None of my research would be possible without the wonderful group of people Dianne has assembled. To Dianne and all the group members I've had the pleasure of working with: Brittany, Caj, Chia, Christian, Dave, David, Elena, Elise, other Elise, Flavia, Gargi, Jessica, Kristy, Kyle, Lina, Lindsey, Lisa, Lucas, Maureen, Megan, Melanie, Michael, Naomi, Nick, Olga, Peter, Ruth, Ryan, Scott, Shannon, Seb, Tahoura, and Will.

A special recognition for my co-authors and collaborators: Suzanne, for never giving up; Ben, for your relentless enthusiasm; Julie, for your supernatural calmness; Kyle, for building excellent settlements; and Stuart, for teaching us biologists where to push the electrons.

To my human friends, Marissa, Josh, and Paul, and my furry friends, Archimedes and Hypatia, for making game night the highlight of my week; and to Natalie Martin, for bringing me food late at night.

And to those with whom I've shared invaluable scientific discussions: Ned Ruby, Ian Booth, Nathan Dalleska, Jens Kaiser, Shu-ou Shan, and Andre Hoelz; and finally to my committee, Doug Rees, Jared Leadbetter, and Sarkis Mazmanian.

Thank you all!

ABSTRACT

The opportunistic pathogen *Pseudomonas aeruginosa* secretes a class of colorful redox-active small molecules known as phenazines. Numerous functions have been proposed for phenazines, including antibiotic activity, virulence, cell-to-cell signaling, iron acquisition, and survival. This thesis delves into mechanisms of the latter role, that of long-term survival under oxidant-limiting conditions. Using a diverse array of methods, I investigated how phenazines support survival and how cells transfer electrons to phenazines, as well as the downstream effects that phenazines have on *P. aeruginosa*.

Direct measurements of NAD(H), ATP, the membrane potential, and fermentation products revealed that phenazines promote redox homeostasis and subsequently ATP synthesis. The ATP is used to maintain a membrane potential through the reverse action of the ATP synthase complex. Even though *P. aeruginosa* does not ferment on sugars, phenazines enable the anaerobic oxidation of glucose to acetate, suggesting *P. aeruginosa* may have previously under-appreciated metabolic flexibility in the absence of terminal electron acceptors. Activity assays with proteins purified natively from *P. aeruginosa* showed that glucose oxidation might be enabled *in vivo* by the pyruvate dehydrogenase complex, which can directly reduce phenazines using pyruvate as an electron donor. Liquid chromatography and mass spectrometry of culture supernatants showed that phenazines alter the chain length distribution of secreted quinolones, which may have indirect downstream signaling effects. Based on this result, combined with data from survival experiments, I hypothesize that phenazine-mediated redox homeostasis promotes β-oxidation and that fatty acid metabolism contributes to long-term survival. Further analysis also showed that *P. aeruginosa* cultures contain several previously-unreported sulfonated phenazines. In its natural environment, *P. aeruginosa* undoubtedly encounters other microbial species that consume or modify its phenazines. At least one of these, a *Mycobacterium*, contains a pyocyanin demethylating

enzyme. The X-ray crystal structure of this protein revealed a novel reaction mechanism wherein the substrate is its own electron acceptor. Together, this work illuminates some of the many ways phenazines shape microbial communities in both clinical and environmental contexts.

PUBLISHED CONTENT AND CONTRIBUTIONS

Glasser, N. R., Saunders, S., and Newman, D. K. (2017) The colorful world of extracellular electron shuttles. *Annual Review of Microbiology*. In Press.

N.R.G. participated in collecting and reviewing the literature, created the figures, and wrote the sections discussing the chemistry and biochemistry of electron shuttling.

Glasser, N. R., Kern, S. E., and Newman, D. K. (2014) Phenazine redox cycling enhances anaerobic survival in *Pseudomonas aeruginosa* by facilitating generation of ATP and a proton-motive force. *Molecular Microbiology* **92**, 399-412. DOI: 10.1111/mmi.12566

N.R.G. collected the data and participated in designing the experiments and writing the manuscript.

Glasser, N. R., Wang, B. X., Hoy, J. A., and Newman, D. K. (2017) The pyruvate and α-ketoglutarate dehydrogenase complexes of *Pseudomonas aeruginosa* catalyze pyocyanin and phenazine-1-carboxylic acid reduction via the subunit dihydrolipoamide dehydrogenase. *Journal of Biological Chemistry* **292**, 5593-5607. DOI: 10.1074/jbc.M116.772848

N.R.G. collected the data, refined the protein structures, wrote the manuscript, and helped design the experiments.

Costa, K. C., Glasser, N. R., Conway, S. J., and Newman, D. K. (2017) Pyocyanin degradation by a tautomerizing demethylase inhibits *Pseudomonas aeruginosa* biofilms. *Science* **355** (6321), 170-173. DOI: 10.1126/science.aag3180

N.R.G. assisted with protein crystallization and solving the X-ray crystal structure, and with writing the relevant methods sections of the manuscript.

TABLE OF CONTENTS

Chapter 1 1
Introduction 1
Overview 3
Literature Cited 5
Chapter 2 6
Background 6
Abstract 6
Introduction 6
Diversity of Endogenous EES and Organisms 9
Chemical diversity of EES 11
Phylogenetic diversity 12
Costs of EES Biosynthesis 15
Cell Biology of Electron Shuttling 16
EES in the Extracellular Environment 20
Shuttle diffusion 20
Electron hopping as an alternative to shuttle diffusion 22
Evolutionary strategies that maintain EES in open environments 22
Outlook 24
Sidebars 25
Sidebar 1. How to characterize a putative EES 25
Sidebar 2. How does redox-potential define an EES? 27
Glossary 28
Acknowledgements 28
Literature Cited 28
Chapter 3 38
Physiology of Phenazine-Mediated Survival 38
Abstract 38
Introduction 39
Results 40
Phenazine redox cycling requires the activity of acetate kinase to promote survival 40
Phenazine redox cycling promotes ATP synthesis during pyruvate fermentation 45
ATP synthesis is limited by redox homeostasis during pyruvate fermentation 47
Arginine supports anaerobic ATP synthesis and survival independently of redox state 50
ATP synthesis is required to maintain the proton-motive force using the F_1F_O-ATPase complex during fermentation 52
Discussion 56
Acknowledgements 60
Materials and Methods 60
Bacterial strains and growth conditions 60
Construction and verification of P. aeruginosa mutants 61
Phenazine redox cycling survival 61
Pyruvate and arginine survival 62
Viability counting 62
Measurement of NAD^+, NADH, and ATP 63
Assessment of membrane potential 64
High performance liquid chromatography 65

Supplemental Material 65
Methods 65
RNA isolation and qRT-PCR analysis 65
Ion chromatography 66
Literature Cited 66
Chapter 4 71
Biochemistry of Phenazine Reduction 71
Abstract 71
Introduction 72
Results 75
Phenazine reduction is catalyzed by cell lysate 75
Multiple enzymes can catalyze phenazine reduction 77
Pyruvate and α-ketoglutarate dehydrogenase catalyze phenazine reduction 81
Dihydrolipoamide dehydrogenase catalyzes phenazine reduction 83
Structural insights into the interaction between LpdG and phenazines 86
Discussion 91
Experimental Procedures 95
Materials 95
Growth conditions 95
PCA reduction by cell lysate 96
Pyruvate and α-ketoglutarate dehydrogenase purification 97
PCA and pyocyanin reduction by purified proteins 99
Fluorescence quenching 100
Curve fitting 100
Cloning 100
Dihydrolipoamide dehydrogenase purification 101
Proteomics 103
Crystallography 103
Acknowledgements 105
Conflict of Interest 106
Author Contributions 106
Literature Cited 106
Chapter 5 111
Profiling the Metabolome of *Pseudomonas aeruginosa* 111
Abstract 111
Introduction 112
Results and Discussion 112
Methods for detecting secreted organic acids 112
Pyocyanin is not required for pyruvate secretion in P. aeruginosa 114
Pyocyanin alters the secretion pattern of quinolones 118
Identification and purification of novel phenazine sulfonates in culture supernatants 128
Detection of intracellular polar metabolites 134
Conclusions 136
Materials and Methods 137
Strains and Culture Conditions 137
Ion Chromatography 137
Organic Acid Analysis 137
Supernatant Analysis 138
Supernatant Analysis by High Resolution LC-MS/MS 139
Intracellular Metabolite Analysis 139

Data Analysis with XCMS 140
Acknowledgements 140
Literature Cited 141
Chapter 6 144
Pyocyanin Degradation 144
Abstract 144
Main text 144
Acknowledgements 154
Author contributions 154
References and Notes 154
Supplemental Material 158
Materials and Methods 158
Strains, medium and growth conditions 158
Generation and analysis of phenazines 159
Protein extraction and purification 160
Enzyme activity and analysis 161
Protein crystallography, X-ray diffraction and analysis 163
Biofilm experiments 164
Biofilm aggregate experiments 166
Oxygen diffusion modeling 167
Figures 168
Tables 176
Table S1. Data collection and refinement statistics for $PodA_{30\text{-}162}$ 176
Table S2. Strains, primers and plasmids used in this study. 177
Supplementary References 178
Chapter 7 180
Conclusions 180
Summary 180
Future Directions 180
Pyocyanin and pyruvate secretion 180
Fatty acid metabolism 181
Phenazine reductases and transporters 182
Diffusion and retention 183
Environmental relevance 183

Chapter 1

INTRODUCTION

One of the most unknowingly influential stories in modern microbiology began in 1859 as an inauspicious anecdote (1) (translated from French):

> *M. Fordos communicates the result of his researches on the cause of the blue coloring which is sometimes observed in pus secreted by wounds under certain unknown conditions of disease. Our colleague has succeeded in isolating from this pus a coloring matter of a peculiar nature...which he designates under the name of* **pyocyanin**.

Contemporaneously with Pasteur's classic experiments disproving spontaneous generation, Fordos noted a special relationship between pyocyanin and air (2) (translated from French):

> *The dissolution of pyocyanin, still containing pus, loses its color from one day to another, if it is preserved in a mouth-flask; but it is sufficient to agitate it in the air in order to restore its original color. The same discoloration phenomenon occurs if the blue solution is heated in a test tube with a few drops of sodium sulphide solution and the blue color is reproduced by stirring the liquor in air. These facts prove that the pyocyanin can, like several coloring matters, become colorless, under the influence of the desoxidants, and then resume its blue color in contact with the oxygen of the air, and explain how a colorless pus can nevertheless color in blue dressing cloths.*

The origin of pyocyanin was clarified when Gessard isolated a pyocyanin-producing bacterium (3,4) known today as *Pseudomonas aeruginosa*. The modern species name is derived from *aerugo*, the Latin word for the blue-green rust of copper, reflecting the coloration that pyocyanin confers upon *P. aeruginosa* cultures.

Pyocyanin's color-changing properties caught the attention of Leonor Michaelis (of Michaelis–Menten kinetics fame) and Ernst Friedheim, who characterized its redox properties and concluded that, in addition to the blue, red, and colorless forms described by Fordos (2),

pyocyanin could reversibly adopt a fourth *green* color (5). The green color represented unequivocal evidence that pyocyanin participates in one-electron redox reactions (6), the first known biological molecule of its kind. Combined with observations that pyocyanin stimulates oxygen consumption and carbon dioxide production (7,8), Friedheim and Michaelis speculated that pyocyanin is involved in cellular respiration in *P. aeruginosa*—and, by extension, that one-electron transfers are essential in biology, a radical notion for the time. With development of the kinetic framework for which Michaelis is now famous, the original work with pyocyanin was extended to quinones and flavins (9), and so our modern understanding of enzyme kinetics and cellular respiration traces back to the colorful properties of pyocyanin.

In the following years, pyocyanin attracted interest as an antimicrobial compound owing to its ability to generate reactive oxygen species (10). As a phenazine derivative, pyocyanin shares properties with other phenazines produced by diverse bacteria and archaea. The precursor to all known bacterial phenazines, phenazine-1-carboxylic acid, can even be found in the literature by its alternate name *tubermycin B* (11), reflecting its activity against *Mycobacterium tuberculosis*. The search for new antimicrobial compounds has dominated phenazine research in recent decades, and the original findings pertaining to bacterial respiration were largely ignored. Until recently, there were surprisingly few studies into the biological function of natural phenazines.

The Newman group has since revisited phenazine biology with a renewed interest in the physiological functions of phenazines. Motivated by the discovery that phenazines promote iron acquisition (12,13) and anaerobic survival (14), along with converging work demonstrating extracellular electron transfer in *Shewanella* species, we have pursued the hypothesis that phenazines can act as a sort of "molecular snorkel" for oxidant-limited cells (15). This idea bears striking resemblance to the original work by Friedheim and Michaelis, who developed their ideas

without even a clear picture of the electron transport chain, and we have made considerable progress thanks to a more rigorous biochemical foundation from decades of prior research.

My own research has focused on the effects that endogenous phenazines have on the metabolism of *P. aeruginosa*. I have strived to explain how phenazines promote anaerobic survival, from a physiological perspective down to a mechanistic biochemical one. This seemingly simple question has carried me on a journey through myriad approaches including electrochemistry, membrane potential measurements, metabolomics, protein purification and X-ray crystallography, and more.

Overview

Before diving into the specifics of phenazines, Chapter 2 reviews the concept of extracellular electron transfer in the environment. It explains our rationale for believing that phenazines are but one example of a diverse set of functionally similar molecules. We explore the environments where electron shuttling might be a viable survival strategy, taking biosynthetic costs and steady-state diffusion into account. Drawing on our experience with phenazines, we also discuss more specific mechanisms of electron shuttle reduction and oxidation.

Chapter 3 focuses more specifically on *P. aeruginosa* and the physiological mechanisms by which phenazine-1-carboxylic acid promotes anaerobic survival. By comparing cultures surviving with phenazines to those surviving via fermentation on pyruvate or arginine, I demonstrate that ATP synthesis is coupled to redox homeostasis and that ATP is required for survival. The ATP is required to maintain a proton-motive force by operating the ATP synthase complex in reverse. This study was enabled by a method to directly detect the membrane potential in *P. aeruginosa*. The physiological effect of phenazines is related to redox homeostasis, which then promotes ATP synthesis and maintenance of the membrane potential.

In Chapter 4, I seek a more detailed biochemical mechanism to explain the results from Chapter 3. By fractionating *P. aeruginosa* lysate and purifying proteins, I show that the pyruvate dehydrogenase and α-ketoglutarate dehydrogenase complexes from *P. aeruginosa* can directly reduce phenazines. These enzymes of central metabolism are directly involved in the findings from Chapter 4, providing a satisfying connection between the physiological and biochemical results. I also report the X-ray crystal structure of the enzyme dihydrolipoamide dehydrogenase to 1.35 Å, the highest resolution structure of this enzyme to date.

While Chapter 4 focuses on a specific subset of enzymes, the data suggest that *P. aeruginosa* contains multiple enzymes that can catalyze phenazine reduction. Such a result always raises the prospect that the activity is an *in vitro* artifact. In hopes of further quantifying the metabolic effects of phenazines, and possibly pinpointing the relevant phenazine reductases *in vivo*, in Chapter 5 I develop a set of metabolomics methods for characterizing *P. aeruginosa*. Preliminary results from analyzing culture supernatants suggest there is a peculiar relationship between pyocyanin and pyruvate that still requires further study. From the detection of 4-hydroxy-2-alkylquinolones and unknown glycerophospholipids, I suggest that pyocyanin affects fatty acid metabolism in *P. aeruginosa*. I also describe several novel sulfonated phenazines that may prove to be useful markers of sulfur metabolism *in situ*.

Chapter 6 returns to the environment and considers the interactions between *P. aeruginosa* and other species. While working on the X-ray crystal structures from Chapter 4, a postdoctoral scholar in the lab discovered and purified a pyocyanin demethylating enzyme from a species of *Mycobacterium*. Working together, we successfully crystallized and solved the structure of this enzyme. The structure revealed a reaction mechanism unique amongst demethylases where the phenazine substrate is its own electron acceptor.

Finally, Chapter 7 provides my concluding thoughts and some areas I feel are exciting avenues for future work.

Literature Cited

1. Fordos, M. J. (1859) Recherches sur la matière colorante des suppurations bleues: pyocyanine. *Recueil des Travaux de la Societé d'Émulation pour les Sciences Pharmaceutiques* **3**, 30
2. Fordos, M. J. (1860) Recherches sur la matière colorante des suppurations blue: pyocyanine. *Comptes rendus hebdomadaires des séances de l'Académie des sciences* **51**, 215-217
3. Gessard, C. (1882) On the blue and green coloration that appears on bandages. *Comptes rendus hebdomadaires des Séances de l'Académie des Sciences* **94**
4. Gessard, C. (1882) *Thèse pour le Doctorat en Médecine: De la pyocyanine et de son microbe. Colorations qui en dépendant dans les liquides organiques (pus et sérosités, sueur, liquides des culture)*, Faculté de Médicine de Paris
5. Friedheim, E., and Michaelis, L. (1931) Potentiometric study of pyocyanine. *Journal of Biological Chemistry* **91**, 355-368
6. Michaelis, L. (1931) The formation of semiquinones as intermediary reduction products from pyocyanine and some other dyestuffs. *Journal of Biological Chemistry* **92**, 211-232
7. Friedheim, E. (1931) Pyocyanine, an accessory respiratory enzyme. *Journal of Experimental Medicine* **54**, 207-221
8. Friedheim, E. (1934) The effect of pyocyanine on the respiration of some normal tissues and tumours. *Biochemical Journal* **28**, 173-179
9. Michaelis, L. (1935) Semiquinones, the intermediate steps of reversible organic oxidation-reduction. *Chemical Reviews* **16**, 243-286
10. Hassan, M., and Fridovich, I. (1979) Intracellular production of superoxide radical and of hydrogen peroxide by redox active compounds. *Archives of Biochemistry and Biophysics* **196**, 385-395
11. Isono, K., Anzai, K., and Suzuki, S. (1958) Tubermycin A and tubermycin B, new antibiotics. *Journal of Antibiotics* **11**, 264-267
12. Cox, C. D. (1986) Role of pyocyanin in the acquisition of iron from transferrin. *Infection and Immunity* **52**, 263-270
13. Wang, Y., Wilks, J. C., Danhorn, T., Ramos, I., Croal, L., and Newman, D. K. (2011) Phenazine-1-carboxylic acid promotes bacterial biofilm development via ferrous iron acquisition. *Journal of Bacteriology* **193**, 3606-3617
14. Wang, Y., Kern, S. E., and Newman, D. K. (2010) Endogenous phenazine antibiotics promote anaerobic survival of *Pseudomonas aeruginosa* via extracellular electron transfer. *Journal of Bacteriology* **192**, 365-369
15. Hernandez, M. E., and Newman, D. K. (2001) Extracellular electron transfer. *Cellular and Molecular Life Sciences* **58**, 1562-1571

Chapter 2

BACKGROUND

This chapter is adapted from an upcoming publication:

Glasser, N. R.*, Saunders, S.*, and Newman, D. K. (2017) The colorful world of extracellular electron shuttles. *Annual Review of Microbiology*. In Press.

*contributed equally

Abstract

Descriptions of the changeable, striking colors associated with secreted natural products date back well over a century. These molecules can serve as extracellular electron shuttles (EES) that permit microbes to access substrates at a distance. In this review, we argue that the colorful world of EES has too-long been neglected. Rather than simply serving as a diagnostic attribute of a particular microbial strain, redox-active natural products likely play fundamental, underappreciated roles in the biology of their producers, particularly those that inhabit biofilms. Here, we describe the chemical diversity and potential distribution of EES producers and users, discuss the costs associated with their biosynthesis, and critically evaluate strategies for their economical usage. We hope this review will inspire efforts to identify and explore the importance of EES cycling by a wide range of microorganisms, so that their contributions to shaping microbial communities can be better assessed and exploited.

Introduction

The microbial world is nothing if not colorful. Colorful figuratively, in that microbes accomplish stunning metabolic feats, which, increasingly, are being recognized for their important roles in promoting human health (1,2), shaping the composition of the atmosphere, lithosphere, and

hydrosphere (3), and biotechnological potential (4), to list only a few examples. Colorful literally, in that they produce a spectacular range of pigments, representing every rainbow hue. This latter aspect of microbial identity is often the first thing one notices about a strain when it is streaked upon a plate, whether its pigments are tightly associated with its colonies or rapidly diffuse away. Flipping through Bergey's Manual of Systematic Bacteriology (5), one can find numerous examples of organisms that have been named after the colors they produce (*e.g. Pseudomonas aeruginosa (6), Pseudoalteromonas luteoviolacia (7), Streptomyces coelicolor (8)*, etc.), yet the biological functions of these defining pigments are seldom discussed. Both old (9) and emerging evidence (10-12), however, suggests that literal colorfulness may underpin figurative colorfulness, particularly when the pigment in question has the property of *changing* color.

Color changes are often indicative of redox-reactions, and the redox properties of many colorful excreted metabolites confer upon them rich potential (bio)chemical reactivity. Such reactivity, when combined with their ability to cycle in and out of the cells that produce them, permit these molecules to serve as extracellular electron shuttles (EES). While we use the word "extracellular" to draw attention to the fact that these metabolites can leave the cell in their reduced state to transfer electrons to a distant extracellular oxidant, equally important to the definition of microbial electron shuttles is that they can return to the cell in the oxidized state, whereupon they are re-reduced (Fig. 1a). It is the cycling of EES and their facilitation of electron transfer both within and without the cell that underpins their important physiological functions. Several years ago, we made a distinction between two types of EES, classifying them according to whether microorganisms produce them (endogenous) or whether they are already present in an environment (exogenous) (12). Endogenous EES, for example, include microbial metabolites that are often considered to be redox-active antibiotics (11); exogenous EES include a chemically heterogeneous fraction of organic compounds derived from the degradation of microbial and plant matter (13,14).

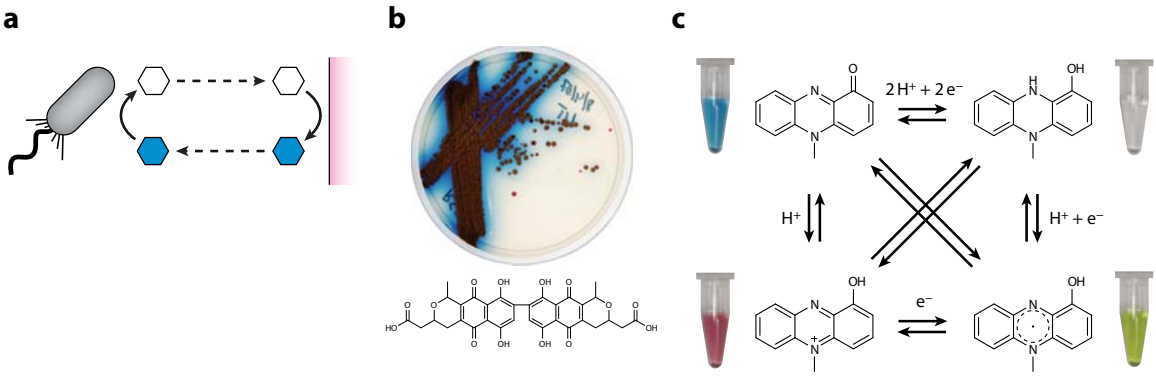

Figure 1. The colorful world of EES. (a) Action at a distance. Cells can perform redox chemistry on small molecules, which then diffuse, or electrically conduct, to extracellular substrates that can be many cell lengths away. (b) The colorful world of microbes as illustrated by Streptomyces coelicolor, producing the blue molecule actinorhodin whose structure is shown. (c) One molecule, four colors. The color of pyocyanin depends on both the pH and reduction potential. The tubes pictured each contain approximately 200 μM pyocyanin in water. The radical and fully reduced forms can be prepared by titrating pyocyanin with sodium dithionite, producing to an immediate and stunning color change.

EES are particularly relevant to situations where microbes have limited access to a critical substrate. For example, an electron acceptor for catabolism might be poorly soluble, as is the case for minerals in many groundwater and sedimentary systems or electrodes in biofuel applications. Alternatively, the substrate might be locally depleted due to rapid consumption by other cells, outpacing its diffusion, as is the case for oxygen in biofilms, be they on the surface of a corroding steel pipeline or in the mucus-filled lungs of an individual living with cystic fibrosis (15-18). Finally, the substrate might be utilized by another organism in an intimate syntrophic partnership, requiring the passage of electrons between different cell types to catalyze an important biogeochemical reaction, such as the anaerobic oxidation of methane achieved by mixed archaeal-bacterial aggregates (19,20). In all of these cases, extracellular electron transfer permits the microbes at a distance from the terminal electron acceptor to remain metabolically active.

Cycling of EES represents a strategy whereby microbes can facilitate extracellular electron transfer, yet is by no means the only one. Over the past three decades, investigations into how

organisms transfer electrons to or from minerals have revealed that many possess outer membrane cytochromes that are critically important for these processes (21). Whether and/or how electrons traverse through "nanowires" or "cables" or some type of extracellular matrix is still being debated (22-25). We simply note that in some organisms such as the mineral-reducing bacteria *Shewanella* and *Geobacter*, the proteinaceous machinery that is required for extracellular electron transfer can interact with and reduce EES of different types (26-30). Thus, it is important to be mindful of the potential involvement of EES in any context where extracellular electron transfer matters—be it the soil of the rhizosphere to the inflamed tissues of chronic infections. Moreover, due to their versatile redox activity, EES can play other important biological roles, such as serving as signaling molecules and promoting iron acquisition (31-34).

In this review, we focus our discussion primarily on colorful, endogenous EES, drawing upon our experience studying phenazines produced by *Pseudomonas aeruginosa* (11,12,31-47) (Fig. 1c). We use phenazines for illustrative purposes only, to pique the reader's curiosity about what other molecules may have similar physiological functions. We critically discuss costs of EES biosynthesis, as well as bioenergetic concerns related to the cell biology of their reduction and potential loss to the environment. Underpinning this review is the conviction that recent advances in mass spectrometry, imaging, and sequencing have the potential to enable dramatic progress in understanding the importance of endogenous EES across diverse microbial systems.

Diversity of Endogenous EES and Organisms

How many endogenous EES exist in nature and which organisms produce them? We are only at the threshold of being able to answer this question. The two most well-characterized EES-producing organisms are *Pseudomonas aeruginosa* and *Shewanella oneidensis*, known for their use of phenazines and flavins, respectively (28,40,44,48,49). Other putative EES-producing organisms, *Lactoccocus lactis, Sphingomonas xenophaga,* and *Klebsiella pneumonia,* are reported to

utilize quinone shuttles (see Table 1) (50-54). A few other observations in the literature hint at the production of EES by diverse organisms, including *Geothrix* and *Geobacter* species (26,55), yet in most cases the molecular nature of the putative EES is unknown. Though many secreted redox-active natural products have been well known for decades, such as indigoidine, only recently have their physiological functions begun to be explored (56). Because these types of natural products are genetically encoded in biosynthetic clusters, bioinformatic analysis predicts that EES production by microorganisms may be extensive (Fig. 2). In this section, we discuss the chemical diversity and potential distribution of EES-producers and users as predicted by current bioinformatics platforms. We emphasize these are *predictions*, which must be validated experimentally (Sidebar 1).

Molecule	Structure	Midpoint potential (mV)	Log K_{ow}*	Organism	Ref
2-amino-3-dicarboxy-1,4-naphthoquinone	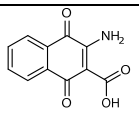	−71	0.15	*Lactococcus lactis*	(50)
4-amino-1,2-naphthoquinone	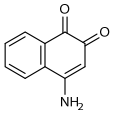	−96	0.81	*Shingomonas xenophaga BN6*	(51)
2,6-Di-*tert*-butyl-1,4-benzoquinone	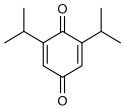	−253	3.9	*Klebsiella pneumonia*	(52)
flavin mononucleotide	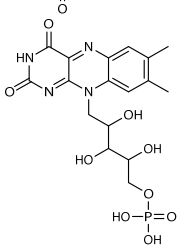	−220	−2.18	Alkaliphilic community, *Shewanella*	(49,57)
phenazine-1-carboxylic acid	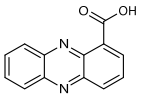	−177	2.17	*Pseudomonas, Streptomyces*	(38)
pyocyanin	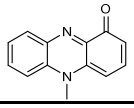	−34	1.6	*Pseudomonas aeruginosa*	(32)

Table 1. Putative EES.

* Log K_{ow} was predicted from Chemspider database (53,54).

Chemical diversity of EES

Much like their intracellular cousins (*e.g.* NAD(P)H, FAD, and quinones), EES are distinguished by the presence of conjugated bonds, often in the form of heterocyclic aromatic rings. It is this system of conjugated bonds that confers color upon EES. Generally, conjugated bonds are also the molecular origin of an electron shuttle's redox activity, as double bonds can be chemically reduced and rearranged at biologically-accessible reduction potentials. Rearrangement of the conjugated bond system necessarily entails a change in the molecule's absorption spectrum, and

so a shuttle's redox activity is inextricably linked to its vibrant and interconvertible colors (Fig. 1c).

Unlike intracellular redox-active metabolites, the endogenous EES described in the literature to date generally lack modifications such as adenylation or lipidation. Instead, they can be decorated with functional groups (*e.g.* amines, carboxylic acids, amides) that tune physical and chemical properties such as the reduction potential, charge state, or solubility. Advances in mass spectrometry and natural product discovery are only beginning to unearth the rich combinatorial diversity of these modifications—as of February 2017, the Dictionary of Natural Products contains over 190 unique phenazine derivatives, 1200 quinones, 1600 napthoquinones, and 2200 anthraquinones (58). While the growth of natural products databases has far outpaced our ability to empirically study the functions of these molecules, computational chemistry has shown recent progress in predicting their properties such as reduction potential (59). We anticipate that a convergence of metabolomics and computational chemistry, together with the on-going detailed study of select molecules such as phenazines, will implicate many of these redox-active natural products as ubiquitous and diverse EES.

Phylogenetic diversity

To predict which organisms may produce or utilize EES, we may consider the phylogenetic distribution of genes used to produce or interact with known EES. We might speculate that most organisms could shuttle electrons, since *S. oneidensis* uses a common cofactor, FMN (48). However, it is unclear how many could use flavins in an analogous manner, so we will instead focus on more specialized natural products. As an example, we will see that biosynthetic clusters for phenazines are widespread, as well as the redox transcription factor, SoxR, which can sense phenazines.

Biosynthetic clusters. Biosynthetic clusters are organized sets of genes that encode enzymes to produce specific metabolites. Bioinformatic tools are rapidly improving our ability to identify specific natural products (e.g. AntiSmash) (60). The authors of the IMG-ABC database showcased their toolkit with phenazines by identifying ~1000 genomes that contained at least 6 of 7 genes required for phenazine biosynthesis. These species included the well-known phenazine producers Streptomyces and Pseudomonads, but also Alphaproteobacteria, Betaproteobacteria, and other Actinobacteria. It was suggested that a much wider set of species probably produces phenazines than previously thought, and that these new putative producers likely synthesize phenazines with novel chemical structures (61). As the accuracy of these type of bioinformatics tools advance, we may be able to predict an organism's ability to make EES from its genome with reasonable confidence.

SoxR redox sensors. One way to identify potential EES users is to search genomes for machinery that can sense them. Presently, the best-known example is the SoxR transcription factor. SoxR was originally studied in *E. coli* for its role in upregulating the oxidative stress response upon exposure to superoxide generating molecules. It was discovered that SoxR sensed redox-active molecules through a Fe-S cluster bound by a unique cysteine motif, and its activation prompted sequence specific binding and transcriptional activation (62). Studies outside of the Enterobacteriacae then showed that SoxR did not upregulate the oxidative stress response in *P. aeruginosa (63)* and *Streptomyces coelicolor (64)*, but that it responded to endogenous redox-active molecules (37,65) and upregulated factors likely to be involved in their cycling. Comparative genomic analysis found that SoxR is widely distributed through the Bacteria, and it predicted that most organisms do not conform to the original *E. coli* oxidative stress paradigm (37).

Today the IMG database contains ~15,000 bacterial genomes with high-confidence SoxR homologues out of ~47,000 total bacterial genomes (66), approximately the same proportion as

the stress sigma factor RpoS. Fig. 2 shows that SoxR homologues are present in 10 bacterial phyla, and that the most representatives are in orders of Proteobacteria and Actinobacteria (67,68). It should be noted that homologues can be found in majorities of Pseudomonadales (2308 genomes) and Streptomycetes (402 genomes), which are well known for their production of natural products (often redox active). Strikingly, SoxR homologues are also identified in the emerging and established pathogens of the Mycobacteria (~400 genomes), the agriculturally important Rhizobia (493 genomes) and Frankia (33 genomes), and recently discovered phyla (6 genomes). Whether these organisms use SoxR to sense endogenous EES remains to be determined, but it suggests they might sense exogenous EES at a minimum. It is even possible that organisms could upregulate their own EES processing machinery to "cheat," analogous to organisms that steal exogenous siderophores (69).

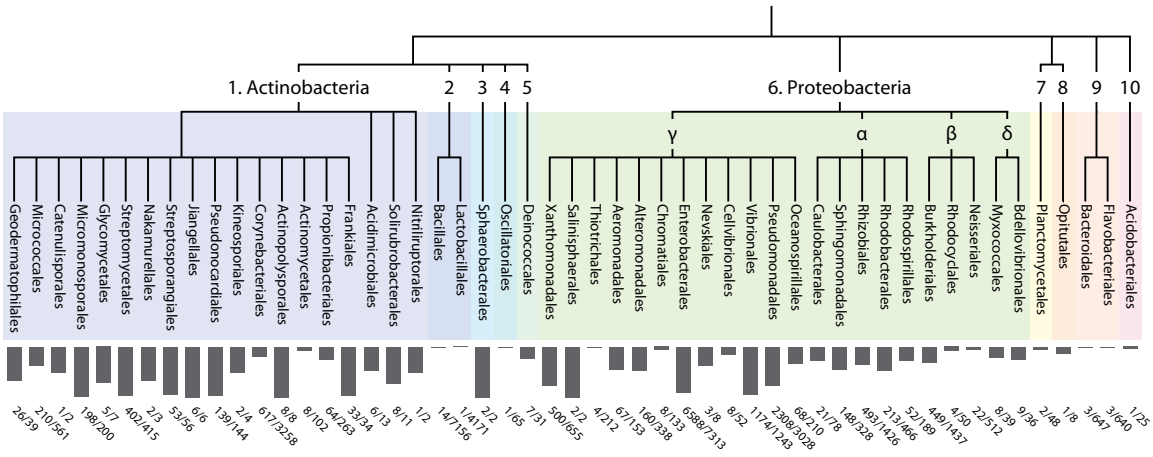

Figure 2. Phylogenetic distribution of SoxR, a transcription factor that senses redox-active metabolites. The phylogenetic tree shows all bacterial orders containing at least one genome with a SoxR homolog in the IMG database (SoxR TIGRfam 01950 (14)). The gray bars represent the percentage of genomes from each order that contain SoxR, with the absolute numbers listed below. The phyla represented are (1) Actinobacteria, (2) Fermicutes, (3) Chloroflexi, (4) Cyanobacteria, (5) Deinococcus, (6) Proteobacteria, with each subphylum labeled separately, (7) Planctomycetes, (8) Verrumicrobia, (9) Bacteroidetes, (10) Acidobacteria. The tree was generated using the NCBI taxonomic classification with PhyloT and the IToL (38, 69).

While the diversity of redox-active metabolites, biosynthetic clusters, and redox sensing homologues satisfy important preconditions for potential widespread EES usage in the microbial world, the numbers we have presented come with two important caveats. First, not all secreted redox-active molecules can serve as EES due to redox-potential constraints (see Sidebar 2). Second, though we have good reason to think that SoxR is a robust predictor of an organism's ability to sense EES, it is just one of many possible transcription factors used to sense, modify, and transport small redox-active molecules (37,70). Our bioinformatic analysis only *suggests* the potential for widespread production and usage of EES in the microbial world, which we hope will stimulate experimental follow-up (Sidebar 1).

Costs of EES Biosynthesis

At first glance, electron shuttles might appear expensive to produce, especially for a molecule that can be lost to diffusion or used by competitors in a microbial community. We discuss strategies for overcoming diffusive losses later, but here we wish to critically ask whether shuttles are 'expensive'. While a cell certainly loses carbon material by secreting a shuttle, the cost should not be compared to the energy that might be gained from fully oxidizing it to CO_2. It is, after all, precisely the condition of oxidant-limitation where EES are important. In a microenvironment where organic carbon is abundant, but oxidants are limited or absent, there is essentially no opportunity cost to discarding carbon. Based on biosynthetic pathways, what is the cost of producing EES?

All the known phenazine-producing bacteria use the same biosynthetic pathway, reviewed in detail elsewhere (71), in which two molecules of chorismate are modified and condensed to produce the core phenazine ring. Chorismate synthesis begins with two ATP equivalents and requires two additional ATP equivalents for completion (72), and so the core phenazine molecule requires a total of 8 ATP. Some quinones require only a single ATP in their conversion from

chorismate (72). Riboflavin synthesis requires only one ATP in its conversion from guanosine triphosphate (73), and including the precursors its cost has been estimated at up to 25 ATP per molecule (49). For these representative examples, the energy required to synthesize a shuttle is on the order of 5 to 25 ATP per molecule. How does this compare to other cellular processes? In protein synthesis, the addition of a single amino acid to a nascent peptide chain requires an estimated 4.5–7.9 ATP per amino acid (74), while RNA transcription further requires one ATP equivalent per nucleotide, and so the biosynthetic proteins themselves may represent a significant portion of a shuttle's cost. A quantitative analysis in *Shewanella* illustrates that its endogenous shuttles, flavin derivatives, cost less than 0.1% of a cell's energy budget to secrete at the necessary concentration (as low as 250 nM) (49).

The striking conclusion is that for a redox-limited microbial community, shuttle synthesis may pose only a minor metabolic cost. Furthermore, bacteria are known to carefully regulate production of secreted molecules. Xavier et al. coined the term metabolic prudence to describe how *P. aeruginosa* specifically secretes carbon-rich rhamnolipids (used for swarming motility) when excess carbon is available and the cost of production is low (75). This regulation ensures that secreting cells are more fit than cheaters in competition experiments, because cost is minimized while the benefit of swarming remains high. Examples from *P. aeruginosa* and *Salmonella typhimurium* suggest that metabolic prudence is a broadly-used strategy for regulating secretions under diverse nutritional conditions, such as iron, phosphate, or nitrogen limitation (76,77). We expect metabolically prudent regulation could further reduce the effective cost of EES under oxidant limitation.

Cell Biology of Electron Shuttling

The biochemical reduction of EES poses a unique topological challenge. Perhaps the best-elucidated mechanism of extracellular electron transport (EET) is in *Shewanella oneidensis* MR-1,

which has been reviewed in detail elsewhere (48,78). This organism uses the Mtr pathway, which is distinguished by a set of proteins that directly transfer electrons through the inner membrane, across the periplasm, and to the outside of the outer membrane where they directly reduce extracellular shuttles (Fig. 3a). The reduction of quinone by NADH dehydrogenase can be accompanied by the translocation of up to four protons across the inner-membrane (79), thus directly contributing to the proton motive force. In contrast, many other membrane-bound quinone reductases, such as succinate dehydrogenase or lactate dehydrogenase, are not known to translocate protons, and so the direct benefit of EET depends on the particular metabolism of a cell.

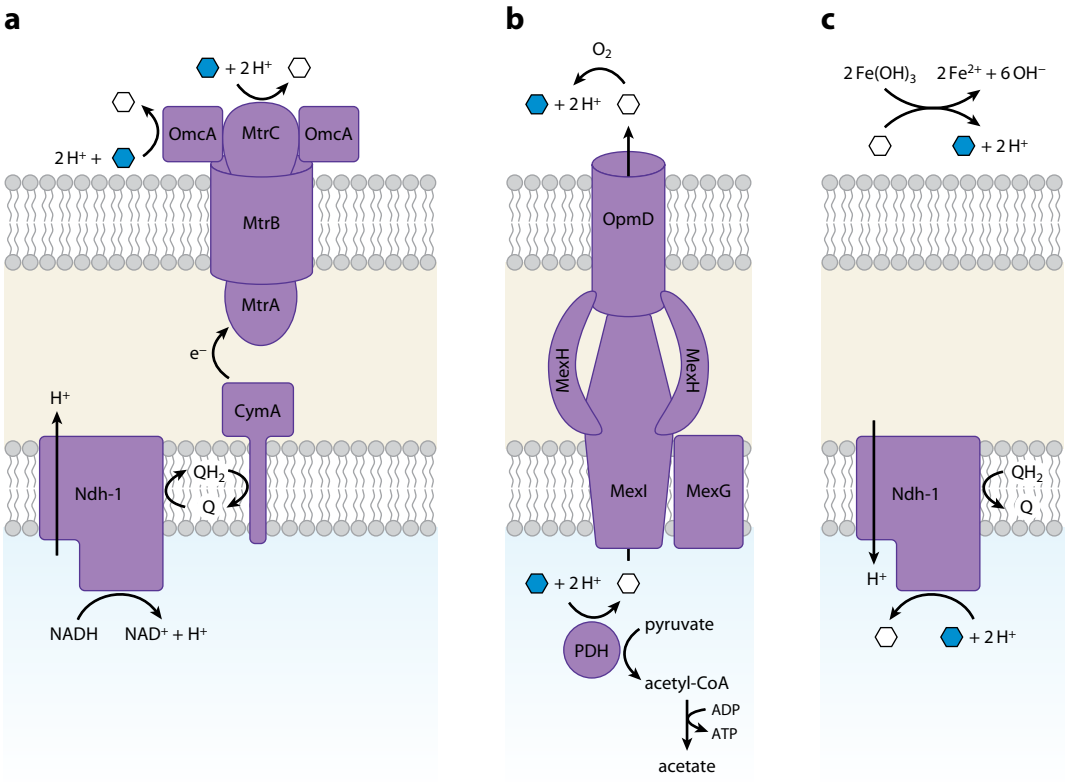

Figure 3. The topology of electron shuttle reduction and oxidation. Filled blue hexagons represent oxidized shuttle, and open white hexagons represent reduced shuttle. (a) The Mtr system in *S. oneidensis* MR-1. Shuttles are reduced extracellularly and do not need to re-enter the cell. (b) A model of phenazine reduction in *P. aeruginosa* that allows for energy conservation by electron shuttling. By substituting for NAD^+ in the pyruvate dehydrogenase complex (PDH), phenazines enable the synthesis of acetyl-CoA, which can drive ATP synthesis through the enzymes phosphate transacetylase and acetate kinase (44,46). Efflux of reduced phenazines by MexGHI-OpmD (70) may be coupled to proton translocation. (c) A condition where electron shuttling is costly. Operating the NADH dehydrogenase in reverse can consume the protonmotive force to drive shuttle reduction. Extracellular reduction of some minerals, such as $Fe(OH)_3$, can alkalize of the medium, possibly depleting the protonmotive force further and causing pH stress for the cell.

In contrast to *Shewanella*, specific pathways of extracellular electron transfer in other systems, such as phenazine shuttling in *P. aeruginosa*, remain ambiguous. Recent work from our laboratory shows that cytoplasmic (flavo)proteins can catalyze phenazine reduction in *P. aeruginosa* (46). Specifically, the enzyme dihydrolipoamide dehydrogenase enables phenazines to substitute for

NAD^+ in the pyruvate and α-ketoglutarate dehydrogenase complexes. This activity may allow phenazines to promote ATP synthesis during glucose oxidation by increasing the flux through pyruvate dehydrogenase and acetate kinase (46) (Fig. 3b). Similar findings have been observed in fermenting organisms, where the presence of humic substances or analogs increases the ratio of oxidized-to-reduced products (80), presumably increasing the ATP yield of fermentation.

The invocation of cytoplasmic EES reduction has interesting implications with respect to the proton-motive force. Upon reduction, phenazines, quinones, and flavins all take on two protons at circumneutral pH (Fig. 1c). The subsequent secretion and oxidation of the reduced shuttle would therefore release those two protons outside the cell, essentially translocating two protons across the inner membrane (Fig. 3b). If this shuttle does not require active transport into our out of the cell, redox cycling of a shuttle could drive the generation of a proton motive force. Conversely, shuttles that accept electrons from the cytoplasmic face of NADH dehydrogenase might consume the proton motive force, such as the artificial compound paraquat (81) (Fig. 3c). Though progress is being made on phenazine transport systems (70), where different phenazines are reduced and how they enter the appropriate efflux pump machinery remain open questions. The take-away message is that the subcellular localization of shuttle reduction greatly influences the energy that can be conserved, and we expect future work will elucidate new and interesting mechanisms to accompany the Mtr system.

Finally, while we have focused here on the mechanisms of EES reduction, electron transfer entails a subtler point with respect to the terminal electron acceptor. The reduction potential of minerals, and the kinetics of their reduction by shuttles (38), depends strongly on pH, and so the free energy available to a cell necessarily depends on its microenvironment. Moreover, mineral reduction is accompanied by alkalization (Fig. 3c), which further inhibits the available free energy and may even negatively affect the proton motive force if it happens close to the cell. From a cell's

perspective, the energy that can be conserved via electron shuttling may depend on the pH-buffering capacity of its environment and the rate of proton diffusion.

EES in the Extracellular Environment

In addition to defining the constraints that shape intracellular EES biosynthesis and processing, central to any predictive understanding of EES usage is knowledge of what happens to EES once they leave the cell. Because most bacteria live in biofilms (82,83), we will consider the extracellular environment to be a self-produced matrix of EPS and water. Here we explore under what conditions EES can be efficiently recycled.

Shuttle diffusion

Two studies have shown that diffusion can theoretically explain electron shuttling-supported metabolism in a closed system (84,85). In any environment, the flux of reduced EES away from cells (J_{red}) (toward electron acceptor) is driven by the concentration gradient that forms as cells reduce EES and the electron acceptor oxidizes them. Simultaneously, the concentration gradient of oxidized EES drives flux (J_{ox}) back to the cells that use EES to run their metabolism (Fig. 4a). We adapted a simple model of 3D diffusion, where an inner sphere of cells shuttle electrons to an outer sphere of electron acceptor, analogous to *P. aeruginosa* biofilms limited for oxygen (Fig. 4c) (86-89). Using realistic values of phenazine diffusion coefficients (~10^{-9}–10^{-10} m^2/s), concentrations (>10μM) and metabolic requirements (M_{min}), the model produces redox gradients that can drive sufficient flux of oxidized EES to support survival (Fig. 4d), in agreement with observed phenazine mediated survival (43,44,85).

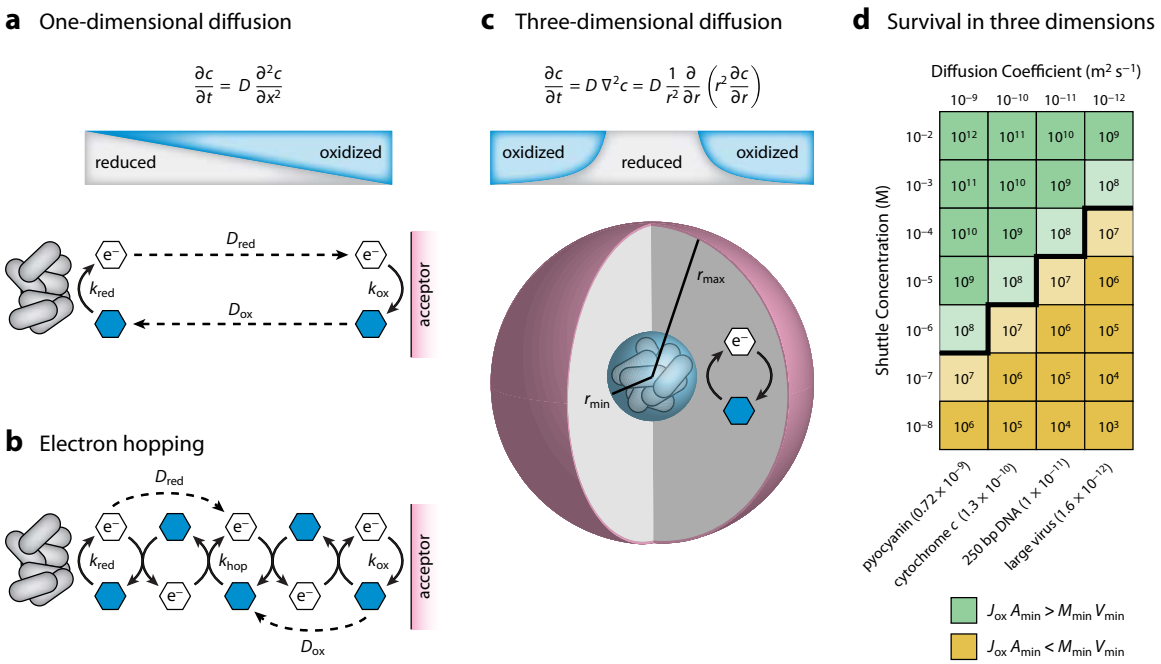

Figure 4. Mechanisms of electron transfer by EES. (a) Diffusion only. The reduced EES can diffuse down its concentration gradient to an electron acceptor, while the oxidized form simultaneously returns along its own concentration gradient. At steady state ($\partial c/\partial t = 0$), the concentration gradients are linear in this closed one-dimensional system. (b) The self-exchange rate (k_{hop}) allows electrons to hop between oxidized and reduced EES. If k_{hop} is significantly faster than the rate of diffusion, electron hopping will accelerate the apparent diffusion of electrons. EES diffusion can also co-occur. (c) In three dimensions, with an inner sphere of cells and an outer sphere of electron acceptor, the concentration gradient at steady state is *non-linear*. The gradient is steeper near the inner sphere, allowing for higher flux than in the one-dimensional case. (d) Results of a closed steady-state model of EES diffusion in three dimensions, with different EES concentrations and diffusion coefficients. Representative aqueous diffusion coefficients are listed below the plot (86,88-90). The numbers in each box correspond to the modeled flux of oxidized EES (J_{ox}) through the surface area (A_{min}) of the inner sphere, in units of molecules per second. Green indicates regions where diffusion can account for the minimum flux needed for cells to survive, while orange indicates regions where diffusion is too slow. The number of molecules per second needed to support the inner sphere with volume V_{min} was calculated to be 1.5×10^7 molecules/s based on published parameters for M_{min}, the minimum energy required for survival in *P. aeruginosa* (85). The inner sphere radius was r_{min} = 10 μm and the outer sphere radius was r_{max} = 100 μm. For simplification, we have taken the diffusion constants of the oxidized and reduced EES (D_{red} and D_{ox}) to be equivalent, and the rates of EES reduction and oxidation (k_{red} and k_{ox}) to be instant.

Electron hopping as an alternative to shuttle diffusion

But what about in an open system, which more accurately models environments where EES operate? An attractive mechanism that might prevent EES loss in an open system is electron hopping between EES bound in the biofilm matrix (84,91). Such conduction would avoid the conflict between turnover and loss within the shuttle diffusion model and might better explain electron shuttling in open systems. The flux of hopping electrons from the cells to the acceptor is considered a diffusive process, which is driven by the concentration gradient of electrons (*i.e.* redox gradient) (92). In this scenario, EES are bound within the extracellular matrix, and electrons propagate from cells to the terminal metabolic electron acceptor (*e.g.* O_2) by sequential electron-transfer reactions among the EES, allowing EES retention and reuse (Fig. 4b). Hopping steps (k_{hop}) are expected to happen rapidly compared to shuttle diffusion (D) (93,94).

Significant theoretical and experimental work has already been done to describe electron hopping in electrode-grown biofilms of *Geobacter sulfurreducens*. Such biofilms, which can exceed tens of microns in thickness, utilize the underlying electrode, poised at a sufficiently oxidizing potential, as the terminal metabolic acceptor. Cells not in direct contact with the electrode can transport their respired electrons to the electrode via hopping through a proposed network of c-type cytochromes as opposed to EES. This model is supported experimentally by measurements of biofilm electrical conductivity (23,91,92,95-100). Much of the theory comes from models of synthetic redox polymers and proteins that contain bound redox cofactors (24,91,101-103). This work provides a proof-of-principle that motivates experiments to test for electron hopping in other biofilms where EES may dominate extracellular electron transfer.

Evolutionary strategies that maintain EES in open environments

Regardless of the electron transfer mechanism, sufficient concentrations of EES must be maintained for viability. What strategies do microbes take in producing and maintaining public

goods in open environments? We view EES as public goods because they are secreted molecules that benefit nearby individuals as well as the producer cell (104). Kin selection theory posits that public good production can evolve when individuals' actions increase not only their own reproductive success, but also the success of genetically related individuals (104). Microbes are therefore more likely to produce public goods when they are highly related to their neighbors, the direct and indirect benefits are high, and the cost of production is low (105).

In this context, it makes sense that EES would be regulated by quorum sensing (QS) molecules, signals that direct population behaviors when cell numbers are high. QS molecules can provide cells with information on nearby relatives and diffusion conditions (106). By dividing quickly and producing an extracellular matrix, many bacteria can establish highly-related microcolonies that favor the evolution of public goods (105). Laboratory studies show that producers of the siderophore, pyoverdine, outcompete non-producer mutants when populations are highly related, but not when strains are mixed (69,107). Because QS molecules are secreted into the environment and subject to diffusion, they enable cells to distinguish between closed and open systems (108). A good example of QS-regulation of EES production can be found in how *Pseudomonas* species regulate phenazine production (31).

Other strategies that can facilitate the viability of EES utilization relate to mechanisms of privatization, such as physical retention or a requirement for special machinery to utilize the secreted molecule (104). Physical retention can be achieved via noncovalent interactions between small molecule and biofilm components, which in the case of EES, could conceivably also provide a scaffold for electron hopping. Marine microbes that retain siderophores by embedding them in the outer membrane with lipophilic sidechains (109) provide an example of selective retention of a secreted metabolite near producing cells. Other chemical mechanisms may facilitate retention, however, such as electrostatic attraction between EES and specific

components of a biofilm matrix. This may help rationalize co-regulation of EES and exopolymeric substances (EPS), as in the case of phenazines, eDNA and particular types of EPS (43,110,111). Discrimination can be achieved with highly specific receptors for siderophores and QS molecules that enable only producers to uptake their secreted products (104,112,113). Another strategy is to make the public good itself toxic, which requires specialized detoxification systems (114). Interestingly, many EES were first identified as antibiotics (11,56), and special proteins are required to deal with their toxic byproducts (115).

Outlook

This is an exciting time to care about microbes that change color. The explosion of computational platforms that can predict structures and properties of natural products, combined with the exponential growth of genomic databases, is ushering in a golden age for EES discovery. Based on these databases, and lessons learned from experimental systems where redox-active pigment production and utilization have been well documented, the available evidence suggests that EES are likely to be widespread and play underappreciated roles in the physiology of diverse microbes.

Going forward, it will be important to prioritize systematic screens to test for EES production and usage. Sidebar 1 provides an example of how one can approach this, yet innovations that would enable high-throughput screens are needed to stimulate the search process. While such technologies could be developed by individual labs at universities, an opportunity for efficient scale-up exists if national labs that are interested in metabolomics, such as the Joint Genome Institute (66,116,117), take on this challenge. The creation of pipelines to interface metabolomics with complementary bioinformatics and physiological screens would greatly accelerate EES discovery. In our view, the identification of genetically-tractable EES-producing microbes should be a priority for future research. Genetically-tractable systems are now more achievable than ever

before (118,119), and thus the isolation of EES-producing or utilizing microbes has the potential to quickly reach a mechanistic-level of understanding.

Identification of machinery that sense and process EES across diverse microorganisms will permit the type of comparative analysis needed to enable general principles to be resolved. For example, the better we understand the conservation of EES transporters or sensors, the more confidently we will be able to scan genomes to predict EES production or usage by new isolates. In this way, we will be able to learn whether the strategies that govern EES cycling by the handful of organisms that have been studied in detail to date represent special cases or broader paradigms. Generally, metabolic strategies fall into a limited number of categories that are viable for cells, thus it will be exciting to discovery the range of strategies that can be used by organisms that employ EES for energy generation and other purposes.

Finally, we end by noting that much of what we understand about microbial metabolism springs from research that has been done when nutrients are replete. Yet microbial existence in the natural world is usually limited by a variety of substrates (120), and it is in this context we believe EES will prove to be important. Not only can EES enable energy generation in oxidant-limited biofilms, which are ubiquitous (82,83), but the broader reactivity of EES can impact the fate and transport of pollutants in soils and sediments (14,121,122). From both fundamental and applied viewpoints, a broader and deeper understanding of EES production, sensing and utilization thus stands to improve our ability to rationalize and control the composition and activities of microbial communities across a variety of natural, engineered, and clinical environments.

Sidebars

Sidebar 1. How to characterize a putative EES

What criteria establish that a molecule functions as an EES? Based on our definition, the molecule must 1) facilitate extracellular electron transfer, 2) undergo multiple redox cycles, and 3) provide

a physiological benefit to its producer via cycling. The following steps can be used to determine whether a particular secreted metabolite is an EES.

Find a tractable extracellular electron transfer phenotype and implicate a soluble EES. Quantifiable extracellular electron transfer phenotypes can be detected in assays with minerals (33), electrodes (40,44,123), or soluble electron acceptors (11,124). Secreted EES can be implicated by demonstrating electron acceptor reduction in the absence of direct cell contact using different strategies, such as separation by agar, permeable membranes, glass frits, or compartments in microfluidic devices.

Isolate and characterize the EES molecule. Once an EES phenotype is established, the responsible molecule can be purified using chromatography and other standard separation methods from organic chemistry. Its spectral properties, biotic and abiotic reactivity, and redox potential can then be measured using different types of spectroscopy (UV–vis, EPR) and cyclic voltammetry, respectively (*e.g.* (9,38,125)).

Genetically inhibit EES biosynthesis. Because EES are not essential under all conditions, it is possible to isolate mutants defective in their production. Such mutants can offer insights into EES biosynthesis, regulation, and even cycling mechanisms (*e.g.* (35,40,126)). Control over EES production, which is enabled by mutant strains, is necessary to rigorously determine the physiological benefits of an EES.

Measure EES turnover. EES uptake and reduction can be quantified using biosynthetic mutants in the presence of a defined EES concentration and oxidant (*e.g.*(40)). The molecule can be defined as an EES if it enables a super-stoichiometric reaction with the distal electron acceptor.

Sidebar 2. How does redox-potential define an EES?

The essence of a shuttle is summarized by its midpoint reduction potential, a broad generalization of a compound's ability to act as electron acceptor or donor. To avoid misusing this parameter, one must remain cognizant that it is descriptive of standard conditions for reactions heading towards thermodynamic equilibrium, conditions that rarely describe biological systems. Importantly, many redox reactions involve proton exchange, and so the true reduction potential depends on the environmental pH. A distinction must also be drawn between the one- and two-electron potentials of a shuttle, which can vary by hundreds of millivolts—this difference has even been exploited by some microorganisms to drive the reduction of low-potential acceptors in a process known as electron bifurcation (127,128). Moreover, the reduction potential says nothing about the kinetics or chemical sensibility of the reaction. A striking example of this distinction is the thermodynamic favorability of biological nitrogen fixation (129), a process that nonetheless requires catalysis and energy input to proceed at rates that support life. Conversely, the artificial redox cycling drug paraquat has a midpoint potential below that of most intracellular donors, rendering paraquat reduction thermodynamically unfavorable *at standard conditions*; even so, the paraquat radical reacts with oxygen at a rate that is nearly diffusion-limited (130), allowing paraquat to drive redox cycling under biological conditions. And so, while a shuttle's reduction potential is a core physical parameter that captures the essence of redox cycling, it must be carefully considered with respect to the environmental conditions, reaction kinetics, and other chemical properties. A rigorous quantitative prediction of these effects remains an ongoing challenge, but further advancements will undoubtedly enrich the already informative natural products databases.

Glossary

Extracellular electron shuttles (EES): A self-produced small molecule that enables a microbe to perform EET by *reversibly* accepting metabolic electrons and donating them to extracellular electron acceptors. Note these molecules can also act as electron donors to metabolism (131).

Biosynthetic clusters: organized sets of genes that encode enzymes to produce specific metabolites.

Redox gradient: A concentration gradient of electrons across a field of redox-active molecules. This gradient can drive physical diffusion of the molecules in different redox states, or electron diffusion via electron transfer between redox-active molecules.

Public goods: Secreted molecules that benefit nearby individuals that did not originally produce the molecules.

Acknowledgements

We thank Leonard Tender and Matthew Yates for helpful comments, and Muir Morrison, Tal Einav, and Manuel Razo for guidance in developing the 3D diffusion model.

Literature Cited

1. Consortium, H. M. P. (2012) Structure, function and diversity of the healthy human microbiome. *Nature* **486**, 207-214
2. Turnbaugh, P. J., Ley, R. E., Hamady, M., Fraser-Liggett, C., Knight, R., and Gordon, J. I. (2007) The human microbiome project: exploring the microbial part of ourselves in a changing world. *Nature* **449**, 804
3. Jelen, B. I., Giovannelli, D., and Falkowski, P. G. (2016) The role of microbial electron transfer in the coevolution of the biosphere and geosphere. *Annual Review of Microbiology* **70**, 45-62
4. Lovley, D. R. (2006) Bug juice: harvesting electricity with microorganisms. *Nature Reviews Microbiology* **4**, 497-508
5. Garrity, G. M., Bell, J. A., and Lilburn, T. G. (2004) Taxonomic outline of the prokaryotes. Bergey's manual of systematic bacteriology. *Springer, New York, Berlin, Heidelberg*

6. Young, G. (1947) Pigment production and antibiotic activity in cultures of *Pseudomonas aeruginosa*. *Journal of Bacteriology* **54**, 109
7. Gauthier, M., and Flatau, G. (1976) Antibacterial activity of marine violet-pigmented Alteromonas with special reference to the production of brominated compounds. *Canadian Journal of Microbiology* **22**, 1612-1619
8. Conn, J. E. (1943) The pigment production of *Actinomyces coelicolor* and *A. violaceus-ruber*. *Journal of Bacteriology* **46**, 133
9. Friedheim, E., and Michaelis, L. (1931) Potentiometric study of pyocyanine. *Journal of Biological Chemistry* **91**, 355-368
10. Grahl, N., Kern, S. E., Newman, D. K., and Hogan, D. A. (2013) The yin and the yang of phenazine physiology. in *Microbial Phenazines* (Chincholkar, S., and Thomashow, L. S. eds.), Springer. pp 43-70
11. Price-Whelan, A., Dietrich, L. E. P., and Newman, D. K. (2006) Rethinking 'secondary' metabolism: physiological roles for phenazine antibiotics. *Nature Chemical Biology* **2**, 221-221
12. Hernandez, M. E., and Newman, D. K. (2001) Extracellular electron transfer. *Cell and Molecular Life Sciences* **58**, 1562-71
13. Roden, E. E., Kappler, A., Bauer, I., Jiang, J., Paul, A., Stoesser, R., Konishi, H., and Xu, H. (2010) Extracellular electron transfer through microbial reduction of solid-phase humic substances. *Nature Geoscience* **3**, 417-421
14. Kappler, A., Benz, M., Schink, B., and Brune, A. (2004) Electron shuttling via humic acids in microbial iron(III) reduction in a freshwater sediment. *FEMS Microbiology Ecology* **47**, 85-92
15. Xu, K. D., Stewart, P. S., Xia, F., Huang, C. T., and McFeters, G. A. (1998) Spatial physiological heterogeneity in *Pseudomonas aeruginosa* biofilm is determined by oxygen availability. *Applied and Environmental Microbiology* **64**, 4035-9
16. Stewart, P. S. (2003) Diffusion in biofilms. *Journal of Bacteriology* **185**, 1485-1491 %@ 0021-9193
17. Cowley, E. S., Kopf, S. H., LaRiviere, A., Ziebis, W., and Newman, D. K. (2015) Pediatric cystic fibrosis sputum can be chemically dynamic, anoxic, and extremely reduced due to hydrogen sulfide formation. *mBio* **6**
18. Lee, A., and Newman, D. (2003) Microbial iron respiration: impacts on corrosion processes. *Applied Microbiology and Biotechnology* **62**, 134-139
19. McGlynn, S. E., Chadwick, G. L., Kempes, C. P., and Orphan, V. J. (2015) Single cell activity reveals direct electron transfer in methanotrophic consortia. *Nature* **526**, 531-535
20. Scheller, S., Yu, H., Chadwick, G. L., McGlynn, S. E., and Orphan, V. J. (2016) Artificial electron acceptors decouple archaeal methane oxidation from sulfate reduction. *Science* **351**, 703-707
21. Shi, L., Dong, H., Reguera, G., Beyenal, H., Lu, A., Liu, J., Yu, H.-Q., and Fredrickson, J. K. (2016) Extracellular electron transfer mechanisms between microorganisms and minerals. *Nature Reviews Microbiology*
22. Malvankar, N. S., Rotello, V. M., Tuominen, M. T., and Lovley, D. R. (2016) Reply to 'Measuring conductivity of living *Geobacter sulfurreducens* biofilms'. *Nature Nanotechnology* **11**, 913-914

23. Yates, M. D., Strycharz-Glaven, S. M., Golden, J. P., Roy, J., Tsoi, S., Erickson, J. S., El-Naggar, M. Y., Barton, S. C., and Tender, L. M. (2016) Measuring conductivity of living *Geobacter sulfurreducens* biofilms. *Nature Nanotechnology* **11**, 910-913
24. Subramanian, P., Pirbadian, S., El-Naggar, M. Y., and Jensen, G. J. (2017) The ultrastructure of *Shewanella oneidensis* MR-1 nanowires revealed by electron cryo-tomography. *bioRxiv*
25. Pfeffer, C., Larsen, S., Song, J., Dong, M., Besenbacher, F., Meyer, R. L., Kjeldsen, K. U., Schreiber, L., Gorby, Y. A., and El-Naggar, M. Y. (2012) Filamentous bacteria transport electrons over centimetre distances. *Nature* **491**, 218-221
26. Tan, Y., Adhikari, R. Y., Malvankar, N. S., Ward, J. E., Nevin, K. P., Woodard, T. L., Smith, J. A., Snoeyenbos-West, O. L., Franks, A. E., and Tuominen, M. T. (2016) The low conductivity of *Geobacter uraniireducens* pili suggests a diversity of extracellular electron transfer mechanisms in the genus *Geobacter*. *Frontiers in Microbiology* **7**
27. Smith, J. A., Tremblay, P.-L., Shrestha, P. M., Snoeyenbos-West, O. L., Franks, A. E., Nevin, K. P., and Lovley, D. R. (2014) Going wireless: Fe(III) oxide reduction without pili by *Geobacter sulfurreducens* strain JS-1. *Applied and Environmental Microbiology* **80**, 4331-4340
28. Kotloski, N. J., and Gralnick, J. A. (2013) Flavin electron shuttles dominate extracellular electron transfer by *Shewanella oneidensis*. *mBio* **4**, e00553-12
29. Lies, D. P., Hernandez, M. E., Kappler, A., Mielke, R. E., Gralnick, J. A., and Newman, D. K. (2005) *Shewanella oneidensis* MR-1 uses overlapping pathways for iron reduction at a distance and by direct contact under conditions relevant for biofilms. *Applied and Environmental Microbiology* **71**, 4414-4426
30. Coates, J. D., Ellis, D. J., Blunt-Harris, E. L., Gaw, C. V., Roden, E. E., and Lovley, D. R. (1998) Recovery of humic-reducing bacteria from a diversity of environments. *Applied and Environmental Microbiology* **64**, 1504-1509
31. Dietrich, L. E., Price-Whelan, A., Petersen, A., Whiteley, M., and Newman, D. K. (2006) The phenazine pyocyanin is a terminal signalling factor in the quorum sensing network of *Pseudomonas aeruginosa*. *Mol Microbiol* **61**, 1308-21
32. Price-Whelan, A., Dietrich, L. E., and Newman, D. K. (2006) Rethinking 'secondary' metabolism: physiological roles for phenazine antibiotics. *Nature Chemical Biology* **2**, 71-8
33. Hernandez, M. E., Kappler, A., and Newman, D. K. (2004) Phenazines and other redox-active antibiotics promote microbial mineral reduction. *Applied and Environmental Microbiology* **70**, 921-8
34. Wang, Y., Wilks, J. C., Danhorn, T., Ramos, I., Croal, L., and Newman, D. K. (2011) Phenazine-1-carboxylic acid promotes bacterial biofilm development via ferrous iron acquisition. *J Bacteriol* **193**, 3606-17
35. Dietrich, L. E., Price-Whelan, A., Petersen, A., Whiteley, M., and Newman, D. K. (2006) The phenazine pyocyanin is a terminal signalling factor in the quorum sensing network of *Pseudomonas aeruginosa*. *Molecular Microbiology* **61**, 1308-21
36. Price-Whelan, A., Dietrich, L. E., and Newman, D. K. (2007) Pyocyanin alters redox homeostasis and carbon flux through central metabolic pathways in *Pseudomonas aeruginosa* PA14. *Journal of Bacteriology* **189**, 6372-81

37. Dietrich, L. E. P., Teal, T. K., Price-Whelan, A., and Newman, D. K. (2008) Redox-active antibiotics control gene expression and community behavior in divergent bacteria. *Science* **321**, 1203-1206
38. Wang, Y., and Newman, D. K. (2008) Redox reactions of phenazine antibiotics with ferric (hydr)oxides and molecular oxygen. *Environ Sci Technol* **42**, 2380-6
39. Ramos, I., Dietrich, L. E., Price-Whelan, A., and Newman, D. K. (2010) Phenazines affect biofilm formation by *Pseudomonas aeruginosa* in similar ways at various scales. *Research in Microbiology* **161**, 187-91
40. Wang, Y., Kern, S. E., and Newman, D. K. (2010) Endogenous phenazine antibiotics promote anaerobic survival of *Pseudomonas aeruginosa* via extracellular electron transfer. *J Bacteriol* **192**, 365-9
41. Sullivan, N. L., Tzeranis, D. S., Wang, Y., So, P. T., and Newman, D. (2011) Quantifying the dynamics of bacterial secondary metabolites by spectral multiphoton microscopy. *ACS Chem Biol* **6**, 893-9
42. Hunter, R. C., Klepac-Ceraj, V., Lorenzi, M. M., Grotzinger, H., Martin, T. R., and Newman, D. K. (2012) Phenazine content in the cystic fibrosis respiratory tract negatively correlates with lung function and microbial complexity. *Am J Respir Cell Mol Biol* **47**, 738-45
43. Dietrich, L. E. P., Okegbe, C., Price-Whelan, A., Sakhtah, H., Hunter, R. C., and Newman, D. K. (2013) Bacterial community morphogenesis is intimately linked to the intracellular redox state. *Journal of Bacteriology* **195**, 1371-1380
44. Glasser, N. R., Kern, S. E., and Newman, D. K. (2014) Phenazine redox cycling enhances anaerobic survival in *Pseudomonas aeruginosa* by facilitating generation of ATP and a proton-motive force. *Mol Microbiol* **92**, 399-412
45. Costa, K. C., Bergkessel, M., Saunders, S., Korlach, J., and Newman, D. K. (2015) Enzymatic degradation of phenazines can generate energy and protect sensitive organisms from toxicity. *mBio* **6**, e01520-15
46. Glasser, N. R., Wang, B. X., Hoy, J. A., and Newman, D. K. (2017) The pyruvate and α-ketoglutarate dehydrogenase complexes of *Pseudomonas aeruginosa* catalyze pyocyanin and phenazine-1-carboxylic acid reduction via the subunit dihydrolipoamide dehydrogenase. *Journal of Biological Chemistry*, jbc. M116. 772848
47. Costa, K. C., Glasser, N. R., Conway, S. J., and Newman, D. K. (2017) Pyocyanin degradation by a tautomerizing demethylase inhibits *Pseudomonas aeruginosa* biofilms. *Science* **355**, 170-173
48. Brutinel, E. D., and Gralnick, J. A. (2012) Shuttling happens: soluble flavin mediators of extracellular electron transfer in *Shewanella*. *Applied Microbiology and Biotechnology* **93**, 41-48
49. Marsili, E., Baron, D. B., Shikhare, I. D., Coursolle, D., Gralnick, J. A., and Bond, D. R. (2008) Shewanella secretes flavins that mediate extracellular electron transfer. *Proceedings of the National Academy of Sciences* **105**, 3968-3973
50. Freguia, S., Masuda, M., Tsujimura, S., and Kano, K. (2009) *Lactococcus lactis* catalyses electricity generation at microbial fuel cell anodes via excretion of a soluble quinone. *Bioelectrochemistry* **76**, 14-18
51. Keck, A., Rau, J., Reemtsma, T., Mattes, R., Stolz, A., and Klein, J. (2002) Identification of quinoide redox mediators that are formed during the degradation of naphthalene-2-

sulfonate by *Sphingomonas xenophaga* BN6. *Applied and Environmental Microbiology* **68**, 4341-4349

52. Deng, L., Li, F., Zhou, S., Huang, D., and Ni, J. (2010) A study of electron-shuttle mechanism in *Klebsiella pneumoniae* based-microbial fuel cells. *Chinese Science Bulletin* **55**, 99-104
53. Pence, H. E., and Williams, A. (2010) ChemSpider: an online chemical information resource. ACS Publications
54. Petrauskas, A. A., and Kolovanov, E. A. (2000) ACD/Log P method description. *Perspectives in Drug Discovery and Design* **19**, 99-116
55. Bond, D. R., and Lovley, D. R. (2005) Evidence for involvement of an electron shuttle in electricity generation by *Geothrix fermentans*. *Applied and Environmental Microbiology* **71**, 2186-2189
56. Cude, W. N., Mooney, J., Tavanaei, A. A., Hadden, M. K., Frank, A. M., Gulvik, C. A., May, A. L., and Buchan, A. (2012) Production of the antimicrobial secondary metabolite indigoidine contributes to competitive surface colonization by the marine roseobacter *Phaeobacter* sp. strain Y4I. *Applied and Environmental Microbiology* **78**, 4771-4780
57. Fuller, S. J., McMillan, D. G., Renz, M. B., Schmidt, M., Burke, I. T., and Stewart, D. I. (2014) Extracellular electron transport-mediated Fe(III) reduction by a community of alkaliphilic bacteria that use flavins as electron shuttles. *Applied and Environmental Microbiology* **80**, 128-137
58. (2017) Dictionary of Natural Products 25.2. Taylor and Francis, http://dnp.chemnetbase.com/
59. Assary, R. S., Brushett, F. R., and Curtiss, L. A. (2014) Reduction potential predictions of some aromatic nitrogen-containing molecules. *RSC Advances* **4**, 57442-57451
60. Weber, T., Blin, K., Duddela, S., Krug, D., Kim, H. U., Bruccoleri, R., Lee, S. Y., Fischbach, M. A., Müller, R., and Wohlleben, W. (2015) antiSMASH 3.0—a comprehensive resource for the genome mining of biosynthetic gene clusters. *Nucleic Acids Research* **43**, W237-W243
61. Hadjithomas, M., Chen, I.-M. A., Chu, K., Ratner, A., Palaniappan, K., Szeto, E., Huang, J., Reddy, T., Cimermančič, P., and Fischbach, M. A. (2015) IMG-ABC: a knowledge base to fuel discovery of biosynthetic gene clusters and novel secondary metabolites. *mBio* **6**, e00932-15
62. Pomposiello, P. J., and Demple, B. (2001) Redox-operated genetic switches: the SoxR and OxyR transcription factors. *Trends in Biotechnology* **19**, 109-114
63. Palma, M., Zurita, J., Ferreras, J. A., Worgall, S., Larone, D. H., Shi, L., Campagne, F., and Quadri, L. E. (2005) *Pseudomonas aeruginosa* SoxR does not conform to the archetypal paradigm for SoxR-dependent regulation of the bacterial oxidative stress adaptive response. *Infection and immunity* **73**, 2958-2966
64. Cruz, R. D., Gao, Y., Penumetcha, S., Sheplock, R., Weng, K., and Chander, M. (2010) Expression of the *Streptomyces coelicolor* SoxR regulon is intimately linked with actinorhodin production. *Journal of Bacteriology* **192**, 6428-6438
65. Singh, A. K., Shin, J. H., Lee, K. L., Imlay, J. A., and Roe, J. H. (2013) Comparative study of SoxR activation by redox-active compounds. *Molecular Microbiology* **90**, 983-996

66. Chen, I.-M. A., Markowitz, V. M., Chu, K., Palaniappan, K., Szeto, E., Pillay, M., Ratner, A., Huang, J., Andersen, E., and Huntemann, M. (2016) IMG/M: integrated genome and metagenome comparative data analysis system. *Nucleic Acids Research*, gkw929
67. Letunic, I., and Bork, P. (2016) Interactive tree of life (iTOL) v3: an online tool for the display and annotation of phylogenetic and other trees. *Nucleic Acids Research* **44**, W242-W245
68. Federhen, S. (2012) The NCBI taxonomy database. *Nucleic Acids Research* **40**, D136-D143
69. Griffin, A. S., West, S. A., and Buckling, A. (2004) Cooperation and competition in pathogenic bacteria. *Nature* **430**, 1024-1027
70. Sakhtah, H., Koyama, L., Zhang, Y., Morales, D. K., Fields, B. L., Price-Whelan, A., Hogan, D. A., Shepard, K., and Dietrich, L. E. (2016) The *Pseudomonas aeruginosa* efflux pump MexGHI-OpmD transports a natural phenazine that controls gene expression and biofilm development. *Proceedings of the National Academy of Sciences*, 201600424
71. Blankenfeldt, W., and Parsons, J. F. (2014) The structural biology of phenazine biosynthesis. *Current Opinion in Structural Biology* **0**, 26-33
72. Dewick, P. M. (1994) The biosynthesis of shikimate metabolites. *Natural Product Reports* **11**, 173-203
73. Bacher, A., Eberhardt, S., Fischer, M., Kis, K., and Richter, G. (2000) Biosynthesis of vitamin B2 (riboflavin). *Annual Review of Nutrition* **20**, 153-167
74. Amthor, J. S. (2000) The McCree–de Wit–Penning de Vries–Thornley respiration paradigms: 30 years later. *Annals of Botany* **86**, 1-20
75. Xavier, J. B., Kim, W., and Foster, K. R. (2011) A molecular mechanism that stabilizes cooperative secretions in *Pseudomonas aeruginosa*. *Molecular Microbiology* **79**, 166-179
76. Gerstel, U., and Römling, U. (2001) Oxygen tension and nutrient starvation are major signals that regulate *agfD* promoter activity and expression of the multicellular morphotype in *Salmonella typhimurium*. *Environmental Microbiology* **3**, 638-648
77. Glick, R., Gilmour, C., Tremblay, J., Satanower, S., Avidan, O., Déziel, E., Greenberg, E. P., Poole, K., and Banin, E. (2010) Increase in rhamnolipid synthesis under iron-limiting conditions influences surface motility and biofilm formation in *Pseudomonas aeruginosa*. *Journal of Bacteriology* **192**, 2973-2980
78. Shi, L., Rosso, K. M., Clarke, T. A., Richardson, D. J., Zachara, J. M., and Fredrickson, J. K. (2012) Molecular underpinnings of Fe(III) oxide reduction by *Shewanella oneidensis* MR-1. *Frontiers in Microbiology*, 46
79. Galkin, A. S., Grivennikova, V. G., and Vinogradov, A. D. (1999) →H+/2e stoichiometry in NADH-quinone reductase reactions catalyzed by bovine heart submitochondrial particles. *FEBS Letters* **451**, 157-161
80. Benz, M., Schink, B., and Brune, A. (1998) Humic acid reduction by *Propionibacterium freudenreichii* and other fermenting bacteria. *Applied and Environmental Microbiology* **64**, 4507-4512
81. Cochemé, H. M., and Murphy, M. P. (2008) Complex I Is the major site of mitochondrial superoxide production by paraquat. *Journal of Biological Chemistry* **283**, 1786-1798
82. Stewart, P. S., and Franklin, M. J. (2008) Physiological heterogeneity in biofilms. *Nature Reviews Microbiology* **6**, 199-210

83. O'Toole, G., Kaplan, H. B., and Kolter, R. (2000) Biofilm formation as microbial development. *Annual Reviews in Microbiology* **54**, 49-79
84. Picioreanu, C., Head, I. M., Katuri, K. P., van Loosdrecht, M. C., and Scott, K. (2007) A computational model for biofilm-based microbial fuel cells. *Water Research* **41**, 2921-2940
85. Kempes, C. P., Okegbe, C., Mears-Clarke, Z., Follows, M. J., and Dietrich, L. E. (2014) Morphological optimization for access to dual oxidants in biofilms. *Proceedings of the National Academy of Sciences* **111**, 208-213
86. Lukacs, G. L., Haggie, P., Seksek, O., Lechardeur, D., Freedman, N., and Verkman, A. (2000) Size-dependent DNA mobility in cytoplasm and nucleus. *Journal of Biological Chemistry* **275**, 1625-1629
87. Phalak, P., Chen, J., Carlson, R. P., and Henson, M. A. (2016) Metabolic modeling of a chronic wound biofilm consortium predicts spatial partitioning of bacterial species. *BMC Systems Biology* **10**, 90
88. Nauman, J. V., Campbell, P. G., Lanni, F., and Anderson, J. L. (2007) Diffusion of insulin-like growth factor-I and ribonuclease through fibrin gels. *Biophysical Journal* **92**, 4444-4450
89. Murray, A. G., and Jackson, G. A. (1992) Viral dynamics: A model of the effects size, shape, motion and abundance of single-celled planktonic organisms and other particles. *Marine ecology progress series. Oldendorf* **89**, 103-116
90. Dhall, S., Do, D. C., Garcia, M., Kim, J., Mirebrahim, S. H., Lyubovitsky, J., Lonardi, S., Nothnagel, E. A., Schiller, N., and Martins-Green, M. (2014) Generating and reversing chronic wounds in diabetic mice by manipulating wound redox parameters. *J Diabetes Res* **2014**, 562625
91. Boyd, D. A., Snider, R. M., Erickson, J. S., Roy, J. N., Strycharz-Glaven, S. M., and Tender, L. M. (2015) Measuring electron transport rates through electrochemically active biofilms in *Biofilms in Bioelectrochemical Systems: from Laboratory Practice o Data Interpretation* (Haluk Beyenal, J. B. ed.), 1 Ed., John Wiley & Sons, Inc. pp
92. Snider, R. M., Strycharz-Glaven, S. M., Tsoi, S. D., Erickson, J. S., and Tender, L. M. (2012) Long-range electron transport in *Geobacter sulfurreducens* biofilms is redox gradient-driven. *Proceedings of the National Academy of Sciences* **109**, 15467-72
93. Uchimiya, M., and Stone, A. T. (2009) Reversible redox chemistry of quinones: Impact on biogeochemical cycles. *Chemosphere* **77**, 451-458
94. Rosso, K. M., Smith, D. M., Wang, Z., Ainsworth, C. C., and Fredrickson, J. K. (2004) Self-exchange electron transfer kinetics and reduction potentials for anthraquinone disulfonate. *The Journal of Physical Chemistry A* **108**, 3292-3303
95. Yates, M. D., Golden, J. P., Roy, J., Strycharz-Glaven, S. M., Tsoi, S., Erickson, J. S., El-Naggar, M. Y., Calabrese Barton, S., and Tender, L. M. (2015) Thermally activated long range electron transport in living biofilms. *Phys Chem Chem Phys* **17**, 32564-70
96. Yates, M. D., and Tender, L. M. (2016) Electrochemical gating measurements of living electrode-grown *Geobacter sulfurreducens* biofilms *Nature Nanotechnology (In press)*
97. Yates, M. D., Strycharz-Glaven, S. M., and Tender, L. M. (2016) Understanding long-distance extracellular electron transport in an electroautotrophic microbial community. *Energy & Environmental Science (in press)*

98. Strycharz-Glaven, S. M., Snider, R. M., Guiseppi-Elie, A., and Tender, L. M. (2011) On the electrical conductivity of microbial nanowires and biofilms. *Energy & Environmental Science* **4**, 4366-4379
99. Phan, H., Yates, M. D., Kirchhofer, N. D., Bazan, G. C., Tender, L. M., and Nguyen, T.-Q. (2016) Biofilm as a redox conductor: a systematic study of the moisture and temperature dependence of its electrical properties. *Physical Chemistry Chemical Physics* **18**, 17815-17821
100. Robuschi, L., Tomba, J. P., Schrott, G. D., Bonanni, P. S., Desimone, P. M., and Busalmen, J. P. (2013) Spectroscopic slicing to reveal internal redox gradients in electricity-producing biofilms. *Angewandte Chemie International Edition* **52**, 925-928
101. Gray, H. B., and Winkler, J. R. (1996) Electron transfer in proteins. *Annual Review of Biochemistry* **65**, 537-561
102. Blauch, D. N., and Saveant, J. M. (1992) Dynamics of electron hopping in assemblies of redox centers. Percolation and diffusion. *Journal of the American Chemical Society* **114**, 3323-3332
103. Pirbadian, S., and El-Naggar, M. Y. (2012) Multistep hopping and extracellular charge transfer in microbial redox chains. *Physical Chemistry Chemical Physics* **14**, 13802-13808
104. West, S. A., Griffin, A. S., Gardner, A., and Diggle, S. P. (2006) Social evolution theory for microorganisms. *Nature Reviews Microbiology* **4**, 597-607
105. Nadell, C. D., Xavier, J. B., and Foster, K. R. (2009) The sociobiology of biofilms. *FEMS Microbiology Reviews* **33**, 206-224
106. Hense, B. A., Kuttler, C., Müller, J., Rothballer, M., Hartmann, A., and Kreft, J.-U. (2007) Does efficiency sensing unify diffusion and quorum sensing? *Nature Reviews Microbiology* **5**, 230-239
107. Diggle, S. P., Griffin, A. S., Campbell, G. S., and West, S. A. (2007) Cooperation and conflict in quorum-sensing bacterial populations. *Nature* **450**, 411-414
108. Redfield, R. J. (2002) Is quorum sensing a side effect of diffusion sensing? *Trends in Microbiology* **10**, 365-370
109. Kümmerli, R., Schiessl, K. T., Waldvogel, T., McNeill, K., and Ackermann, M. (2014) Habitat structure and the evolution of diffusible siderophores in bacteria. *Ecology Letters* **17**, 1536-1544
110. Das, T., and Manefield, M. (2012) Pyocyanin promotes extracellular DNA release in *Pseudomonas aeruginosa*. *PLoS One* **7**, e46718
111. Das, T., Kutty, S. K., Tavallaie, R., Ibugo, A. I., Panchompoo, J., Sehar, S., Aldous, L., Yeung, A. W., Thomas, S. R., Kumar, N., Gooding, J. J., and Manefield, M. (2015) Phenazine virulence factor binding to extracellular DNA is important for *Pseudomonas aeruginosa* biofilm formation. *Scientific Reports* **5**, 8398
112. Neilands, J. (1981) Iron absorption and transport in microorganisms. *Annual Review of Nutrition* **1**, 27-46
113. Schuster, M., Joseph Sexton, D., Diggle, S. P., and Peter Greenberg, E. (2013) Acyl-homoserine lactone quorum sensing: from evolution to application. *Annual Review of Microbiology* **67**, 43-63
114. Schertzer, J. W., Boulette, M. L., and Whiteley, M. (2009) More than a signal: non-signaling properties of quorum sensing molecules. *Trends in Microbiology* **17**, 189-195

115. Hassan, H. M., and Fridovich, I. (1979) Intracellular production of superoxide radical and of hydrogen peroxide by redox active compounds. *Archives of Biochemistry and Biophysics* **196**, 385-395
116. Baran, R., Ivanova, N. N., Jose, N., Garcia-Pichel, F., Kyrpides, N. C., Gugger, M., and Northen, T. R. (2013) Functional genomics of novel secondary metabolites from diverse cyanobacteria using untargeted metabolomics. *Marine Drugs* **11**, 3617-3631
117. Silva, L. P., and Northen, T. R. (2015) Exometabolomics and MSI: deconstructing how cells interact to transform their small molecule environment. *Current Opinion in Biotechnology* **34**, 209-216
118. Cobb, R. E., Wang, Y., and Zhao, H. (2014) High-efficiency multiplex genome editing of *Streptomyces* species using an engineered CRISPR/Cas system. *ACS Synthetic Biology* **4**, 723-728
119. Peters, J. M., Silvis, M. R., Zhao, D., Hawkins, J. S., Gross, C. A., and Qi, L. S. (2015) Bacterial CRISPR: accomplishments and prospects. *Current Opinion in Microbiology* **27**, 121-126
120. Bergkessel, M., Basta, D. W., and Newman, D. K. (2016) The physiology of growth arrest: uniting molecular and environmental microbiology. *Nature Reviews Microbiology* **14**, 549-562
121. Kappler, A., and Haderlein, S. B. (2003) Natural organic matter as reductant for chlorinated aliphatic pollutants. *Environmental Science & Technology* **37**, 2714-2719
122. Jiang, J., and Kappler, A. (2008) Kinetics of microbial and chemical reduction of humic substances: implications for electron shuttling. *Environmental Science & Technology* **42**, 3563-3569
123. Emde, R., Swain, A., and Schink, B. (1989) Anaerobic oxidation of glycerol by *Escherichia coli* in an amperometric poised-potential culture system. *Applied Microbiology and Biotechnology* **32**, 170-175
124. Khan, M. T., Duncan, S. H., Stams, A. J., Van Dijl, J. M., Flint, H. J., and Harmsen, H. J. (2012) The gut anaerobe *Faecalibacterium prausnitzii* uses an extracellular electron shuttle to grow at oxic–anoxic interphases. *The ISME journal* **6**, 1578-1585
125. Scott, D. T., McKnight, D. M., Blunt-Harris, E. L., Kolesar, S. E., and Lovley, D. R. (1998) Quinone moieties act as electron acceptors in the reduction of humic substances by humics-reducing microorganisms. *Environmental Science & Technology* **32**, 2984-2989
126. Pierson III, L. S., and Thomashow, L. S. (1992) Cloning and Heterologous Expression of the Phenazine Biosynthetic. *Molecular Plant-Microbe Interactions* **5**, 330-339
127. Li, F., Hinderberger, J., Seedorf, H., Zhang, J., Buckel, W., and Thauer, R. K. (2008) Coupled ferredoxin and crotonyl coenzyme A (CoA) reduction with NADH catalyzed by the butyryl-CoA dehydrogenase/Etf complex from *Clostridium kluyveri*. *Journal of Bacteriology* **190**, 843-850
128. Herrmann, G., Jayamani, E., Mai, G., and Buckel, W. (2008) Energy conservation via electron-transferring flavoprotein in anaerobic bacteria. *Journal of Bacteriology* **199**, 784-791
129. Alberty, R. A. (1994) Thermodynamics of the nitrogenase reactions. *Journal of Biological Chemistry* **269**, 7099-7102
130. Farrington, J. A., Ebert, M., Land, E. J., and Fletcher, K. (1973) Bipyridylium quaternary salts and related compounds. V. Pulse radiolysis studies of the reaction of paraquat radical

with oxygen. Implications for the mode of action of bipyridyl herbicides. *Biochimica et Biophysica Acta (BBA) - Bioenergetics* **314**, 372-381

131. Coates, J. D., Cole, K. A., Chakraborty, R., O'Connor, S. M., and Achenbach, L. A. (2002) Diversity and ubiquity of bacteria capable of utilizing humic substances as electron donors for anaerobic respiration. *Applied and Environmental Microbiology* **68**, 2445-2452

Chapter 3

PHYSIOLOGY OF PHENAZINE-MEDIATED SURVIVAL

This chapter is adapted from:

Glasser, N. R., Kern, S. E., and Newman, D. K. (2014) Phenazine redox cycling enhances anaerobic survival in *Pseudomonas aeruginosa* by facilitating generation of ATP and a proton-motive force. *Molecular Microbiology* **92**, 399-412.

Abstract

While many studies have explored the growth of *Pseudomonas aeruginosa*, comparatively few have focused on its survival. Previously, we reported that endogenous phenazines support the anaerobic survival of *P. aeruginosa*, yet the physiological mechanism underpinning survival was unknown. Here, we demonstrate that phenazine redox cycling enables *P. aeruginosa* to oxidize glucose and pyruvate into acetate, which promotes survival by coupling acetate and ATP synthesis through the activity of acetate kinase. By measuring intracellular NAD(H) and ATP concentrations, we show that survival is correlated with ATP synthesis, which is tightly coupled to redox homeostasis during pyruvate fermentation but not during arginine fermentation. We also show that ATP hydrolysis is required to generate a proton-motive force using the ATP synthase complex during fermentation. Together, our results suggest that phenazines enable maintenance of the proton-motive force by promoting redox homeostasis and ATP synthesis. Our results demonstrate the more general principle that small redox-active molecules, such as phenazines, can broaden the metabolic versatility of microorganisms by facilitating redox homeostasis.

Introduction

Pseudomonas aeruginosa is an opportunistic pathogen that forms both acute and chronic infections. It is well known to form biofilms in diverse environments, and microbial stasis within biofilms is thought to complicate the treatment of many persistent infections. For example, cells at the base of *P. aeruginosa* biofilms enter a dormant state with decreased levels of transcription and translation, and they undergo physiological adaptations to hypoxic conditions (1,2). These cells are substantially more resistant to antibiotics than actively growing cells (2). Moreover, nutrient deprivation triggers active responses for *P. aeruginosa* that increase antibiotic resistance in growth-arrested cells (3). Even under active growth, many bacterial species, including *P. aeruginosa*, maintain a small population of phenotypically resistant cells called persisters (4). The persister state is thought to be controlled by stochastic changes in cell physiology and metabolism (4-6). Together, these subpopulations of resistant non-replicating cells can serve as reservoirs for recurrent infections (4). Our incomplete understanding of the metabolic changes underpinning microbial quiescence thus limits our ability to treat chronic infections.

In addition to forming biofilms and persister cells during infections, pseudomonads synthesize a class of redox-active pigments collectively termed phenazines (7,8). Phenazines are important virulence factors (9) that serve as antibiotics towards microbial competitors (10) and damage mammalian cells (11). Phenazines can benefit *P. aeruginosa* by serving as signaling molecules (12), regulating persister cell formation (13), influencing colony morphology (14,15), and promoting iron acquisition and biofilm development (16).

We previously reported that micromolar concentrations of phenazines can support anaerobic survival by transferring electrons to an extracellular oxidant (17). Although the physiological basis for this survival mechanism was unknown, phenazine redox cycling was correlated with a more oxidized intracellular environment for planktonic cultures (18,19) and colony biofilms (15),

suggesting that phenazines alter metabolism. *P. aeruginosa* is thought to form biofilms within the lungs of cystic fibrosis patients (20,21), and in many patients, the lung sputum contains phenazines at concentrations that can support anaerobic survival (17,22,23). Phenazines are positively correlated with the progression of *P. aeruginosa* lung infections (23), and so they may directly alter the physiology of *P. aeruginosa* infections *in situ*.

Here, we sought to elucidate the physiological basis for phenazine-promoted anaerobic survival in *P. aeruginosa*. We discovered that phenazines facilitate the conversion of glucose and pyruvate into acetate. Our data support a model where phenazines dissipate excess reducing equivalents, allowing for the coupling of acetate and ATP synthesis through the activity of acetate kinase. ATP is required for survival, in part to maintain the proton-motive force through the ATP synthase complex. Our results highlight the interplay between redox homeostasis and ATP synthesis in the context of long-term survival, and illuminate the important role extracellular redox active metabolites can play in facilitating core metabolism.

Results

Phenazine redox cycling requires the activity of acetate kinase to promote survival

Phenazine redox cycling occurs when a phenazine molecule undergoes alternating reduction and oxidation reactions, resulting in the transfer of electrons from the reductant (*e.g.* NAD(P)H) to the oxidant (*e.g.* oxygen). Phenazines can cross cell membranes, enabling the transfer of reducing equivalents from inside the cell to the extracellular environment. We have previously shown that this transfer of reducing equivalents can promote anaerobic survival (17). We found that a carbon source, specifically glucose, is required for anaerobic survival in the presence of oxidized phenazines (17). To understand how phenazines promote anaerobic survival, we began by exploring the role of glucose.

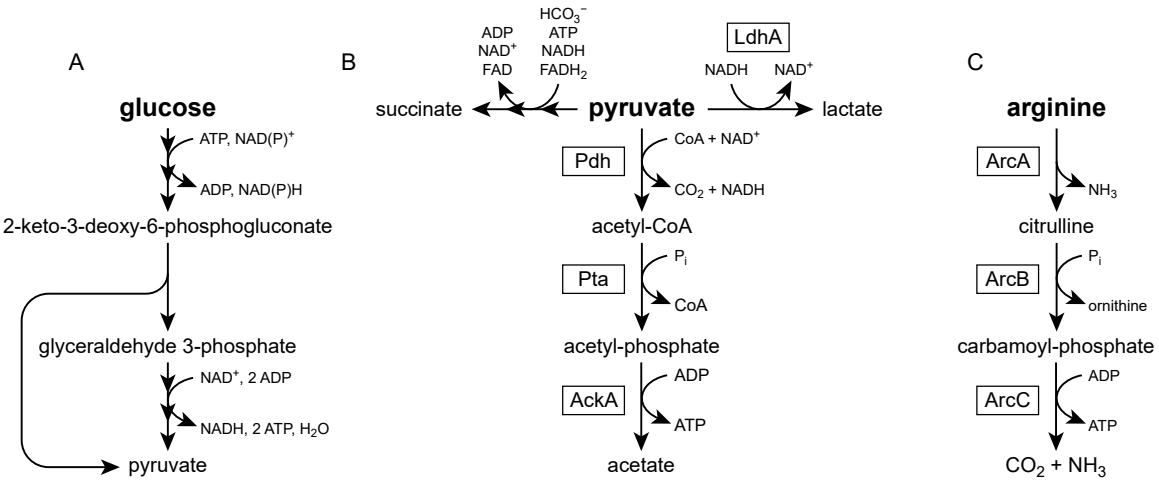

Figure 1. Metabolic pathways in *P. aeruginosa*. Multiple arrowheads indicate that several reaction steps have been condensed for clarity. Boxes indicate the enzyme that catalyzes each reaction. (A) Glucose oxidation via the Entner-Doudoroff pathway. For clarity, the pathway is abbreviated to the key intermediates of glycolysis. (B) Pyruvate fermentation (Eschbach *et al.*, 2004). LdhA, lactate dehydrogenase; Pdh, pyruvate dehydrogenase; Pta, phosphate acetyltransferase; AckA, acetate kinase. (C) The arginine deiminase pathway (Vander Wauven *et al.*, 1984). ArcA, arginine deiminase; ArcB, ornithine carbamoyltransferase; ArcC, carbamate kinase.

To metabolize glucose, *P. aeruginosa* uses the Entner-Doudoroff pathway to convert one glucose molecule into two pyruvate molecules (Figure 1a). This process is coupled to the synthesis of one net ATP molecule and two excess reducing equivalents (NAD(P)H) (Figure 1a). Pyruvate can be further converted into acetate to produce additional ATP and reducing equivalents (Figure 1b). To sustain anaerobic glycolysis, *P. aeruginosa* must regenerate the oxidants (*i.e.* NAD^+ and $NADP^+$) that were consumed during pyruvate and acetate synthesis. We therefore hypothesized that phenazines, by dissipating excess reducing equivalents, might promote the oxidation of glucose into acetate during anaerobic glycolysis. In this model, acetate synthesis is coupled to ATP synthesis through the activity of acetate kinase (Figure 1b), and it is the ATP synthesis that we expected to promote survival.

To address this hypothesis, we tested mutants with markerless deletions of pyruvate metabolism genes in a phenazine redox cycling survival assay. In this experiment, early stationary phase cells were resuspended in anoxic MOPS-buffered minimal medium containing glucose as the sole carbon and energy source. To control the concentration of phenazines, we used strains with deletions in both phenazine biosynthetic operons (Δ*phzA1-G1* Δ*phzA2-G2*, abbreviated Δ*phz1/2*) (12) and added phenazine-1-carboxylic acid (PCA) back to the culture at a physiologically relevant concentration (75 μM) (23). We chose PCA because it is the biosynthetic precursor of all other phenazines in *P. aeruginosa* and other pseudomonads (24,25), and also because it is synthesized whether oxygen is present or not. While oxygen and ferric iron are likely oxidants of phenazines in infection environments (26), we instead supplied an electrode poised at a potential sufficient to oxidize phenazines in our culture vessels (E^0 = +207 mV).

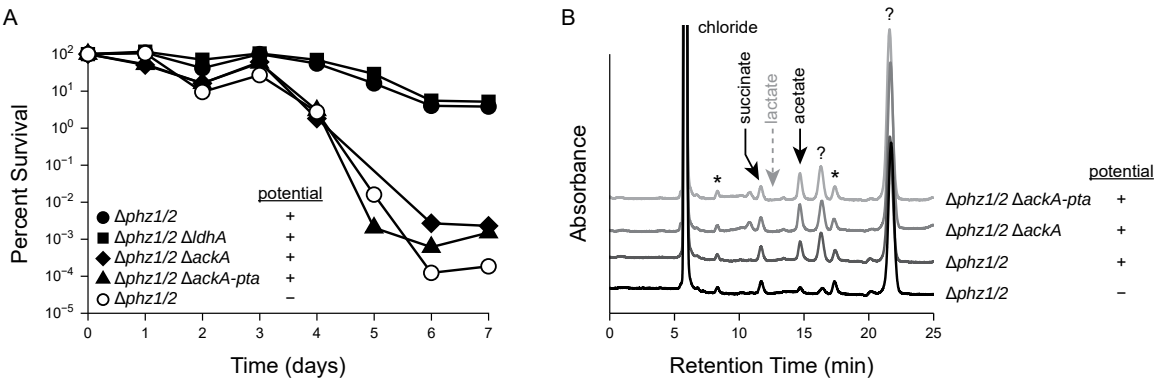

Figure 2. Phenazine redox cycling in *P. aeruginosa* PA14 Δ*phz1/2*. Cells were grown aerobically in LB to an OD_{500} of 2.8 and then pelleted, washed, and resuspended in anoxic MOPS-buffered minimal medium with 20 mM glucose. Where noted in the 'potential' column of the legend, cultures also included 75 μM PCA and an electrode poised at a potential to oxidize any reduced PCA. Results are typical of at least three independent experiments. (A) Survival of strains with deletions of pyruvate metabolism genes. 100% survival represents approximately 7×10^8 CFU/mL. (B) HPLC traces from culture supernatants after three days of phenazine cycling as in panel A. Peaks were identified by comparing retention times to known standards. The dashed gray arrow indicates the retention time of lactate, which was not observed in this experiment. Question marks (?) indicate unidentified products. Asterisks (*) indicate trace contaminants that were present from the start of the experiment.

Consistent with the fact that *P. aeruginosa* is not known to ferment glucose, cultures declined to about 0.0001% viability after seven days when provided with glucose alone (Figure 2a). As previously reported (17), the addition of phenazines and an extracellular oxidizing potential improved anaerobic survival to 10% after seven days (Figure 2a). A strain lacking lactate dehydrogenase, Δ*ldhA*, was not impaired in survival relative to the Δ*phz1/2* parent strain (Figure 2a). However, strains lacking acetate kinase that are unable to generate ATP by converting pyruvate into acetate, Δ*ackA* and Δ*ackA-pta*, failed to survive relative to the parent strain, with only about 0.001% of cells remaining viable after seven days (Figure 2a).

We detected current through the extracellular electrode only when phenazines were present (Supplemental Figure 1), consistent with the model that phenazines mediate electron transfer from inside the cells to the electrode. After three days of survival, before we observed a loss in viability (Figure 2a), the Δ*phz1/2* strain transferred a total charge of 11 C to the electrode. Using the relationship $Q = 2F(acv)$, where Q is the total charge transferred (11 C), F is Faraday's constant (96,485 C mole^{-1}), c is the concentration of PCA (7.5×10^{-5} M), v is the reaction volume (0.1 L), and a is the average number of redox cycles, we calculated an average of 8 redox cycles per molecule of PCA, a value similar to previous measurements (17).

To test if acetate is produced during phenazine redox cycling, we used high performance liquid chromatography (HPLC) to directly measure the secreted metabolic products in our experiment. We detected the production of acetate, succinate, and two additional unknown products whose identification is a work in progress. Consistent with our hypothesis, cultures with oxidized phenazines produced more acetate than did cultures without phenazines (Figure 2b). After three days, in duplicate measurement, the Δ*phz1/2* strain produced 5.9×10^{-8} nanomoles CFU^{-1} (350 μM) and 5.0×10^{-8} nanomoles CFU^{-1} (330 μM) of acetate with phenazine redox cycling but only 1.3×10^{-8} nanomoles CFU^{-1} (78 μM) and 2.1×10^{-8} nanomoles CFU^{-1} (130 μM) of acetate

without phenazine redox cycling. Succinate and one unknown compound were produced in approximately equal amounts irrespective of phenazines (Figure 2a), with the Δ*phz1/2* strain producing 2.4×10^{-8} nanomoles CFU^{-1} of succinate after three days with oxidized phenazines. The other unknown product was produced in greater amounts in cultures with oxidized phenazines than in cultures without phenazines (Figure 2a).

We expected that acetate would be synthesized by acetate kinase (Figure 1b), which couples acetate synthesis to ATP synthesis. To our surprise, the Δ*ackA* and Δ*ackA-pta* mutants produced similar amounts of acetate as the parent strain during phenazine redox cycling with glucose (Figure 2b), suggesting that acetate kinase is not the only active acetate-producing enzyme in our experiment. The *P. aeruginosa* PA14 genome contains the gene *poxB*, which codes for a putative pyruvate oxidase that converts pyruvate to acetate and CO_2 without directly generating ATP or NADH (27). Using quantitative reverse-transcription PCR, we detected *poxB* transcripts during exponential growth, early stationary phase, and after resuspension in anaerobic MOPS-buffered minimal medium with glucose and 75 μM oxidized PCA. We also measured an increase in the relative abundance of pyruvate oxidase transcripts to control gene transcripts (pyruvate dehydrogenase and the housekeeping genes *clpX* and *recA*) after resuspension in minimal medium when compared to exponential growth (Supplemental Figure 2). Pyruvate oxidase, encoded by *poxB*, may therefore account for the observed acetate synthesis in the Δ*ackA* and Δ*ackA-pta* mutants during phenazine redox cycling. Pyruvate oxidase may also account for some acetate synthesis in the WT strain.

Together, the survival defect of the Δ*ackA* and Δ*ackA-pta* mutants (Figure 2a) demonstrates that the activity of acetate kinase is essential for long-term survival in our phenazine redox cycling experiment. As the Δ*ackA* and Δ*ackA-pta* mutants still produce acetate (Figure 2b), it is unlikely

that acetate itself is sufficient for survival. Instead, our data are consistent with a model where ATP synthesis by acetate kinase is required for anaerobic survival.

Phenazine redox cycling promotes ATP synthesis during pyruvate fermentation

In keeping with the fact that the Δ*phz1/2* Δ*ldhA* mutant survived as well as the parent strain Δ*phz1/2* (Figure 2a), we did not observe lactate synthesis during phenazine redox cycling with glucose (Figure 2b). This suggests that lactate dehydrogenase is not used to maintain redox homeostasis during anaerobic glycolysis. In contrast, lactate dehydrogenase is required for survival during pyruvate fermentation (28). During pyruvate fermentation, *P. aeruginosa* converts pyruvate into succinate, lactate, and acetate (Figure 1b). This process supports anaerobic survival but not growth (28) and uses acetate kinase to synthesize ATP (Figure 1b). If phenazine redox cycling is a general mechanism for maintaining redox homeostasis, we predicted that phenazine redox cycling should support redox homeostasis and ATP synthesis during pyruvate fermentation.

To test this prediction, we measured the anaerobic survival of the Δ*phz1/2* Δ*ldhA* strain using pyruvate as the sole carbon and energy source. As expected, this strain was unable to survive by fermenting pyruvate (Figure 3a). Consistent with our prediction, however, the addition of PCA and an extracellular oxidizing potential improved the survival of the Δ*phz1/2* Δ*ldhA* strain during pyruvate fermentation (Figure 3a).

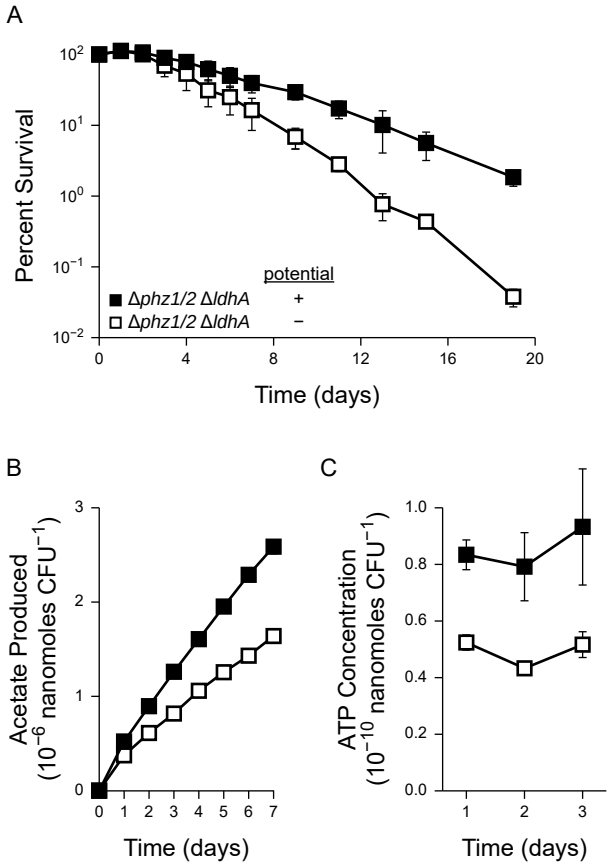

Figure 3. Pyruvate fermentation in the PA14 Δ*phz1/2* Δ*ldhA* strain with 40 mM pyruvate. Cultures were incubated without phenazines or an oxidizing potential (open squares) or with 75 μM PCA and an oxidizing potential (closed squares). Error bars indicate the standard error of three independent experiments. (A) Survival of the Δ*phz1/2* Δ*ldhA* strain during pyruvate fermentation. 100% survival represents approximately 1.4 × 10^9 CFU/mL. (B) Acetate produced during pyruvate fermentation in the Δ*phz1/2* Δ*ldhA* strain. The amount of acetate produced in each experiment was normalized to the CFU measurement at day 0. Error bars are present but smaller than the data points. (C) ATP concentrations during pyruvate fermentation in the Δ*phz1/2* Δ*ldhA* strain.

In our model of survival, redox homeostasis allows for additional acetate and ATP synthesis through the oxidative branch of the pyruvate fermentation pathway (Figure 1b). To further confirm this model, we used HPLC to measure acetate synthesis during pyruvate fermentation. The Δ*phz1/2* Δ*ldhA* strain produced more acetate when provided with phenazines and an extracellular oxidizing potential (Figure 3b). We observed a difference in acetate production

before the Δ*phz1/2* Δ*ldhA* cultures began to lose viability (on day 3), suggesting that the difference in acetate synthesis was not simply due to a difference in survival.

To confirm that phenazine redox cycling provides an energetic benefit to *P. aeruginosa,* we also measured the ATP concentrations of cultures with and without phenazine redox cycling. Consistent with a coupling between acetate and ATP synthesis, Δ*phz1/2* Δ*ldhA* cultures with oxidized phenazines maintained higher ATP concentrations than those without phenazines (Figure 3c). This difference was again observed before the cultures began to lose viability, suggesting that the difference in ATP concentration was not simply a consequence of cell death.

ATP synthesis is limited by redox homeostasis during pyruvate fermentation

Our model suggests that, by helping to maintain redox homeostasis, phenazines promote the conversion of pyruvate to acetate through the activity of acetate kinase. This model predicts that redox homeostasis is the limiting factor for ATP synthesis during pyruvate fermentation. From the stoichiometry of pyruvate fermentation, acetate and lactate synthesis are coupled through the common cofactor NAD(H) (Figure 1b). Sustained pyruvate oxidation to acetate, and thus ATP synthesis, requires the regeneration of NADH to NAD^+, which can be accomplished by the activity of lactate dehydrogenase. To determine whether this is indeed the case, we compared the concentration of relevant metabolites during pyruvate fermentation for wild type (WT) *P. aeruginosa* PA14 and different mutant strains.

To initiate pyruvate fermentation, we cultured PA14 using pyruvate as the sole carbon source aerobically, shifted the cells to an anoxic environment, and washed and resuspended the cells in fresh anoxic medium. As expected, anaerobic WT cultures with pyruvate survived for at least seven days, while cultures without pyruvate quickly declined in viability (Figure 4a). In contrast to previous studies with PAO1 (28,29), which demonstrated nearly complete survival, in our study we observed only 50% survival after 7 days of anaerobic incubation with pyruvate.

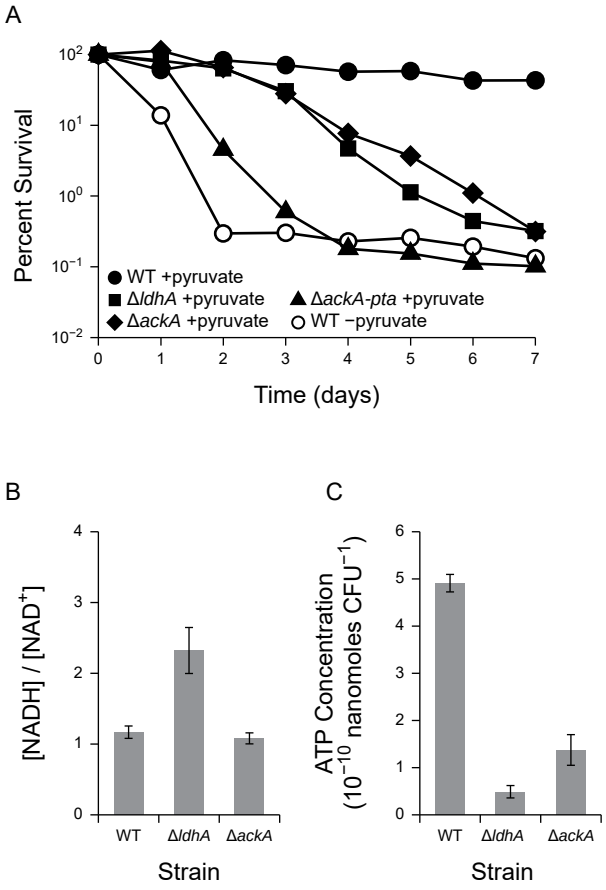

Figure 4. Survival with pyruvate fermentation in *P. aeruginosa*. Where shown, error bars indicate the standard error of three independent experiments. (A) Anaerobic survival for wild type PA14 (WT), PA14 Δ*ldhA* (Δ*ldhA*), PA14 Δ*ackA* (Δ*ackA*), and PA14 Δ*ackA-pta* (Δ*ackA-pta*) in the presence of 40 mM pyruvate (+pyruvate, closed points). WT PA14 without pyruvate is shown for comparison (–pyruvate, open points). 100% survival represents approximately 4×10^8 CFU/mL. Results are typical of least three independent experiments. (B) The [NADH]/[NAD^+] ratio after 24 hours of pyruvate fermentation in PA14 WT, Δ*ldhA*, and Δ*ackA*. (C) ATP concentrations from the same experiments shown in panel B.

As expected, mutants deficient in the conversion of pyruvate to acetate, Δ*ackA* and Δ*ackA-pta*, displayed a survival defect during pyruvate fermentation (Figure 4a). A mutant deficient in the conversion of pyruvate to lactate, Δ*ldhA*, had a survival defect similar to that of the Δ*ackA* mutant (Figure 4a). To our surprise, a mutant unable to convert acetyl-CoA to acetyl-phosphate, Δ*ackA-pta*, was more defective in survival than the Δ*ackA* mutant (Figure 4a). The survival difference

between the Δ*ackA* and Δ*ackA-pta* mutants might result from a difference in intracellular acetyl-phosphate concentrations, as acetyl-phosphate can serve as a phosphate donor in signaling pathways (30). Alternatively, the Δ*ackA-pta* mutant might accumulate acetyl-CoA, starving other essential pathways that require coenzyme A. Similar results have been observed in *E. coli*, where the expression of a pathway to consume acetyl-CoA enhances the survival of a Δ*pta* mutant in stationary phase (31).

We used ion chromatography to confirm the biosynthesis of acetate, lactate, and succinate from pyruvate as previously reported (28) (Supplemental Figure 3). As expected, both the Δ*ackA-pta* and Δ*ldhA* mutants produced significantly less acetate than the WT strain (Supplemental Figure 3), suggesting that the Δ*ldhA* mutant is limited in its ability to generate acetate and ATP using acetate kinase.

To confirm that the Δ*ldhA* strain is impaired in redox homeostasis and ATP synthesis, we measured the NAD^+, NADH, and ATP concentrations in cultures fermenting pyruvate. After 24 hours of anaerobic incubation with pyruvate as the sole carbon and energy source, both the WT strain and Δ*ackA* mutant maintained an $[NADH]/[NAD^+]$ ratio of approximately 1 (Figure 4b). In contrast, the Δ*ldhA* mutant contained a more reduced intracellular environment with an $[NADH]/[NAD^+]$ ratio of approximately 2 (Figure 4b). The Δ*ldhA* mutant also contained significantly less total NAD(H) than the WT strain and Δ*ackA* mutant (Supplemental Figure 4). In support of our model, both the Δ*ldhA* and Δ*ackA* mutants contained significantly less ATP than the WT strain (Figure 4c).

The reduced acetate synthesis and depleted ATP concentration in the Δ*ldhA* mutant suggest that the Δ*ldhA* mutant is unable to synthesize ATP through acetate kinase. The elevated $[NADH]/[NAD^+]$ ratio suggests that acetate and ATP synthesis are limited by redox

homeostasis, corroborating the fact that phenazine redox cycling improves survival in the Δ*phz1/2* Δ*ldhA* mutant during pyruvate fermentation (Figure 3a).

Arginine supports anaerobic ATP synthesis and survival independently of redox state

The survival defects of the Δ*ackA* and Δ*ldhA* mutants during pyruvate fermentation suggest that ATP synthesis is an essential component of survival in *P. aeruginosa*. To test this hypothesis using an independent anaerobic metabolism that produces ATP, we investigated survival using arginine as the sole carbon and energy source. Arginine is used as an ATP source during anaerobic growth through the arginine deiminase pathway (32) (Figure 1c). Previous work has shown that mutants in the arginine deiminase pathway have reduced anaerobic survival in undefined complex media (29), but to our knowledge there have been no reports of arginine alone serving as a sufficient energy source for survival.

To determine whether arginine is sufficient for anaerobic survival, we cultured *P. aeruginosa* PA14 aerobically using arginine as the sole carbon source, shifted the cells to an anoxic environment, and washed and resuspended the cells in fresh anoxic medium with arginine. As with pyruvate, arginine alone was sufficient as an energy source to promote anaerobic survival (Figure 5a). WT PA14 dropped to 30% viability after one day of anaerobic incubation and slowly decreased in viability to 15% after seven days. In contrast, cells incubated without arginine declined to 0.1% viability after seven days (Figure 5a). A transposon insertion mutant in the arginine deiminase pathway, *arcC*::MAR2xT7 (33), rapidly declined in viability to 0.02% after seven days despite the presence of arginine (Figure 5a). Similar results were obtained with a second independent transposon insertion mutant, *arcA*::MAR2xT7, disrupting another gene in the same pathway (Figure 1c) (data not shown). This demonstrates that arginine is sufficient to promote anaerobic survival through the arginine deiminase pathway.

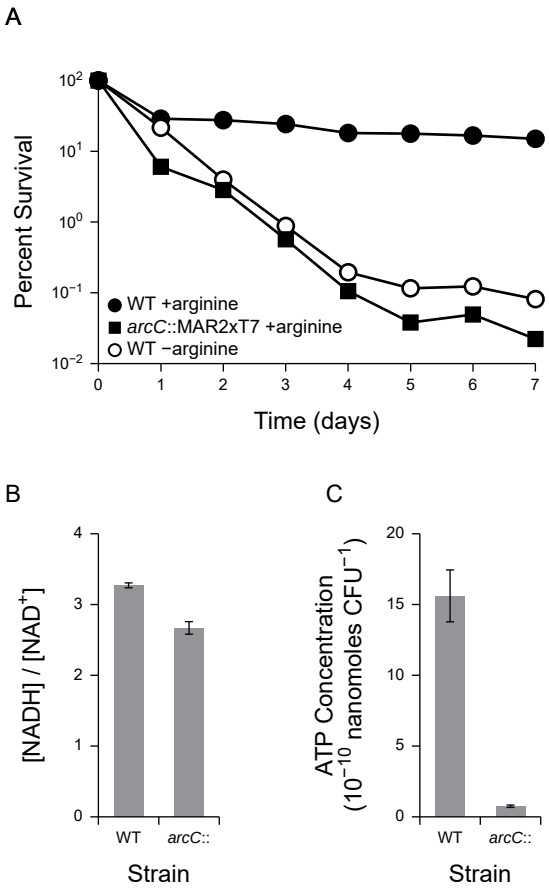

Figure 5. Survival with the arginine deiminase pathway in *P. aeruginosa*. Where shown, error bars indicate the standard error of three independent experiments (A) Anaerobic survival for wild type PA14 (WT) and PA14 *arcC*::MAR2xT7 (*arc*::) in the presence of 40 mM arginine. WT PA14 without arginine is shown for comparison (−arginine, open points). 100% survival represents approximately 4×10^8 CFU/mL. Results are typical of at least three independent experiments. (B) The [NADH]/[NAD$^+$] ratio after 24 hours of anaerobic incubation with arginine in PA14 WT and *arcC*::MAR2xT7. (C) ATP concentrations from the same experiments shown in panel B.

To confirm that disrupting the arginine deiminase pathway also disrupted ATP synthesis, we measured NAD$^+$, NADH, and ATP concentrations in cultures incubated with arginine. After 4 hours of anaerobic incubation with arginine as the sole carbon and energy source, both the WT strain and *arcC*::MAR2xT7 mutant maintained similarly high [NADH]/[NAD$^+$] ratios of approximately 3 (Figure 5b). However, the *arcC*::MAR2xT7 mutant contained significantly less

ATP than the WT strain (Figure 5c), consistent with the disruption of the ATP-generating step in the arginine deiminase pathway. The ability of the WT strain to anaerobically generate ATP from arginine, despite an elevated [NADH]/[NAD^+] ratio, is consistent with the fact that the arginine deiminase pathway does not involve redox reactions (Figure 1c).

Together, these measurements are consistent with the hypothesis that ATP synthesis, rather than the [NADH]/[NAD+] ratio itself, is essential for long-term anaerobic survival in *P. aeruginosa*. Although redox homeostasis is essential when it is coupled to ATP synthesis, as in glycolysis and pyruvate fermentation, survival correlates most directly with ATP synthesis itself.

ATP synthesis is required to maintain the proton-motive force using the F_1F_O-ATPase complex during fermentation

The requirement for ATP suggests that *P. aeruginosa* consumes ATP during long-term survival. During fermentation in many bacteria, the F_1F_O-ATPase complex, also known as ATP synthase, hydrolyses ATP to extrude protons from the cytoplasm to the periplasm, thereby generating a proton-motive force (PMF) (34). Previous studies have highlighted numerous reasons why a PMF might be required for survival; for example, the PMF is required for the exchange of metabolites and other ions (34), the localization of cell division and cytoskeletal proteins (35), protonation of the peptidoglycan layer (36), and the regulation of autolysis (37). We therefore hypothesized that *P. aeruginosa* requires ATP to maintain its PMF during fermentation.

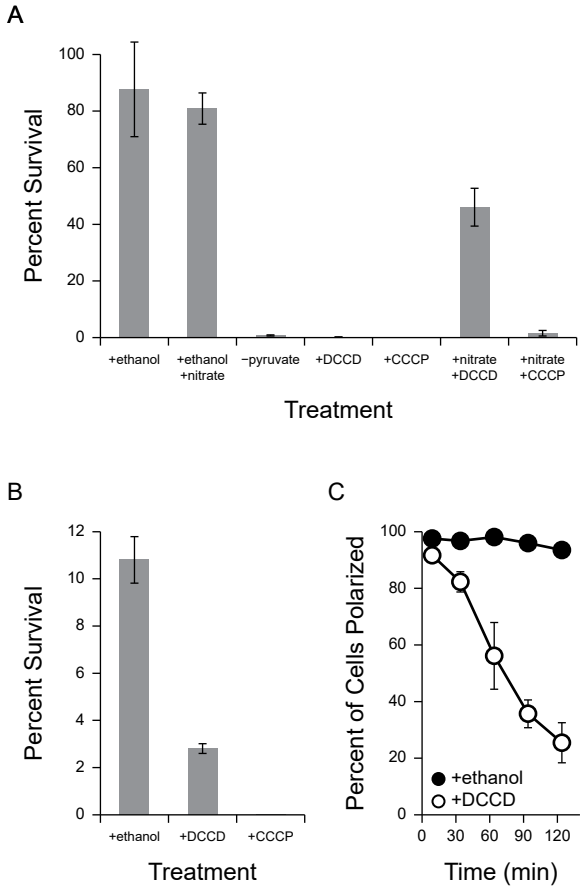

Figure 6. Response of *P. aeruginosa* PA14 to drugs that disrupt the proton-motive force. Error bars represent the standard error of at least three independent experiments. 100% survival represents approximately 4×10^8 CFU/mL. (A) Anaerobic survival of *P. aeruginosa* PA14 after two days of anaerobic incubation with 40 mM pyruvate. At the start of anaerobiosis, potassium nitrate (50 mM), DCCD (2 mM), and/or CCCP (100 μM) were added as indicated. DCCD and CCCP were dissolved in ethanol, and so as a control ethanol was added to a final concentration of 0.2% where indicated. A culture incubated without pyruvate is shown for comparison (−pyruvate). (B) Anaerobic survival after two days of anaerobic incubation with 40 mM arginine. At the start of anaerobiosis, ethanol (0.2%), DCCD (2 mM), or CCCP (100 μM) were added as indicated. (C) Effect of DCCD on membrane polarization. After 24 hours of anaerobiosis, 2 mM DCCD was added to cultures surviving anaerobically on 40 mM pyruvate (+DCCD, open circles). Since DCCD was dissolved in ethanol, an equivalent concentration of ethanol (0.2%) was added to control cultures (+ethanol, closed circles). Membrane polarization was monitored over time as described in Methods (for an example analysis, see Supplemental Figure 5). Time 0 indicates the addition of DCCD and ethanol to the cultures.

To test this hypothesis, we incubated pyruvate-fermenting cells anaerobically with *N,N'*-dicyclohexylcarbodiimide (DCCD), an inhibitor of the proton-translocation channel in the F_O subunit of ATP synthase (38). DCCD (dissolved in ethanol) was efficient at killing anaerobic *P. aeruginosa*, reducing viability to 0.16% ± 0.07% after two days (Figure 6a). Ethanol from the addition of DCCD did not significantly affect survival, as a control culture with 0.2% ethanol maintained 88 ± 17% viability (Figure 6a). This suggests that the activity of ATP synthase is required for survival during pyruvate fermentation in *P. aeruginosa*.

To confirm that the PMF is required for survival, we incubated cells with carbonyl cyanide 3-chlorophenylhydrazone (CCCP), an ionophore that equilibrates the proton concentration across cell membranes and dissipates the PMF (39). CCCP (dissolved in ethanol) reduced the viability of anaerobic cultures to below 0.01% after two days (Figure 6a), confirming that the PMF is required for survival.

If the PMF is required for survival, then restoring the PMF should recover survival even in the presence of DCCD. Although DCCD will inhibit oxidative phosphorylation, the cells can still synthesize ATP through pyruvate fermentation. To recover the PMF after DCCD treatment, we incubated cells anaerobically with nitrate, which serves as an alternate terminal electron acceptor for the electron transport chain in *P. aeruginosa* (40,41). Cultures incubated with pyruvate, DCCD, and nitrate sustained 46% ± 7% viability after two days (Figure 6a), demonstrating that respiration mitigates the killing effects of DCCD. Nitrate also improved the survival of cultures that were depolarized with CCCP to 2% ± 1% (Figure 6a). We did not observe significant growth after two days in cultures incubated with pyruvate, 0.2% ethanol, and nitrate, although we did observe growth after three days (data not shown), suggesting a long lag phase for growth by anaerobic nitrate respiration.

Because both pyruvate fermentation and the arginine deiminase pathway support anaerobic ATP synthesis, we also tested the effects of DCCD and CCCP on cultures surviving anaerobically with arginine. Cultures treated with 0.2% ethanol maintained 11% ± 1% viability after two days (Figure 6b), consistent with the incomplete long-term survival we observed with arginine (Figure 5a). As with survival on pyruvate, DCCD inhibited the survival of cultures incubated with arginine, reducing viability to 2.8% ± 0.2% (Figure 6b), and 100 μM CCCP reduced viability to below 0.001% (Figure 6b). This suggests that maintenance of the PMF by the F_1F_O-ATPase complex is a general survival strategy used by *P. aeruginosa* during fermentation.

To validate that DCCD caused death by preventing the generation of a PMF, rather than by some non-specific mechanism, we used flow cytometry with the dye $DiOC_2(3)$ to assess the membrane potential of DCCD-treated cultures. $DiOC_2(3)$ is a green-excitable dye that accumulates intracellularly in polarized cells, where it undergoes a red fluorescence shift that is indicative of a membrane potential (42). Since this assay is not quantitative in Gram-negative bacteria (43), we assessed the membrane potential qualitatively by comparing DCCD-treated samples to controls depolarized with CCCP (for an example analysis, see Supplemental Figure 5). As expected, pyruvate-fermenting cells maintained a detectable membrane potential. We observed a time-dependent depolarization of the cells after treatment with DCCD (Figure 6c), while an ethanol-treated control remained almost fully polarized (Figure 6c), demonstrating that DCCD prevents maintenance of the PMF and induces depolarization of the cell membrane.

These results indicate that *P. aeruginosa* uses the ATP generated during fermentation to maintain a PMF using the F_1F_O-ATPase complex, and that the PMF is required for long-term anaerobic survival. To integrate our findings, we measured the membrane potential of cells surviving anaerobically on glucose in our phenazine redox cycling experiment. After three days of survival, 38% ± 6% of cells maintained a detectable membrane polarization in the presence of oxidized

phenazines, while less than 1% of cells maintained a detectable membrane potential in the absence of phenazines. Together, our results suggest that the ATP generated during phenazine redox cycling is used to maintain the PMF.

Discussion

In this study, we sought an explanation for how phenazines promote anaerobic survival in *P. aeruginosa* be it in planktonic (17) or biofilm (15) cultures. We found that phenazines help *P. aeruginosa* convert glucose and pyruvate into acetate (Figure 2b, 3b). This was an interesting result because *P. aeruginosa* is not known to ferment glucose or other sugars (28,44). Previous studies have shown that small molecule electron carriers can couple fermentation to extracellular oxidants, leading to the synthesis of more oxidized fermentation products (45-48). Our results suggest that phenazines perform a similar role, enabling *P. aeruginosa* to generate ATP by oxidizing glucose into acetate. This anaerobic glycolysis promotes survival but not growth (Figure 2a), underscoring the importance of studying survival phenotypes independently from growth phenotypes.

In Figure 7, we integrate the known survival pathways and processes in *P. aeruginosa* with a focus on redox homeostasis and ATP synthesis. By comparing phenazine redox cycling, pyruvate fermentation, and the arginine deiminase pathway, our combined results suggest that ATP synthesis is a key feature of long-term survival. The ATP synthesized during fermentation and phenazine redox cycling is required, in part, to maintain the PMF using the ATP synthase complex.

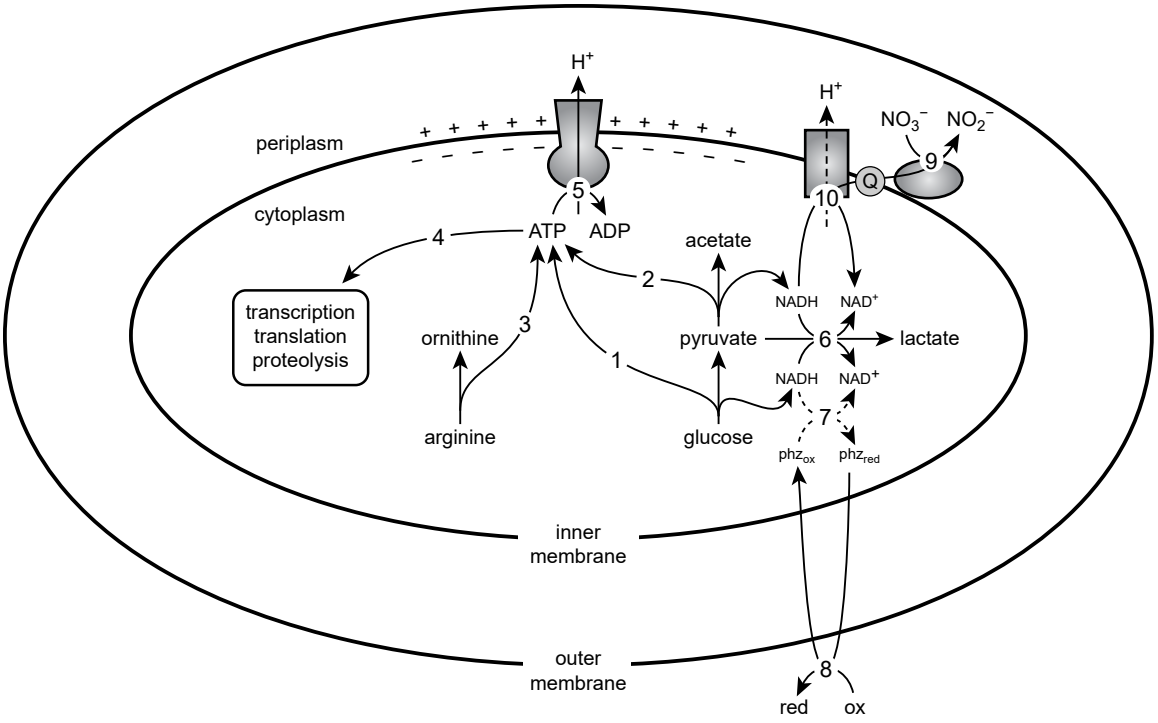

Figure 7. A metabolic model of survival in *P. aeruginosa*. The ATP synthesized from glycolysis [1], pyruvate fermentation [2], and the arginine deiminase pathway [3] is used for essential processes including transcription, translation, and proteolysis [4]. The F_1F_O-ATPase complex hydrolyses ATP to translocate protons across the inner membrane [5], thereby generating a proton-motive force. Excess reducing equivalents from pyruvate oxidation can be dispensed by converting pyruvate to lactate [6]. Phenazines can also regenerate oxidants for metabolism [7]; although NAD(P)H is a possible electron donor for phenazines *in vivo* (Price-Whelan *et al.*, 2007), the dashed lines indicate that the nature of this interaction has not been elucidated. Phenazines are then oxidized extracellularly [8] and can be reused. Nitrate reductase can reduce nitrate to nitrite using electrons from the quinone pool [9], permitting oxidation of NADH via NADH dehydrogenase [10], which can result in proton translocation depending on which dehydrogenase complex is used.

During pyruvate fermentation, pyruvate dehydrogenase converts NAD^+ to NADH in a pathway that allows acetate kinase to synthesize ATP (Figure 1b). NAD^+ is regenerated by reducing pyruvate to lactate or succinate (Figure 1b). *P. aeruginosa* produces significantly more lactate than succinate during pyruvate fermentation (Supplemental Figure 3) (28), and so lactate synthesis by lactate dehydrogenase appears to be the primary pathway for NAD^+ regeneration. This effectively couples the activities of acetate kinase and lactate dehydrogenase through the NAD(H) pool. As

a result, the Δ*ldhA* mutant has an elevated [NADH]/[NAD^+] ratio during pyruvate fermentation (Figure 4b) and is also unable to maintain ATP levels as high as the WT strain (Figure 4c). Phenazine redox cycling can serve as an alternate pathway for redox homeostasis in the Δ*ldhA* mutant and restore ATP synthesis (Figure 3c) and survival (Figure 3a).

In contrast to pyruvate fermentation, ATP synthesis by the arginine deiminase pathway does not involve redox reactions (Figure 1c). During anaerobic incubation with arginine, both the WT strain and the *arcC*::MAR2xT7 mutant developed an [NADH]/[NAD^+] ratio even higher than the Δ*ldhA* mutant did during pyruvate fermentation (Figure 5b). Nonetheless, the WT strain maintained ATP levels considerably higher than the *arcC*::MAR2xT7 mutant (Figure 5c), demonstrating that the arginine deiminase pathway can proceed even with large intracellular redox imbalances. Despite maintaining a high [NADH]/[NAD^+] ratio, cultures incubated with arginine were able to survive through the arginine deiminase pathway (Figure 5a). Pyruvate and arginine may therefore offer alternative sources of ATP during long-term anaerobic survival.

The requirement for ATP suggests that *P. aeruginosa* is not dormant during long-term survival. The ATP synthase inhibitor DCCD killed anaerobic PA14 cultures that were fermenting pyruvate or arginine (Figure 6a,b) and also depolarized cultures that were fermenting pyruvate (Figure 6c), demonstrating that *P. aeruginosa* actively maintains its PMF using the ATP synthase complex during fermentation. Previous studies have shown that survival also requires transcription (49), translation (50), and proteolysis (51), all of which consume ATP. By promoting ATP synthesis, phenazine redox cycling can therefore facilitate a variety of cellular processes that are required for long-term survival.

We do not yet know how native phenazines such as PCA are reduced *in vivo*. Phenazines oxidize NAD(P)H *in vitro* (52), and so PCA might directly oxidize NAD(P)H within the cell. Redox cycling compounds such as phenazines are oxidants of flavins and iron-sulfur clusters (53), and so

metabolic enzymes such as NADH dehydrogenase, pyruvate dehydrogenase, or pyruvate oxidase might also reduce phenazines. Synthetic electron shuttles such as anthraquinone-2,6-disulfonate and paraquat do not support anaerobic survival by redox cycling because they are reduced slowly by *P. aeruginosa* (17), suggesting that cells specifically reduce native phenazines. Our preliminary studies indicate PCA reduction is enzymatically catalyzed, and we are attempting to identify the proteins responsible for this activity.

Consistent with our finding that phenazines can alter metabolism, WT *P. aeruginosa* cultures grown aerobically with glucose secrete pyruvate in the oxygen-limited late stationary phase of growth, while phenazine-null mutant cultures do not (18). It was suggested that superoxide or pyocyanin radicals may inhibit pyruvate dehydrogenase, leading to pyruvate accumulation in the culture supernatant (18). Our results suggest an additional interpretation where glycolysis is limited by the availability of intracellular NAD^+. By promoting redox homeostasis, phenazines might accelerate the conversion of glucose to pyruvate faster than pyruvate can be consumed. After the consumption of glucose, the secreted pyruvate can be fermented or oxidized in the tricarboxylic acid cycle, depending on the metabolic needs of the cell.

Together, this work underscores the importance of environmental metabolites that are not always accounted for in metabolic pathways. Extracellular electron shuttles, such as phenazines, may permit cells to utilize unexpected energy sources by alleviating redox constraints on a pathway. An understanding of environmental parameters that interface with metabolism is therefore essential to assess the true metabolic potential of some organisms. Furthermore, a distinction must be drawn between growth and survival when considering the environment. Numerous studies have demonstrated the metabolic versatility of *P. aeruginosa* (for example, (54,55)), and here we have shown how several anaerobic pathways might enable survival under clinically relevant conditions. Characterizations of cystic fibrosis sputum indicate the presence of up to 100

μM phenazines (23) and significant quantities of nitrate, arginine, and glucose (56). Nitrate concentrations may be as high as 350 μM (57) and oxygen levels vary widely (21,58), potentially resulting in extended periods of slow growth or quiescence. Given the metabolic heterogeneity of biofilms (2) and the likely heterogeneity of infections, *P. aeruginosa* cells throughout infection environments might exhibit a range of growth rates, including survival without replication. As a result, understanding the multitude of survival mechanisms used by *P. aeruginosa* may be key to identifying new drug targets.

Acknowledgements

This work was supported by the Howard Hughes Medical Institute (HHMI). DKN is an HHMI Investigator, and NRG and SEK were both supported by NSF graduate research fellowships. This work was supported in part by the National Research Service Award (T32GM07676) from the National Institute of General Medical Sciences. We thank Nathan Dalleska and the Environmental Analysis Center (Caltech) for help with metabolite analyses, Ron Grimm for help with electrodes, and Ian Booth and members of the Newman lab for helpful discussions. The authors declare no conflicts of interest.

Materials and Methods

Bacterial strains and growth conditions

The strains and plasmids used in this study are shown in Supplemental Table 1. For routine growth, *P. aeruginosa* and *E. coli* were cultured at 37 °C in lysogeny broth (LB) containing 10 g/L tryptone, 5 g/L yeast extract, 10 g/L NaCl, and optionally 15 g/L agar for solid medium. *S. cerevisiae* was cultured at 30 °C in YPD medium containing 10 g/L yeast extract, 20 g/L peptone, 20 g/L D-glucose, and optionally 20 g/L agar for solid medium. Specific experimental growth conditions are described where appropriate. For aerobic growth, liquid cultures were shaken at 250 rpm.

Construction and verification of P. aeruginosa mutants

Unmarked deletions in *P. aeruginosa* PA14 were constructed using a modification of previously described methods (59). Briefly, PCR was used to amplify approximately 1-kilobase fragments flanking the target gene. Homologous recombination in yeast was used to assemble these fragments into the *sacB*-counterselectable suicide shuttle vector pMQ30. The knockout vector was transformed into *E. coli* DH5α, and triparental mating with DH5α and *E. coli* HB101/pRK2013 was used to conjugate the constructed knockout vector into PA14; merodiploids containing the chromosomally integrated vector were selected on cetrimide agar (HiMedia) containing 100 μg mL^{-1} gentamicin sulfate. Merodiploids were cultured overnight in nonselective LB, and resolved merodiploids were then selected on LB agar plates with 10% sucrose. Potential deletion mutants were screened using colony PCR with primers flanking the target gene, and clean deletions were confirmed by DNA sequencing of the PCR product (Retrogen). Transposon insertions were verified using colony PCR with primers flanking the annotated transposon position. Primer sequences for constructing and confirming the genetic mutants used in this study are listed in Supplemental Table 2.

Phenazine redox cycling survival

The assay for anaerobic survival enabled by phenazine redox cycling was performed as previously described (17). Briefly, strains of PA14 deleted in the core phenazine biosynthesis operons (Δ*phz1/2*) (12) were grown overnight in LB. The overnight cultures were used to inoculate 250 mL of LB in 1-L flasks to an OD_{500} of 0.05. At early stationary phase (OD_{500} of 2.8) the cells were pelleted, washed twice aerobically in MOPS-buffered medium (100 mM 3-(N-morpholino)propanesulfonic acid (MOPS), 3.5 μM $FeSO_4$, 43 mM NaCl, 3.7 mM KH_2PO_4, 9.3 mM NH_4Cl at pH 7.2), and resuspended to a concentrated OD_{500} of 70 before being transferred to a nitrogen-only atmosphere (MBraun Unilab glove box). There, 1 mL of concentrated cells was added to sealed glass vessels containing 100 mL of anoxic MOPS-buffered medium amended with

75 μM phenazine-1-carboxylic acid and 20 mM D-glucose or 40 mM sodium pyruvate. To oxidize PCA, a graphite rod (Alfa Aesar #14738) working electrode was poised at a potential of +207 mV vs. NHE against a homemade platinum mesh counter electrode, which was placed in buffer within an attached small chamber separated from the bulk solution by a glass frit. Electrochemical parameters were maintained by a potentiostat (Gamry). An Ag/AgCl electrode (BaSi #RE5B) was used as the reference electrode. Anaerobic cultures of cells were stirred vigorously and maintained at 31˚C for the duration of the experiment, with daily sampling for colony forming units. Phenazine turnover was confirmed by the accumulated charge over the duration of the experiment as previously described (17).

Pyruvate and arginine survival

For measuring anaerobic survival using pyruvate or arginine as a sole carbon source, cultures were grown overnight at 37 °C in a minimal medium containing 14.15 mM KH_2PO_4, 35.85 mM K_2HPO_4, 42.8 mM NaCl, 9.3 mM NH_4Cl, 1 mM $MgSO_4$, 7.2 μM $FeCl_2$ and trace elements (60), and 40 mM sodium pyruvate or 40 mM arginine (pH adjusted to 7.2 with NaOH or HCl). Overnight cultures were diluted at least 100-fold with fresh medium to an OD_{500} of 0.01 and incubated at 37 °C in shaking flasks to an OD_{500} of 0.4. After centrifuging the culture for 15 min at 5000×g, the supernatant was removed and the pellet was transferred to a glove chamber (Coy) containing an atmosphere of 15% CO_2, 80% N_2, and 5% H_2. The pellet was washed twice with fresh anoxic medium and then resuspended to a final OD_{500} of approximately 0.4 in rubber-stoppered tubes. The sealed tubes were incubated at 37 °C in the anaerobic chamber without shaking.

Viability counting

For measurements of colony forming units (CFU), 20 μL of each culture was sampled anaerobically and then serially diluted in aerobic phosphate-buffered saline. Relevant dilutions

were plated in drips of 10 μL on LB agar plates and incubated aerobically for 24 hours at 37 ˚C. The average of at least 4 pipetting replicates was taken as the CFU count for a given CFU measurement.

Measurement of NAD^+, NADH, and ATP

The method for measuring NAD^+ and NADH in this study was based on established protocols (18,61). For each condition, two 1-mL samples in 1.7 ml tubes were centrifuged for 1 min at maximum speed (16,000×g). The supernatant was removed and 200 μL of either 0.2 M HCl (for NAD^+ extraction) or 0.2 M NaOH (for NADH extraction) was added and mixed by vortexing. The samples were then incubated for 10 minutes at 55 °C, cooled on ice, and partially neutralized drop-wise with 200 μL of 0.1 M NaOH (for NAD^+) or 0.1 M HCl (for NADH). Cell debris was pelleted by centrifugation (5 minutes at maximum speed) and 150 μL of the supernatant was transferred to a fresh tube for immediate analysis. To assay the amount of NAD^+ or NADH in each sample, 5 μL of sample was added to 90 μL of the reagent mix in a 96-well microtiter plate. The reagent mix contained 2x bicine buffer (1.0 M, pH 8.0), 1x water, 1x 40 mM EDTA, 1x 100% ethanol, 1x 4.2 mM thiazolyl blue, and 2x 16.6mM phenazine ethosulfate. The 96-well plate was then heated to 30 °C. To initiate the colorimetric assay, 5 μL of a 1 mg mL^{-1} solution of alcohol dehydrogenase II (Sigma A3263) in 0.1 M bicine pH 8.0 was added to each well. A BioTek Synergy 4 plate reader was used to incubate the plate at 30 °C and record the absorbance of reduced thiazolyl blue at 570 nm every minute for 30 minutes. The rate of increase in absorbance at 570 nm over time was used as the measure of NAD(H) concentration. Unknown concentrations of NAD^+ and NADH were determined from the slope and intercept of a standard curve derived from known concentrations of NADH.

For ATP measurement, 20 μL of culture was added to 180 μL of dimethyl sulfoxide (DMSO) to quench and dissolve the cells. The sample was then diluted with 800 μL of 0.1 M HEPES (pH 7.5)

and stored at −80 °C for up to 7 days. ATP was quantified by mixing 25 µL of sample with 25 µL of Promega BacTiter-Glo reagent in a 96-well opaque white microtiter plate. The BacTiter-Glo reagent uses luciferase to produce luminescence in an ATP-dependent manner. Total luminescence was measured at 30 °C in a BioTek Synergy 4 plate reader. In control experiments using pure ATP, DMSO had no effect on luminescence at a final concentration of 9% (data not shown). Unknown concentrations of ATP were determined from the slope and intercept of a standard curve derived from known concentrations of ATP.

Assessment of membrane potential

The membrane potential was measured qualitatively using the dyes 3,3′-diethyloxacarbocyanine iodide ($DiOC_2(3)$) and TO-PRO-3. Cultures were diluted at least 100-fold into a permeabilization buffer containing 100 mM Tris, 1 mM EDTA, and 80 mM NaCl (pH adjusted to 7.4 using HCl). $DiOC_2(3)$ and TO-PRO-3 (both dissolved in DMSO) were then added to a final concentration of 30 µM and 100 nM, respectively. For depolarized controls, CCCP (dissolved in DMSO) was added to a final concentration of 15 µM. The final DMSO concentration did not exceed 2%. The samples were incubated for 2-5 minutes at room temperature and then analyzed on an Accuri C6 flow cytometer. $DiOC_2(3)$ fluorescence was measured using excitation at 488 nm and emission at 530 ± 15 nm (FL1) and 610 ± 10 nm (FL3). TO-PRO-3 fluorescence was measured using excitation at 640 nm and emission at 675 ± 12.5 nm (FL4). Intact cells were gated on a log-scale scatter plot of FL4 vs. FL2 (585 ± 20 nm) for further analysis. Cells with a membrane potential were distinguished by an increased red/green (FL3/FL1) fluorescence ratio relative to depolarized controls. For an example analysis, see Supplemental Figure 5.

High performance liquid chromatography

Metabolite samples were collected by centrifuging 550 μL of culture and passing the supernatant through a 0.2 μm nylon centrifugal filter. Samples were stored at −80 °C until analysis. Pyruvate, acetate, and succinate were quantified using an Agilent 1100 Series HPLC. A G1312A binary pump was used to a draw a continuous flow of 8 mN H_2SO_4 at 0.6 mL/min through a G1322A degasser. Samples were injected using a G1313A autosampler, and separation was effected using an Aminex HPX-87H column (Bio-Rad). Each sample was analyzed using a G1315A diode array detector to measure the UV absorbance at 206 nm referenced to 260 nm (bandwidth 16 nm) with a total run time of 25 min. Retention times for analytes were validated with single species standards. For each analyte, standards ranging from 0 to 40 mM were used to calibrate peak area against a known concentration. Data were analyzed using the ChemStation software (Agilent).

SUPPLEMENTAL MATERIAL

Methods

RNA isolation and qRT-PCR analysis

Gene transcription was analyzed as previously described (Kreamer, N.N.K., Wilks, J.C., Marlow, J.J., Coleman, M.L., and Newman, D.K. (2012) *J Bacteriol* **194**: 1195–1204). To stabilize mRNA prior to analysis, 1 mL of culture was mixed with 1 mL of RNAprotect (Qiagen) and the sample was stored at −80 °C until analysis. An RNeasy Mini Kit (Qiagen) was used to extract total RNA from the samples according to the manufacturer's protocol, including the optional DNase treatment step. cDNA was synthesized using the isolated RNA as a template for the iScript DNA Synthesis Kit (Bio-Rad) according to the manufacturer's protocol. The synthesized cDNA was used as a template for quantitative PCR (Real Time 7500 PCR machine, Applied Biosystems) using SYBR green with the ROX detection system (Bio-Rad). The primers used were: for *recA*, TCTACGGCAAGGGCATCTAC and TCCAGTACCGAACCGATTTC; for *clpX*,

CCTGTGCAATGACATCATCC and TTCTTGTCACGCTGGTTGAG; for *poxB*, GAACAATGCCTCGCTGAA and TGGCCGAACTCGATCTT; for *aceE*, GGCATGGAAGGCATGTT and GGAAGCCGAACATCGAATAG. C_t values for the PCR reactions were determined using the 7500 Fast System SDS Software.

Ion chromatography

To quantify pyruvate, lactate, acetate, and succinate, we used ion chromatography on a Dionex DX-500 ion chromatography system. A continuous flow of ultrapure water (18.2 megaohm, produced from a milliQ Gradient system, Millipore) at 1.00 mL/min was maintained with a Dionex GP40 pump, passed through an anion trap column to remove remaining anionic impurities, then through a potassium hydroxide eluent generator cartridge controlled by an EG40 module and subsequently through a six-port value configured for sample loop injection. A 10-microliter sample loop was loaded from a Dionex (Sunnyvale, CA) AS40 autosampler. Separation was effected on Dionex AG-19 (4x50 mm) and AS-19 (4x250mm) columns in series, the eluent was returned to neutral pH with a SRS-300 suppressor operating at 50 mA, and finally analytes were detected with a conductivity cell monitored by an ED-40 detector in conductivity mode. The suppressor was operated in eluent recycle mode. The hydroxide gradient began at 0.01 mM KOH 11 minutes before injection and was held at that concentration until injection. The concentration was increased linearly to 6.0 mM at 15 minutes, then to 15.0 mM at 25 minutes, and finally to 38 mM at 35 minutes where it was held for 3 minutes. Data were analyzed with Chromeleon 6.8 (Dionex).

Literature Cited

1. Alvarez-Ortega, C., and Harwood, C. S. (2007) Responses of *Pseudomonas aeruginosa* to low oxygen indicate that growth in the cystic fibrosis lung is by aerobic respiration. *Mol Microbiol* **65**, 153-165
2. Williamson, K. S., Richards, L. A., Perez-Osorio, A. C., Pitts, B., McInnerney, K., Stewart, P. S., and Franklin, M. J. (2012) Heterogeneity in *Pseudomonas aeruginosa* biofilms includes expression of ribosome hibernation factors in the antibiotic-tolerant

subpopulation and hypoxia-induced stress response in the metabolically active population. *J Bacteriol* **194**, 2062-2073

3. Nguyen, D., Joshi-Datar, A., Lepine, F., Bauerle, E., Olakanmi, O., Beer, K., McKay, G., Siehnel, R., Schafhauser, J., Wang, Y., Britigan, B. E., and Singh, P. K. (2011) Active starvation responses mediate antibiotic tolerance in biofilms and nutrient-limited bacteria. *Science* **334**, 982-986
4. Lewis, K. (2010) Persister cells. *Annu Rev Microbiol* **64**, 357-372
5. Keren, I., Shah, D., Spoering, A., Kaldalu, N., and Lewis, K. (2004) Specialized persister cells and the mechanism of multidrug tolerance in Escherichia coli. *J Bacteriol* **186**, 8172-8180
6. Allison, K. R., Brynildsen, M. P., and Collins, J. J. (2011) Metabolite-enabled eradication of bacterial persisters by aminoglycosides. *Nature* **473**, 216-220
7. Price-Whelan, A., Dietrich, L. E. P., and Newman, D. K. (2006) Rethinking 'secondary' metabolism: physiological roles for phenazine antibiotics. *Nature Chem Biol* **2**, 71-78
8. Mavrodi, D. V., Blankenfeldt, W., and Thomashow, L. S. (2006) Phenazine compounds in fluorescent Pseudomonas spp. biosynthesis and regulation. *Annu Rev Phytopathol* **44**, 417-445
9. Lau, G. W., Hassett, D. J., and Britigan, B. E. (2005) Modulation of lung epithelial functions by *Pseudomonas aeruginosa*. *Trends Microbiol* **13**, 389-397
10. Baron, S. S., and Rowe, J. J. (1981) Antibiotic action of pyocyanin. *Antimicrob Agents Chemother* **20**, 814-820
11. Britigan, B. E., Roeder, T. L., and Rasmussen, G. T. (1992) Interaction of the *Pseudomonas aeruginosa* secretory products pyocyanin and pyochelin generates hydroxyl radical and causes synergistic damage to endothelial cells. *J Clin Invest* **90**, 2187-2196
12. Dietrich, L. E. P., Price-Whelan, A., Petersen, A., Whiteley, M., and Newman, D. K. (2006) The phenazine pyocyanin is a terminal signalling factor in the quorum sensing network of *Pseudomonas aeruginosa*. *Mol Microbiol* **61**, 1308-1321
13. Möker, N., Dean, C. R., and Tao, J. (2010) *Pseudomonas aeruginosa* increases formation of multidrug-tolerant persister cells in response to quorum-sensing signaling molecules. *J Bacteriol* **192**, 1946-1955
14. Dietrich, L. E. P., Teal, T. K., Price-Whelan, A., and Newman, D. K. (2008) Redox-active antibiotics control gene expression and community behavior in divergent bacteria. *Science* **321**, 1203-1206
15. Dietrich, L. E. P., Okegbe, C., Price-Whelan, A., Sakhtah, H., Hunter, R. C., and Newman, D. K. (2013) Bacterial Community Morphogenesis Is Intimately Linked to the Intracellular Redox State. *J Bacteriol* **195**, 1371-1380
16. Wang, Y., Wilks, J. C., Danhorn, T., Ramos, I., Croal, L., and Newman, D. K. (2011) Phenazine-1-carboxylic acid promotes bacterial biofilm development via ferrous iron acquisition. *J Bacteriol* **193**, 3606-3617
17. Wang, Y., Kern, S. E., and Newman, D. K. (2010) Endogenous phenazine antibiotics promote anaerobic survival of *Pseudomonas aeruginosa* via extracellular electron transfer. *J Bacteriol* **192**, 365-369
18. Price-Whelan, A., Dietrich, L. E. P., and Newman, D. K. (2007) Pyocyanin alters redox homeostasis and carbon flux through central metabolic pathways in *Pseudomonas aeruginosa* PA14. *J Bacteriol* **189**, 6372-6381

19. Sullivan, N. L., Tzeranis, D. S., Wang, Y., So, P. T. C., and Newman, D. K. (2011) Quantifying the dynamics of bacterial secondary metabolites by spectral multiphoton microscopy. *ACS Chem Biol* **6**, 893-899
20. Singh, P. K., Schaefer, A. L., Parsek, M. R., Moninger, T. O., Welsh, M. J., and Greenberg, E. P. (2000) Quorum-sensing signals indicate that cystic fibrosis lungs are infected with bacterial biofilms. *Nature* **407**, 762-764
21. Worlitzsch, D., Tarran, R., Ulrich, M., Schwab, U., Cekici, A., Meyer, K. C., Birrer, P., Bellon, G., Berger, J., Weiss, T., Botzenhart, K., Yankaskas, J. R., Randell, S., Boucher, R. C., and Döring, G. (2002) Effects of reduced mucus oxygen concentration in airway *Pseudomonas* infections of cystic fibrosis patients. *J Clin Invest* **109**, 317-325
22. Wilson, R., Sykes, D. A., Watson, D., Rutman, A., Taylor, G. W., and Cole, P. J. (1988) Measurement of *Pseudomonas aeruginosa* phenazine pigments in sputum and assessment of their contribution to sputum sol toxicity for respiratory epithelium. *Infect Immun* **56**, 2515-2517
23. Hunter, R. C., Klepac-Ceraj, V., Lorenzi, M. M., Grotzinger, H., Martin, T. R., and Newman, D. K. (2012) Phenazine content in the cystic fibrosis respiratory tract negatively correlates with lung function and microbial complexity. *Am J Respir Cell Mol Biol* **47**, 738-745
24. Mavrodi, D. V., Bonsall, R. F., Delaney, S. M., Soule, M. J., Phillips, G., and Thomashow, L. S. (2001) Functional analysis of genes for biosynthesis of pyocyanin and phenazine-1-carboxamide from *Pseudomonas aeruginosa* PAO1. *J Bacteriol* **183**, 6454-6465
25. Mavrodi, D. V., Parejko, J. A., Mavrodi, O. V., Kwak, Y.-S., Weller, D. M., Blankenfeldt, W., and Thomashow, L. S. (2013) Recent insights into the diversity, frequency and ecological roles of phenazines in fluorescent *Pseudomonas* spp. *Environ Microbiol* **15**, 675-686
26. Wang, Y., and Newman, D. K. (2008) Redox Reactions of Phenazine Antibiotics with Ferric (Hydr)oxides and Molecular Oxygen. *Environ Sci Technol* **42**, 2380-2386
27. Chang, Y.-Y., and Cronan, J. E. (1983) Genetic and Biochemical Analyses of *Escherichia coli* Strains having a Mutation in the Structural Gene (*poxB*) for Pyruvate Oxidase. *J Bacteriol* **154**, 756-672
28. Eschbach, M., Schreiber, K., Trunk, K., Buer, J., Jahn, D., and Schobert, M. (2004) Long-term anaerobic survival of the opportunistic pathogen *Pseudomonas aeruginosa* via pyruvate fermentation. *J Bacteriol* **186**, 4596-4604
29. Schreiber, K., Boes, N., Eschbach, M., Jaensch, L., Wehland, J., Bjarnsholt, T., Givskov, M., Hentzer, M., and Schobert, M. (2006) Anaerobic survival of *Pseudomonas aeruginosa* by pyruvate fermentation requires an Usp-type stress protein. *J Bacteriol* **188**, 659-668
30. Klein, A. H., Shulla, A., Reimann, S. A., Keating, D. H., and Wolfe, A. J. (2007) The Intracellular Concentration of Acetyl Phosphate in *Escherichia coli* Is Sufficient for Direct Phosphorylation of Two-Component Response Regulators. *J Bacteriol* **189**, 5574-5581
31. Chang, D.-E., Shin, S., Rhee, J.-S., and Pan, J.-G. (1999) Acetate Metabolism in a *pta* Mutant of *Escherichia coli* W3110: Importance of Maintaining Acetyl Coenzyme A Flux for Growth and Survival. *J Bacteriol* **181**, 6656-6663
32. Vander Wauven, C., Piérard, A., Kley-Raymann, M., and Haas, D. (1984) *Pseudomonas aeruginosa* mutants affected in anaerobic growth on arginine: evidence for a four-gene cluster encoding the arginine deiminase pathway. *J Bacteriol* **160**, 928-934

33. Liberati, N. T., Urbach, J. M., Miyata, S., Lee, D. G., Drenkard, E., Wu, G., Villanueva, J., Wei, T., and Ausubel, F. M. (2006) An ordered, nonredundant library of *Pseudomonas aeruginosa* strain PA14 transposon insertion mutants. *Proc Natl Acad Sci USA* **103**, 2833-2838
34. Krulwich, T. A., Sachs, G., and Padan, E. (2011) Molecular aspects of bacterial pH sensing and homeostasis. *Nature Rev Microbiol* **9**, 330-343
35. Strahl, H., and Hamoen, L. W. (2010) Membrane potential is important for bacterial cell division. *Proc Nat Acad USA* **107**, 12281-12286
36. Calamita, H. G., Ehringer, W. D., Koch, A. L., and Doyle, R. J. (2001) Evidence that the cell wall of *Bacillus subtilis* is protonated during respiration. *Proc Nat Acad USA* **98**, 15260-15263
37. Jolliffe, L. K., Doyle, R. J., and Streips, U. N. (1981) The Energized Membrane and Cellular Autolysis in Bacillus subtilis. *Cell* **25**, 753-763
38. Sebald, W., Machleidt, W., and Wachter, E. (1980) *N,N'*-dicyclohexylcarbodiimide binds specifically to a single glutamyl residue of the proteolipid subunit of the mitochondrial adenosinetriphosphatases from *Neurospora crassa* and *Saccharomyces cerevisiae*. *Proc Natl Acad Sci USA* **77**, 785-789
39. Hopfer, U., Lehninger, A. L., and Thompson, T. E. (1968) Protonic conductance across phospholipid bilayer membranes induced by uncoupling agents for oxidative phosphorylation. *Proc Natl Acad Sci USA* **59**, 484-490
40. Carlson, C. A., and Ingraham, J. L. (1983) Comparison of denitrification by *Pseudomonas stutzeri*, *Pseudomonas aeruginosa*, and *Paracoccus denitrificans*. *Appl Environ Microbiol* **45**, 1247-1253
41. Van Alst, N. E., Sherrill, L. A., Iglewski, B. H., and Haidaris, C. G. (2009) Compensatory periplasmic nitrate reductase activity supports anaerobic growth of *Pseudomonas aeruginosa* PAO1 in the absence of membrane nitrate reductase. *Can J Microbiol* **55**, 1133-1144
42. Novo, D., Perlmutter, N. G., Hunt, R. H., and Shapiro, H. M. (1999) Accurate flow cytometric membrane potential measurement in bacteria using diethyloxacarbocyanine and a ratiometric technique. *Cytometry* **35**, 55-63
43. Shapiro, H. M., and Nebe-von-Caron, G. (2004) *Multiparameter flow cytometry of bacteria*,
44. Barnishan, J., and Ayers, L. W. (1979) Rapid identification of nonfermentative gram-negative rods by the Corning N/F system. *J Clin Microbiol* **9**, 239-243
45. Emde, R., Swain, A., and Schink, B. (1989) Anaerobic oxidation of glycerol by Escherichia coli in an amperometric poised-potential culture system. *Appl Microbiol Biot* **32**, 170-175
46. Emde, R., and Schink, B. (1990) Oxidation of glycerol, lactate, and propionate by Propionibacterium freudenreichii in a poised-potential amperometric culture system. *Arch Microbiol* **153**, 506-512
47. Benz, M., Schink, B., and Brune, A. (1998) Humic acid reduction by Propionibacterium freudenreichii and other fermenting bacteria. *Appl Environ Microbiol* **64**, 4507-4512
48. Beck, S., and Schink, B. (1995) Acetate oxidation through a modified citric acid cycle in Propionibacterium freundenreichii. *Arch Microbiol* **163**, 182-187

49. Hu, Y., and Coates, A. R. (1999) Transcription of the stationary-phase-associated hspX gene of Mycobacterium tuberculosis is inversely related to synthesis of the 16-kilodalton protein. *J Bacteriol* **181**, 1380-1387
50. Reeve, C. A., Amy, P. S., and Matin, A. (1984) Role of protein synthesis in the survival of carbon-starved *Escherichia coli* K-12. *J Bacteriol* **160**, 1041-1046
51. Weichart, D., Querfurth, N., Dreger, M., and Hengge-Aronis, R. (2003) Global role for ClpP-containing proteases in stationary-phase adaptation of *Escherichia coli*. *J Bacteriol* **185**, 115-125
52. Cox, C. D. (1986) Role of pyocyanin in the acquisition of iron from transferrin. *Infect Immun* **52**, 263-270
53. Gu, M., and Imlay, J. A. (2011) The SoxRS response of *Escherichia coli* is directly activated by redox-cycling drugs rather than by superoxide. *Molecular Microbiology* **79**, 1136-1150
54. Behrends, V., Ebbels, T. M. D., Williams, H. D., and Bundy, J. G. (2009) Time-resolved metabolic footprinting for nonlinear modeling of bacterial substrate utilization. *Appl Environ Microbiol* **75**, 2453-2463
55. Stover, C. K., Pham, X. Q., Erwin, A. L., Mizoguchi, S. D., Warrener, P., Hickey, M. J., Brinkman, F. S., Hufnagle, W. O., Kowalik, D. J., Lagrou, M., Garber, R. L., Goltry, L., Tolentino, E., Westbrock-Wadman, S., Yuan, Y., Brody, L. L., Coulter, S. N., Folger, K. R., Kas, A., Larbig, K., Lim, R., Smith, K., Spencer, D., Wong, G. K., Wu, Z., Paulsen, I. T., Reizer, J., Saier, M. H., Hancock, R. E., Lory, S., and Olson, M. V. (2000) Complete genome sequence of *Pseudomonas aeruginosa* PAO1, an opportunistic pathogen. *Nature* **406**, 959-964
56. Palmer, K. L., Aye, L. M., and Whiteley, M. (2007) Nutritional cues control *Pseudomonas aeruginosa* multicellular behavior in cystic fibrosis sputum. *J Bacteriol* **189**, 8079-8087
57. Palmer, K., Mashburn, L., and Singh, P. (2005) Cystic fibrosis sputum supports growth and cues key aspects of *Pseudomonas aeruginosa* physiology. *J Bacteriol* **187**, 5267-5277
58. Kolpen, M., Kühl, M., Bjarnsholt, T., Moser, C., Hansen, C. R., Liengaard, L., Kharazmi, A., Pressler, T., Høiby, N., and Jensen, P. Ø. (2014) Nitrous Oxide Production in Sputum from Cystic Fibrosis Patiens with Chronic *Pseudomonas aeruginosa* Lung Infection. *PLOS ONE* **9**, e84353
59. Shanks, R. M. Q., Caiazza, N. C., Hinsa, S. M., Toutain, C. M., and O'Toole, G. A. (2006) *Saccharomyces cerevisiae*-based molecular tool kit for manipulation of genes from gram-negative bacteria. *Appl Environ Microbiol* **72**, 5027-5036
60. Widdel, F., Kohring, G.-W., and Mayer, F. (1983) Studies on dissimilatory sulfate-reducing bacteria that decompose fatty acids. *Arch Microbiol* **134**, 286-294
61. San, K.-Y., Bennett, G. N., Berríos-Rivera, S. J., Vadali, R. V., Yang, Y.-T., Horton, E., Rudolph, F. B., Sariyar, B., and Blackwood, K. (2002) Metabolic engineering through cofactor manipulation and its effects on metabolic flux redistribution in *Escherichia coli*. *Metab Eng* **4**, 182-192

Chapter 4

BIOCHEMISTRY OF PHENAZINE REDUCTION

This chapter is adapted from:

Glasser, N. R., Wang, B. X., Hoy, J. A., and Newman, D. K. (2017) The pyruvate and α-ketoglutarate dehydrogenase complexes of *Pseudomonas aeruginosa* catalyze pyocyanin and phenazine-1-carboxylic acid reduction via the subunit dihydrolipoamide dehydrogenase. *Journal of Biological Chemistry* **292**, 5593-5607.

Abstract

Phenazines are a class of redox-active molecules produced by diverse bacteria and archaea. Many of the biological functions of phenazines, such as mediating signaling, iron acquisition, and redox homeostasis, derive from their redox activity. While prior studies have focused on extracellular phenazine oxidation by oxygen and iron, here we report a search for reductants and catalysts of intracellular phenazine reduction in *Pseudomonas aeruginosa*. Enzymatic assays in cell-free lysate, together with crude fractionation and chemical inhibition, indicate that *P. aeruginosa* contains multiple enzymes that catalyze the reduction of the endogenous phenazines pyocyanin and phenazine-1-carboxylic acid in both cytosolic and membrane fractions. We used chemical inhibitors to target general enzyme classes and found that an inhibitor of flavoproteins and heme-containing proteins, diphenyleneiodonium, effectively inhibited phenazine reduction *in vitro*, suggesting that most phenazine reduction derives from these enzymes. Using natively purified proteins, we demonstrate that the pyruvate and α-ketoglutarate dehydrogenase complexes directly catalyze phenazine reduction with pyruvate or α-ketoglutarate as electron donors. Both complexes transfer electrons to phenazines through the common subunit dihydrolipoamide dehydrogenase, a flavoprotein encoded by the gene *lpdG*. Although we were unable to co-

crystalize LpdG with an endogenous phenazine, we report its X-ray crystal structure in the apo form (refined to 1.35 Å), bound to NAD^+ (1.45 Å), and bound to NADH (1.79 Å). In contrast to the notion that phenazines support intracellular redox homeostasis by oxidizing NADH, our work suggests that phenazines may substitute for NAD^+ in LpdG and other enzymes, achieving the same end by a different mechanism.

Introduction

Over a century ago, *Pseudomonas aeruginosa* was identified as the source of a blue pigment observed in infected wounds (1). This pigment, a phenazine derivative known as pyocyanin (Figure 1), was the first natural organic molecule shown to undergo one-electron reduction (2-4). This distinctive property inspired early studies into bacterial respiration. As early as 1931, Friedheim and Michaelis demonstrated that pyocyanin stimulates oxygen consumption and carbon dioxide production in both *P. aeruginosa* (5) and human tissue (6), and so initially pyocyanin was considered an accessory respiratory pigment analogous to quinones (5). This interpretation predated an understanding of the electron transport chain, and today pyocyanin is understood to alter redox homeostasis more generally (7,8) though methanophenazine can substitute for quinones in the electron transport chains of certain methanogenic archaea (9). Later researchers recognized that reduced pyocyanin and other phenazines react with molecular oxygen to form toxic superoxide radicals (10). Phenazines also poison cells by oxidizing iron-sulfur clusters (11), short-circuiting electron transfer (12), covalently modifying proteins (13), and intercalating into DNA (14). This broad spectrum of toxicity became the focus of phenazine research for several decades, and so today phenazines are best known as antibiotics and virulence factors.

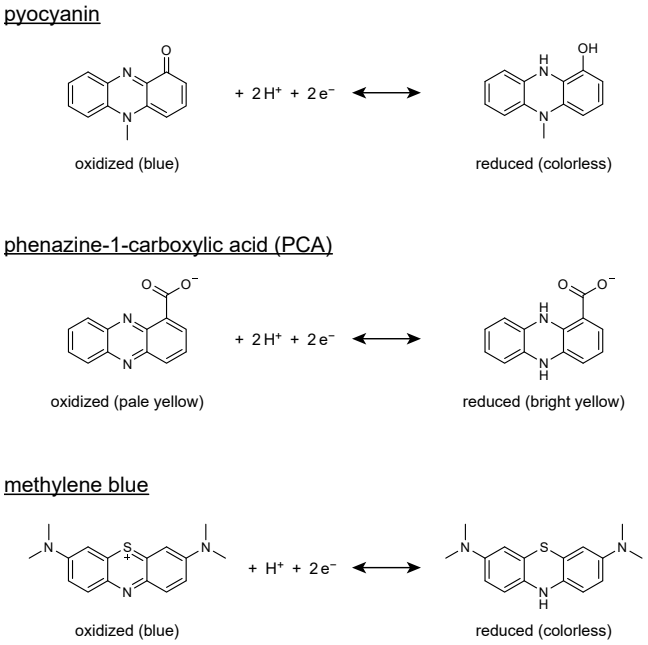

Figure 1. Chemical structures and redox chemistry of the redox-active substrates employed in this study.

Our interest in phenazines stems from the discovery that the *P. aeruginosa* phenazines can reduce extracellular minerals (15,16). Rather than merely inhibiting the growth of competing organisms, we hypothesized that phenazine "antibiotics" could directly benefit *P. aeruginosa* by promoting iron acquisition and redox homeostasis (17,18). This hypothesis has motivated several experiments that illustrate physiological functions for the endogenous phenazines of *P. aeruginosa*. We previously showed that phenazine redox cycling promotes anaerobic survival on glucose (19,20). Although *P. aeruginosa* does not ferment glucose, phenazines serve as an electron acceptor that enables glucose oxidation to acetate with concomitant ATP synthesis (20). We also showed that phenazines, by acting as electron shuttles, expand the habitable zone of colony biofilms into the anoxic portion (8). These findings paint a nuanced view where phenazines are multi-functional molecules, in some contexts possessing antibiotic activity and in others supporting redox homeostasis or iron acquisition.

In addition to pyocyanin, *P. aeruginosa* synthesizes at least six other phenazine derivatives. The precursor molecule, phenazine-1-carboxylic acid (PCA) (Figure 1), is synthesized from chorismic acid by enzymes encoded in the homologous *phzABCDEFG1* and *phzABCDEFG2* operons (21,22). Additional enzymes catalyze structural modifications of PCA to pyocyanin, phenazine-1-hydroxide, and phenazine-1-carboxamide (22). Other endogenous *P. aeruginosa* phenazines have been observed with amination (23) and sulfonation (24) modifications, although the pathways for these modifications are unknown. Beyond *P. aeruginosa*, over 180 naturally occurring phenazines have been described in the literature from a variety of bacteria and archaea (25). This diverse array of structurally similar molecules suggests particular phenazines might be tuned for certain functions or properties. In support of this interpretation, the endogenous *P. aeruginosa* phenazines have different pH-dependent solubilities, toxicities, and reactivities towards oxygen and iron (16,26).

Despite their structural diversity, the key biological functions of phenazines, be it promoting anaerobic energy generation or facilitating iron acquisition, derive from their redox activity. The environmentally relevant extracellular oxidants, molecular oxygen and ferric iron, are well characterized (16). In stark contrast, there is a dearth of information about biologically catalyzed phenazine reduction. While pyocyanin and PCA are known to oxidize the electron donors NAD(P)H, dihydrolipoamide, and glutathione *in vitro* (15,27), it is unknown whether this is relevant *in vivo* or whether it is enzymatically catalyzed. To address this unknown, previous work in our laboratory attempted to identify phenazine reductases by screening transposon mutants (28,29). Mutants in glycerol-3-phosphate dehydrogenase and the cytochrome bc_1 complex were found to be deficient in pyocyanin reduction (28), but these mutants are generally unhealthy and carry a number of pleiotropic effects (28), rendering it impossible to ascribe pyocyanin reduction to these proteins from the physiological data alone.

As an alternative to our prior genetic screens, in this study we used a biochemical approach to identify *P. aeruginosa* enzymes with endogenous phenazine reductase activity. Our results suggest that *P. aeruginosa* might not express an enzyme evolved to specifically reduce phenazines; rather, our findings implicate flavoproteins and/or heme-containing proteins as important non-specific catalysts for phenazine reduction. Illustrating this principle, we identified and characterized the pyruvate and α-ketoglutarate dehydrogenase complexes as models for flavoprotein-mediated phenazine reduction. Our data indicate that under energy-limited anoxic conditions, phenazine substitution for NAD^+ in these enzymes might contribute to the maintenance of intracellular redox homeostasis.

Results

Phenazine reduction is catalyzed by cell lysate

We first asked whether *P. aeruginosa* produces enzymes that catalyze phenazine reduction. We focused on phenazine-1-carboxylic acid (PCA) (Figure 1) because it is the precursor for all biological phenazines in *P. aeruginosa* (22) and it promotes anaerobic energy generation by redox cycling (19,20). It conveniently undergoes a color change to bright yellow after reduction (30), enabling a colorimetric detection of PCA reduction. To avoid re-oxidation by atmospheric oxygen, we monitored PCA reduction using a plate reader housed within an anaerobic chamber. Among the many possible intracellular electron carriers, we tested NADH, NADPH, and glutathione as electron donors that are important determinants of the intracellular redox state (7,31). Compared to pyocyanin, PCA reacts relatively slowly with these donors, minimizing the risk of misinterpreting non-enzymatic reduction for enzyme activity. Because phenazines alter the metabolic flux of *P. aeruginosa* (7,20), we reasoned that intermediates of central metabolism might also serve as electron donors, and so we also tested pyruvate, citrate, isocitrate, α-ketoglutarate, succinate, and malate. We prepared cell lysate from late-exponential phase cultures grown on succinate, a preferred carbon source of *P. aeruginosa* (32). Because phenazines induce a

transcriptional response in *P. aeruginosa* (33), and so may regulate the activity of their endogenous reductases, we harvested the cultures several hours after the onset of phenazine production as indicated by the blue color of pyocyanin.

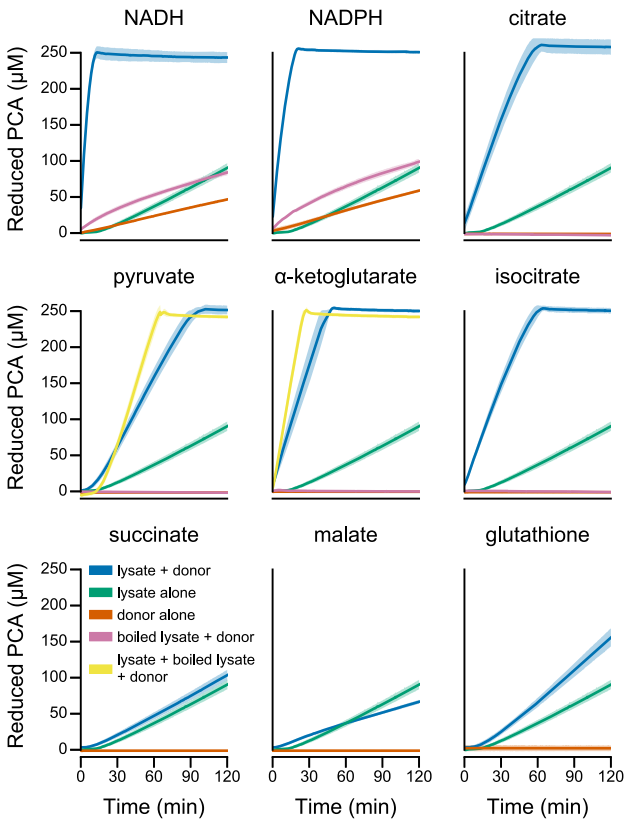

Figure 2. Catalytic reduction of PCA by P. aeruginosa cell-free lysate. Each panel illustrates a time course of PCA reduction using the indicated electron donor. The line and shaded region represent the mean and standard deviation, respectively, from three independent assays using lysate prepared from independent cultures. The final concentrations in the assay were 1 mM for NADH and NADPH, 5 mM for racemic DL-isocitrate (to give 2.5 mM D-isocitrate), and 2.5 mM for all other donors.

In the absence of cell lysate, PCA did not react with the organic acid metabolic intermediates and it reacted only slowly with NADH, NADPH, and glutathione (Figure 2). Similarly, in the absence of an exogenous electron donor, cell lysate slowly reduced PCA over time (Figure 2), likely

deriving some reducing equivalents from metabolites already present within the lysate. Relative to lysate or electron donor alone, lysate rapidly reduced PCA when supplemented with NADH, NADPH, citrate, isocitrate, pyruvate, or α-ketoglutarate (Figure 2). Glutathione slightly increased the rate of PCA reduction, whereas malate and succinate had no stimulatory effect when added to lysate (Figure 2). Boiling the cell lysate beforehand effectively eliminated PCA reduction even with the addition of exogenous electron donors (Figure 2), demonstrating that the lysate catalyzed reduction rather than indirectly accelerating reduction through a change in ionic strength or pH. Additionally, we found that adding boiled lysate to un-boiled lysate could further accelerate reduction with pyruvate and α-ketoglutarate (Figure 2), suggesting the presence of additional cofactors or substrates in cell lysate that are required for PCA reduction. Together, these results demonstrate that *P. aeruginosa* produces one or more enzymes with PCA reduction activity.

We attempted to purify an NADH:PCA or NADPH:PCA oxidoreductase from *P. aeruginosa* cell lysate using anion-exchange, cation-exchange, and hydrophobic interaction chromatography. Unfortunately, our efforts were hampered by the abiotic reaction between NAD(P)H and PCA, which is greatly accelerated at higher salt concentrations involved in protein chromatography. We struggled to locate chromatographic peaks of activity from the high background. To learn more about the types of proteins that might catalyze phenazine reduction, we opted to characterize the phenazine reduction activity in terms of cellular localization and sensitivity towards chemical inhibitors.

Multiple enzymes can catalyze phenazine reduction

We wondered whether the electron transport chain catalyzes phenazine reduction, because pyocyanin is reported to stimulate respiration (5,6) and phenazines induce morphological changes in colony biofilms that are consistent with increased respiration (8). To test if PCA

reduction activity derives mostly from the membrane-bound electron transport chain, we separated membrane-associated components from the lysate by ultracentrifugation (note that some soluble components, such as ribosomes, β-oxidation machinery, and 2-oxoacid dehydrogenases, can also be pelleted by ultracentrifugation). We saved the supernatant containing soluble proteins and resuspended the membrane pellet with a gentle non-ionic detergent. We then tested the three fractions—crude lysate, soluble proteins, and membrane-associated proteins—for PCA reduction in terms of absolute rate and specific activity.

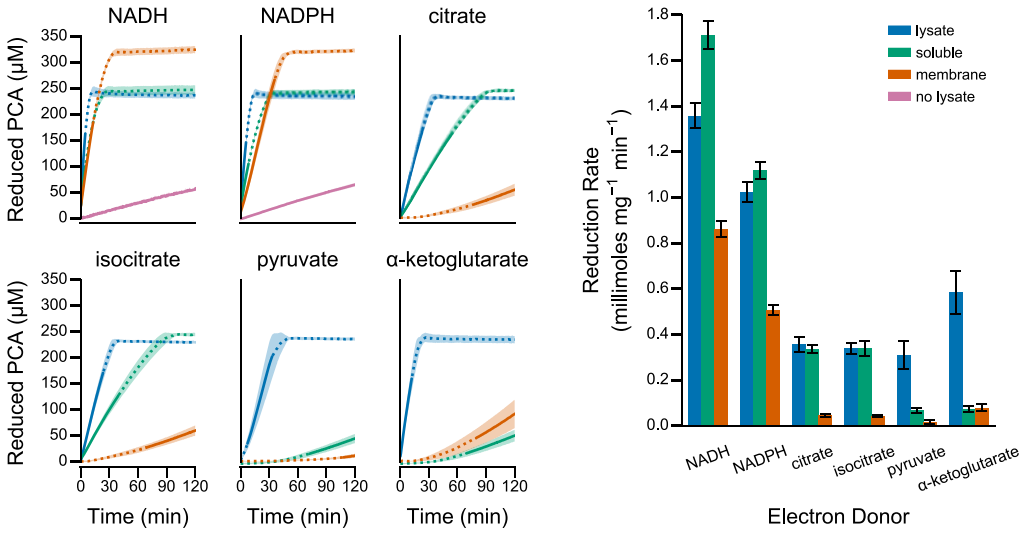

Figure 3. Fractionation of PCA reductase activity in cell-free lysate. Cell-free lysate was fractionated into soluble- and membrane-associated components by ultracentrifugation. The fractions were assayed for their ability to catalyze PCA reduction. (Left) Each panel illustrates a time course of PCA reduction using the indicated electron donor. The line and shaded region represent the mean and standard deviation, respectively, from four independent assays using lysate prepared from independent cultures. The solid portion of each line indicates the linear region used for quantification. (Right) The specific activity for each fraction was determined by normalizing the rate of PCA reduction, illustrated with a solid line in the left panels, by the protein concentration of each fraction. Error bars represent the standard deviation from four independent biological replicates.

Both the soluble and membrane fractions contained approximately equal activity, but specific activity (activity normalized by protein concentration) was 2-fold greater in the soluble fraction relative to the membrane fraction (Figure 3). In the membrane samples, the calculated final concentration of reduced PCA (300–350 μM) was greater than the amount initially added to the spectrophotometric assay (250 μM) (Figure 3). This artifact may be due to redox-active cytochromes absorbing at the same wavelength as PCA, or residual endogenous phenazines associated with the membrane, and so our data might overestimate the rate of PCA reduction in membrane fractions. Citrate and isocitrate stimulated PCA reduction primarily in the soluble fraction (Figure 3). Notably, for the 2-oxoacids pyruvate and α-ketoglutarate, ultracentrifugation significantly lowered PCA reduction activity but we did not recover this activity in the membrane fraction (Figure 3). Because many enzymes in central metabolism use NAD(P)H as an electron carrier, from these data we infer that the cell lysate contains at least two NAD(P)H:PCA oxidoreductases that are distributed between the soluble and membrane fractions, with more activity residing in the soluble fraction. This implies that the electron transport chain does not exclusively reduce PCA *in vitro*. Additional enzymes might also use citrate, isocitrate, pyruvate, or α-ketoglutarate as electron donors.

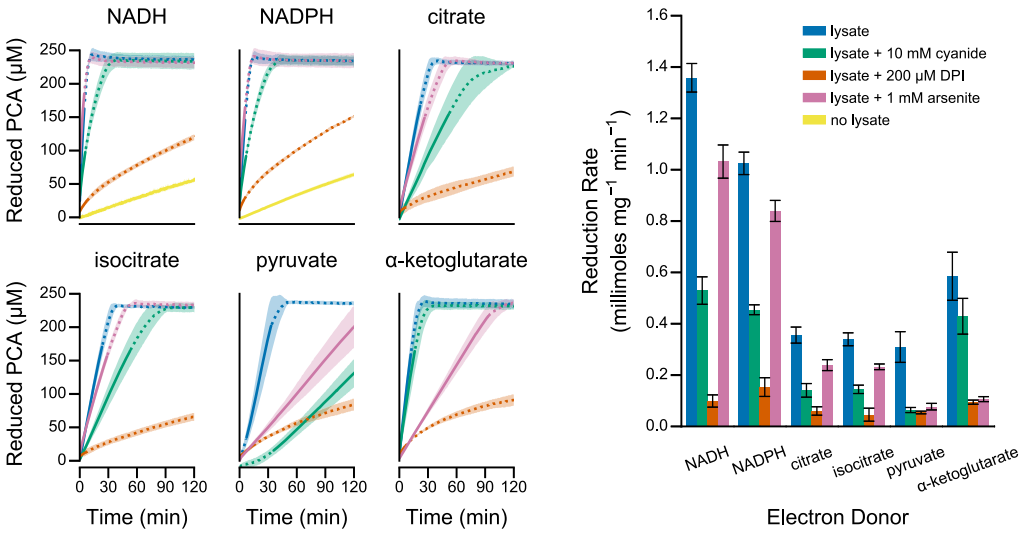

Figure 4. Inhibition of PCA reduction activity in cell-free lysate. Unfractionated cell-free lysate was assayed for its ability to catalyze PCA reduction in the presence of the indicated inhibitors. (Left) Each panel illustrates a time course of PCA reduction using the indicated electron donor. The line and shaded region represent the mean and standard deviation, respectively, from four independent assays using lysate prepared from independent cultures. The solid portion of each line indicates the linear region used for quantification. (Right) The specific activity for each fraction was determined by normalizing the rate of PCA reduction, illustrated with a solid line in the left panels, by the protein concentration of each sample. Error bars represent the standard deviation of four independent biological replicates.

We further probed the lysate using three inhibitors: (a) cyanide to inhibit metalloproteins and heme-containing proteins (34), (b) diphenyleneiodonium to inhibit flavoproteins and some heme-containing proteins (35), and (c) arsenite to inhibit thiol-dependent proteins (36). Cyanide only slightly inhibited activity, while diphenyleneiodonium greatly inhibited activity with all of the electron donors tested (Figure 4). Arsenite specifically inhibited activity only for pyruvate and α-ketoglutarate (Figure 4). Together, the differential localization and inhibitor activities suggest that *P. aeruginosa* lysate contains multiple enzymes that catalyze PCA reduction. The strong inhibition by diphenyleneiodonium (Figure 4) further suggests that flavoproteins and/or heme-containing proteins may catalyze PCA reduction.

Pyruvate and α-ketoglutarate dehydrogenase catalyze phenazine reduction

Our experiments with cell lysate suggested a role for the pyruvate and α-ketoglutarate dehydrogenases in PCA reduction. Not only did pyruvate and α-ketoglutarate stimulate PCA reduction (Figure 3), but the pattern of localization and inhibition was consistent with the conserved mechanism of the 2-oxoacid dehydrogenase complexes (reviewed in (37,38)). In the 2-oxoacid dehydrogenase complexes, the E1 subunit, the substrate dehydrogenase, conjugates the substrate to thiamine pyrophosphate (TPP) with concomitant decarboxylation. The TPP cofactor is regenerated by transferring the substrate onto a lipoamide cofactor covalently attached to the E2 subunit. The E2 subunit, dihydrolipoyl transacetylase, then regenerates lipoamide by transferring the substrate to CoA, producing dihydrolipoamide. The dihydrolipoamide is finally re-oxidized by the E3 subunit, dihydrolipoamide dehydrogenase (DLDH), by transferring electrons to NAD^+ through a flavin in the form of a tightly bound FAD.

We recognized that the megadalton-sized 2-oxoacid dehydrogenases can be pelleted by ultracentrifugation, which would explain why 2-oxoacid-dependent activity was depleted by ultracentrifugation (Figure 3), and the cofactor requirement could explain why activity was not recovered in the membrane fraction (Figure 3) because cofactors would remain in the soluble fraction. The obligate reduction and oxidation of the lipoamide thiols is consistent with inhibition by arsenite (Figure 4). Moreover, oxidation of the lipoamide cofactor requires a flavoprotein subunit, consistent with inhibition by diphenyleneiodonium (Figure 4). We therefore asked whether the pyruvate and α-ketoglutarate dehydrogenase complexes were sufficient to catalyze phenazine reduction, and if so, what electron transfer pathway was employed.

To answer this question, we isolated the native pyruvate and α-ketoglutarate dehydrogenase complexes from *P. aeruginosa* (detailed in Experimental Procedures). As judged by Coomassie staining of an SDS-PAGE gel, the complexes were approximately 90% pure (Figure 5a). The α-

ketoglutarate dehydrogenase preparation contained no detectable pyruvate dehydrogenase (<0.1%), while the pyruvate dehydrogenase preparation contained a small amount of contaminating α-ketoglutarate dehydrogenase (approximately 4%) as measured by NAD^+ reduction activity.

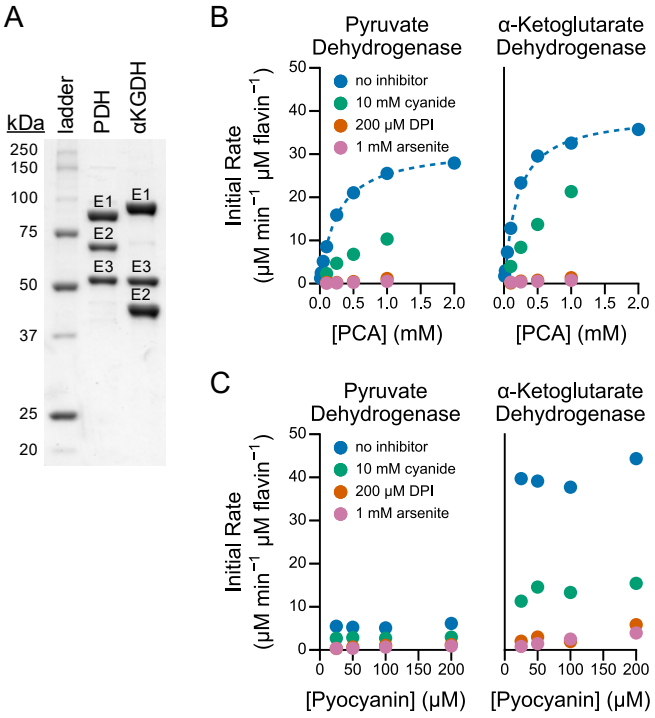

Figure 5. Preparation and characterization of the pyruvate and α-ketoglutarate dehydrogenase complexes. (A) A Coomassie Blue-stained SDS-PAGE gel of the purified pyruvate dehydrogenase (PDH) and α-ketoglutarate (αKGDH) complexes. The three prominent bands represent the three subunits of the complex as labeled. PDH: E1 (pyruvate dehydrogenase, AceE), E2 (dihydrolipoamide acetyltransferase, AceF), E3 (dihydrolipoamide dehydrogenase, LpdG); αKGDH: E1 (α-ketoglutarate dehydrogenase, SucA), E2 (dihydrolipoamide succinyltransferase, SucB), E3 (dihydrolipoamide dehydrogenase, LpdG). (B and C) PCA (B) and pyocyanin (C) reduction by the purified complexes in the absence or presence of the indicated inhibitors. The dashed line represents the fitted Michaelis-Menten binding curve.

The purified complexes catalyzed PCA (Figure 5b) and pyocyanin (Figure 5c) reduction using their respective electron donors. We normalized the reaction rate to the protein flavin content (as a measure of dihydrolipoamide dehydrogenase) rather than defining the number of active sites in

a large, potentially heterogeneous complex with multiple reaction steps. A Michaelis-Menten kinetic model fit to the initial rate of PCA reduction (Figure 5b) yielded a K_m of 260 μM and V_{max} of 32 min^{-1} for pyruvate dehydrogenase and a K_m of 190 μM and V_{max} of 40 min^{-1} for α-ketoglutarate dehydrogenase. The initial rates of pyocyanin reduction did not depend on the pyocyanin concentration (Figure 5c), implying a K_m of less than 25 μM for pyocyanin. Interestingly, while the pyruvate and α-ketoglutarate dehydrogenase complexes reduced PCA at similar rates (Figure 5b), pyruvate dehydrogenase reduced pyocyanin considerably slower than did α-ketoglutarate dehydrogenase (Figure 5c).

Cyanide, diphenyleneiodonium, and arsenite inhibited PCA and pyocyanin reduction by the purified complexes (Figure 5b,c). The relative inhibition of the purified complexes mirrored that of whole cell lysate (Figure 4), with cyanide partially inhibiting PCA reduction and both arsenite and diphenyleneiodonium more fully inhibiting PCA reduction (Figure 5b,c), indicating that the 2-oxoacid dehydrogenase complexes can account for the activity in lysate.

In control experiments, PCA and pyocyanin reduction by the purified complexes required all known substrates and cofactors. We detected no activity when the electron donor (pyruvate or α-ketoglutarate), coenzyme A, or magnesium were omitted from the reaction mixture. We observed residual activity (<1%) in the absence of TPP, possibly due to co-purification of trace amounts of this cofactor with the protein. Although we cannot rule out catalysis by a contaminant in our enzyme preparation, the inhibition by arsenite and diphenyleneiodonium, and the requirement for the known cofactors of pyruvate and α-ketoglutarate dehydrogenase, indicate that the 2-oxoacid dehydrogenase complexes directly catalyze PCA and pyocyanin reduction.

Dihydrolipoamide dehydrogenase catalyzes phenazine reduction

We next asked which 2-oxoacid dehydrogenase subunit catalyzes phenazine reduction. In the absence of CoA, the E1 subunit catalyzes ferricyanide and dichloroindophenol reduction (39,40).

However, we observed no PCA or pyocyanin reduction in the absence of CoA, suggesting these phenazines are not reduced by the E1 subunit. As the E3 subunit has long been recognized to reduce methylene blue (40), a molecule structurally similar to phenazines (Figure 1), and the porcine and malarial E3 subunits have been shown to catalyze pyocyanin reduction (27), we hypothesized that the *P. aeruginosa* E3 subunit (dihydrolipoamide dehydrogenase, DLDH) catalyzes phenazine reduction.

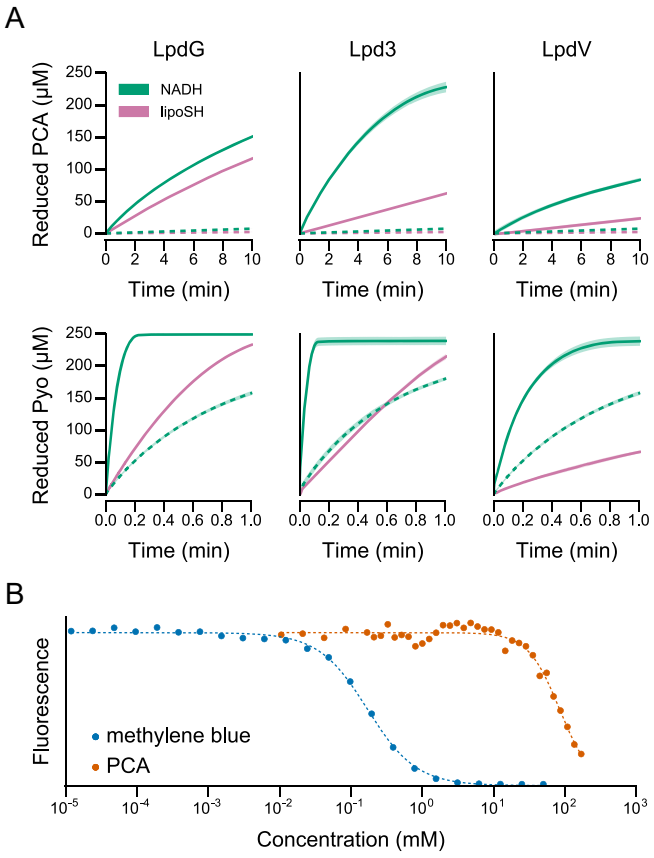

Figure 6. Phenazine reduction and binding by DLDH homologs of *P. aeruginosa*. (A) Time courses of PCA and pyocyanin reduction by DLDH using both NADH and dihydrolipoamide (lipoSH) as electron donors. Solid lines indicate the presence of 2 μM enzyme. Dashed lines indicate the absence of enzyme. Shaded regions indicate the standard deviation of three technical replicates. (B) Affinity of LpdG for PCA and methylene blue as measured by fluorescence quenching. The dashed line indicates the binding curve fitted to the data. The data points are normalized to the maximum and minimum values of the fitted curve.

Strain PA14 encodes three DLDH homologs in its genome: LpdG (PA14_43970), Lpd3 (PA14_63850), and LpdV (PA14_35490) (41,42). We purified His-tagged versions of each protein. All three enzymes catalyzed PCA and pyocyanin reduction using both NADH and dihydrolipoamide as electron donors (Figure 6a). Phenazine reduction by both dihydrolipoamide and NADH—the substrate and product of the physiological reaction, respectively—is consistent with the FAD cofactor acting as a bidirectional electron-transfer intermediate, suggesting that phenazines interact with the flavin during the catalytic cycle of DLDH. In the context of the full 2-oxoacid dehydrogenase complexes, we propose that phenazines can substitute for NAD^+ as the final electron acceptor of pyruvate and α-ketoglutarate oxidation. This contrasts with our previous assumption that phenazines serve as an oxidant for NADH (20).

Before probing the interaction between phenazines and DLDH, we determined the enzymatically relevant DLDH homolog for the 2-oxoacid dehydrogenase complexes. Although the pyruvate dehydrogenase complex of *P. aeruginosa* has been purified before (43), the precise identity of its constituent DLDH was not determined, and the operon encoding pyruvate dehydrogenase does not contain an associated DLDH. In contrast, the operon encoding α-ketoglutarate dehydrogenase encodes all three subunits (E1, E2, and E3 (LpdG)). Phenotypic evidence in *Pseudomonas putida* suggests the E3 component of pyruvate dehydrogenase is LpdG, but Lpd3 may substitute in the absence of LpdG (44). To address this ambiguity, we excised the band corresponding to DLDH from an SDS-PAGE gel (Figure 5a), performed an in-gel trypsin digest, and analyzed the resulting peptide fragments using LC-MS/MS. As expected from its operon structure, the DLDH peptides from α-ketoglutarate dehydrogenase mapped to LpdG (Table 1). The DLDH peptides from pyruvate dehydrogenase also mapped to LpdG (Table 1), with only 0.03% of peptide intensity mapping to Lpd3, indicating that LpdG is the primary DLDH of the *P. aeruginosa* PA14 pyruvate dehydrogenase. We detected no peptides corresponding to LpdV in either complex (Table 1). We also confirmed the identity of dihydrolipoamide acetyltransferase

in our pyruvate dehydrogenase preparation (Table 1), as this band migrated slower than expected for its predicted size of 56.7 kDa (Figure 5a).

Having established LpdG as the enzymatically relevant DLDH for both pyruvate and α-ketoglutarate dehydrogenase, we quantified the interaction between LpdG and phenazines in more detail. We measured the binding affinity, K_d, by exploiting the intrinsic fluorescence of the flavin moiety in the FAD cofactor of LpdG. We anticipated that binding of an aromatic group near the flavin would quench fluorescence, thereby providing a direct measure of substrate binding. This prediction was borne out experimentally. High concentrations of PCA were sufficient to quench fluorescence (Figure 6b), consistent with binding near the flavin. The extrapolated K_d is 84 mM with a Hill coefficient of 1.95 (Figure 6b). In support of a cooperative model of binding, a non-cooperative model (Hill coefficient = 1) required a nonsensical large negative minimum fluorescence and an unrealistically large K_d (>1000 mM). In contrast to PCA, the positively charged methylene blue quenched fluorescence with a K_d of 170 μM and a Hill coefficient of 1.27 (Figure 6b). We were unable to apply this method to pyocyanin, which is water-soluble at pH 7.5 only to approximately 1 mM, or to phenazine-1-hydroxide and phenazine-1-carboxamide, which are even less soluble. Hill coefficients of less than two are consistent with the dimeric structure of DLDH. Cooperative substrate binding in DLDH has been observed for NADH (45) and may originate from the architecture of the active site, which contains residues from both chains of the DLDH homodimer (46,47), potentially allowing for substrate binding to induce long-range conformational changes within the protein.

Structural insights into the interaction between LpdG and phenazines

Although the affinity of the *P. aeruginosa* LpdG for PCA appears to be low, we were encouraged by the comparatively high affinity for methylene blue, and so we attempted to solve the X-ray crystal structure of LpdG bound to a phenazine or methylene blue. LpdG crystallized in multiple

screens using polyethylene glycol as a precipitant, similar to previously discovered conditions for DLDH. During optimization, we discovered a new crystal form in which over 90% of crystals diffracted to 1.8 Å or better in the space group $P2_1$. One crystal diffracted to 1.43 Å (Figure 7a) with a signal-to-noise cutoff of 2.0, which we refined to 1.35 Å using paired refinement (48), representing the highest published resolution of any DLDH to date.

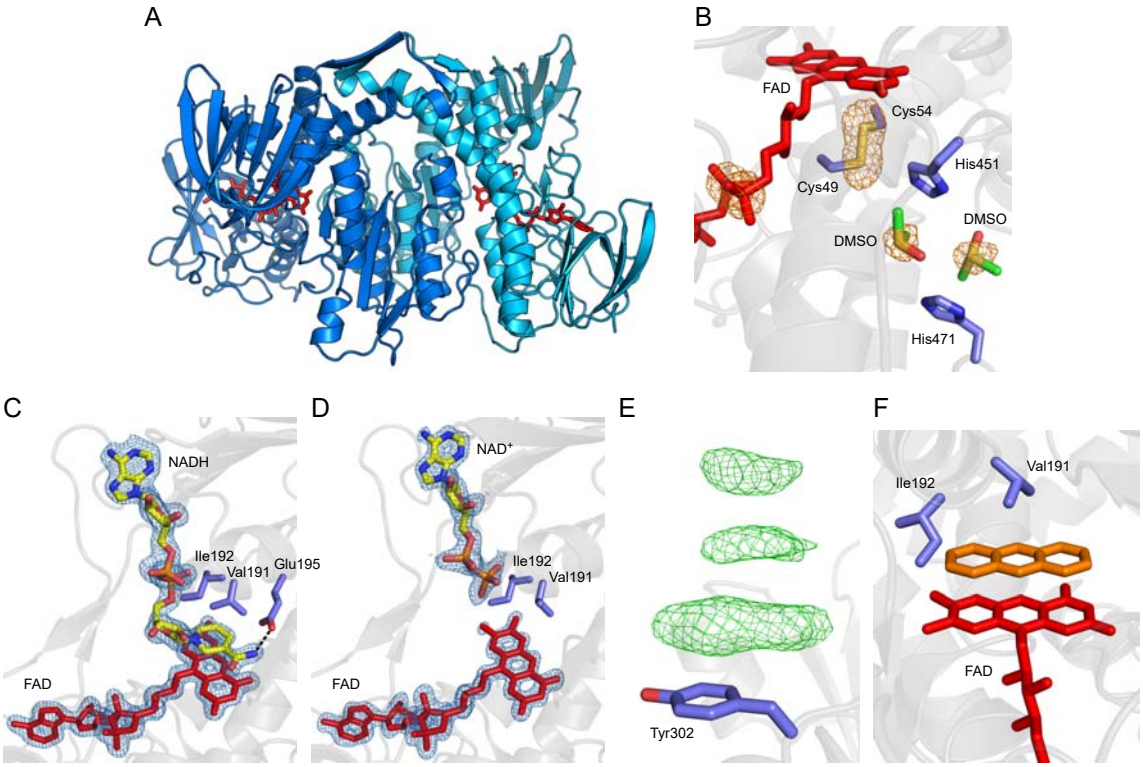

Figure 7. Structural analysis of LpdG. Where visible, the embedded FAD cofactor is shown in red. Protein side chain carbons are shown in purple. (A) Overview of the LpdG dimer. The two polypeptides of the biological assembly are shown in shades of blue. (B) Close-up of DMSO bound in the lipoamide binding pocket. The orange mesh represents the anomalous difference map contoured at 4σ, which highlights sulfur atoms and the phosphorous atoms in FAD. The DMSO carbon atoms are shown in green. (C and D) Close-up of NADH (C) and NAD^+ (D) bound to LpdG. Electron density was not visible for the oxidized nicotinamide group in NAD^+ and so this group has not been modeled. The blue mesh represents the $2mF_o - DF_c$ map of electron density for FAD and NAD(H) contoured at 1.5σ. The NAD(H) carbon atoms are shown in yellow. The dashed line illustrates a hydrogen-bond interaction. (E) Example of π-stacking interactions at a surface residue in a crystal soaked with 225 mM PCA. The green mesh represents positive density in the $mF_o - DF_c$ difference map contoured at 3σ. (F) Hypothetical illustration of a phenazine (orange) substituting for NADH, demonstrating a steric clash with Ile192. The phenazine was placed manually in Coot and does not represent a real dataset.

Apart from minor rotamer corrections and the orientations of some surface residues, our model of LpdG at 1.35 Å is essentially identical to the previously reported structure at 2.8 Å (the root mean square deviation is less than 0.4 over 470 α-carbons), and so we defer to the original

publication by Mattevi *et al.* (46) for a full structural description. A noteworthy feature unique to our model is the association of LpdG with the cryoprotectant DMSO. We observed two molecules of DMSO inside the active site where dihydrolipoamide is postulated to bind (Figure 7b). This orientation appears to be stabilized by a sulfur-π interaction between the central sulfur atom of DMSO and a histidine sidechain. This configuration might mimic the binding of the dihydrolipoamide sulfhydryl groups in the active site of LpdG. Crystals soaked for one hour with 10 mM NADH or NAD^+ yielded electron densities corresponding to the soaked substrate (Figure 7c,d). As previously observed with human DLDH (49), we could not resolve electron density for the nicotinamide group of NAD^+ (Figure 7d), suggesting the oxidized cofactor is disordered or present in multiple conformations. Statistics for the apo, NAD^+-, and NADH-bound structures are shown in Table 2.

Our initial screens yielded no crystals when 2 mM methylene blue or 250 mM PCA was included in the protein solution, so for these substrates we focused on soaking into preformed crystals. Unfortunately, we observed no electron density assignable to a phenazine after soaking for up to one week with 10 mM pyocyanin, 10 mM phenazine-1-carboxamide, 10 mM phenazine-1-hydroxide, 5 mM methylene blue, or up to 175 mM PCA. We were similarly unsuccessful when the soaks included up to 100 mM dithionite or 100 mM dihydrolipoamide to generate the reduced forms of LpdG and substrate. Above 200 mM PCA, we observed electron density characteristic of a π-stacking interaction between PCA and aromatic residues on the surface of the protein (Figure 7e), but this interaction is unlikely to be physiologically relevant because of the high PCA concentration it requires.

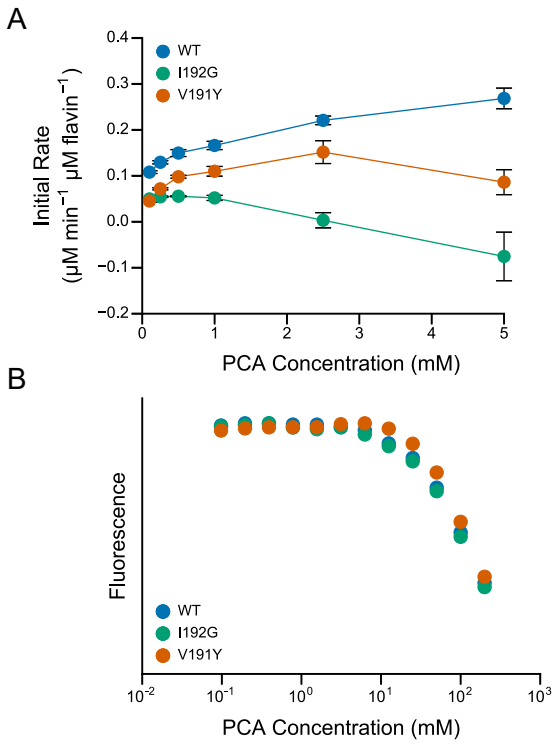

Figure 8. Site-directed mutagenesis of LpdG. (A) PCA reduction by site-directed mutants of LpdG. The initial rate of reduction was normalized by the concentration of protein (2 μM) and subtracted by the abiotic rate of reduction as measured without protein. Error bars represent the standard deviation of four technical replicates. (B) Affinity of site-directed mutants of LpdG for PCA as measured by fluorescence quenching. The fluorescence values are normalized to the maximum fluorescence for each mutant.

The crystal structure reveals a carefully structured nicotinamide binding site that sterically excludes larger molecules such as phenazines (Figure 7c,d), likely explaining why we were unable to obtain crystals bound to a phenazine. In particular, an isoleucine sidechain (Ile192) restricts access to the flavin. The smaller nicotinamide moiety of NADH forms a π-stack with the flavin that is further stabilized by hydrogen bonding of the amide group with Glu195 and the peptide backbone (Figure 7c). Assuming no other conformational changes, extending nicotinamide to contain three rings yields a steric clash with Ile192 and disrupts the stabilizing hydrogen bonds (Figure 7f). Based on this structural interpretation, we hypothesized that mutating Ile192 to a

smaller residue might increase accessibility of the flavin to phenazines, thereby accelerating DLDH-catalyzed phenazine reduction. We were also interested in Val191 which sits above the flavin–nicotinamide π-stack. In other homologs, and the closely related glutathione reductase, this residue is a tyrosine that may regulate NADH binding or reactivity through additional π-stacking and compression (50). We therefore generated two site-directed mutants of LpdG: I192G and V191Y. Contrary to our expectations, the I192G mutant catalyzed PCA reduction more slowly than wildtype LpdG and also appeared to be substrate-inhibited (Figure 8a). The V191Y mutation also lowered enzyme activity and conferred substrate inhibition (Figure 8a). The mutations did not affect the PCA concentration required to quench LpdG fluorescence (Figure 8b), demonstrating that the binding affinity remained unchanged in the mutants. Together, these results indicate that residues V191 and I192 do not sterically hinder PCA from binding to LpdG.

Discussion

The search for phenazine reductases was motivated by our interest in phenazine-mediated anaerobic survival and energy generation (19,20). Our work here suggests that, rather than possessing an enzyme with specific phenazine reductase activity, *P. aeruginosa* makes a variety of redox-active enzymes that adventitiously reduce phenazines under anoxic conditions. By subsequently reacting with molecular oxygen or ferric iron (16), phenazines would enable the oxidation of metabolites in a manner independent of the electron transport chain. The electron donor for this process could be the metabolite itself, for example pyruvate or α-ketoglutarate, without involvement of another cofactor such as NAD(P)H. Through extracellular electron transport in a microbial community (8), this mechanism would allow multiple metabolic pathways, such as glycolysis or pyruvate oxidation (20), to support energy generation for cells locally starved of an electron acceptor (*i.e.* oxygen or nitrate).

We identified the pyruvate and α-ketoglutarate dehydrogenase complexes as phenazine reductases (Figure 5) based on activity assays in whole cell lysate (Figure 2) and the pattern of fractionation and inhibition (Figures 3,4). We focused on this specific subset of enzymes because we previously found that phenazines enable ATP synthesis through the conversion of glucose to acetate by serving as an electron acceptor (20). Notably, this pathway requires pyruvate dehydrogenase. In our prior work, we hypothesized that phenazines stimulate pyruvate dehydrogenase by converting NADH to NAD^+ (20), a limiting substrate in the absence of a terminal electron acceptor. Our results here suggest that phenazines may instead directly substitute for NAD^+ in the pyruvate dehydrogenase complex during anaerobic survival. Under NAD^+-limiting conditions (*e.g.* hypoxia), phenazines could therefore increase metabolic flux through pyruvate dehydrogenase. The phenazine reduction activity of pyruvate dehydrogenase is admittedly low (V_{max} = 32 min^{-1} for PCA) (Figure 5), but it may be compatible with the low metabolic activities observed in anoxic planktonic models of survival (20,51).

Importantly, the affinity we measured of pyruvate dehydrogenase for phenazines (K_m of 260 μM for PCA and <25 μM for pyocyanin) is within the physiological range produced by *P. aeruginosa*, which can reach up to 200 μM within infection contexts (52). We observed a large mismatch between the ligand binding affinity of the catalytic subunit LpdG (*i.e.* K_d, Figure 6b) and the concentration required to saturate the reaction rate in the full complex (*i.e.* K_m, Figure 5b,c). LpdG is natively associated with the larger complex, and so the rate saturation of the full complex likely represents the more physiologically meaningful result. The large disparity in magnitude suggests that LpdG is not rate limiting within the full complex, and/or that binding to the complex induces substantial changes in the affinity of LpdG for its substrates. Given the high K_d for PCA, we would not expect PCA to outcompete NAD^+ unless the concentration of available NAD^+ were very low, but we note that this is precisely the condition where phenazines manifest a physiological benefit for *P. aeruginosa* (7,8,19,20).

The phenazine reductase activity of pyruvate dehydrogenase is particularly intriguing in the context of biofilm maintenance and development. The inner core of established biofilms is anoxic (8,53) and enters a metabolically-repressed state with decreased respiration and increased substrate-level phosphorylation (53). In the absence of oxygen, *P. aeruginosa* can survive by mixed-acid fermentation of pyruvate to acetate and lactate (51), a process that is enhanced by phenazine redox cycling (20). This suggests a model where cells at the anoxic core of a biofilm may use pyruvate dehydrogenase, with phenazines as an electron acceptor and coupled to substrate-level phosphorylation, to maintain a basal level of energy generation; reduced phenazines could then be re-oxidized at the oxygen-rich surface of the biofilm. In addition to maintaining energy generation in anoxic regions of biofilms (8), phenazines can also stimulate biofilm formation through iron acquisition (54), extracellular DNA release (55), and other unknown mechanisms (54-56). In context of our work here, it is striking that early biofilm development in *P. aeruginosa* requires pyruvate fermentation and redox homeostasis (57). It is tempting to speculate that the biofilm-promoting behavior of phenazines and pyruvate fermentation could be mechanistically linked through the activity of pyruvate dehydrogenase.

We do not mean to suggest that pyruvate and α-ketoglutarate dehydrogenase are the only relevant phenazine reductases *in vivo*. Indeed, NADH and NADPH are more effective than the 2-oxoacids at stimulating PCA reduction in cell lysate (Figures 2–4). The 2-oxoacid:PCA oxidoreductase activity in lysate could be explained by the 2-oxoacid dehydrogenases reducing NAD^+ to NADH, enabling the activity of an NADH:PCA oxidoreductase. Similarly, the stimulation by citrate and isocitrate (Figures 2–4) could result from the downstream production of NAD(P)H. Therefore, our results with cell lysate are best interpreted as an upper limit to the overall PCA reductase activity of pyruvate and α-ketoglutarate dehydrogenase. With that caveat, we also found that diphenyleneiodonium is a strong inhibitor of PCA reduction (Figure 4). Notably, diphenyleneiodonium is a known flavoprotein inhibitor that conjugates to reduced flavins via a

radical-mediated mechanism, although it can also inhibit some heme-proteins (35). This is consistent with our finding that the flavoenzyme LpdG, the E3 subunit of the 2-oxoacid dehydrogenases studied here (Table 1), directly catalyzes PCA and pyocyanin reduction (Figure 6). Together, these findings suggest that flavoproteins, and possibly some heme-containing proteins, account for the majority of phenazine reductase activity in *P. aeruginosa*.

Ultimately, pyruvate and α-ketoglutarate dehydrogenase serve to demonstrate that many electron donors, through the activity of their catabolic enzymes, could support phenazine reduction. By accepting electrons from flavoproteins, a ubiquitous class of proteins important for metabolism, phenazines could potentially alter metabolic flux through a number of pathways. A quantitative prediction of this activity *de novo* is presently impossible. Even for the adventitious reduction of oxygen, the most studied side-reaction of flavoproteins, the parameters that govern reaction rates (which differ by at least 6 orders of magnitude) are still unclear (58). Mirroring this uncertainty, our prediction that sterics are the rate-limiting factor for phenazine reduction by LpdG did not hold up to site-directed mutagenesis (Figure 8), suggesting that even for the restricted active site of LpdG, the enzyme-specific particulars of electronic structure and transition state are important. Beyond enzyme kinetics, phenazine reduction varies by growth phase (7), and so we expect the overall effects of phenazines on metabolism to be heavily context-dependent. For example, within a heterogeneous and stratified biofilm community, different enzymes likely catalyze phenazine reduction under (hyp)oxic and anoxic conditions. The results of this study, indicating that oxidized PCA and pyocyanin can substitute for NAD^+, allow us to postulate that under strictly anaerobic conditions, where NAD^+ may be limited (7,20), substitution of phenazines for NAD^+ in enzymes like LpdG would facilitate redox homeostasis. This is in a manner distinct from what we have previously assumed (the coupling of NADH oxidation to phenazine reduction) but results in the same net effect: maintenance of a higher NAD^+/NADH ratio. Such substitution would allow for flux through pathways that would otherwise not proceed, including, but not

limited to, energy-generation pathways such as pyruvate oxidation (20). A comprehensive understanding of phenazine metabolism *in vivo* will require a synthesis of biochemical and genetic approaches, yet this study helps focus our attention on potentially important enzymatic catalysts and pathways.

Experimental Procedures

Materials

The reagents used for growth media and protein purification were from Sigma-Aldrich or Acros Organics and were of ACS grade or better. Pyocyanin was from Cayman Chemicals. Phenazine-1-carboxylic acid and phenazine-1-carboxamide were from Princeton Biosciences. Phenazine-1-hydroxide was from TCI America. NAD^+, NADH, thiamine pyrophosphate, coenzyme A, $MgCl_2$, lipoamide, potassium cyanide, diphenyleneiodonium chloride, and sodium (meta)arsenite were from Sigma-Aldrich. Dihydrolipoamide was synthesized from lipoamide by reduction with sodium borohydride (59) and stored desiccated at −20 °C. For crystallography, PEG-3350 (50% solution) was from Hampton Research and DMSO, HEPES, KOH, and KCl were from Sigma-Aldrich. Ni-Sepharose and Sephacryl S-400 were from GE Healthcare. CHT hydroxyapatite was from Bio-Rad. Thrombin was from EMD Millipore. Other chemicals were from Sigma-Aldrich unless stated otherwise. All phosphate buffers were prepared with KH_2PO_4 and adjusted to the appropriate pH with KOH at room temperature. Anaerobic buffers were prepared by autoclaving and transferring the still-warm solution into an anaerobic chamber; other anaerobic solutions were prepared by dissolving solid compounds with anaerobic buffers within the anaerobic chamber.

Growth conditions

For routine culturing, *P. aeruginosa* and *Escherichia coli* were grown in lysogeny broth containing 10 g/L tryptone, 5 g/L yeast extract, and 10 g/L NaCl. Solid agar plates contained 15 g/L agar.

The succinate minimal medium for *P. aeruginosa* contained 14.15 mM KH_2PO_4, 35.85 mM K_2HPO_4, 42.8 mM NaCl, 9.3 mM NH_4Cl, 40 mM disodium succinate, 1 mM $MgSO_4$, 7.5 μM $FeCl_2{\cdot}4H_2O$, 0.5 μM $ZnCl_2$, 0.5 μM $MnCl_2{\cdot}4H_2O$, 0.1 μM H_3BO_3, 0.8 μM $CoCl_2{\cdot}6H_2O$, 0.01 μM $CuCl_2{\cdot}2H_2O$, 0.1 μM $NiCl_2{\cdot}6H_2O$, and 0.15 μM Na_2MoO_4. The minimal medium was sterilized by autoclaving; to avoid precipitation, the metals were prepared as a separate solution (1000×) and added immediately prior to inoculation. All liquid cultures were incubated in a New Brunswick Innova 44R incubator at 37 °C shaking at 250 rpm (2.54 cm stroke length).

PCA reduction by cell lysate

Wildtype *P. aeruginosa* PA14 was incubated in 250-mL Erlenmeyer flasks containing 50 mL of succinate minimal medium and grown to an OD_{500} of 2.4–2.8 (approximately 11 hours from a starting OD_{500} of 0.01). The cells were harvested by centrifugation for 15 minutes at 6,800×g, washed twice with 1 mL of 50 mM KH_2PO_4, pH 7.5, and resuspended to a final volume of 1 mL with 50 mM KH_2PO_4, pH 7.5, and 1 mM phenylmethylsulfonyl fluoride (PMSF). The cells were lysed by sonication on ice using a ThermoScientific Sonic Dismembrator 550 set to power level 3 with a pulse setting of 1 s on, 4 s off for 3 min total sonication time. Large debris and unlysed cells were removed by centrifugation for 15 min at 8,000×g. Where applicable, membrane-associated proteins were separated by ultracentrifugation using a Beckman Optima ultracentrifuge with a TLA-100.3 fixed-angle rotor. The lysate was centrifuged for one hour at 70,000 rpm (208,000×*g* average) and the supernatant was saved. The pellet was resuspended by gently pipetting an equivalent volume of 50 mM KH_2PO_4, pH 7.5, with 1% n-dodecyl β-D-maltoside and 1 mM PMSF. Undissolved material was removed by centrifugation for 15 min at 8,000×*g*. Protein concentration was measured using the bicinchoninic acid assay (Pierce) (60) calibrated with BSA standards (Pierce). Boiled lysate was prepared by placing an aliquot into a boiling water bath for 5 minutes; the precipitated material was removed by centrifugation at 17,000×*g* for 5 min.

PCA reduction assays were performed inside an anaerobic glove box (Coy) with an atmosphere of 3–4% H_2 and 97–96% N_2. Reactions were performed at 28 °C in a 96-well plate with each well containing 50 µL of lysate, 50 µL of electron donor (dissolved in 50 mM KH_2PO_4, pH 7.5), and 50 µL of buffer (50 mM KH_2PO_4, pH 7.5) or boiled lysate. Where applicable, inhibitors were added using 2 µL of a 100× stock solution (KCN and $NaAsO_2$ were dissolved in water; diphenyleneiodonium chloride was dissolved in DMSO). The reaction was initiated by adding 50 µL of PCA (1 mM stock in 50 mM KH_2PO_4, pH 7.5; 250 µM final concentration). The reaction was monitored by measuring absorbance at 440 nm using a BioTek Synergy 4 plate reader housed within the anaerobic glove box. The reaction progress was normalized against four averaged control wells containing 250 µM PCA and 10 mM sodium dithionite as a measure of 100% PCA reduction.

Pyruvate and α-ketoglutarate dehydrogenase purification

The pyruvate and α-ketoglutarate dehydrogenase complexes were prepared natively from *P. aeruginosa* PA14 Δ*phz1/2* (33). This phenazine-null strain was used to minimize the generation of reactive oxygen species during the initial stages of purification. Cells were grown in 1 L of the succinate minimal medium (with 80 mM disodium succinate to achieve higher cell density) in a 2.8-L baffled Fernbach flask to an OD_{500} of 4–6. In a typical preparation, 6 L of cells were harvested by centrifugation for 15 min at 8000×*g*. The cells were resuspended in 200 mL of 50 mM KH_2PO_4, adjusted to pH 7.5 with KOH, with 1 mM EDTA and a cOmplete ULTRA protease inhibitor tablet (Roche). The cells were lysed using 3 or 4 passes through an Avestin Emulsiflex-C3 operating at 20,000 PSI. The lysate was centrifuged for 30 min at 30,000×*g* and the pellet was discarded. In subsequent steps, the activity of the complexes was followed using a reaction mix containing 50 mM KH_2PO_4, pH 7.5, 1 mM $MgCl_2$, 100 µM TPP, 100 µM CoA, 500 µM NAD^+, and 2.5 mM pyruvate or α-ketoglutarate. Activity was indicated by an absorbance increase over time at 340 nm after adding 1–5 µL of lysate or protein to 199–195 µL of the reaction mix.

After adjusting the lysate dropwise with 5% acetic acid to pH 6.0 on ice, 0.17 volumes of 2% protamine sulfate were added and the mixture was gently stirred on ice for 30 min. The mixture was centrifuged for 30 min at 30,000×*g* and the pellet was discarded. The lysate was further clarified by adding 0.2 volumes of ice-cold acetone, stirring the mixture on ice for 15 min, centrifuging for 15 min at 30,000×*g*, and discarding the pellet. The dehydrogenase complexes were then precipitated by slowly adding an additional 0.4 volumes of ice-cold acetone. The mixture was gently stirred for 30 min on ice and centrifuged for 30 min at 30,000×g. The supernatant was discarded.

The precipitated proteins were dissolved in 50 mL of ice-cold 100 mM KH_2PO_4, pH 7.5, with 0.5 mM PMSF. Undissolved material was removed by centrifugation for 15 min 15,000×*g*. The supernatant was applied to a CHT ceramic hydroxyapatite (Type I, 40 μm particle size) column (dimensions 2.2×16.5 cm) at a flow rate of 2.0 mL/min using an Äkta Express system at room temperature. The column was washed with 2 column volumes of 100 mM KH_2PO_4, pH 7.5. The complexes were eluted at a flow rate of 5 mL/min using a linear gradient over 2 column volumes to 500 mM KH_2PO_4, pH 7.5, with 2 mL fraction collection. Fractions were assayed for pyruvate and α-ketoglutarate dehydrogenase activity and pooled accordingly. The complexes were concentrated using an Amicon ultra centrifugal filter (30 kDa cutoff) to a volume of less than 1 mL. The complexes were further purified using gel filtration over a Sephacryl S-400 column (dimensions 1.6×38.0 cm) run isocratically with 100 mM KH_2PO_4, pH 7.5, and 1 mM EDTA at 0.5 mL/min with an Äkta Purifier system at 4 °C. Fractions containing pyruvate or α-ketoglutarate dehydrogenase activity were again pooled and concentrated using an Amicon ultra centrifugal filter. Purity was assessed using an SDS-PAGE gel stained with Coomassie Blue.

PCA and pyocyanin reduction by purified proteins

Phenazine reduction by purified proteins was measured using a Thermo Scientific Evolution 260 Bio spectrometer housed within an anaerobic chamber. PCA reduction was followed at 440 nm at 5 Hz with an integration time of 0.2 s. Pyocyanin reduction was followed at 690 nm at 5 or 20 Hz with an integration time of 0.2 s or 0.05 s, respectively. The extinction coefficients used were $\varepsilon_{440} = 2206\ M^{-1}\ cm^{-1}$ for reduced PCA, $\varepsilon_{440} = 35.4\ M^{-1}\ cm^{-1}$ for oxidized PCA, $\varepsilon_{690} = 4306\ M^{-1}\ cm^{-1}$ for oxidized pyocyanin, and $\varepsilon_{690} = 0\ M^{-1}\ cm^{-1}$ for reduced pyocyanin. PCA was dissolved to a stock concentration of 20 mM in 300 mM KH_2PO_4, pH 7.5. Pyocyanin was dissolved to a stock concentration of 10 mM in 20 mM HCl. All reactions were performed at 30 °C. The limit of detection was approximately 25 μM, corresponding to a change in absorbance of approximately 0.01 before the rate became non-linear.

The pyruvate and α-ketoglutarate dehydrogenase complexes were assayed using 0.5–0.9 μM LpdG (as measured by flavin content) in 50 mM KH_2PO_4, pH 7.5, 1 mM EDTA, 3 mM $MgCl_2$, 200 μM TPP, 200 μM CoA, and 2.5 mM pyruvate or α-ketoglutarate. Where applicable, inhibitors were added from a 100× stock solution. The reaction was initiated by adding an equal volume of a 2× solution of phenazine.

DLDH was assayed using 2 μM of protein (as measured by flavin content) in phosphate buffer, pH 7.5, with 1 mM EDTA and 1 mM NADH or 1 mM dihydrolipoamide (dissolved in 50% isopropanol as a 100 mM stock solution). Because the enzymes required different ionic strengths for stability, LpdG and Lpd3 were assayed using 300 mM KH_2PO_4 and LpdV was assayed using 50 mM KH_2PO_4. For PCA, the reaction was initiated by adding an equal volume of 2× PCA; for pyocyanin, the reaction was initiated by adding an equal volume of 2× NADH or dihydrolipoamide.

Fluorescence quenching

The fluorescence of LpdG was measured in a black half-area microtiter plate using a BioTek Synergy 4 plate reader. Each well contained 100 μL of 2 μM protein in 300 mM KH_2PO_4, pH 7.5, with the appropriate concentration of ligand. Fluorescence was measured using a tungsten lamp with a 485±10 nm excitation filter and a 528±10 nm emission filter. The background fluorescence of a control well, without protein but with the same ligand concentration, was subtracted from the protein fluorescence.

Curve fitting

Non-linear curve fitting was performed using the curve_fit function from SciPy's optimization package. Fluorescence quenching data were fit with the formula $F = ([S]^N / ([S]^N + K_d^N)) \times (F_s - F_o) + F_o$, where F is the observed fluorescence, $[S]$ is the substrate concentration, N is the measure of cooperativity (Hill coefficient), K_d is the dissociation constant, F_s is the fluorescence at a saturating substrate concentration, and F_o is the fluorescence in the absence of substrate. Kinetic data were fit with the equation $R = V_{max} \cdot [S] / (K_m + [S])$, where R is the rate of reaction, V_{max} is the maximum reaction velocity, $[S]$ is the substrate concentration, and K_m is the substrate concentration at half of V_{max}.

Cloning

Heterologous expression vectors for LpdG, Lpd3, and LpdV were prepared similarly as follows. The full ORFs were amplified with PCR from *P. aeruginosa* PA14 genomic DNA. The forward and reverse primers contained an additional stop codon and restriction sites for cloning into the Novagen pET-15b expression vector (MilliporeSigma). For LpdG, the forward primer was AGAGAGcatatgAGCCAGAAATTCGACGTG and the reverse primer was ACACACggatccTTATTATCAGCGCTTCTTGCGGTT. For Lpd3, the forward primer was AGAGAGcatatgATGGAAAGCTATGACGTGATCGTG and the reverse primer was

ACACACggatccTTATTATCAGTTCTGCATGGCCCG. For LpdV, the forward primer was AGAGAGcatatgAGCCAGATCCTGAAGACTTC and the reverse primer was ACACACctcgagTTATTATCAGATGTGCAGGGCGTG. The products for LpdG and Lpd3, and the pET15b vector, were digested with NdeI and BamHI. The product for LpdV, and the pET15b vector, were digested with NdeI and XhoI. The digests were purified using the Qiagen PCR Purification Kit and the resulting ORF and plasmid products were ligated together with T4 DNA ligase. The ligated product was transformed into *E. coli* Top10 (Invitrogen) and selected for on LB agar plates with 50 μg/mL carbenicillin. Individual colonies were cultured and the constructed plasmid was isolated using a Qiagen Miniprep Kit and sequenced (Retrogen) to verify that no mutations were introduced. The plasmid was then transformed into *E. coli* BL21(DE3) (61) for protein expression.

Site-directed mutants of LpdG were created by PCR-amplification of the LpdG-pET15b vector. The wildtype vector was amplified using primers that contained appropriate mismatches. The resulting PCR product was phosphorylated using T4 polynucleotide kinase, blunt-end ligated using T4 DNA ligase, and transformed into *E. coli* Top10 and BL21 as described above. For LpdG I192G, the primers were GGCCTGGAGCTGGGTTC and GCCGACGCCGGCGCCGAT. For LpdG V191Y, the primers were ATTGGCCTGGAGCTGGGT and ATAGCCGGCGCCGATCACAC.

Dihydrolipoamide dehydrogenase purification

His_6-tagged DLDH homologs and mutants were purified using the same procedure. *E. coli* BL21 harboring the expression plasmid (see Cloning) was cultured at 37 °C to an OD_{600} of approximately 0.8 in terrific broth containing 12 g/L tryptone, 24 g/L yeast extract, 4 mL/L glycerol, 17 mM KH_2PO_4, 72 mM K_2HPO_4, 8 mM $MgSO_4$, and 100 μg/mL ampicillin. A typical purification used 1 L of cells grown in a 2.8-L baffled Fernbach flask. All steps after culturing were

performed at 4 °C. The cells were harvested by centrifugation for 15 min at 5,000×g. The pellet was resuspended in 2.5 volumes of 50 mM KH_2PO_4, pH 7.5, 200 mM KCl, 50 mM imidazole, and 1 mM PMSF. The cells were lysed using 3–4 passes through an Avestin Emulsiflex-C3 operating at 15,000 PSI and the lysate was clarified by centrifugation for 30 min at 30,000×*g*. The supernatant was applied to a 5-mL HisTrap HP column (GE Healthcare) with an Äkta Purifier system running at 3 mL/min. The column was washed with 5 column volumes of 50 mM KH_2PO_4, pH 7.5, 200 mM KCl, and 50 mM imidazole and proteins were eluted using a linear gradient over 5 column volumes to 50 mM KH_2PO_4, pH 7.5, 200 mM KCl, and 500 mM imidazole. The yellow fractions were pooled, concentrated using an Amicon ultra centrifugal filter (30 kDa) to a volume of less than 3 mL, and desalted using a HiPrep 26/10 desalting column (GE Healthcare) into a buffer containing 300 mM KH_2PO_4, pH 7.5. The yellow fractions were again pooled and stored at 4 °C. All of the preparations were at least 95% pure as judged by Coomassie Blue staining of an SDS-PAGE gel.

For crystallography, LpdG was purified as described above except that protein was purified from 6 L of cell culture using a 20-mL HisPrep FF 16/10 column (GE Healthcare). Prior to desalting, the protein was incubated overnight at 4 °C with 50 U of thrombin (EMD Millipore). The protein was concentrated and desalted into 50 mM KH_2PO_4, pH 7.5, 500 mM KCl, and 20 mM imidazole. Uncleaved protein, and other contaminants that bind to the HisPrep column, were removed by passing the protein back through the HisPrep column and collecting the flowthrough. The flowthrough was applied to a CHT ceramic hydroxyapatite (Type I, 40 μm particle size) column (dimensions 2.2×16.5 cm) at a flow rate of 5.0 mL/min. The column was washed with 2 column volumes of 100 mM KH_2PO_4, pH 7.5, and highly pure LpdG was eluted using a linear gradient over 2 column volumes to 500 mM KH_2PO_4, pH 7.5. The yellow fractions were pooled, concentrated and desalted into 25 mM HEPES, pH 7.5, with 600 mM KCl, and stored at 4 °C.

Flavoprotein concentrations were determined spectrophotometrically. An aliquot of protein was first boiled in the dark for 5 min. The precipitated protein was removed by centrifugation, and the concentration of liberated flavin was determined using the FAD extinction coefficient of ε_{450} = 11300 M^{-1} cm^{-1}.

Proteomics

In-gel digests were performed as previously described (62) and LC-MS/MS analysis was performed at the Caltech Proteome Exploration Laboratory (63).

Crystallography

Initial crystal screens were performed using vapor diffusion in sitting drop plates. The five screens used were Crystal Screen HT (Hampton), Index HT (Hampton), PEGRx HT (Hampton), JCSG-*plus* HT-96 (Molecular Dimensions), and Wizard Classic 1 and 2 (Rigaku). An Art Robins Gryphon Nano liquid-handling robot was used to mix 0.2 µL of screen solution with 0.2 µL of protein solution (30 mg/mL in 25 mM HEPES, pH 7.5, with 600 mM KCl). The plates were sealed with transparent film and incubated at 20 °C. The plates were monitored every several days for crystal growth using a stereoscopic microscope. For each well that formed crystals, a secondary screen was performed using similar conditions with a wider concentration of salt, pH, and PEG.

The optimized crystals were grown in a hanging-drop format using Hampton VDX plates with sealant and siliconized glass cover slides. Drops were created by mixing 1.5 µL of mother liquor with 2 µL of protein solution and 0.5 µL of seed solution. The mother liquor contained 500 µL of 22% PEG-3350 with 530 mM HEPES at pH 6.1. The protein solution contained 6 mg/mL of LpdG (as measured by the BCA assay) in 400 mM HEPES, pH 6.1, with 100 mM KCl. The seed solution contained several crystals, crushed by vortexing with a glass bead and diluted approximately 1000-fold, in 22% PEG-3350 with 10 mM HEPES, pH 6.5. The pH 6.1 HEPES buffers were prepared using a stock of 1 M HEPES with 50 mM MES, and so the final drop

solution contained 11% PEG-3350, 400 mM HEPES, 50 mM KCl, and 23 mM MES. The initial seed crystal formed under similar conditions at pH 7.5 and was propagated to the lower pH through several rounds of crystallization and seeding. Crystals formed as yellow cubes or bricks and were apparent after 5 hours at pH 6.5–7.0 or overnight at pH 6.1. The best-diffracting crystals were grown for 24–48 hours and were 50–100 μm in each dimension.

Ligand soaking and cryoprotection were performed delicately because the crystals were highly susceptible to cracking from osmotic strength changes. Crystals were first transferred to 8 μL of mother liquor on a cover slip. Serial dilutions (2-fold) were created of the soaking or cryo solution with the mother liquor, and the crystals were slowly acclimated by mixing in 0.5–1 μL of new solution with a pipette tip. The same volume was removed from the drop and iteratively replaced until Schlieren lines were no longer visible, and the process was repeated using a higher concentration of ligand or cryoprotectant. Typically, batches of 10 crystals were acclimated at a time over 30–45 minutes. The final cryoprotection solution contained 50 mM HEPES, pH 7.0, 20% PEG-3350, 20% DMSO, and the final desired ligand concentration. Crystals were flash frozen by plunging into liquid nitrogen.

Data collection was performed at the Stanford Synchotron Radiation Lightsource, beamline 12-2. Diffraction images were collected every 0.15° for a full 360° around a single axis (2400 images total) using X-rays at 12658 eV. Data completion was frequently low (<90%) because of the low symmetry in $P2_1$ and the dead spaces between detector tiles of the Pilatus 6M, and so a second dataset was collected for each crystal utilizing a detector offset of 10 mm in the X- and Y-directions. For well-diffracting crystals with minimal radiation damage, this process was repeated with X-rays at 6900 eV to capture the anomalous signal from sulfur. The datasets were integrated with XDS (64), scaled together with XSCALE, and then processed with POINTLESS (65), merged with AIMLESS (66), and converted to structure factors with CTRUNCATE in the CCP4

suite (67). The structure was solved by molecular replacement with Phaser (68) using a search model consisting of chain A from the structure 1LPF in the PDB. The structure was refined using phenix.refine (69) and ligands (FAD and NADH) were placed using phenix.ligandfit (70). For the structure containing NAD^+, a fragment of the NAD^+ ligand was placed manually in Coot (71) because electron density was not apparent for the full ligand. Side chains were trimmed in Coot where there was undefined electron density. Further refinement was performed with phenix.refine and iterative model building in Coot to the resolution that provided an arbitrary signal-to-noise cutoff of 2.0. Paired refinement (48) was then used in 0.05-0.08 Å increments to establish the resolution limit of useful data. Riding-hydrogens considerably improved R_{free} and overall geometry and so they were including in all models. Compared to a simpler TLS model of anisotropy, a fully anisotropic model improved R_{free} and overall geometry for the apo and NAD^+ structures, and so these models were refined using anisotropic *b*-factors. TLS parameters for the lower-resolution NADH structure were determined and refined with PHENIX. A large number of DMSO molecules, originating from the cryoprotectant, were placed manually in Coot with guidance from the low-energy anomalous difference map. The high resolution apo structure suggested deviations from planarity in the flavin ring of FAD, and so the final rounds of refinement in the apo and NAD^+ structures were performed using relaxed planarity restraints for FAD.

Acknowledgements

We thank the Howard Hughes Medical Institute, National Institutes of Health (5R01HL117328-03), National Science Foundation (1144469), and the Amgen Scholars Program for funding this work. We also thank Dr. Doug Rees and the Caltech Molecular Observatory for providing essential guidance, training, and materials for X-ray crystallography, the Caltech Proteome Exploration Laboratory for its services, and the SSRL staff. Members of the Newman lab (past and present) provided constructive feedback on the manuscript.

Conflict of Interest

The authors declare that they have no conflicts of interest with the contents of this article.

Author Contributions

N.R.G. and D.K.N. designed the experiments. N.R.G. collected the data, refined the protein structures, and wrote the manuscript. B.X.W. created the protein expression vectors, assisted with protein purification, and performed preliminary enzyme kinetics. B.X.W. and J.A.H. performed the initial crystallography screens and optimized crystal growth conditions. J.A.H. discovered the high-resolution crystal form of LpdG and provided crystallography training. N.R.G. further optimized crystallization and cryoprotection. D.K.N. coordinated the project. All authors reviewed the manuscript.

Literature Cited

1. Gessard, C. (1882) *Thèse pour le Doctorat en Médicine: De la pyocyanine et de son microbe. Colorations qui en dépendant de les liquides organiques (pus et sérosités, suer, liquides des culture)*, Faculté de Médicine de Paris
2. Elema, B. (1931) Studies on the oxidation-reduction of pyocyanine: Part II. Redox potentials of pyocyanine. *Recueil des Travaux Chimiques des Pays-Bas* **50**, 807-826
3. Friedheim, E., and Michaelis, L. (1931) Potentiometric study of pyocyanine. *Journal of Biological Chemistry* **91**, 355-368
4. Michaelis, L. (1931) The formation of semiquinones as intermediary reduction products from pyocyanine and some other dyestuffs. *Journal of Biological Chemistry* **92**, 211-232
5. Friedheim, E. (1931) Pyocyanine, an accessory respiratory enzyme. *Journal of Experimental Medicine* **54**, 207-221
6. Friedheim, E. (1934) The effect of pyocyanine on the respiration of some normal tissues and tumours. *Biochemical Journal* **28**, 173-179
7. Price-Whelan, A., Dietrich, L. E. P., and Newman, D. K. (2007) Pyocyanin alters redox homeostasis and carbon flux through central metabolic pathways in *Pseudomonas aeruginosa* PA14. *Journal of Bacteriology* **189**, 6372-6381
8. Dietrich, L. E. P., Okegbe, C., Price-Whelan, A., Sakhtah, H., Hunter, R. C., and Newman, D. K. (2013) Bacterial community morphogenesis is intimately linked to the intracellular redox state. *Journal of Bacteriology* **195**, 1371-1380
9. Abken, H.-J., Tietze, M., Brodersen, J., Bäumer, S., Beifuss, U., and Deppenmeier, U. (1998) Isolation and characterization of methanophenazine and function of phenazines in membrane-bound electron transport of *Methanosarcina mazei* Gö1. *Journal of Bacteriology* **180**, 2027-2032

10. Hassan, M., and Fridovich, I. (1979) Intracellular production of superoxide radical and of hydrogen peroxide by redox active compounds. *Archives of Biochemistry and Biophysics* **196**, 385-395
11. Gu, M., and Imlay, J. (2011) The SoxRS response of *Escherichia coli* is directly activated by redox-cycling drugs rather than by superoxide. *Molecular Microbiology* **79**, 1136-1150
12. Armstrong, A., and Stewart-Tull, D. E. S. (1971) The site of the activity of extracellular products of *Pseudomonas aeruginosa* in the electron-transport chain in mammalian cell respiration. *Journal of Medical Microbiology* **4**, 263-270
13. Morales, D. K., Jacobs, N. J., Rajamani, S., Krishnamurthy, M., Cubillos-Ruiz, J. R., and Hogan, D. A. (2010) Antifungal mechanisms by which a novel *Pseudomonas aeruginosa* phenazine toxin kills *Candida albicans* in biofilms. *Molecular Microbiology* **78**, 1379-1392
14. Hollstein, U., and Gernert, R. J. V. (1971) Interaction of phenazines with polydeoxyribonucleotides. *Biochemistry* **10**, 497-504
15. Cox, C. D. (1986) Role of pyocyanin in the acquisition of iron from transferrin. *Infection and Immunity* **52**, 263-270
16. Wang, Y., and Newman, D. K. (2008) Redox reactions of phenazine antibiotics with ferric (hydr)oxides and molecular oxygen. *Environmental Science and Technology* **42**, 2380-2386
17. Hernandez, M. E., and Newman, D. K. (2001) Extracellular electron transfer. *Cellular and Molecular Life Sciences* **58**, 1562-1571
18. Price-Whelan, A., Dietrich, L. E. P., and Newman, D. K. (2006) Rethinking 'secondary' metabolism: physiological roles for phenazine antibiotics. *Nature Chemical Biology* **2**, 71-78
19. Wang, Y., Kern, S. E., and Newman, D. K. (2010) Endogenous phenazine antibiotics promote anaerobic survival of *Pseudomonas aeruginosa* via extracellular electron transfer. *Journal of Bacteriology* **192**, 365-369
20. Glasser, N. R., Kern, S. E., and Newman, D. K. (2014) Phenazine redox cycling enhances anaerobic survival in *Pseudomonas aeruginosa* by facilitating generation of ATP and a proton-motive force. *Molecular Microbiology* **92**, 399-412
21. Mavrodi, D. V., Ksenzenko, V. N., Bonsall, R. F., Cook, R. J., Boronin, A. M., and Thomashow, L. S. (1998) A seven-gene locus for synthesis of phenazine-1-carboxylic acid by *Pseudomonas fluorescens* 2-79. *Journal of Bacteriology* **180**, 2541-2548
22. McDonald, M., Mavrodi, D. V., Thomashow, L. S., and Floss, H. G. (2001) Phenazine biosynthesis in *Pseudomonas fluorescens*: branchpoint from the primary shikimate biosynthetic pathway and role of phenazine-1,6-dicarboxylic acid. *Journal of the American Chemical Society* **123**, 9459-9460
23. Holliman, F. G. (1969) Pigments of *Pseudomonas* species: Part I. Structure and synthesis of aeruginosin A. *Journal of the Chemical Society C*, 2514-2516
24. Herbert, R. B., and Holliman, F. G. (1969) Pigments of *Pseudomonas* species: Part II. Structure of aeruginosin B. *Journal of the Chemical Society C*, 2517-2520
25. Wallace, R. J., Swenson, J. M., Silcox, V. A., Good, R. C., Tschen, J. A., and Stone, M. S. (1983) Spectrum of disease due to rapidly growing *Mycobacteria*. *Reviews of Infectious Diseases* **5**, 657-679
26. Cezairliyan, B., Vinayavekhin, N., Grenfell-Lee, D., Yuen, G. J., Saghatelian, A., and Ausubel, F. M. (2013) Identification of *Pseudomonas aeruginosa* phenazines that kill *Caenorhabditis elegans*. *PLoS Pathogens* **9**, e1003101

27. Kasozi, D. M., Gromer, S., Adler, H., Zocher, K., Rahlfs, S., Wittlin, S., Fritz-Wolf, K., Schirmer, R. H., and Becker, K. (2011) The bacterial redox signaller pyocyanin as an antiplasmodial agent: comparisons with its thioanalog methylene blue. *Redox Report* **16**, 154-165
28. Price-Whelan, A. M. (2009) *Physiology and mechanisms of pyocyanin reduction in Pseudomonas aeruginosa*, California Institute of Technology
29. Kern, S. E. (2013) *Consequences of redox-active phenazines on the physiology of the opportunistic pathogen Pseudomonas aeruginosa*, Massachusetts Institute of Technology
30. Sullivan, N. L., Tzeranis, D. S., Wang, Y., So, P. T. C., and Newman, D. K. (2011) Quantifying the dynamics of bacterial secondary metabolites by spectral multiphoton microscopy. *ACS Chemical Biology* **6**, 893-899
31. Masip, L., Veeravalli, K., and Georgioui, G. (2006) The many faces of glutathione in bacteria. *Antioxidants & Redox Signaling* **8**, 753-762
32. Huang, J., Sonnleitner, E., Ren, B., Xu, Y., and Haas, D. (2012) Catabolite repression control of pyocyanin biosynthesis at an intersection of primary and secondary metabolism in *Pseudomonas aeruginosa*. *Applied and Environmental Microbiology* **78**, 5016-5020
33. Dietrich, L. E. P., Price-Whelan, A., Petersen, A., Whiteley, M., and Newman, D. K. (2006) The phenazine pyocyanin is a terminal signalling factor in the quorum sensing network of *Pseudomonas aeruginosa*. *Molecular Microbiology* **61**, 1308-1321
34. Williams, H. D., Zlosnik, J. E. A., and Ryall, B. (2007) Oxygen, cyanide and energy generation in the cystic fibrosis pathogen *Pseudomonas aeruginosa*. *Advances in Microbial Physiology* **52**, 1-71
35. O'Donnell, V. B., Tew, D. G., Jones, O. T. G., and England, P. J. (1993) Studies on the inhibitory mechanism of iodonium compounds with special reference to neutrophil NADPH oxidase. *Biochemical Journal* **290**, 41-49
36. Carter, D. E., Aposhian, H. V., and Gandolfi, A. J. (2003) The metabolism of inorganic arsenic oxides, gallium arsenide, and arsine: a toxicochemical review. *Toxicology and Applied Pharmacology* **193**, 309-334
37. Reed, L. J. (1974) Multienzyme complexes. *Accounts of Chemical Research* **7**, 40-46
38. de Kok, A., Hengeveld, A. F., Martin, A., and Westphal, A. H. (1998) The pyruvate dehydrogenase multi-enzyme complex from Gram-negative bacteria. *Biochimica et Biophysica Acta* **1385**, 353-366
39. Gruys, K. J., Datta, A., and Frey, P. A. (1989) 2-Acetylthiamin pyrophosphate (acetyl-TPP) pH-rate profile for hydrolysis of acetyl-TPP and isolation of acetyl-TPP as a transient species in pyruvate dehydrogenase catalyzed reactions. *Biochemistry* **28**, 9071-9080
40. Corran, H. S., Green, D. E., and Straub, F. B. (1939) On the catalytic function of heart flavoprotein. *Biochemical Journal* **33**, 793-801
41. Lee, D. G., Urbach, J. M., Wu, G., Liberati, N. T., Feinbaum, R. L., Miyata, S., Diggins, L. T., He, J., Saucier, M., Déziel, E., Friedman, L., Li, L., Grills, G., Montgomery, K., Kucherlapati, R., Rahme, L. G., and Ausubel, F. M. (2006) Genomic analysis reveals that *Pseudomonas aeruginosa* virulence is combinatorial. *Genome Biology* **7**, R90

42. Winsor, G. L., Griffiths, E. J., Lo, R., Dhillon, B. K., Shay, J. A., and Brinkman, F. S. L. (2016) Enhanced annotations and features for comparing thousands of *Pseudomonas* genomes in the *Pseudomonas* genome database. *Nucleic Acids Research* **44**, D646-D653
43. Jeyaseelan, K., Guest, J. R., and Visser, J. (1980) The pyruvate dehydrogenase complex of *Pseudomonas aeruginosa* PAO. Purification, properties and characterization of mutants. *Journal of General Microbiology* **120**, 393-402
44. Burns, G., Sykes, P. J., Hatter, K., and Sokatch, J. R. (1989) Isolation of a third lipoamide dehydrogenase from *Pseudomonas putida*. *Journal of Bacteriology* **171**, 665-668
45. Sahlman, L., and Williams, C. H., Jr. (1989) Lipoamide dehydrogenase from *Escherichia coli*. Steady-state kinetics of the physiological reaction. *Journal of Biological Chemistry* **264**, 8039-8045
46. Mattevi, A., Obmolova, G., Kalk, K. H., van Berkel, W. J. H., and Hol, W. G. J. (1993) Three-dimensional structure of lipoamide dehydrogenase from *Pseudomonas fluorescens* at 2.8 Å resolution: Analysis of redox and thermostability properties. *Journal of Molecular Biology* **230**, 1200-1215
47. Mattevi, A., Obmolova, G., Sokatch, J. R., Betzel, C., and Hol, W. G. J. (1992) The refined crystal structure of *Pseudomonas putida* lipoamide dehydrogenase complexed with NAD^+ at 2.45 Å resolution. *Proteins: Structure, Function, and Bioinformatics* **13**, 336-351
48. Karplus, P. A., and Diederichs, K. (2012) Linking crystallographic model and data quality. *Science* **336**, 1030-1033
49. Brautigam, C. A., Chuang, J. L., Tomchick, D. R., Machius, M., and Chuang, D. T. (2005) Crystal structure of human dihydrolipoamide dehydrogenase: NAD^+/NADH binding and the structural basis of disease-causing mutations. *Journal of Molecular Biology* **350**, 543-552
50. Berkholz, D. S., Faber, H. R., Savvides, S. N., and Karplus, P. A. (2008) Catalytic cycle of human glutathione reductase near 1 Å resolution. *Journal of Molecular Biology* **382**, 371-384
51. Eschbach, M., Schreiber, K., Trunk, K., Buer, J., Jahn, D., and Schobert, M. (2004) Long-term anaerobic survival of the opportunistic pathogen *Pseudomonas aeruginosa* via pyruvate fermentation. *Journal of Bacteriology* **186**, 4596-4604
52. Hunter, R. C., Asfour, F., Dingemans, J., Osuna, B. L., Samad, T., Malfroot, A., Cornelis, P., and Newman, D. K. (2013) Ferrous iron is a significant component of bioavailable iron in cystic fibrosis airways. *MBio* **4**, e00557-13
53. Williamson, K. S., Richards, L. A., Perez-Osorio, A. C., Pitts, B., McInnerney, K., Stewart, P. S., and Franklin, M. J. (2012) Heterogeneity in *Pseudomonas aeruginosa* biofilms includes expression of ribosome hibernation factors in the antibiotic-tolerant subpopulation and hypoxia-induced stress response in the metabolically active population. *Journal of Bacteriology* **194**, 2062-2073
54. Wang, Y., Wilks, J. C., Danhorn, T., Ramos, I., Croal, L., and Newman, D. K. (2011) Phenazine-1-carboxylic acid promotes bacterial biofilm development via ferrous iron acquisition. *Journal of Bacteriology* **193**, 3606-3617
55. Das, T., Ibugo, A. I., Klare, W., and Manefield, M. (2016) Role of pyocyanin and extracellular DNA in facilitating *Pseudomonas aeruginosa* biofilm formation. in *Microbial Biofilms - Importance and Applications*, InTech. pp 23-42

56. Ramos, I., Dietrich, L. E. P., Price-Whelan, A., and Newman, D. K. (2010) Phenazines affect biofilm formation by *Pseudomonas aeruginosa* in similar ways at various scales. *Research in Microbiology* **161**, 187-191
57. Petrova, O. E., Schurr, J. R., Schurr, M. J., and Sauer, K. (2012) Microcolony formation by the opportunistic pathogen *Pseudomonas aeruginosa* requires pyruvate and pyruvate fermentation. *Molecular Microbiology* **86**, 819-835
58. Massey, V. (1994) Activation of molecular oxygen by flavins and flavoproteins. *Journal of Biological Chemistry* **269**, 22459-22462
59. Patel, M. S., Vettakkorumakankav, N. N., and Liu, T.-C. (1995) Dihydrolipoamide dehydrogenase: activity assays. *Methods in Enzymology* **252**, 186-195
60. Smith, P. K., Krohn, R. I., Hermanson, G. T., Mallia, A. K., Gartner, F. H., Provenzano, M. D., Fujimoto, E. K., Goeke, N. M., Olson, B. J., and Klenk, D. C. (1985) Measurement of protein using bicinchoninic acid. *Analytical Biochemistry* **150**, 76-85
61. Studier, F. W., and Moffatt, B. A. (1986) Use of bacteriophage T7 RNA polymerase to direct selective high-level expression of cloned genes. *Journal of Molecular Biology* **189**, 113-130
62. Babin, B. M., Bergkessel, M., Sweredoski, M. J., Moradian, A., Hess, S., Newman, D. K., and Tirrell, D. A. (2016) SutA is a bacterial transcription factor expressed during slow growth in *Pseudomonas aeruginosa*. *Proceedings of the National Academy of Sciences USA* **113**, E597-E605
63. Kalli, A., and Hess, S. (2012) Effect of mass spectrometric parameters on peptide and protein identification rates for shotgun proteomic experiments on an LTQ-orbitrap mass analyzer. *Proteomics* **12**, 21-31
64. Kabsch, W. (2010) XDS. *Acta Crystallographica Section D* **66**, 125-132
65. Evans, P. (2006) Scaling and assessment of data quality. *Acta Crystallographica Section D* **62**, 72-82
66. Evans, P. R., and Murshudov, G. N. (2013) How good are my data and what is the resolution? *Acta Crystallographica Section D* **69**, 1204-1214
67. Winn, M. D., Ballard, C. C., Cowtan, K. D., Dodson, E. J., Emsley, P., Evans, P. R., Keegan, R. M., Krissinel, E. B., Leslie, A. G. W., McCoy, A., McNicholas, S. J., Murshudov, G. N., Pannu, N. S., Potterton, E. A., Powell, H. R., Read, R. J., Vagin, A., and Wilson, K. S. (2011) Overview of the CCP4 suite and current developments. *Acta Crystallographica Section D* **67**, 235-242
68. McCoy, A. J., Grosse-Kunstleve, R. W., Adams, P. D., Winn, M. D., Storoni, L. C., and Read, R. J. (2007) Phaser crystallographic software. *Journal of Applied Crystallography* **40**, 658-674
69. Afonine, P. V., Grosse-Kunstleve, R. W., Echols, N., Headd, J. J., Moriarty, N. W., Mustyakimov, M., Terwilliger, T. C., Urzhumtsev, A., Zwart, P. H., and Adams, P. D. (2012) Towards automated crystallographic structure refinement with phenix.refine. *Acta Crystallographica Section D* **68**, 352-367
70. Terwilliger, T. C., Klei, H., Adams, P. D., Moriarty, N. W., and Cohn, J. D. (2006) Automated ligand fitting by core-fragment fitting and extension into density. *Acta Crystallographica Section D* **62**, 915-922
71. Emsley, P., Lohkamp, B., Scott, W. G., and Cowtan, K. (2010) Features and development of Coot. *Acta Crystallographica Section D* **66**, 486-501

Chapter 5

PROFILING THE METABOLOME OF *PSEUDOMONAS AERUGINOSA*

Abstract

Endogenous phenazine are known to alter metabolic flux in *P. aeruginosa*, but the full scope and biochemical basis of this interaction is unknown. To facilitate future studies into the metabolism of *P. aeruginosa*, I have developed several methods using high performance liquid chromatography and mass spectrometry to characterize both extracellular and intracellular metabolites. Preliminary results show that pyocyanin is not required for pyruvate secretion in *P. aeruginosa* and that pyocyanin alters the secretion of numerous other compounds. Using high-resolution LCMS, I show that pyocyanin shifts the chain-length distribution of the secreted 4-hydroxy-2-alkylquinolones such that longer chains are less abundant and shorter chains are more abundant. Quinolones are well-established signaling molecules, and so pyocyanin may indirectly affect cell-to-cell signaling via the distribution of quinolones. Pyocyanin also alters the production of certain glycerophospholipids whose precise identity has not been determined. These results are consistent with the notion that phenazines promote redox homeostasis, which might in turn promote β-oxidation and drive shifts in the fatty acid pool. I also identified several novel sulfonated phenazines and further purified a pyocyanin sulfonate from culture supernatants. These phenazines could arise from reactions with reactive sulfur species (sulfite or sulfide) that form during sulfate assimilation, raising the prospect that they might be useful markers of *in situ* sulfur metabolism in clinical samples. Finally, I have begun to extend these methods to the analysis of intracellular polar metabolites, especially those of central metabolism. Together, this method development will enable powerful new studies into the interactions between phenazines and metabolism.

Introduction

Converging evidence suggests that phenazines, the colorful redox-active molecules secreted by diverse bacteria and archaea, significantly alter the metabolic flux of *Pseudomonas aeruginosa*. For instance, during anaerobic survival on glucose, phenazine-1-carboxylic acid (PCA) stimulates the secretion of acetate and the production of ATP (1). During aerobic growth on glucose, pyocyanin stimulates pyruvate secretion in stationary phase (2). Elucidating the metabolic origins of these phenotypes requires tools to characterize both intracellular and extracellular metabolites. In this Chapter, I describe my progress towards analyzing complex mixtures of metabolites. With current technology, it is not possible to measure every molecule with a single method, and so I will discuss three different methods and preliminary insights they have given into the relationship between phenazines and metabolism in *P. aeruginosa*. The first method uses traditional chromatography for the targeted quantification of specific organic acids. The second method uses low- and high-resolution liquid chromatography and mass spectrometry (LCMS) for the untargeted identification of unknown molecules in culture supernatants. The third method, which is technically challenging and requires further optimization, extends high-resolution LCMS to the identification of polar intracellular metabolites. My preliminary results suggest that pyocyanin's metabolic effects on *P. aeruginosa* are more extensive and indirect than previously appreciated.

Results and Discussion

Methods for detecting secreted organic acids

Small organic acids, such as acetate, succinate, pyruvate, are ubiquitous intermediates in metabolism, and many are secreted by microorganisms. When grown on glucose, *P. aeruginosa* is known to secrete α-ketoglutarate during nitrogen limitation (3). It can also secrete pyruvate during glucose oxidation (4), and pyruvate secretion during the oxygen-limited stationary phase of growth is stimulated by pyocyanin (2). *P. aeruginosa* also secretes acetate, lactate, and succinate when surviving by fermentation on pyruvate (5,6), and it secretes acetate during phenazine-

mediated anaerobic survival on glucose (1). A method to quantify extracellular organic acids is therefore a versatile tool to study metabolism in *P. aeruginosa*.

My first attempts to measure organic acids in culture supernatants used ion chromatography on a Dionex DX-500 instrument (1), but this method struggled to separate acetate and lactate for quantification (Figure 1). For my compounds of interest (primarily pyruvate, acetate, lactate, and succinate), I found greater success using high performance liquid chromatography (HPLC), and so this method is not fully optimized. However, it may prove superior for quantifying other acids or for simultaneously quantifying inorganic anions (*e.g.* chloride and phosphate).

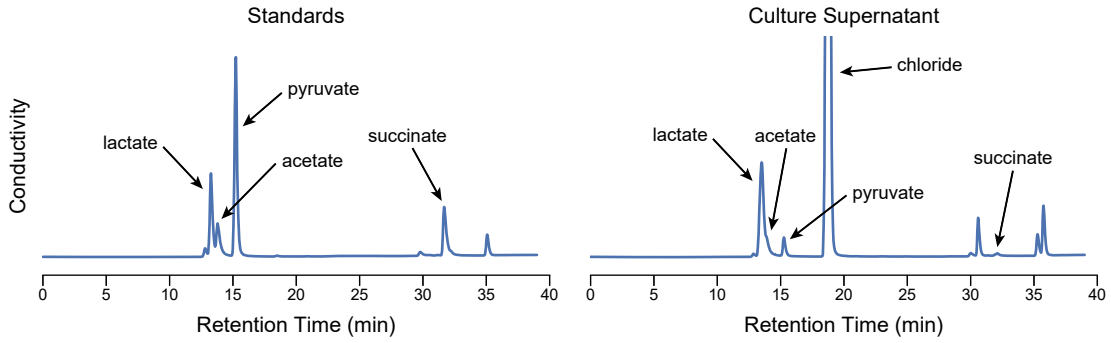

Figure 1. Separation of organic acids using ion chromatography. The indicated compounds were analyzed as described previously (1) (see Supplemental Information). (Left) Injection of a mixture of pure standards. (Right) Injection of supernatant from an anaerobic culture of *P. aeruginosa* incubated with pyruvate. Note the poor separation of lactate and acetate, which precluded an accurate quantification of acetate.

For better quantification of organic acids, HPLC using an Aminex HPX-87H (Bio-Rad) anion-exclusion column proved to be simple and effective. I have used this column on multiple instruments (Agilent 1100, Waters Alliance, and Beckman Gold) with comparable results, and it is my preferred method for studying fermentation (1). This method adequately separates pyruvate, acetate, lactate, and succinate in culture supernatants. It can also measure other acids,

including α-ketoglutarate, citrate, malate, and fumarate (Figure 2). The method uses a simple isocratic elution using 5 mM H_2SO_4 or 0.2% phosphoric acid with UV detection at 206–210 nm. For enhanced signal-to-noise and improved sensitivity, the signal at 206 nm can be referenced to 260 nm. While the overall chromatographic resolution is not as high as in the ion chromatography method (compare peak widths in Figure 1 and Figure 2), some compounds are better resolved (note the separation between pyruvate and lactate), and the relative simplicity of this method makes it easier for routine use.

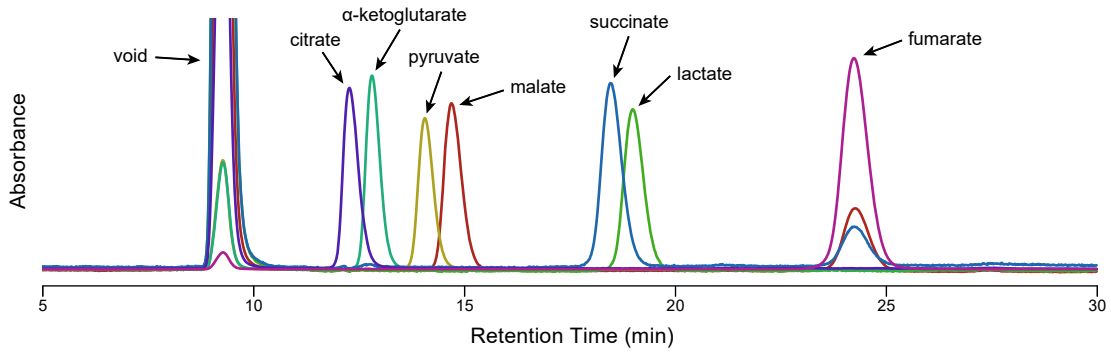

Figure 2. Separation of organic acids using HPLC. Organic acid standards (1 mM) were dissolved in minimal medium and separated on an Aminex HPX-87H column with a Beckman Gold system. Compounds were eluted isocratically using 5 mM H_2SO_4 and detected at 206 nm. The chromatograms have been rescaled so that the relevant peaks are approximately the same height. The commercial sources of malate and succinate appear to be contaminated with fumarate, which absorbs strongly at 206 nm.

Pyocyanin is not required for pyruvate secretion in P. aeruginosa

Previously it was hypothesized that pyocyanin might promote pyruvate secretion by inhibiting pyruvate dehydrogenase (2). An alternative, but not mutually exclusive, hypothesis is that pyocyanin increases the rate of glucose oxidation to pyruvate (1). I attempted to distinguish these hypotheses by measuring pyruvate secretion from different carbon sources. If pyocyanin acts by inhibiting pyruvate dehydrogenase, then only carbon sources that feed through pyruvate dehydrogenase (*e.g.* glucose, gluconate, and mannitol, but not succinate) should lead to pyruvate

secretion. I cultured *P. aeruginosa* in a minimal medium containing 20 mM glucose, 20 mM gluconate, 20 mM mannitol, or 30 mM succinate and monitored organic acid secretion in the culture supernatant using HPLC with the Aminex HPX-87H column.

Representative HPLC traces for these experiments are shown in Figure 3, along with pure pyruvate and α-ketoglutarate standards for reference. I did not detect pyruvate secretion in glucose as previously described (2); however, I sampled earlier timepoints in a medium that contained less glucose and ammonium than previously used. I detected α-ketoglutarate in both wild type and Δ*phz1/2* cultures growing on succinate and gluconate (Figure 3). I also detected pyruvate in Δ*phz1/2* cultures growing on gluconate (Figure 3). Mannitol yielded slow growth rates (generation time ~2–3 hours) and no detectable organic acid secretion. The identities of α-ketoglutarate and pyruvate were confirmed by spiking samples with pure standards and observing only a single peak, as well as by the full UV–vis spectrum of the peak which showed absorbance at ~320 nm, a characteristic of α-keto acids.

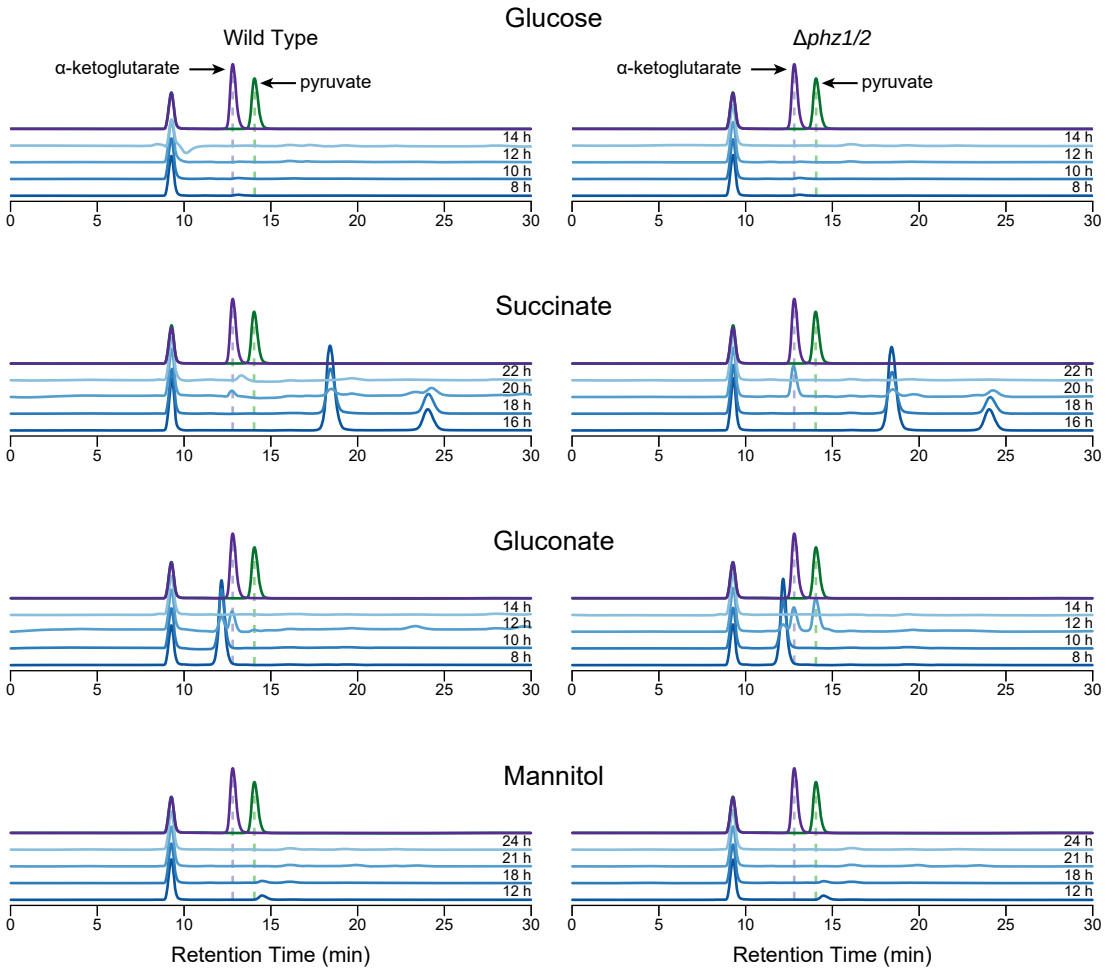

Figure 3. Representative HPLC traces of supernatants from cultures grown on the indicated carbon sources. The *y*-axis represents absorbance at 206 nm (arbitrary units). Separation was performed using an Aminex HPX-87H column. The left plots show traces from wild type cultures and the right plots show traces from Δ*phz1/2* mutant cultures. Dashed lines indicate the retention times of α-ketoglutarate (purple) and pyruvate (green) (standards at 1 mM in culture medium). The time point of sampling, measured from inoculation of the shaking flask, is shown to the right of each trace.

In shaking flasks, I also did not detect pyruvate secretion using the MOPS-buffered medium with 50 mM glucose and 93 mM NH_4Cl as originally published (2). However, in one experiment, increasing the glucose concentration in my medium to 50 mM yielded pyruvate secretion during stationary phase (Figure 4).

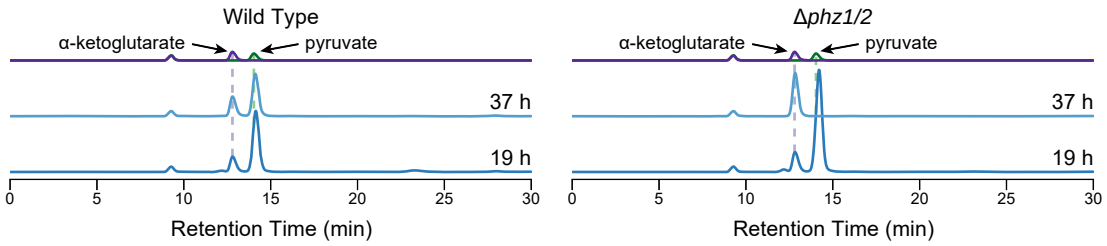

Figure 4. Pyruvate and α-ketoglutarate secretion in wild type and Δ*phz1/2* cultures with 50 mM glucose. The plots are arranged as in Figure 3.

Unfortunately, I was unable to consistently reproduce the pyruvate secretion phenotype. Hypothesizing that subtle differences in aeration affected the outcome, I tested cultures containing 20, 50, and 100 mL in 250-mL flasks, but none yielded consistent pyruvate secretion above a few micromolar. Adjusting the amount of iron in acid-washed glassware (from 7.2 μM to 30 μM), to control for variable metal concentrations adsorbed to glassware, also did not yield pyruvate secretion, nor did increasing the NH_4Cl concentration (from 9.3 mM to 30 mM).

Pyruvate secretion by *P. aeruginosa*, and its relationship to pyocyanin, appears to be more complicated than previously reported (2). The observation of pyruvate in Δ*phz1/2* cultures (Figures 3 and 4) demonstrates that pyocyanin is not required for pyruvate secretion. During aerobic growth, *P. aeruginosa* metabolizes glucose via gluconate as an intermediate (7,8), and so pyruvate secretion during growth on gluconate (Figure 3) is consistent with secretion in glucose. It is possible that subtle differences in culture conditions, such as the difference between shaking flasks (this study) and shaking tubes (2), differences in flask shape between manufacturers, or lot-to-lot variations in the chemicals used (note the trace fumarate contamination in some carbon sources (Figure 2)), lead to seemingly random variation in the total pyruvate secreted by stationary-phase cultures. In addition, the transient nature of pyruvate and α-ketoglutarate accumulation (appearing within 2 hours and disappearing within 2 hours later (Figure 3)) may lead to false-negatives. Elucidating the specific growth conditions where pyocyanin specifically

induces pyruvate secretion, and those where it does not, may yield insight into the interaction between pyocyanin and metabolism in *P. aeruginosa*.

Pyocyanin alters the secretion pattern of quinolones

While testing different growth conditions, such as changing carbon source or nitrogen availability, I observed a range of colors in the cultures including colorless, green, blue, brown, and yellow. Inexplicably, the colors sometimes varied between replicate cultures, originating from the same medium bottle, in acid-washed flasks from the same manufacturer and incubated adjacently. This was true for both wild type and Δ*phz1/2* cultures, suggesting the variation is caused partly by pigments other than phenazines. I speculated that, even if I could not reproduce pyruvate secretion, pyocyanin may regulate the secretion of other metabolites.

To explore the variation of unknown secreted compounds, I used a reversed-phase HPLC method with the Waters Atlantis T3 column. In this method, compounds are eluted in approximate order of increasing hydrophobicity. A comparison of supernatants from wild type and Δ*phz1/2* cultures grown in succinate demonstrates several differentially secreted metabolites (Figure 5a). Note that these chromatograms are shown for the wavelength 260 nm; compounds that absorb at lower wavelengths are obscured by the background of formic acid in the eluent, and so there might be additional unseen differences. Without a pure standard, it is difficult to equate the peaks to an absolute concentration.

Interestingly, I observed only trace amounts of 1-hydroxyphenazine in my cultures (Figure 5a and others not shown). This demethylated pyocyanin derivative is frequently cited as an endogenous phenazine of *P. aeruginosa* (9,10). Based on my results and a review of the literature, it seems that *P. aeruginosa* may not directly produce significant amounts of 1-hydroxyphenazine. Rather, this compound might originate from the abiotic base-catalyzed demethylation of pyocyanin. Pyocyanin biosynthesis begins with methylation of PCA to form 5MPCA by the enzyme PhzM.

This reactive intermediate is converted to pyocyanin by the oxidative decarboxylase PhzS. It has been suggested that PhzS can also act on PCA to directly produce 1-hydroxyphenazine. However, it was also noted that the Δ*phzM* mutant produces considerably less 1-hydroxyphenazine than the wild type (10), a peculiar result when one might expect this mutation to increase the PCA available for direct decarboxylation to 1-hydroxyphenazine. These experiments were performed in unbuffered Pseudomonas isolation agar or Pseudomonas broth (10). In my hands, growth of *P. aeruginosa* in such unbuffered media, including lysogeny broth (LB), leads to alkalization of the medium to pH ~9, presumably from the release of ammonium during the catabolism of amino acids in peptone or other protein digests. At basic pH, pyocyanin spontaneously demethylates to form 1-hydroxyphenazine (11). While PhzS may act slowly on PCA to form 1-hydroxyphenazine, the decreased production by the Δ*phzM* strain is readily explained if most 1-hydroxyphenazine originates from pyocyanin.

The differences observed between wild type and Δ*phz1/2* cultures (Figure 5a) might be caused by phenazines. Alternatively, phenazine biosynthesis could deplete the shikimate and chorismite pools (12), leading to indirect changes in shikimate- or chorismite-derived compounds. To test if phenazines directly alter the secretion of metabolites, I complemented Δ*phz1/2* cultures with pyocyanin at approximately the same OD_{500} where phenazine biosynthesis is induced. Some of the differences between wild type and Δ*phz1/2* cultures were recapitulated by pyocyanin addition (Figure 5b), clearly demonstrating that pyocyanin stimulates the accumulation of some metabolites and inhibits the accumulation of others. The remaining differences between wild type and Δ*phz1/2* cultures (the peak differences that weren't recapitulated by pyocyanin addition) might be caused by the other endogenous phenazines (*e.g.* phenazine-1-carboxylic acid and phenazine-1-carboxamide), but this has not been confirmed.

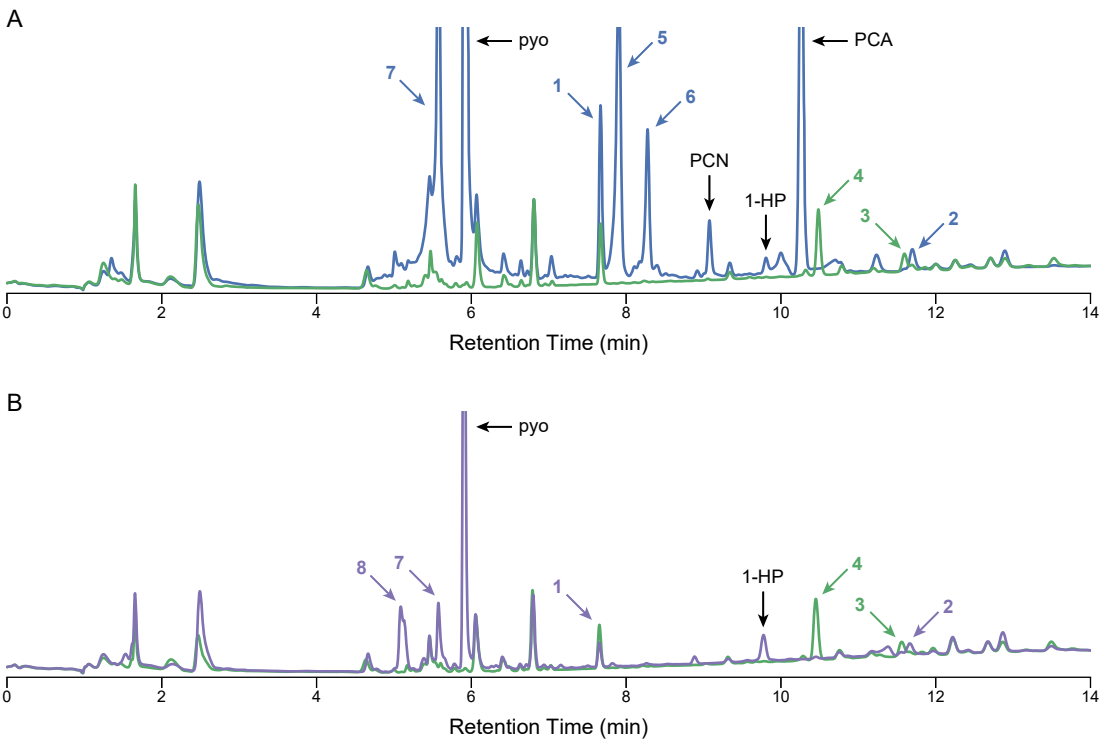

Figure 5. Analysis of succinate-grown culture supernatants using reversed-phase chromatography. The *y*-axis represents absorbance at 260 nm (arbitrary units). Peaks representing the endogenous phenazines are labeled with black arrows (pyo, pyocyanin; PCN, phenazine-1-carboxamide; PCA, phenazine-1-carboxylic acid; 1-HP, 1-hydroxyphenazine). Peaks unique to a condition are indicated with appropriately colored arrows. (A) Comparison of wild type (blue) and Δ*phz1/2* (green) culture supernatants incubated for 20 h. (B) Comparison of Δ*phz1/2* (green) and Δ*phz1/2* with exogenous pyocyanin (purple) culture supernatants. After 10 h of growth (OD_{500} ~ 1), pyocyanin was added to a concentration of 100 μM. Cultures were sampled after an additional 10 h. The stock of pyocyanin was contaminated with small amounts of 1-hydroxyphenazine. Compounds of interest are numbered in order of discussion in the main text.

To characterize the unknown compounds, I collected mass spectrometry data in the same HPLC runs with a Waters Acquity QDa detector using electrospray ionization in both positive and negative scanning modes, yielding mass information accurate to ~0.2 Da. I then analyzed representative samples with a similar chromatography method on a Waters Xevo G2-XS QTof mass spectrometer, providing mass accuracy to within 5 ppm, sufficient to establish a probable

chemical formula. By comparing masses and UV-spectra between the methods, I could assign formulas to the peaks labeled in Figure 5. I also used the XCMS package (13) to identify peaks within each dataset, identifying up to 800 putative compounds within each sample depending on the parameters used. Most of the masses represent unknown compounds with no reasonable hits in the METLIN database (14). Notable exceptions include hits for pyochelin, rhamnolipids, the Pseudomonas quinolone signal, and nucleotide monophosphates. I used short chromatography runs for the high-resolution data, making it difficult to analyze the fragmentation patterns for every identified mass, and so here I focus my discussion only on the peaks labeled in Figure 5.

Compound 1 has absorbance peaks at 270, 279, and 313 nm. It yields the ions 160.0375^{1-} and 162.0575^{1+}, consistent with the neutral formula $C_9H_7NO_2$. The UV spectrum matches precisely with that of 2,4-dihydroxyquinolone (15) (Figure 6), which has previously been detected by LC-MS/MS in *P. aeruginosa* cultures (16). When grown on glucose, this compound was nearly absent in the Δ*phz1/2* cultures but abundant in wild type cultures (data not shown).

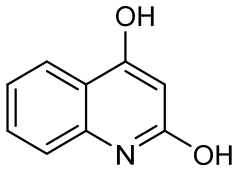

Figure 6. Structure of compound **1**, 2,4-dihydroxyquinolone.

Compound 2 has an absorbance peak at 341 nm. QDa detected the ions 260.2^{1+} and 258.3^{1-}. Xevo detected 260.1667^{1+} and 258.1470^{1-}, consistent with the neutral formula $C_{16}H_{21}NO_2$. Based on the UV-spectrum and mass, this compound is likely the Pseudomonas quinolone signal (PQS, 2-heptyl-3-hydroxy-4-quinolone) or HQNO (N-oxo-2-heptyl-4-hydroxyquinoline) (Figure 7). Further analysis suggests this peak may be an artifact of the chromatography. While two peaks of mass 260.17 were observed on the Atlantis T3 column with the QDa detector (Figure 8), only a

single peak of this mass was observed in the Xevo dataset. I have observed that several aromatic compounds, including pyocyanin, elute as multiple peaks (Figure 8), possibly because they interact with other aromatic analytes bound to the column. The samples were analyzed on the Xevo after the QDa, and so alternatively, the compound of interest (PQS or NQNO) degraded over time.

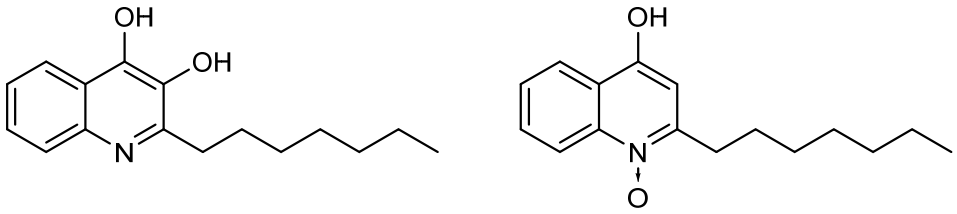

Figure 7. Possible structures of compound **2**. (Left) 2-heptyl-3-hydroxy-4-quinolone (the Pseudomonas quinolone signal, PQS). (Right) N-oxo-2-heptyl-4-hydroxyquinoline (HQNO).

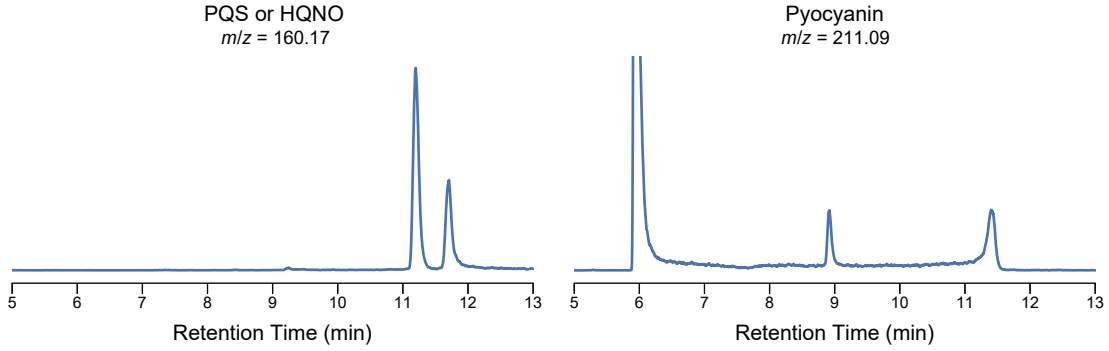

Figure 8. Potential chromatography artifacts, detected by mass spectrometry, where certain compounds elute as two or more well-defined peaks. These traces represent extracted ion chromatograms from QDa data (positive mode) with a Waters Atlantis T3 column.

Compound 3 has an absorbance peak at 338 nm. QDa detected masses of 314.0^{1+}, 298.2^{1+}, 276.2^{1+}, and 573.3^{1+}, with 276.2^{1+} being the most abundant. The high-resolution mass spectrum yielded the following ions and corresponding formulas:

+		−	
276.1609	**$C_{16}H_{22}NO_3$**	274.1454	$C_{16}H_{20}NO_3$
258.1500	$C_{16}H_{20}NO_2$	218.1549	$C_{14}H_{20}NO$
178.0500	**$C_9H_8NO_3$**	175.0271	$C_9H_5NO_3$
162.0547	**$C_9H_{10}NO_3$**	148.0400	$C_8H_6NO_2$
160.0395	**$C_9H_6NO_2$**	120.0450	C_7H_6NO
146.0599	**C_9H_8NO**	92.0506	C_6H_6N
144.0440	**C_9H_6NO**		
134.0599	C_8H_8NO		
132.0445	**C_8H_6NO**		
125.0961	$C_8H_{13}O$		
104.0498	C_7H_6N		
97.1017	C_7H_{13}		

The rows in bold illustrate all of the fragments from a previous study (17) that reported the putative structure 3-heptyl-2,3-dihydroxy-4-quinolone (Figure 9), a possible identity of this compound.

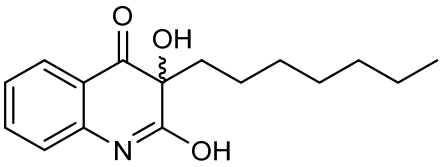

Figure 9. Putative structure of compound **3**, 3-heptyl-2,3-dihydroxy-4-quinolone, based on comparison to the mass spectrum from a previous study (17).

Compound 4 has absorbance peaks at 267 and 329 nm. QDa detected masses of 292.1^{1+} and 120.1^{1+}, and 290.2^{1-}. Xevo yielded the following ions and corresponding formulas:

+		−	
292.1554	$C_{16}H_{22}NO_4$	290.1403	$C_{16}H_{20}NO_4$
		246.1499	$C_{15}H_{20}NO_2$
		218.1549	$C_{14}H_{20}NO$
		125.0966	$C_8H_{13}O$
		92.0503	C_6H_6N

This compound eluted close to PQS (or HQNO), making it difficult to discern the appropriate fragmentation pattern in the positive channel, but it ionized well in the negative channel and gave easily identifiable fragments. The loss of CO_2 (290 → 246), a mass difference not observed in compound **5**, suggests the presence of a carboxylic acid group in a similar molecule; however, addition of a carboxylic acid to the heptyl chain produces a hypothetical molecule that is 2 Da too small to match the data. It is more abundant in the absence of pyocyanin (Figure 10).

Analysis using XCMS also revealed the following compound:

+		−	
291.1714	$C_{16}H_{23}N_2O_3$	289.1563	$C_{16}H_{21}N_2O_3$
246.1497	$C_{15}H_{20}NO_2$	271.1459	$C_{16}H_{19}N_2O_2$
147.0554	$C_8H_7N_2O$	246.1502	$C_{15}H_{20}NO_2$
130.0287	C_8H_4NO	146.0243	$C_8H_4NO_2$
120.0445	C_7H_6NO	92.0504	C_6H_6N
102.0342	C_7H_4N		
92.0501	C_6H_6N		

This compound was also more abundant in the absence of pyocyanin (Figure 10), along with a related compound with a shorter alkyl chain. These compounds may be hydroxylated and aminated derivatives of compound **5**, with the observed fragments resulting from a more complex rearrangement (17,18). Nonetheless, the smaller mass fragments are consistent with a quinolone.

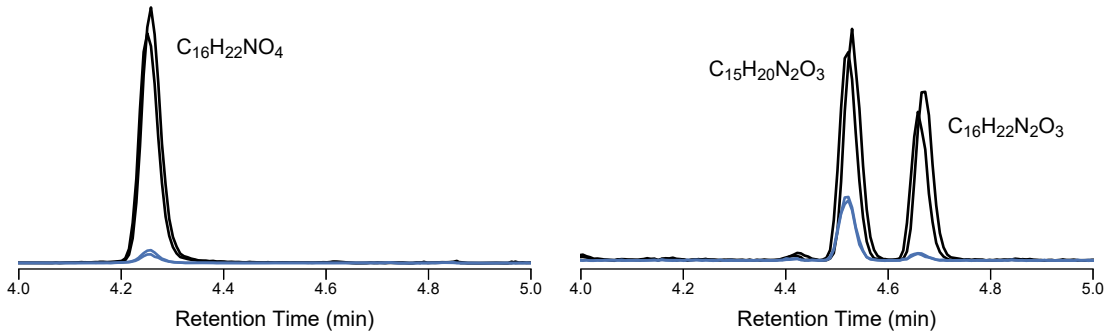

Figure 10. Derivatives of quinolones that are more abundant in the absence of pyocyanin. The compounds were detected by high-resolution LC-MS/MS. The *y*-axis represents intensity (arbitrary units). Two traces from independent succinate-grown Δ*phz1/2* supernatants are shown for the absence (black) and presence (blue) of 100 μM pyocyanin.

A more detailed inspection of the high-resolution datasets suggests that pyocyanin affects the distribution of several quinolone derivatives (Figure 11). Cultures with pyocyanin had increased amounts of shorter 4-hydroxy-2-alkylquinolones (HAQs), while cultures without pyocyanin produced more of the longer chain length derivatives (Figure 11). Cultures without pyocyanin also produced more of the putative 3-alkyl-2,3-dihydroxy-4-quinolones. The relative abundance of PQS appeared unchanged (Figure 11).

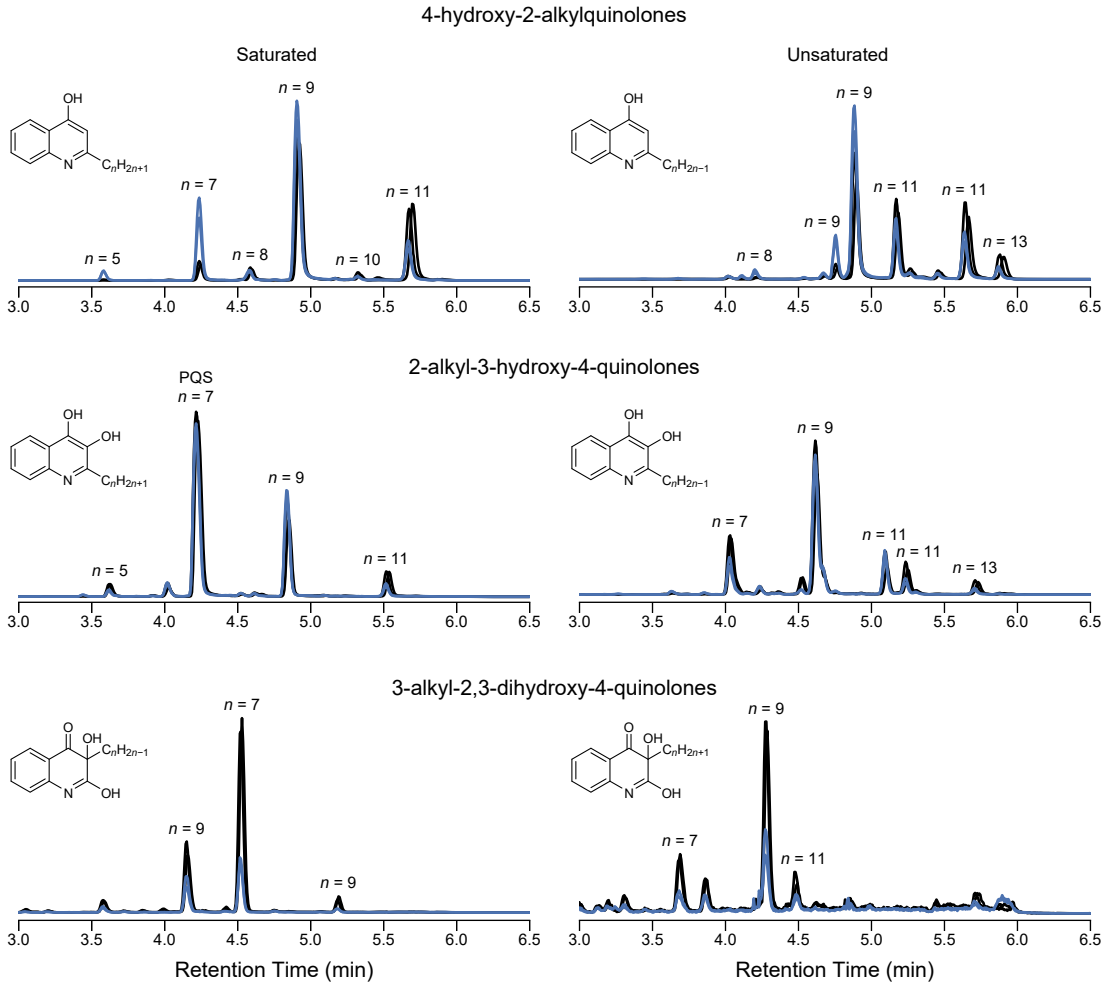

Figure 11. LCMS-based characterization of quinolones in duplicate succinate-grown Δ*phz1/2* (black) and Δ*phz1/2* + 100 μM pyocyanin (blue) culture supernatants. The *y*-axis represents signal intensity (arbitrary units).

Quinolones are signaling molecules in *P. aeruginosa* (19,20) that are required for the full expression of phenazines (21,22). The Pseudomonas quinolone signal, 2-heptyl-3-hydroxy-4-quinolone, and HHQ, 4-hydroxy-2-heptylquinolone, induce a transcriptional response by binding to the regulator MvfR, and both are required for the maximal expression of pyocyanin (23). The data presented here suggest that this regulatory network might act reciprocally, with pyocyanin altering the expression of multiple quinolones, particularly HHQ (Figure 11). While the literature focuses primarily on PQS, HHQ, and HQNO, *P. aeruginosa* produces several dozen

related molecules with varying chain lengths (17,20) (Figure 11), and here I have detected still others with additional hydroxylation and amination modifications (Figure 10). Depending on the response of MvfR to these modifications and varying chain lengths, pyocyanin could exert a regulatory effect through the action of quinolones.

Pyocyanin induces a direct transcriptional response in *P. aeruginosa* by activating the transcriptional regulator SoxR (24), but none of the reported targets appear related to quinolone biosynthesis. Quinolones are synthesized from anthranilic acid by conversion to 2-aminobenzoylacetate, which is then joined with a fatty acid and cyclized to form the 2-alkyl-4-quinolone (25). The related molecule 2,4-dihydroxyquinolone (Figure 6) originates from the spontaneous cyclization of 2-aminobenzoylacetate (25). The alkyl chain originates directly from fatty acids, as demonstrated by the incorporation of isotope-labeled octanoic acid (25). It has been further suggested that the fatty acids incorporated into quinolones originate from β-oxidation, not *de novo* synthesis, because intermediates of synthesis are covalently bound to the acyl carrier protein, and labeled decanoic acid was incorporated into quinolones with a shorter chain (25). Together, these results suggest that pyocyanin may alter the secreted quinolones (Figures 10 and 11) by altering β-oxidation and the fatty acid pool in stationary phase cultures. Because β-oxidation produces a large excess of reducing equivalents, pyocyanin might stimulate β-oxidation by promoting redox homeostasis (2), consistent with the production of shorter-chain quinolones in cultures with pyocyanin (Figure 11). In addition, XCMS identified several differences in pyocyanin-treated cultures that are likely phospholipids (not shown). Although these are only preliminary findings, requiring confirmation by additional replicates and more thorough statistics, along with investigations into the effects of carbon source and growth phase, this hypothesis is well-suited for the application of LCMS-based lipidomics and may yield new insights into the regulatory mechanisms of phenazines.

Identification and purification of novel phenazine sulfonates in culture supernatants

The remaining peaks labeled in Figure 5, compounds **5–8**, all had absorbance peaks near 269–280 nm and 393 with spectra nearly identical to that of pyocyanin. For both compounds **5** and **6**, QDa identified the same ions 334.9^{1+}, 319^{1+}, 320.0^{1+}, 255.1^{1+}, 188.2^{1+}, and 333.1^{1-}, suggesting they are isomers of each other. Xevo detected the following ions:

+		−	
335.0347	$C_{16}H_{22}NO_4$	335.0314	$C_{14}H_{11}N_2O_6S$
319.0400	**$C_{14}H_{11}N_2O_5S$**	333.0173	$C_{14}H_9N_2O_6S$
275.0495	$C_{13}H_{11}N_2O_3S$	318.0300	$C_{14}H_{10}N_2O_5S$
274.0421	$C_{13}H_{10}N_2O_3S$	317.0218	$C_{14}H_9N_2O_5S$
271.0725	$C_{14}H_{11}N_2O_4$	305.0210	$C_{13}H_9N_2O_5S$
255.0776	$C_{14}H_{11}N_2O_3$	303.0062	$C_{13}H_7N_2O_5S$
		273.0316	$C_{13}H_9N_2O_3S$
		259.0162	$C_{12}H_7N_2O_3S$
		195.0541	$C_{12}H_7N_2O$

These compounds were undetectable in the Δ*phz1/2* strain (Figure 5), even with exogenous pyocyanin, suggesting they are not adducts of pyocyanin, but their UV-spectrum and mass fragmentation into 195^{1-} (the same mass as 1-hydroxyphenazine) suggest they are phenazine derivatives. Based on a more thorough investigation into compound **7**, I propose that compounds **5** and **6** are sulfonated derivatives of 5-methylphenazine-1-carboxylic acid (5MPCA) (Figure 12), a precursor to pyocyanin (10) with a reported absorbance peak at 387 nm (26), similar to that of acidic pyocyanin.

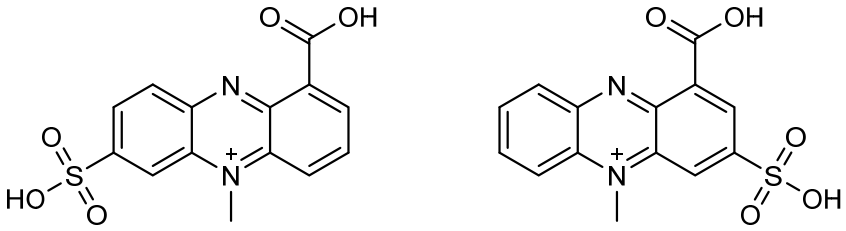

Figure 12. Proposed structures of compounds **5** and **6**.

This interpretation is consistent with the prominent mass peak at 319^{1+} (bold in the table above). The peak for 317^{1-} was barely distinguishable from the background noise in the mass spectrum, likely because the formation of three charged groups in such a small molecule is disfavored during electrospray ionization. The higher masses 335^{1+}, 333^{1-}, and 335^{1-} represent formic acid adducts of smaller fragments.

Compound 7 yielded the following ions and corresponding formulas:

+		−	
291.0447	$C_{13}H_{11}N_2O_4S$	289.0284	$C_{13}H_9N_2O_4S$
263.0490	$C_{12}H_{11}N_2O_3S$	274.0045	$C_{12}H_6N_2O_4S$
227.0824	$C_{13}H_{11}N_2O_2$	246.0112	$C_{11}H_6N_2O_3S$
210.0789	$C_{13}H_{10}N_2O$	210.0426	$C_{12}H_6N_2O_2$
199.0870	$C_{12}H_{11}N_2O$	182.0478	$C_{11}H_6N_2O$
184.0631	$C_{11}H_8N_2O$		
157.0762	$C_{10}H_9N_2$		

Based on the similarity of the UV-spectrum to that of pyocyanin, and the mass fragmentation pattern, I hypothesized that this compound is a pyocyanin sulfonate (Figure 13). This hypothesis was guided by a few key features of the mass spectrum. The fragmentation 291 → 263 represents loss of the ketone group (through a radical-mediated rearrangement) as seen in other cyclic ketones (27). I also observed the loss of the *N*-methyl group (289 → 274) and the sulfonate group

(291 → 210). Other fragmentations with the loss of SO_2 likely involve a rearrangement that retains one of the oxygen atoms of the sulfonate. I did not observe a fragment corresponding to the loss of SO_4, which argues in favor of a sulfonate (CSO_3H) rather than a sulfate ($COSO_3H$) group.

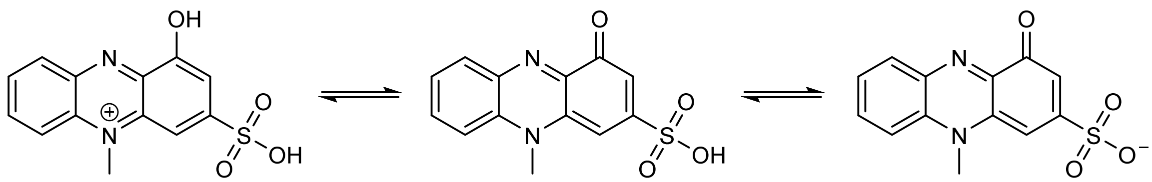

Figure 13. Proposed structure of compound **7**, pyocyanin sulfonate.

Guided by this hypothetical structure, I attempted to purify the putative pyocyanin sulfonate from a *P. aeruginosa* culture. As determined by HPLC, pyocyanin bound to the hydrophobic resin SP850 but the sulfonate derivative did not. The anion-exchange resin 1X8 (Dowex) adsorbed the remaining pyocyanin and the putative sulfonate from the SP850-treated supernatant. Washing the 1X8 resin with water eluted surprisingly pure pyocyanin (Figure 14a) in the pink (acidic) form. Following a second wash with acetonitrile, I eluted the sulfonate using 10% acetonitrile in water with 5% formic acid to yield relatively pure compound **7** (Figure 14a). The similarity between the UV–vis spectra supports the conclusion that the compound is a pyocyanin derivative (Figure 14b), and the difference in retention time establishes it as distinct from pyocyanin (Figure 14a).

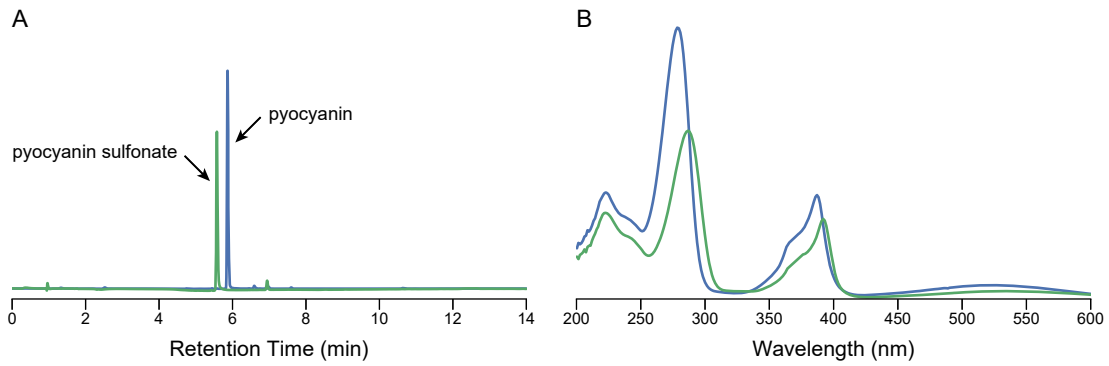

Figure 14. (A) Overlaid traces of purified pyocyanin and pyocyanin sulfonate, demonstrating a difference in retention time. The *y*-axis represents absorbance at 280 nm (arbitrary units). (B) Overlaid UV–vis spectra of pyocyanin (blue) and pyocyanin sulfonate (green). The spectra were collected from a Waters 2998 HPLC detector and represent the acidified forms of pyocyanin (in 0.1% formic acid).

I attempted to scale-up the purification by treating culture supernatant directly with 1X8, eluting the pyocyanin sulfonate with 5% formic acid, and further purifying the compound using semi-preparative HPLC. I obtained approximately 0.5 mg of compound from 2 L of glucose-grown wild type culture supernatant. I was unable to collect an interpretable ^{1}H-NMR spectrum because of many interfering peaks that resembled peptides. Contaminating proteins or small peptides may have co-purified with the anion-exchange chromatography and eluted similarly in the preparative HPLC; the analytical HPLC (Figure 14a) used formic acid in the eluent, which obscures the UV signal below approximately 250 nm, making it difficult to detect such contaminants. Further purification and a larger scale will be required to obtain NMR-confirmation of the proposed structure (Figure 13).

Finally, **compound 8** yielded the following ions and corresponding formulas:

+		−	
371.0013	$C_{13}H_{11}N_2O_7S_2$	368.9868	$C_{13}H_9N_2O_7S_2$
356.9851	$C_{12}H_9N_2O_7S_2$	354.9709	$C_{12}H_7N_2O_7S_2$
		305.0245	$C_{13}H_{19}N_2O_5S$
		290.0011	$C_{12}H_6N_2O_5S$
		262.0054	$C_{11}H_6N_2O_4S$
		260.9975	$C_{11}H_5N_2O_4S$
		241.0620	$C_{13}H_9N_2O_3$
		226.0383	$C_{12}H_6N_2O_3$
		198.0428	$C_{11}H_6N_2O_2$

Based on the mass spectrum, and analysis of compounds **5**–**7**, this compound appears to be a disulfonate derivative of pyocyanin. Closer inspection of compound **7**, the pyocyanin sulfonate, suggests it may elute as two closely related molecules with a split HPLC peak. I hypothesize that compound **8** is the doubly sulfonated version representing the two isomers of compound **7**.

Biological aromatic sulfonates, as in Figure 13, are extremely rare in the literature. A notable exception is an old report of aeruginosin B, a modification of 5MPCA by both amination and sulfonation (28), which has been claimed as only known example of a biological aromatic sulfonate (29). The sulfonated phenazines reported here (Figures 12 and 13) may have the same origin as aeruginosin B. While I have not fully elucidated the position of the sulfonate, a task which will require NMR spectroscopy and/or direct synthesis, the structures drawn (Figure 12 and 13) represent the locations known to be targeted by nucleophiles in previous reports. Specifically, it has recently become appreciated that amines and thiols can covalently conjugate to phenazines (30,31), and even ammonia can modify 5MPCA to produce aeruginosin A (26). Aeruginosin B was reported to form spontaneously from aeruginosin A in the presence of sulphite (32,33) along with a second disulfonated derivative (33). As noted in its original characterization, "aeruginosin B may be an artefact arising through the biological reduction of sulphate to sulphite and its

reaction with aeruginosin A" (33). *P. aeruginosa* assimilates sulfate by first incorporating it into ATP as 5′-adenylyl sulfate, where the sulfate is then reduced to free sulfite and then to sulfide (34), and so phenazine sulfonates may represent a side-reaction with the sulfite intermediate. Alternatively, they might be generated from a reaction with sulfide (HS^-) followed by oxidation with molecular oxygen or reactive oxygen species. As 5MPCA is an intermediate of pyocyanin synthesis, the accumulation of sulfonated 5MPCA suggests that sulfonation might protect the intermediate from the decarboxylating enzyme that produces pyocyanin (PhzS). Pyocyanin sulfonate was observed even in the Δ*phz1/2* strain, demonstrating that it can be produced from pyocyanin directly rather than deriving from sulfonated 5MPCA.

If sulfonated phenazines originate via an uncatalyzed reaction with reactive sulfur species (*e.g.* sulfite and sulfide), their accumulation in lung sputum or other infection contexts could provide a useful marker of sulfur metabolism *in situ*. Hydrogen sulfide has been detected in sputum samples from patients with cystic fibrosis (35), and hydrogen sulfide has been shown to promote antibiotic resistance in *P. aeruginosa* (36), making it a particularly noteworthy sulfur species. In contrast to the direct detection of sulfur species, reaction products with phenazines (or other molecules) could give a preserved record of sulfite or sulfide accumulation over time. Extraction of such compounds from complex samples may prove difficult. Phenazines are generally extracted using organic solvents such as chloroform or ethyl acetate, but the sulfonated derivatives and 5MPCA are highly water soluble, possibly explaining why the diversity of sulfonated phenazines has not been reported before. However, phenazines have been quantified directly from filtered sputum (37), and so detection by LCMS might enable a simple path to sulfonate detection in complex clinical samples.

Detection of intracellular polar metabolites

HPLC often utilizes columns containing C18-derivatized silica ("reversed phase"), which provides excellent chromatography for hydrophobic molecules using solvents that are compatible with mass spectrometry. A major technical hurdle for the analysis of small polar molecules (*e.g.* pyruvate, ATP, glucose) is their poor retention on traditional C18 columns. While alternative separations are possible based on underivatized silica ("normal phase"), ion-exchange, or ion-exclusion, these methods generally involve solvents, additives, or salt concentrations that are incompatible with mass spectrometry.

Hydrophilic interaction liquid chromatography (HILIC) has gained popularity for its ability to separate polar compounds for mass spectrometry. In HILIC, a column derivatized with polar headgroups (*e.g.* amides, amines, carboxylates) is equilibrated with organic solvent containing a small portion of water. The water preferentially associates with the polar groups in the column, providing a water-enriched layer that polar analytes can partition into. Polar analytes can then be eluted using an increasing concentration of water. In the case of charged head groups (*e.g.* amines and carboxylates), this can be combined with weak ion exchange for a hybrid mode of chromatography. Several groups have successfully applied such a hybrid HILIC-anion exchange approach for the quantification of polar metabolites. Here I briefly report my efforts towards adapting this method to the instrumentation available at Caltech.

The published method (38), developed a decade ago, uses a long (250 mm) Phenomenex Luna NH_2 column with a relatively large particle size (5 μm). To fully utilize the improved separations available on more modern UPLC instruments, I attempted a similar method using a shorter (150 mm) column with a smaller particle size (3 μm). This column provided unacceptably long retention times for multiply phosphorylated compounds (*e.g.* ATP), which translated to poor sensitivity, but many compounds behaved well. Increasing the pH to ~9.6 (to reduce the portion

of protonated NH_2 groups on the column) enabled faster elution and better sensitivity for negatively charged compounds.

Using this optimized method (described in Materials and Methods), I have detected many intracellular metabolites from crude extractions with minimal sample preparation. The extracted ion chromatograms for representative metabolites are shown in Figure 15. However, detailed comparisons between pyocyanin treated and untreated Δ*phz1/2* cultures have been unsuccessful. I have struggled to obtain suitable sensitivity for many metabolites (*e.g.* succinate and other TCA cycle intermediates), possibly due to ion suppression from the ammonium acetate in the method. Analysis with XCMS often detects differences in compounds that are likely glycerophospholipids, but their precise structure is unknown. In addition, I have observed that while organic solvents solubilize nearly the entire pellet from *E. coli* cultures, they leave behind most *P. aeruginosa* cell material. Extraction from filters also fails to solubilize most of the visible *P. aeruginosa* colony growth, suggesting that the poor sensitivity is a symptom of poor extraction. Over-extraction can also reduce sensitivity through ion suppression (39), and so extraction efficiency will likely need to be optimized for the compounds of interest.

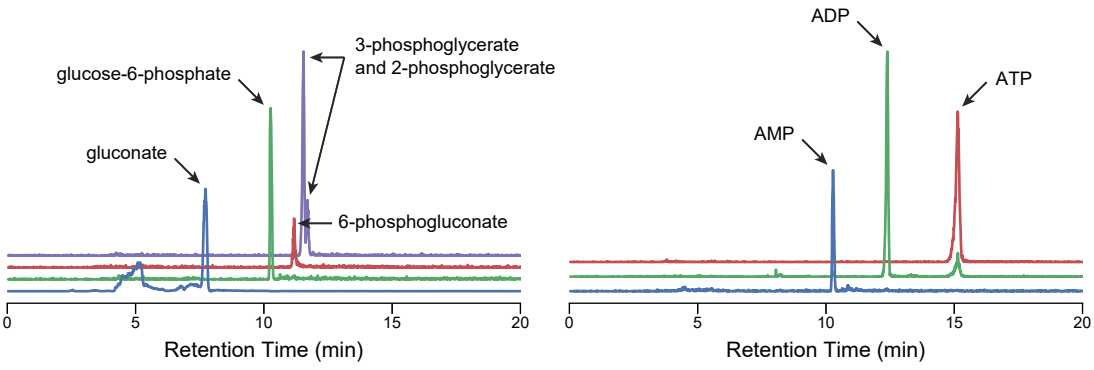

Figure 15. Extracted ion chromatograms for representative metabolites (left, intermediates of glycolysis; right, nucleotide phosphates) from *P. aeruginosa*. The *y*-axis represents signal intensity (arbitrary units).

Despite the technical challenges, my preliminary results suggest a suitable method for intracellular polar metabolite characterization in *P. aeruginosa* is within reach. Such a method will allow absolute quantification (40) (via ^{13}C labeling with coinjection of ^{12}C standards) or direct comparisons between two conditions (by mixing ^{12}C-labeled samples with ^{13}C-labeled samples). This will enable direct measurements of metabolic flux and any changes induced by phenazines. I predict that phenazines will preferentially affect the flux through specific pathways, which will indicate potential enzyme–phenazine interactions and may even reveal the relevant phenazine reductases *in vivo*.

Conclusions

Metabolomics is a powerful discovery tool. Using a simple HPLC method that works on virtually any instrument, organic acid quantification in culture supernatants can be a routine procedure. Although the relationship between pyocyanin and pyruvate secretion is still unclear, organic acid analysis nonetheless revealed the qualitative fact that pyocyanin is not essential for pyruvate secretion. While it is less accessible and costlier to operate, HPLC with high resolution mass spectrometry revealed an astounding number of unknown compounds secreted by *P. aeruginosa*. By comparing two conditions (with and without pyocyanin) to winnow the list to differentially secreted compounds, I identified quinolone secretion as a potential indirect target of pyocyanin. Using similar analyses in different comparisons, LC-MS/MS will likely be a cornucopia of low-hanging fruit for follow-up study. With additional optimization, this approach can be extended to *in vivo* metabolites and metabolic flux studies, providing a new and powerful tool to study the physiological effects of phenazines.

Materials and Methods

Strains and Culture Conditions

The two *P. aeruginosa* strains used were wild type PA14 (41) and the mutant Δ*phz1/2* (24), which has clean deletions in the *phzA1B1C1D1E1F1G1* and *phzA2B2C2D2E2F2G2* operons and does not produce endogenous phenazine-1-carboxylic acid. These strains were cultured as previously described (5) (repeated here from Chapter 4). For routine culturing, *P. aeruginosa* was maintained with lysogeny broth containing 10 g/L tryptone, 5 g/L yeast extract, and 10 g/L sodium chloride. Solid agar plates contained 15 g/L agar. The minimal medium contained 14.15 mM KH_2PO_4, 35.85 mM K_2HPO_4, 42.8 mM NaCl, 9.3 mM NH_4Cl, 1 mM $MgSO_4$, 7.5 μM $FeCl_2{\cdot}4H_2O$, 0.5 μM $ZnCl_2$, 0.5 μM $MnCl_2{\cdot}4H_2O$, 0.1 μM H_3BO_3, 0.8 μM $CoCl_2{\cdot}6H_2O$, 0.01 μM $CuCl_2{\cdot}2H_2O$, 0.1 μM $NiCl_2{\cdot}6H_2O$, and 0.15 μM Na_2MoO_4. The minimal medium was sterilized by autoclaving; to avoid precipitation, the metals were prepared as a separate solution (1000×) and added immediately prior to inoculation. The carbon source was also added after autoclaving (to a final concentration of 20 or 50 mM glucose, 30 mM disodium succinate, 20 mM sodium gluconate, or 20 mM mannitol).

For metabolite analysis, a 5-mL culture was grown overnight to an OD_{500} of at least 1.0. The culture was then diluted to an OD_{500} of 0.01 in 50 mL of fresh medium in a 250-mL flask (VWR #10536-914 or Fisher #FB500250) covered with aluminum foil. All liquid cultures were incubated in a New Brunswick Innova 44R incubator at 37 °C shaking at 250 rpm (2.54 cm stroke length).

Ion Chromatography

Ion chromatography was performed as previously described (1) (Chapter 3).

Organic Acid Analysis

For sample collection, 1 mL of culture was centrifuged for 2 min at 16,873×g. To inhibit microbial growth, 600 μL of sample was mixed with 600 μL of 2% phosphoric acid. The sample was

incubated at 4 °C and precipitated material (primarily phenazine-1-carboxylic acid) was removed by additional centrifugation for 2 min at 16,873×g, and 1 mL of the supernatant was transferred to an HPLC sample vial.

Analysis was performed using a Beckman Gold HPLC equipped with a model 126P solvent module, a model 168 photodiode array detector, and a model 508 autosampler. The column used was an Aminex HPX-78H (Bio-Rad) ion exclusion column (7.8×300 mm, 9 μm particle size). Organic acids were separated isocratically at 0.4 mL/min using 5 mM H_2SO_4 in water with a sample injection volume of 20 μL. Detection was performed at 206 nm referenced to 260 nm. The total run time per sample was 30 min. Similar separations could be performed on an Agilent 1100 system as described previously (1) (Chapter 3) or on a Waters Alliance system with a 2695 separations module and a 2998 photodiode array detector. An eluent with 0.2% phosphoric acid performed similarly to 5 mM sulfuric acid on the Alliance system.

Supernatant Analysis

To analyze other compounds in culture supernatants, samples were collected as for organic acid analysis except that 2% formic acid was used instead of 2% phosphoric acid. Analysis was performed using a Waters Alliance system with a 2695 separations module, a 2998 photodiode array detector, and a QDa quadrupole mass spectrometer detector (connected to the outlet of the photodiode array detector). The column used was a Waters Atlantis T3 C18 column (2.1×100 mm, 3 μm particle size) equipped with a VanGuard cartridge holder and Atlantis T3 VanGuard cartridge. The injection volume was 5 μL and the flow rate was 0.3 mL/min. Solvents A and B both contained 10 mM ammonium formate adjusted to pH 3.0 with formic acid, with A being 100% water and B being 20% water and 80% acetonitrile. Compounds were eluted using a linear gradient of 0% to 100% B over 0–10 min, 100% B over 10–12 min, and 0% B over 12–20 min. UV–vis data were collected from 200 to 600 nm on the 2998 photodiode array detector. Mass

scans from 50 to 700 Da in both positive and negative ionization modes were collected simultaneously using the QDa detector with a cone voltage of 5 V and a capillary voltage of 1.5 kV. The instrument was controlled using the software Empower (Waters).

Supernatant Analysis by High Resolution LC-MS/MS

Representative samples from the culture supernatants were additionally analyzed on a Waters Acquity I-Class system with an Acquity UPLC PDA detector and a Xevo G2-XS QToF mass spectrometer. The column used was a Waters Acquity HSS T3 column (2.1×100 mm, 1.8 μm particle size). The injection volume was 2 μL and the flow rate was 0.3 mL/min. The column was maintained at 30 °C using an Acquity UPLC column heater. Solvent A was 0.1% formic acid in water and solvent B was 0.1% formic acid in acetonitrile. Compounds were eluted using a linear gradient of 0% to 90% B over 0–5 min, 90% B over 5–5.5 min, and 0% B over 5.5–8 min. UV–vis data were collected from 200 to 500 nm on the PDA detector. Mass scans from 50 Da to 800 Da in positive and negative ionization modes were collected in separate runs using the Xevo QToF detector with a cone voltage of 15 V and a capillary voltage of 2.5 kV. A second data channel was also simultaneously collected using a collision energy of 30 eV. The desolvation temperature was 550 °C and the desolvation gas flow rate was 800 L/h. A solution of 20 pg/μL leucine enkephalin was used as the LockSpray solution. The instrument was controlled using the software MassLynx (Waters).

Intracellular Metabolite Analysis

To minimize metabolic perturbations during extraction, *P. aeruginosa* was cultured on filter discs similarly to a previously described method for *E. coli* (39), except that a smaller 47 mm Nylon filter with a 0.2 μm pore size (Millipore) was used. Cultures were grown in minimal medium containing 20 mM glucose as described above, and 2 mL of culture was filtered onto the disc. The disc was then placed onto an agar plate containing minimal medium with 20 mM glucose and 15

g/L noble agar. Filter cultures were grown for 4 h or 18 h at 37 °C. Metabolite extraction was performed using a mixture of 20:40:40 water:methanol:acetonitrile with 1% formic acid, similar to the previously described method (39). The filters were placed cell-side down into a dish containing 2 mL of extraction solution at −20 °C. After 15 min of incubation in the freezer, the solution was collected, centrifuged for 5 min at 16,873×g at 4 °C, and 1 mL was transferred to an autosampler vial.

Metabolite analysis was performed on the same Waters Acquity system with a Xevo G2-XS QToF detector. The column used was a Phenomenex Luna NH_2 column (2.0×150 mm, 3 μm particle size). The injection volume was 5 μL and the flow rate was 0.25 mL/min. The injection purge solution was 80:20 acetonitrile:water. Solvent A was 20 mM ammonium acetate and 40 mM ammonium hydroxide (pH ~9.6) in 90% water and 10% acetonitrile. Solvent B was 20 mM ammonium acetate and 40 mM ammonium hydroxide in 20% water and 80% acetonitrile. Compounds were eluted using a linear gradient of 85% to 0% B over 0–10 min, 0% B over 10–20 min, and 85% B over 20–30 min.

Data Analysis with XCMS

The XCMS package (13) was used to identify differences between duplicate pyocyanin treated and untreated Δ*phz1/2* cultures. Lock mass corrected chromatograms were exported using DataBridge (Waters) to the CDF format for processing by XCMS. Mass peaks were identified using the centWave method with a peak width of 5–10 s, noise cutoff of 1000, a signal-to-noise cutoff of 100, and a ppm setting of 10. Retention times were corrected by allowing up to 4 missing or extra peaks.

Acknowledgements

This study was made possible by the Caltech Environmental Analysis Center, which provided essential instrument access and training, especially for the high-resolution mass spectrometry.

Literature Cited

1. Glasser, N. R., Kern, S. E., and Newman, D. K. (2014) Phenazine redox cycling enhances anaerobic survival in *Pseudomonas aeruginosa* by facilitating generation of ATP and a proton-motive force. *Molecular Microbiology* **92**, 399-412
2. Price-Whelan, A., Dietrich, L. E. P., and Newman, D. K. (2007) Pyocyanin alters redox homeostasis and carbon flux through central metabolic pathways in *Pseudomonas aeruginosa* PA14. *Journal of Bacteriology* **189**, 6372-6381
3. Duncan, M. G., and Campbell, J. J. R. (1962) Oxidative assimilation of glucose by *Pseudomonas aeruginosa*. *Journal of Bacteriology* **84**, 784-792
4. Tomlinson, G. A., and Campbell, J. J. R. (1963) Patterns of oxidative assimilation in strains of *Pseudomonas* and *Achromobacter*. *Journal of Bacteriology* **86**, 434-444
5. Glasser, N. R., Wang, B. X., Hoy, J. A., and Newman, D. K. (2017) The pyruvate and α-ketoglutarate dehydrogenase complexes of *Pseudomonas aeruginosa* catalyze pyocyanin and phenazine-1-carboxylic acid reduction via the subunit dihydrolipoamide dehydrogenase. *Journal of Biological Chemistry* **292**, 5593-5607
6. Eschbach, M., Schreiber, K., Trunk, K., Buer, J., Jahn, D., and Schobert, M. (2004) Long-term anaerobic survival of the opportunistic pathogen *Pseudomonas aeruginosa* via pyruvate fermentation. *Journal of Bacteriology* **186**, 4596-4604
7. Hunt, J. C., and Phibbs, P. V. (1983) Regulation of alternate peripheral pathways of glucose catabolism during aerobic and anaerobic growth of *Pseudomonas aeruginosa*. *Journal of Bacteriology* **154**, 793-802
8. Norris, F. C., and Campbell, J. J. R. (1949) The intermediate metabolism of *Pseudomonas aeruginosa*: the application of paper chromatography to the identification of gluconic and 2-ketogluconic acids, intermediates in glucose oxidation. *Canadian Journal of Research* **27c**, 253-261
9. Price-Whelan, A., Dietrich, L. E. P., and Newman, D. K. (2006) Rethinking 'secondary' metabolism: physiological roles for phenazine antibiotics. *Nature Chemical Biology* **2**, 71-78
10. Mavrodi, D. V., Bonsall, R. F., Delaney, S. M., Soule, M. J., Phillips, G., and Thomashow, L. S. (2001) Functional analysis of genes for biosynthesis of pyocyanin and phenazine-1-carboxamide from *Pseudomonas aeruginosa* PAO1. *Journal of Bacteriology* **183**, 6454-6465
11. Watson, D., MacDermot, J., Wilson, R., Cole, P. J., and Taylor, G. W. (1986) Purification and structural analysis of pyocyanin and 1-hydroxyphenazine. *European Journal of Biochemistry* **159**, 309-313
12. McDonald, M., Mavrodi, D. V., Thomashow, L. S., and Floss, H. G. (2001) Phenazine biosynthesis in *Pseudomonas fluorescens*: branchpoint from the primary shikimate biosynthetic pathway and role of phenazine-1,6-dicarboxylic acid. *Journal of the American Chemical Society* **123**, 9459-9460
13. Smith, C. A., Want, E. J., O'Maille, G., Abagyan, R., and Siuzdak, G. (2006) XCMS: Processing mass spectrometry data for metabolite profiling using nonlinear peak alignment, matching, and identification. *Analytical Chemistry* **78**, 779-787
14. Smith, C. A., O'Maille, G., Want, E. J., Qin, C., Trauger, S. A., Brandon, T. R., Custodio, D. E., Abagyan, R., and Siuzdak, G. (2005) METLIN: a metabolite mass spectral database. *Ther Drug Monit* **27**, 747-51

15. Rouge, P., Cornu, A., Biesse-Martin, A.-S., Lyan, B., Rochut, N., and Graulet, B. (2013) Identification of quinoline, carboline and glycinamide compounds in cow milk using HRMS and NMR. *Food Chemistry* **141**, 1888-1894
16. Lépine, F., Dekimpe, V., Lesic, B., Milot, S., Lesimple, A., Mamer Orval, A., Rahme Laurence, G., and Déziel, E. (2007) PqsA is required for the biosynthesis of 2,4-dihydroxyquinoline (DHQ), a newly identified metabolite produced by *Pseudomonas aeruginosa* and *Burkholderia thailandensis*. in *Biological Chemistry*
17. Lépine, F., Milot, S., Déziel, E., He, J., and Rahme, L. G. (2004) Electrospray/mass spectrometric identification and analysis of 4-hydroxy-2-alkylquinolines (HAQs) produced by *Pseudomonas aeruginosa*. *Journal of the American Society for Mass Spectrometry* **15**, 862-869
18. Clugston, D. M., and MacLean, D. B. (1966) Mass spectra of oxygenated quinolines. *Canadian Journal of Chemistry* **44**, 781-788
19. McKnight, S. L., Iglewski, B. H., and Pesci, E. C. (2000) The Pseudomonas quinolone signal regulates rhl quorum sensing in *Pseudomonas aeruginosa*. *Journal of Bacteriology* **182**, 2702-2708
20. Déziel, E., Lépine, F., Milot, S., He, J., Mindrinos, M. N., Tompkins, R. G., and Rahme, L. G. (2004) Analysis of P*seudomonas aeruginosa* 4-hydroxy-2-alkylquinolines (HAQs) reveals a role for 4-hydroxy-2-heptylquinoline in cell-to-cell communication. *Proceedings of the National Academy of Sciences of the United States of America* **101**, 1339-1344
21. Recinos, D. A., Sekedat, M. D., Hernandez, A., Cohen, T. S., Sakhtah, H., Prince, A. S., Price-Whelan, A., and Dietrich, L. E. P. (2012) Redundant phenazine operons in *Pseudomonas aeruginosa* exhibit environment-dependent expression and differential roles in pathogenicity. *Proceedings of the National Academy of Sciences* **109**, 19420-19425
22. Gallagher, L. A., McKnight, S. L., Kuznetsova, M. S., Pesci, E. C., and Manoil, C. (2002) Functions required for extracellular quinolone signaling by *Pseudomonas aeruginosa*. *Journal of Bacteriology* **184**, 6472-6480
23. Xiao, G., Déziel, E., He, J., Lépine, F., Lesic, B., Castonguay, M.-H., Milot, S., Tampakaki, A. P., Stachel, S. E., and Rahme, L. G. (2006) MvfR, a key *Pseudomonas aeruginosa* pathogenicity LTTR-class regulatory protein, has dual ligands. *Molecular Microbiology* **62**, 1689-1699
24. Dietrich, L. E. P., Price-Whelan, A., Petersen, A., Whiteley, M., and Newman, D. K. (2006) The phenazine pyocyanin is a terminal signalling factor in the quorum sensing network of *Pseudomonas aeruginosa*. *Molecular Microbiology* **61**, 1308-1321
25. Dulcey, Carlos E., Dekimpe, V., Fauvelle, D.-A., Milot, S., Groleau, M.-C., Doucet, N., Rahme, Laurence G., Lépine, F., and Déziel, E. (2013) The end of an old hypothesis: The *Pseudomonas* signaling molecules 4-hydroxy-2-alkylquinolines derive from fatty acids, not 3-ketofatty acids. *Chemistry & Biology* **20**, 1481-1491
26. Hansford, G. S., Holliman, F. G., and Herbert, R. B. (1972) Pigments of *Pseudomonas* species. Part IV. In vitro and in vivo conversion of 5-methylphenazinium-1-carboxylate into aeruginosin A. *Journal of the Chemical Society, Perkin Transactions 1*, 103-105
27. Demarque, D. P., Crotti, A. E. M., Vessecchi, R., Lopes, J. L. C., and Lopes, N. P. (2016) Fragmentation reactions using electrospray ionization mass spectrometry: an important tool for the structural elucidation and characterization of synthetic and natural products. *Natural Product Reports* **33**, 432-455

28. Herbert, R. B., and Holliman, F. G. (1964) Aeruginosin B—A naturally occuring phenazinesulphonic acid. *Proceedings of the Chemical Society*, 19
29. Kertesz, M. A. (2000) Riding the sulfur cycle—metabolism of sulfonates and sulfate esters in Gram-negative bacteria. *FEMS Microbiology Reviews* **24**, 135-175
30. Heine, D., Sundaram, S., Beudert, M., Martin, K., and Hertweck, C. (2016) A widespread bacterial phenazine forms S-conjugates with biogenic thiols and crosslinks proteins. *Chemical Science* **7**, 4848-4855
31. Morales, D. K., Jacobs, N. J., Rajamani, S., Krishnamurthy, M., Cubillos-Ruiz, J. R., and Hogan, D. A. (2010) Antifungal mechanisms by which a novel *Pseudomonas aeruginosa* phenazine toxin kills *Candida albicans* in biofilms. *Molecular Microbiology* **78**, 1379-1392
32. Bentley, R. K., and Holliman, F. G. (1966) Aeruginosin B-A synthesis. *Chemical Communications (London)*, 312a-312a
33. Bentley, R. K., and Holliman, F. G. (1970) Pigments of *Pseudomonas* species. Part III. The synthesis of demethylaeruginosin B and aeruginosin B. *Journal of the Chemical Society C: Organic*, 2447-2457
34. Bick, J. A., Dennis, J. J., Zylstra, G. J., Nowack, J., and Leustek, T. (2000) Identification of a new class of 5′-adenylylsulfate (APS) reductases from sulfate-assimilating bacteria. *Journal of Bacteriology* **182**, 135-142
35. Cowley, E. S., Kopf, S. H., LaRiviere, A., Ziebis, W., and Newman, D. K. (2015) Pediatric cystic fibrosis sputum can be chemically dynamic, anoxic, and extremely reduced due to hydrogen sulfide formation. *mBio* **6**
36. Shatalin, K., Shatalina, E., Mironov, A., and Nudler, E. (2011) H_2S: A universal defense against antibiotics in bacteria. *Science* **334**, 986
37. Hunter, R. C., Klepac-Ceraj V Fau - Lorenzi, M. M., Lorenzi Mm Fau - Grotzinger, H., Grotzinger H Fau - Martin, T. R., Martin Tr Fau - Newman, D. K., and Newman, D. K. Phenazine content in the cystic fibrosis respiratory tract negatively correlates with lung function and microbial complexity.
38. Bajad, S. U., Lu, W., Kimball, E. H., Yuan, J., Peterson, C., and Rabinowitz, J. D. (2006) Separation and quantitation of water soluble cellular metabolites by hydrophilic interaction chromatography-tandem mass spectrometry. *Journal of Chromatography A* **1125**, 76-88
39. Rabinowitz, J. D., and Kimball, E. (2007) Acidic acetonitrile for cellular metabolome extraction from *Escherichia coli*. *Analytical Chemistry* **79**, 6167-6173
40. Bennett, B. D., Yuan, J., Kimball, E. H., and Rabinowitz, J. D. (2008) Absolute quantitation of intracellular metabolite concentrations by an isotope ratio-based approach. *Nature Protocols* **3**, 1299-1311
41. Rahme, L. G., Stevens, E. J., Wolfort, S. F., Shao, J., Tompkins, R. G., and Ausubel, F. M. (1995) Common virulence factors for bacterial pathogenicity in plants and animals. *Science* **268**, 1899-902

Chapter 6

PYOCYANIN DEGRADATION

This chapter is adapted from:

Costa, K. C., Glasser, N. R., Conway, S. J., and Newman, D. K. (2017) Pyocyanin degradation by a tautomerizing demethylase inhibits *Pseudomonas aeruginosa* biofilms. *Science* **355** (6321), 170-173.

My specific contributions were assisting with the PodA protein crystallization and solving the X-ray crystal structure.

Abstract

The opportunistic pathogen *Pseudomonas aeruginosa* produces colorful redox-active metabolites called phenazines, which underpin biofilm development, virulence and clinical outcomes. Though phenazines exist in many forms, the best studied is pyocyanin. Here, we describe pyocyanin demethylase (PodA), a hitherto uncharacterized protein that oxidizes the pyocyanin methyl group to formaldehyde and reduces the pyrazine ring via an unusual tautomerizing demethylation reaction. Treatment with PodA disrupts *P. aeruginosa* biofilm formation similarly to DNase, suggesting interference with the pyocyanin-dependent release of extracellular DNA into the matrix. PodA-dependent pyocyanin demethylation also restricts established biofilm aggregate populations experiencing anoxic conditions. Together, these results show that modulating extracellular redox-active metabolites can influence the fitness of biofilms.

Main text

Bacteria from phylogenetically diverse taxa secrete colorful redox-active metabolites, such as the well-studied phenazines produced by multiple species, including *Pseudomonas aeruginosa* (*1, 2*)

(Fig. 1A,B). Phenazines can be toxic to other cells but also benefit their producers by facilitating extracellular electron transfer and survival in anoxic environments (*3-6*). These latter functions support the growth of antibiotic-resistant biofilms, and *P. aeruginosa* mutants that cannot make phenazines are defective in biofilm development (*5*). Accordingly, we reasoned that selectively manipulating phenazines might present a means to control biofilms. One way to influence extracellular metabolites is through active modification or degradation by other organisms (*7-9*). Recently, we described a group of mycobacteria that enzymatically degrade phenazines and identified genes that catalyze distinct steps in degradation (*9*). Here, we focus on the structure and function of a previously uncharacterized protein from *Mycobacterium fortuitum* encoded by MFORT_14352 (NCBI Accession number: EJZ13467) that catalyzes pyocyanin (PYO) degradation (*9*).

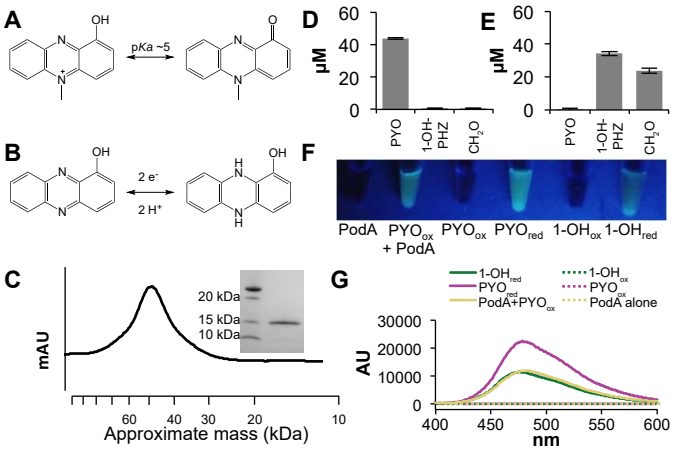

Figure 1. Biochemical analysis of the PodA reaction. PodA catalyzes the demethylation of PYO (**A**) to reduced 1-OH-PHZ (**B**). (**C**) $PodA_{30\text{-}162}$ purifies as a trimer by gel filtration chromatography (45.6 kDa). Inset is a denaturing gel demonstrating the size of monomeric $PodA_{30\text{-}162}$. Incubations of $PodA_{30\text{-}162}$ with PYO show the conversion of the starting material (**D**) to 1-OH-PHZ and formaldehyde (**E**). Data are average measurements from six reactions and error bars represent one standard deviation around the mean. Formaldehyde is derivatized to facilitate detection; the derivatization competes with other compounds in the mixture so stoichiometric production was not observed. (**F**) $PodA_{30\text{-}162}$ is active under anoxic conditions, and the PYO containing reaction mixture fluoresces under UV illumination. This fluorescent product has an emission spectrum (250 nm excitation) consistent with a reduced phenazine (**G**). While both reduced PYO and 1-OH-PHZ have similar emission maxima (50 µM phenazine), the magnitude of the peak is consistent with the generation of reduced 1-OH-PHZ by $PodA_{30\text{-}162}$.

To characterize its activity, we purified a heterologously expressed, truncated version of this protein (lacking a predicted N-terminal, membrane-spanning helix (*10*)), hereafter referred to as $PodA_{30\text{-}162}$ (PYO demethylase), from *Escherichia coli* (Fig. 1C). $PodA_{30\text{-}162}$ converts PYO to 1-hydroxyphenazine (1-OH-PHZ) and formaldehyde (Fig. 1D,E), indicating that it functions as a demethylase. Generally, enzyme-catalyzed *N*-demethylations proceed by oxidation of the methyl group to formaldehyde with electron transfer to a bound cofactor or iron-sulfur cluster (*11, 12*). Surprisingly, we found that $PodA_{30\text{-}162}$ generates 1-OH-PHZ in the absence of either flavin or 2-oxoglutarate, which are required for most known *N*-demethylases (Fig. S1). Additionally, $PodA_{30\text{-}162}$ functions under anoxic conditions, suggesting a mechanism distinct from the oxygen-

dependent Rieske-iron type demethylases (*13*). Kinetic analysis suggests that PodA is a high affinity PYO demethylase (K_m < 1 μM and k_{cat} = 1.20 ± 0.07 s^{-1}) that operates over a wide regime of pH (<4.9–8.7) and salt concentrations (0–400 mM) (Fig. S2) with specificity for *N*-methylated phenazines (Fig S3). Under anoxic conditions, $PodA_{30\text{-}162}$ catalyzes the formation of a reduced phenazine, suggesting that its substrate serves as the electron acceptor (Fig. 1F,G). This mechanism has not previously been observed for demethylases (*11, 12*). We propose the following reaction for PodA, wherein oxidized PYO (PYO_{ox}) is converted to reduced 1-OH-PHZ (1-OH-PHZ_{red}) (Fig. 1A,B):

$$C_{13}H_{10}N_2O\ (PYO_{ox}) + H_2O \longrightarrow C_{12}H_{10}N_2O\ (1\text{-OH-PHZ}_{red}) + CH_2O$$

To test this model and better understand how $PodA_{30\text{-}162}$ reduces its substrate, we solved the X-ray crystal structure at 1.8 Å resolution (Table S1) by molecular replacement using a search model generated by Robetta (*14-16*) (Fig. S4). $PodA_{30\text{-}162}$ crystalized as a trimer in the asymmetric unit (Fig. 2A). Crystal formation occurred only in the presence of 1-OH-PHZ, which was visible in a putative solvent-exposed active site (Fig. 2B,C). We found no evidence of a bound cofactor or metals in the electron density of the active site (Fig. S5) further supporting the hypothesis that PodA catalyzes a novel demethylation reaction. Within the active site, there are several charged and polar residues (D68, D72, H121, E154, and Y156) and a nearby disulfide that are candidate catalytic residues (*17*); additionally, 1-OH-PHZ appears to bind via a π-π stacking interaction with F70 (Fig. 2B).

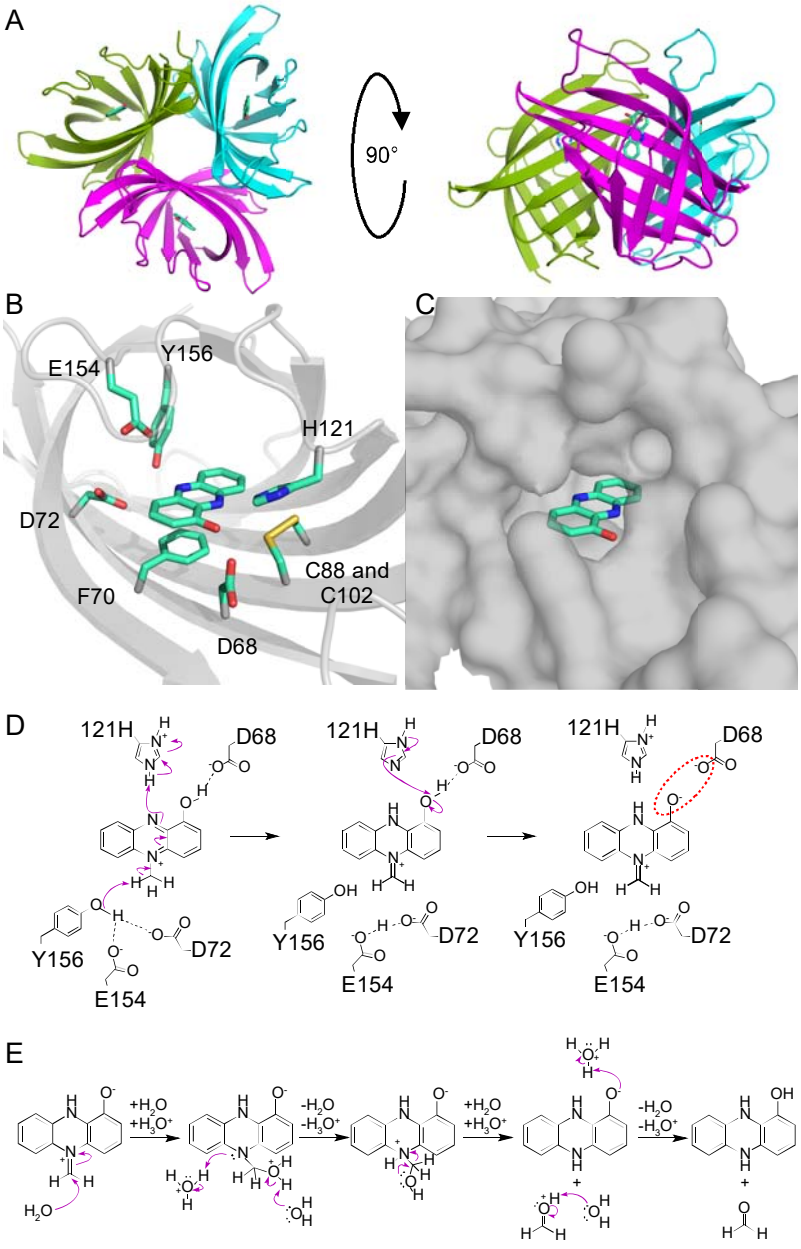
A
90°
B
E154
Y156
H121
D72
C88 and
C102
F70
D68
C
D
121H
D68
Y156
D72
E154
E
+H2O
+H3O+
-H2O
-H3O+
OH

Figure 2. 1.8 Å crystal structure of $PodA_{30\text{-}162}$. (**A**) View of the $PodA_{30\text{-}162}$ trimer with 1-OH-PHZ bound. The PodA active site (**B**) is solvent exposed (**C**) and contains charged and polar residues. There is a nearby disulfide ~3.5 Å from 1-OH-PHZ. (**D**) A proposed reaction mechanism based on the residues present in the active site. The model predicts that D72, E154, and Y156 are necessary for methyl deprotonation. H121 protonates the unmethylated N atom of the pyrazine ring, and D68 reprotonates H121. Formation of the negatively charged phenolate ion promotes product release due to an unfavorable electrostatic interaction (red dashed circle). D72 and E154 remain protonated, acidifying the active site to assist in formation of hydroxylated PYO (Fig. 1A) in the next catalytic cycle. (**E**) Hydrolysis of the product is spontaneous and occurs after release from the active site.

Based on the active site structure, we propose a mechanism relying on the presence of H121 functioning as an acid and D72, E154 and Y156 collectively functioning as a base (Fig. 2D). PYO binds in the phenol tautomeric form (Fig. 1A). Deprotonation of the methyl group results in iminium ion formation and concomitant reduction of the pyrazine ring, with the second nitrogen atom protonated by H121. H121 is then reprotonated by PYO's hydroxyl group (pK_a of His ~6 versus PYO ~5). The unfavorable interaction between the negatively charged phenolate ion and D68 drives product release. We hypothesize that PodA catalyzes the tautomerization of PYO to an iminium ion that is susceptible to hydrolysis outside of the enzyme: the structure indicates that the active site cannot accommodate both the substrate and a water molecule (Fig. 2B–E) (*11*). D72 and E154 remain protonated in this scenario, acidifying the active site, perhaps to ensure that PYO is in the hydroxylated form in subsequent reaction cycles (Fig. 1A). This scheme highlights the significance of the hydroxyl group of PYO to recharge PodA for subsequent reaction cycles and to drive product release. An alternative substrate, methoxyphenazine methosulfate (methoxy-PMS), which lacks the hydroxyl group, displays an initial burst of activity followed by a slower steady state (Fig. 3A), which is consistent with our model.

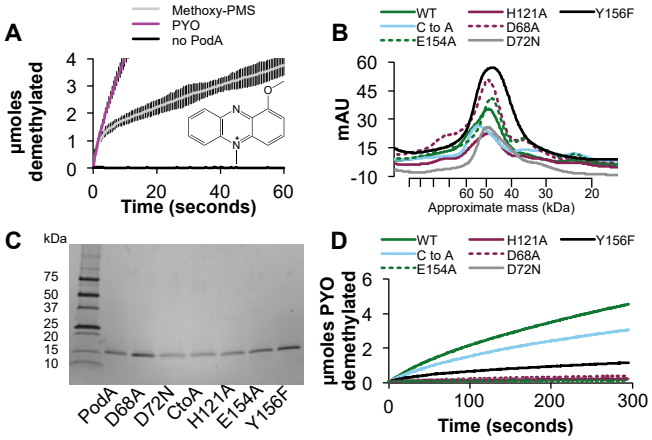

Figure 3. Molecular analysis of the PodA reaction mechanism. (**A**) An alternative substrate — methoxy-PMS, inset — is demethylated by PodA$_{30\text{-}162}$, but the reaction rate slows significantly after an initial burst, highlighting the importance of the hydroxyl group of PYO for catalysis and/or driving product release after deprotonation. Data are averages from triplicate measurements and error bars represent one standard deviation from the mean. (**B**) Residues in the PodA active site (Fig. 2B) were mutated and the resulting proteins purified; H121A, D68A, E154A, D72N, Y156F, and the C88A, C102A (C to A) double mutant all purify as a trimer by gel filtration chromatography. (**C**) Mutant proteins were pure as assayed by reducing SDS-PAGE. (**D**) Activity of mutant proteins shows that the disulfide bond is not essential for activity. Y156F has ~25% wild type activity, and all other residues appear essential for catalysis.

To probe the proposed mechanism, we performed mutagenesis for each of the putative catalytic residues. H121A, E154A, D68A, and D72N mutants all formed a trimer (Fig. 3B,C) but had <10% wild type activity, consistent with the postulated catalytic mechanism (Fig. 3D). Y156F formed a trimer but retained ~25% wild type activity, consistent with this residue facilitating proton transfer to D72 and E154 but not being essential. A possible alternative mechanism could utilize the disulfide in the active site forming a covalent adduct with the phenazine, in analogy to some flavoproteins (*18*). However, our mutagenesis results indicate that the disulfide bond near the active site is not essential for catalytic activity although it may be important for structural stability (Fig. 3B–D) (Fig. S6).

Because PodA requires only water and substrate for activity (Figs. 2D,E, S1, and S2), we hypothesized that it could degrade PYO during active production by *P. aeruginosa* (Fig. S7). $PodA_{30\text{-}162}$ addition to *P. aeruginosa* planktonic culture results in the conversion of PYO to 1-OH-PHZ in both rich and minimal medium (Fig. S8). Encouraged by these findings, we assessed the impact of PodA on biofilm formation. Extracellular DNA (eDNA) comprises >50% of the *P. aeruginosa* biofilm matrix (*19*), and recently PYO was shown to drive eDNA release (*20, 21*) which is important early in biofilm development (*19*). We hypothesized that $PodA_{30\text{-}162}$ might inhibit *P. aeruginosa* biofilms in part by attenuating DNA release, thereby removing an important matrix component and changing biofilm architecture. Because PYO does not completely block DNA release (*20, 21*), it is also possible that downstream PYO-DNA interactions may be important. We checked whether $PodA_{30\text{-}162}$ could access PYO in the presence of DNA, as PYO is a known DNA intercalator (*22*); $PodA_{30\text{-}162}$ catalyzed PYO demethylation in this context (Fig S8). We grew *P. aeruginosa* biofilms for 5 hours, staining them with DAPI to image biofilm structure. HPLC analysis of supernatants confirmed the conversion of PYO to 1-OH-PHZ by $PodA_{30\text{-}162}$ in these cultures (Fig. 4A). Overall biofilm formation, as assayed by surface coverage (*22*), was reduced by $PodA_{30\text{-}162}$ but not by the inactive PodA control (Fig. 4B-D), consistent with a role for PYO in early biofilm development. As previously shown, treatment with DNase independently inhibited biofilms (*22*). Interestingly, DNase or $PodA_{30\text{-}162}$ treatment inhibited biofilms to the same extent, and dual treatment did not have an additive effect (Fig. 4D).

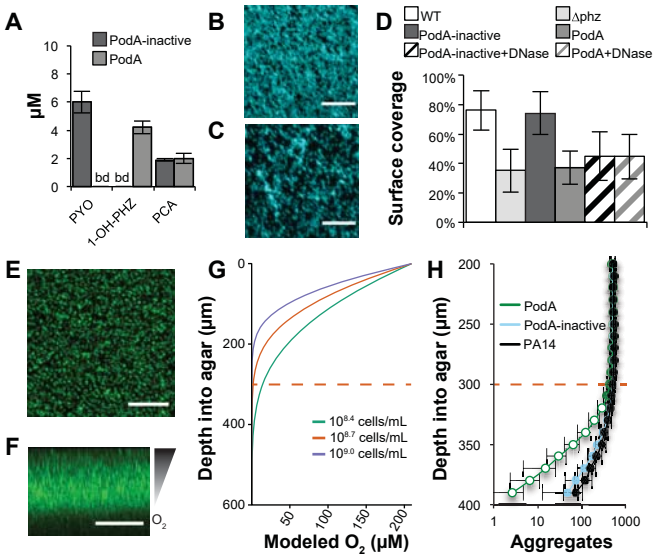

Figure 4. PodA$_{30\text{-}162}$ inhibits biofilm formation and anoxic fitness of *P. aeruginosa*. (**A**) Phenazines were measured by HPLC in biofilm supernatants after 5 hours of growth. PCA, phenazine-1-carboxylic acid. (**B**) *P. aeruginosa* forms a robust biofilm in the presence of inactivated PodA$_{30\text{-}162}$ after 5 hours. (**C**) In the presence of PodA$_{30\text{-}162}$, biofilm surface coverage was decreased. Surface coverage was 43.5 percent compared with 82.7 percent in the absence of PodA$_{30\text{-}162}$ in the representative images shown. Scale Bars = 20 μm. (**D**) Surface coverage was lower in the presence of PodA$_{30\text{-}162}$ ($p < 10^{-6}$ vs. PodA-inactive, two-tailed Student's t-test). DNase addition decreased surface coverage ($p < 10^{-3}$ vs. PodA-inactive), but DNase and PodA$_{30\text{-}162}$ combined did not have an additive effect ($p > 0.05$), consistent with an interaction between PYO and eDNA in supporting biofilms (*22*). Data are averages of 12 replicates taken from independent cultures. Error bars represent one standard deviation around the mean. Δ*phz*, PA14 mutant incapable of making phenazines. (**E**) Top down and (**F**) side views of *P. aeruginosa* grown embedded in 0.5% agar blocks for 27 hours. Scale bars = 200 μm. Oxygen depletion occurs at lower depths as a result of biological consumption outpacing diffusion from the surface, resulting in decreased biomass. (**G**) Oxygen diffusion model predicting the shape of the oxycline in agar blocks. Cell densities were estimated at $10^{8.7}$ cells mL^{-1} based on aggregate number and volume. Modeling this concentration and 2-fold higher and lower densities suggests that oxygen depletion occurs ~300 μm ± 100 μm below the agar surface. Dashed red line indicates the approximate oxic-anoxic interface. (**H**) Biofilm aggregates detected at 10 μm increments below the agar surface. At depths near the oxic/anoxic interface (dashed red line), total biomass begins to decline. In assays treated for the last 5 hours with PodA$_{30\text{-}162}$, there is an apparent biomass defect specifically at anoxic depths compared to untreated and inactive PodA treated controls, consistent with the importance of PYO for anoxic survival in *P. aeruginosa*. Data are averages of six independent experiments and error bars represent one standard deviation around the mean. Open symbols, $p < 0.01$, two-tailed Student's t-test.

In addition to impacting early stages in biofilm development, phenazines can expand the habitable zone within established biofilms (*5, 23*). As *P. aeruginosa* biofilms mature, cells in deeper layers of the biofilm begin to experience oxygen limitation and redox stress (*4, 23*); these cells are believed to be slow growing and are highly resistant to antibiotics (*24*). Phenazines facilitate anoxic survival and alleviate redox stress (*3, 25*). Because PYO reacts with oxygen more efficiently than 1-OH-PHZ (*26*), we hypothesized that PodA activity might decrease anoxic fitness by disrupting PYO dependent electron shuttling to oxygen. To capture key features of *in vivo* biofilm aggregates (*27, 28*), cells were grown suspended in agar blocks at 37 °C for 22 hours to establish an oxygen gradient before a 5 hour treatment with $PodA_{30\text{-}162}$ (Fig. 4E,F). Owing to constraints imposed by the incubator, we were unable to measure oxygen gradients directly, so we used a previously validated model to estimate the oxic-anoxic transition zone (*29*). Modeling our aggregate population indicated that anoxia occurs ~300 μm below the surface as a result of microbial consumption (Fig. 4G), consistent with what is known about oxygen diffusion into *in vivo* biofilms (*29*). We observed a decrease in detectable aggregates at depths 300–400 μm below the agar surface; additionally, cultures treated with $PodA_{30\text{-}162}$ had a sharper decline in detectable aggregates below this depth (Fig. 4H). There was no significant difference in aggregate numbers above the predicted oxic-anoxic transition zone. How PYO demethylation restricts the aggregate population is unknown.

In conclusion, the discovery of a PYO demethylase that simultaneously catalyzes substrate reduction shows that redox-active pigments can participate in their own enzyme-catalyzed modification. Though PodA is the first member of a new class of tautomerizing demethylases that utilizes an oxidized substrate as the electron acceptor, this reaction is reminiscent of reduced flavin acting as the electron donor in its own destruction in vitamin B_{12} biosynthesis (*30*). It seems likely that the processing of other redox-active pigments and cofactors may operate by a similar mechanism where the redox activity of the substrate enables catalysis. That PodA can inhibit *P.*

aeruginosa at different stages of biofilm development raises the possibility that selective degradation of extracellular electron shuttles may facilitate treatment of intractable infections.

Acknowledgements

The final model and native data set for PodA were submitted to the wwPDB under accession code 5K21. We thank Elena Perry, Lucas Meirelles, William DePas, and Douglas Rees for assistance in experimental design and interpretation. KCC was supported by a Ruth L. Kirschstein National Research Service Award from the National Institutes of Health, National Institute of Allergy and Infectious Diseases, Grant no. F32AI112248. NRG was supported by the National Science Foundation Graduate Research Fellowship, Grant no. 1144469. This work was further supported by the Howard Hughes Medical Institute (HHMI), NIH (Grant 5R01HL117328-03) and the Molecular Observatory at the Beckman Institute, California Institute of Technology through the Gordon and Betty Moore Foundation and the Sanofi-Aventis Bioengineering Research Program at Caltech. Additional support was provided by the Stanford Synchrotron Radiation Lightsource, which is funded by the US DOE and NIH. SJC thanks St Hugh's College, Oxford for research support.

Author contributions

KCC and DKN conceived the project. KCC, NRG, and DKN designed the experiments. KCC and NRG performed the experiments. KCC, NRG, SJC, and DKN analyzed and interpreted the results. KCC, SJC and DKN wrote the paper.

References and Notes

1. J. M. Turner, A. J. Messenger, Occurrence, biochemistry and physiology of phenazine pigment production. *Adv Microb Physiol* **27**, 211-275 (1986).
2. L. E. Dietrich, T. K. Teal, A. Price-Whelan, D. K. Newman, Redox-active antibiotics control gene expression and community behavior in divergent bacteria. *Science* **321**, 1203-1206 (2008).

3. N. R. Glasser, S. E. Kern, D. K. Newman, Phenazine redox cycling enhances anaerobic survival in *Pseudomonas aeruginosa* by facilitating generation of ATP and a proton-motive force. *Mol Microbiol* **92**, 399-412 (2014).
4. A. Price-Whelan, L. E. Dietrich, D. K. Newman, Pyocyanin alters redox homeostasis and carbon flux through central metabolic pathways in *Pseudomonas aeruginosa* PA14. *J Bacteriol* **189**, 6372-6381 (2007).
5. I. Ramos, L. E. Dietrich, A. Price-Whelan, D. K. Newman, Phenazines affect biofilm formation by *Pseudomonas aeruginosa* in similar ways at various scales. *Res Microbiol* **161**, 187-191 (2010).
6. Y. Wang *et al.*, Phenazine-1-carboxylic acid promotes bacterial biofilm development via ferrous iron acquisition. *J Bacteriol* **193**, 3606-3617 (2011).
7. W. J. Moree *et al.*, Interkingdom metabolic transformations captured by microbial imaging mass spectrometry. *Proc Natl Acad Sci U S A* **109**, 13811-13816 (2012).
8. Z. J. Yang *et al.*, Isolation, identification, and degradation characteristics of phenazine-1-carboxylic acid-degrading strain *Sphingomonas* sp. DP58. *Curr Microbiol* **55**, 284-287 (2007).
9. K. C. Costa, M. Bergkessel, S. Saunders, J. Korlach, D. K. Newman, Enzymatic degradation of phenazines can generate energy and protect sensitive organisms from toxicity. *MBio* **6**, e01520-01515 (2015).
10. A. Krogh, B. Larsson, G. von Heijne, E. L. Sonnhammer, Predicting transmembrane protein topology with a hidden Markov model: application to complete genomes. *J Mol Biol* **305**, 567-580 (2001).
11. R. Anand, R. Marmorstein, Structure and mechanism of lysine-specific demethylase enzymes. *J Biol Chem* **282**, 35425-35429 (2007).
12. J. M. Hagel, P. J. Facchini, Biochemistry and occurrence of O-demethylation in plant metabolism. *Front Physiol* **1**, 14 (2010).
13. R. M. Summers *et al.*, Novel, highly specific N-demethylases enable bacteria to live on caffeine and related purine alkaloids. *J Bacteriol* **194**, 2041-2049 (2012).
14. Y. Song *et al.*, High-resolution comparative modeling with RosettaCM. *Structure* **21**, 1735-1742 (2013).
15. S. Raman *et al.*, Structure prediction for CASP8 with all-atom refinement using Rosetta. *Proteins* **77 Suppl 9**, 89-99 (2009).
16. D. E. Kim, D. Chivian, D. Baker, Protein structure prediction and analysis using the Robetta server. *Nucleic Acids Res* **32**, W526-531 (2004).
17. A. Gutteridge, J. M. Thornton, Understanding nature's catalytic toolkit. *Trends Biochem Sci* **30**, 622-629 (2005).
18. C. T. Walsh, T. A. Wencewicz, Flavoenzymes: versatile catalysts in biosynthetic pathways. *Nat Prod Rep* **30**, 175-200 (2013).
19. C. B. Whitchurch, T. Tolker-Nielsen, P. C. Ragas, J. S. Mattick, Extracellular DNA required for bacterial biofilm formation. *Science* **295**, 1487 (2002).
20. T. Das, M. Manefield, Pyocyanin promotes extracellular DNA release in *Pseudomonas aeruginosa*. *PLoS One* **7**, e46718 (2012).
21. T. Das, M. Manefield, Phenazine production enhances extracellular DNA release via hydrogen peroxide generation in *Pseudomonas aeruginosa*. *Commun Integr Biol* **6**, e23570 (2013).

22. T. Das *et al.*, Phenazine virulence factor binding to extracellular DNA is important for *Pseudomonas aeruginosa* biofilm formation. *Sci Rep* **5**, 8398 (2015).
23. L. E. Dietrich *et al.*, Bacterial community morphogenesis is intimately linked to the intracellular redox state. *J Bacteriol* **195**, 1371-1380 (2013).
24. G. Borriello *et al.*, Oxygen limitation contributes to antibiotic tolerance of *Pseudomonas aeruginosa* in biofilms. *Antimicrob Agents Chemother* **48**, 2659-2664 (2004).
25. Y. Wang, S. E. Kern, D. K. Newman, Endogenous phenazine antibiotics promote anaerobic survival of *Pseudomonas aeruginosa* via extracellular electron transfer. *J Bacteriol* **192**, 365-369 (2010).
26. Y. Wang, D. K. Newman, Redox reactions of phenazine antibiotics with ferric (hydr)oxides and molecular oxygen. *Environ Sci Technol* **42**, 2380-2386 (2008).
27. T. Bjarnsholt *et al.*, The in vivo biofilm. *Trends Microbiol* **21**, 466-474 (2013).
28. K. N. Kragh *et al.*, Role of Multicellular Aggregates in Biofilm Formation. *MBio* **7**, e00237 (2016).
29. E. S. Cowley, S. H. Kopf, A. LaRiviere, W. Ziebis, D. K. Newman, Pediatric cystic fibrosis sputum can be chemically dynamic, anoxic, and extremely reduced due to hydrogen sulfide formation. *MBio* **6**, e00767 (2015).
30. M. E. Taga, N. A. Larsen, A. R. Howard-Jones, C. T. Walsh, G. C. Walker, BluB cannibalizes flavin to form the lower ligand of vitamin B12. *Nature* **446**, 449-453 (2007).
31. L. E. Dietrich, A. Price-Whelan, A. Petersen, M. Whiteley, D. K. Newman, The phenazine pyocyanin is a terminal signalling factor in the quorum sensing network of *Pseudomonas aeruginosa*. *Mol Microbiol* **61**, 1308-1321 (2006).
32. L. G. Rahme *et al.*, Common virulence factors for bacterial pathogenicity in plants and animals. *Science* **268**, 1899-1902 (1995).
33. F. W. Studier, B. A. Moffatt, Use of bacteriophage T7 RNA polymerase to direct selective high-level expression of cloned genes. *J Mol Biol* **189**, 113-130 (1986).
34. S. K. DasGupta, S. Jain, D. Kaushal, A. K. Tyagi, Expression systems for study of mycobacterial gene regulation and development of recombinant BCG vaccines. *Biochem Biophys Res Commun* **246**, 797-804 (1998).
35. Y. P. Shih, H. C. Wu, S. M. Hu, T. F. Wang, A. H. Wang, Self-cleavage of fusion protein in vivo using TEV protease to yield native protein. *Protein Sci* **14**, 936-941 (2005).
36. M. M. Bradford, A rapid and sensitive method for the quantitation of microgram quantities of protein utilizing the principle of protein-dye binding. *Anal Biochem* **72**, 248-254 (1976).
37. T. Nash, The colorimetric estimation of formaldehyde by means of the Hantzsch reaction. *Biochem J* **55**, 416-421 (1953).
38. S. B. Jones, C. M. Terry, T. E. Lister, D. C. Johnson, Determination of submicromolar concentrations of formaldehyde by liquid chromatography. *Anal. Chem.* **71**, 4030-4033 (1999).
39. N. L. Sullivan, D. S. Tzeranis, Y. Wang, P. T. So, D. Newman, Quantifying the dynamics of bacterial secondary metabolites by spectral multiphoton microscopy. *ACS Chem Biol* **6**, 893-899 (2011).
40. D. V. Mavrodi *et al.*, Functional analysis of genes for biosynthesis of pyocyanin and phenazine-1-carboxamide from *Pseudomonas aeruginosa* PAO1. *J Bacteriol* **183**, 6454-6465 (2001).

41. G. Kemmer, S. Keller, Nonlinear least-squares data fitting in Excel spreadsheets. *Nat Protoc* **5**, 267-281 (2010).
42. H. McIlwain, The phenazine series. Part IV. Reactionsof alkyl phenazonium salts; the phenazyls. *J Chem Soc*, 1704-1711 (1937).
43. W. Kabsch, Xds. *Acta Crystallogr D Biol Crystallogr* **66**, 125-132 (2010).
44. W. Kabsch, Integration, scaling, space-group assignment and post-refinement. *Acta Crystallogr D Biol Crystallogr* **66**, 133-144 (2010).
45. P. Evans, Scaling and assessment of data quality. *Acta Crystallogr D Biol Crystallogr* **62**, 72-82 (2006).
46. P. R. Evans, G. N. Murshudov, How good are my data and what is the resolution? *Acta Crystallogr D Biol Crystallogr* **69**, 1204-1214 (2013).
47. J. E. Padilla, T. O. Yeates, A statistic for local intensity differences: robustness to anisotropy and pseudo-centering and utility for detecting twinning. *Acta Crystallogr D Biol Crystallogr* **59**, 1124-1130 (2003).
48. M. D. Winn *et al.*, Overview of the CCP4 suite and current developments. *Acta Crystallogr D Biol Crystallogr* **67**, 235-242 (2011).
49. A. J. McCoy *et al.*, Phaser crystallographic software. *J Appl Crystallogr* **40**, 658-674 (2007).
50. P. Emsley, B. Lohkamp, W. G. Scott, K. Cowtan, Features and development of Coot. *Acta Crystallogr D Biol Crystallogr* **66**, 486-501 (2010).
51. T. C. Terwilliger *et al.*, Iterative model building, structure refinement and density modification with the PHENIX AutoBuild wizard. *Acta Crystallogr D Biol Crystallogr* **64**, 61-69 (2008).
52. J. J. Headd *et al.*, Use of knowledge-based restraints in phenix.refine to improve macromolecular refinement at low resolution. *Acta Crystallogr D Biol Crystallogr* **68**, 381-390 (2012).
53. P. V. Afonine *et al.*, Towards automated crystallographic structure refinement with phenix.refine. *Acta Crystallogr D Biol Crystallogr* **68**, 352-367 (2012).
54. T. C. Terwilliger, P. D. Adams, N. W. Moriarty, J. D. Cohn, Ligand identification using electron-density map correlations. *Acta Crystallogr D Biol Crystallogr* **63**, 101-107 (2007).
55. T. C. Terwilliger, H. Klei, P. D. Adams, N. W. Moriarty, J. D. Cohn, Automated ligand fitting by core-fragment fitting and extension into density. *Acta Crystallogr D Biol Crystallogr* **62**, 915-922 (2006).
56. P. D. Adams *et al.*, PHENIX: a comprehensive Python-based system for macromolecular structure solution. *Acta Crystallogr D Biol Crystallogr* **66**, 213-221 (2010).
57. N. W. Moriarty, R. W. Grosse-Kunstleve, P. D. Adams, electronic Ligand Builder and Optimization Workbench (eLBOW): a tool for ligand coordinate and restraint generation. *Acta Crystallogr D Biol Crystallogr* **65**, 1074-1080 (2009).
58. M. D. Winn, M. N. Isupov, G. N. Murshudov, Use of TLS parameters to model anisotropic displacements in macromolecular refinement. *Acta Crystallogr D Biol Crystallogr* **57**, 122-133 (2001).
59. T. Das, S. K. Kutty, N. Kumar, M. Manefield, Pyocyanin facilitates extracellular DNA binding to *Pseudomonas aeruginosa* influencing cell surface properties and aggregation. *PLoS One* **8**, e58299 (2013).
60. C. A. Schneider, W. S. Rasband, K. W. Eliceiri, NIH Image to ImageJ: 25 years of image analysis. *Nat Methods* **9**, 671-675 (2012).

61. S. Bolte, F. P. Cordelieres, A guided tour into subcellular colocalization analysis in light microscopy. *J Microsc* **224**, 213-232 (2006).
62. D. Cohen *et al.*, Oligoribonuclease is a central feature of cyclic diguanylate signaling in *Pseudomonas aeruginosa*. *Proc Natl Acad Sci U S A* **112**, 11359-11364 (2015).

SUPPLEMENTAL MATERIAL

Materials and Methods

Strains, medium and growth conditions.

Primers, strains and plasmids are listed in Table S2 (*31-33*). All expression constructs were derivatives of the IPTG inducible plasmid pET-20b(+) (Novagen). The gene for MFORT_14352 lacking the N-terminal 29 amino acids ($podA_{30\text{-}162}$) was PCR amplified from *Mycobacterium fortuitum* ATCC 6841 using primers listed in Table S2 and first placed into the NdeI and PstI sites of plasmid pSD5 (*34*) to verify expression of a His tag construct in a vector we used previously for *podA* expression in *Rhodococcus* sp. JVH1 (*9*). Primers encoded both a TEV protease cleavage site and a 6x-His tag on the C-terminus. Activity was observed in the *Escherichia coli* cloning strain, so we transferred the $podA_{30\text{-}162}$ construct to an *E. coli* expression vector for further analysis. PCR product was digested with NdeI and NotI and ligated into digested pET-20b(+) before transfer into *E. coli* BL21(DE3) cells by electroporation (*33*). Mutant proteins were generated by PCR amplifying pET-20b(+) containing $podA_{30\text{-}162}$ with primers encoding the relevant mutation (Table S2). Product was cut with DpnI to remove WT vector, phosphorylated with T4 polynucleotide kinase, and ligated to generate a circular mutant protein expression construct. For D72N and Y156F mutants, DNA fragments encoding the mutation were synthesized (Integrated DNA Technologies) and cloned into pET-20b(+) as for the wild type sequence. Enzymes for cloning were purchased from New England Biolabs. Constructs were transferred to *E. coli* BL21(DE3) for expression. All mutations were confirmed by Sanger sequencing (Laragen and Retrogen). When necessary, 100 μg mL^{-1} carbenicillin was included in

all growth media to maintain selection for the plasmid. To measure the effect of $PodA_{30-162}$ on phenazine production in planktonically grown *P. aeruginosa*, cultures were grown overnight in 5 mL volumes of tryptic soy broth (TSB) or succinate minimal medium (arginine medium recipe from Glasser *et al.*, 2014 with 40 mM sodium succinate in place of arginine) (*3*) in the presence 1 μg mL^{-1} $PodA_{30-162}$. Cells were removed by centrifugation and supernatants were analyzed by HPLC as previously described (*9*). See below for a description of biofilm growth of *P. aeruginosa* PA14.

To induce protein expression, an overnight culture was inoculated 1/1000 in Terrific Broth (BD Difco). Cultures were grown in baffled Erlenmeyer flasks (1 L culture per 3 L flask) at 37 °C with 150 rpm agitation in a shaking incubator (Innova 44 shaking incubator, New Brunswick). After 3-4 hours, the temperature was changed to 16 °C and cultures were induced with 50 μM (final concentration) IPTG and left to incubate overnight. Cells were then pelleted by centrifugation, flash frozen in liquid N_2, and stored at −80 °C for up to 1 month before protein purification.

Generation and analysis of phenazines

Pyocyanin (PYO) was purified directly from cultures of *P. aeruginosa* PA14 grown on succinate minimal medium using a previously established protocol (*31*). Briefly, culture supernatants were first extracted with 0.4 volume dichloromethane (DCM). DCM extracts were treated 1:1 with 0.01 M HCl to acidify PYO and extract it back into the aqueous phase. Finally, 1 M NaOH was added to pH7, and PYO was extracted back into DCM and dried in vacuo. This crude preparation was used for routine analysis of FPLC fractions for activity. To further purify PYO, extracts were dried and purified by reverse phase HPLC as described (*26, 31*). 1-hydroxy-phenazine (1-OH-PHZ) was manufactured by TCI America. Phenazine-1-carboxylic acid (PCA) and phenazine-1-carboxamide (PCN) standards were purchased from Princeton Biomolecular Research, Inc.

Phenazines from culture supernatants were analyzed and measured by HPLC as described previously (*6, 9*).

Protein extraction and purification

Frozen cell pellets were thawed at room temperature and suspended in 25 mL wash buffer (200 mM KCl, 20 mM imidazole, Tris, pH 7.6). Cell suspensions were homogenized in an Emulsiflex device (Avestin). Cell debris was removed by centrifugation (Avanti J-25 centrifuge, J-series JA-25.50 rotor, Beckman-Coulter) at 50,000 xg and supernatant was applied to a nickel GE Healthcare HisTrap HP 5 mL nickel column on a GE Healthcare ÄKTAxpress FPLC. All protein purification steps were carried out at room temperature. The column with bound protein was washed with wash buffer until the UV (280 nm) trace stabilized below 20 mAU. Proteins were eluted across a gradient of 20-500 mM imidazole applied over 10 column volumes. PYO demethylase activity generally eluted around 300 mM imidazole. Eluted protein was concentrated to ~3 mL (Amicon Ultra-15 centrifugal filters, Ultracel 3K MWCO) and treated overnight with 1% wt/wt TEV protease (*35*) while dialyzing (Spectra/Por Biotech Dialysis membrane, MWCO: 3.5-5 kD) into buffer containing 200 mM KCl and 20 mM Tris, pH7.6 at 4 C. Samples were run back through the nickel column and PYO demethylase activity was collected in the flow through. Protein was concentrated to 250-500 µL (Amicon Ultra – 0.5 mL centrifugal filters, Ultracel – 3K MWCO) and loaded on a GE Healthcare HiLoad 16/60 Superdex 200 prep grade gel filtration column and run at 1 mL min^{-1} with gel filtration buffer (100 mM $CaCl_2$, 20 mM Tris, pH 7.6). $CaCl_2$ in the buffer was necessary for maximal $PodA_{30\text{-}162}$ activity. Activity eluted after ~83 mL. For applications requiring highly purified $PodA_{30\text{-}162}$ (e.g., crystallography), an acid precipitation step (400 mM phosphate/citrate, pH 4.2) was added either before or after gel filtration chromatography to precipitate trace contaminants that were not apparent by SDS-PAGE. PYO demethylase activity remained in the supernatant. For acid precipitation, sample was dialyzed into 20 mM Tris, pH 7.6 between steps to avoid mixing $CaCl_2$ and phosphate buffers. Purified $PodA_{30\text{-}}$

$_{162}$ was dialyzed into 20 mM Tris, pH7.6 and stored at 4 °C; protein remained stable with no apparent loss of activity for as long as tested (up to 4 months). To determine the approximate molecular weight of purified proteins, the elution peak was compared to Bio-Rad gel filtration standards run across the same column with gel filtration buffer. Mutant proteins were purified on the same day as wild type and fractions where activity was seen in wild type were also collected for mutant preparations. Protein quantification was carried out by Bradford assay (*36*) (Quick Start 1x Bradford Dye Reagent, Bio-Rad) using pre-diluted Bovine Serum Albumin standards (Thermo Scientific) to establish a standard curve. A purification from 6 liters of culture typically yielded 1-2 mg protein. Purified proteins were routinely subject to SDS-PAGE using 4-20% Mini-PROTEAN TGX precast protein gels (Bio-Rad) and stained with Coomassie Blue. All protein preparations were colorless, indicating that flavins were not present in the purified protein.

Enzyme activity and analysis

PYO demethylation by $PodA_{30\text{-}162}$ was first determined by HPLC analysis as described previously (*6, 9*). To detect formaldehyde evolution, 150 nM protein was mixed with 50 μM PYO in 1 mL of 20 mM Tris pH 7.6 amended with 200 μL Nash reagent (2 M ammonium acetate, 50 mM acetic acid, 20 mM acetylacetone) and incubated at 55 °C until the reaction proceeded to completion (*37, 38*). The products were determined by HPLC using the same method as used for phenazine quantification. To monitor the formation of reduced phenazine, protein and 50 μM PYO were placed into an anaerobic chamber (Coy Laboratory Products) under an atmosphere of H_2/N_2 (5:95) and left overnight before allowing the reaction to proceed. To generate reduced PYO and 1-OH-PHZ, 50 μM were mixed with 1 mM sodium dithionite. The formation of reduced phenazine products was assayed visually under UV illumination (*39*). A BioTek Synergy 4 microplate reader (BioTek) plate reader in the anaerobic chamber was used to measure the emission spectrum of products with excitation at 250 nm.

To determine the activity of $PodA_{30-162}$ in the presence of glycerol, salts, or varying pH, 30 nM protein was suspended in 500 µL buffer, 40 µM PYO was mixed with 2x solution containing the buffer of interest (500 µL), and solutions were preheated to 30 C. For pH range measurements, the following buffers were used (40 mM, adjusted with KOH): acetic acid, pH 4.9; MES, pH 5.4 and 5.7; HEPES, pH 6.1; Tris, pH 6.9 and 7.5; Bicine, pH 7.8, 8.3 and 8.7; CHES, pH 9.4. To measure reaction rates, cuvettes containing the 2x PYO solution were placed in an Evolution 260Bio UV-Vis spectrophotometer (Thermo Scientific) and 500 µL of 30 nM protein was added at time 0 (15 nM protein and 20 µM PYO, final concentration). Reaction progress was monitored by measuring absorbance at 313 nm (*40*) every 0.5 seconds for 5 minutes. To measure kinetic parameters (k_{cat}, K_m) 15 nM protein was used in a reaction buffer of Bicine, pH 7.8; reactions were monitored as before with measurements every 0.2 seconds. The rate from the first 10 seconds of the reaction was used for the determination of kinetic parameters. Kinetic parameters were calculated in Microsoft Excel using the Solver plug-in and fitting data to ideal Michaelis-Menten plots with non-linear regression of experimental data (*41*). For measurements of the rate of methoxy-PMS demethylation, 300 nM protein was used and methoxy-PMS loss from the reaction mixture was monitored at 500 nm wavelength. methoxy-PMS was purchased from TCI America. For assays with mutant proteins, 60 nM protein was used. The stimulatory effects of flavin or 2-oxoglutarate addition was determined by adding 25 µM flavin or 2-oxoglutarate to 20 µM PYO and 15 nM $PodA_{30-162}$ and monitoring the reaction.

Experiments testing alternative substrates were carried out using in 1 mL reaction volumes containing 20 mM Tris (pH 7.6) and 50 µg mL^{-1} $PodA_{30-162}$. Alternative substrates tested were 10-methylphenothiazine (Alfa Aesar), phenazine methosulfate (Alfa Aesar), methoxyphenazine methosulfate (TCI America), and 4-keto-N-ethylphenazine. 4-keto-N-ethylphenazine was synthesized from phenazine ethosulfate (Sigma-Aldrich) by incubating under fluorescent light overnight followed by purification by HPLC as described (*6, 42*). As phenazine methosulfate is

light sensitive and spontaneously converts to PYO in the presence of light, all reactions were carried out in the dark, and activity was assessed by end point analysis by HPLC after 4 hours (*9*).

Protein crystallography, X-ray diffraction and analysis

Crystallization screens were performed with the JCSG+ screen (Molecular Dimensions) using vapor diffusion in sitting drop format with assistance from the California Institute of Technology Molecular Observatory. A Crystal Gryphon liquid-handling robot (Art Robins) was used to mix 0.2 μL of screen solution with 0.2 μL of protein solution (5 mg mL^{-1} in 20 mM Tris, pH 7.6 amended with 200 μM 1-OH-PHZ in DMSO (1% final concentration)). Crystals formed in JCSG+ conditions C1, C6, and D12 after 3 days at 20 °C. Varying the salt and polymer concentrations in a 24-well plate showed that JSCG+ condition C1 gave robust crystal growth in vapor diffusion sitting drop format using 2 μL drops in Micro-Bridges (Hampton Research). Protein (5 mg mL^{-1}) was mixed with mother liquor (1μL:1μL) composed of 20% w/v PEG 8000, 200 mM NaCl, 200 μM 1-OH-PHZ, 1% DMSO, and 100 mM sodium phosphate dibasic/citric acid, pH 4.2. Crystals generally formed within 3 days at 20 °C and were rod shaped with typical dimensions of 50 x 50 x 100 μm. Crystals were equilibrated into a cryoprotectant solution (12% w/v PEG 8000, 20% w/v PEG 300, 100 mM NaCl, 100 μM 1-OH-PHZ, 0.5% DMSO, and 50 mM sodium phosphate dibasic/citric acid, pH 4.2) by gradually replacing the sitting drop solution with cryoprotectant solution over the span of 10–15 minutes. Crystals were then mounted in a nylon loop and flash frozen in liquid nitrogen.

Data collection was performed at 100 K at the Stanford Synchrotron Radiation Lightsource (SSRL) beamline 12-2 equipped with a PILATUS 6M Pixel Array Detector. X-ray diffraction data were collected at 12,000 eV with a beamstop distance of 32.7 mm and a detector distance of 280 nm. Images were collected every 0.15° for a full 360° of rotation around a single axis (generating a total of 2400 images). For well-diffracting crystals, an additional dataset was collected at 7,000 eV

to capture the anomalous signal from sulfur and calcium. Diffraction images were integrated and scaled using the XDS package (*43*). To ensure maximum data completion, the two highest quality datasets were combined using XSCALE and further processed using POINTLESS, AIMLESS and CTRUNCATE in the CCP4 software suite (*44-48*). The structure was solved by molecular replacement in PHASER (*49*) using a search model derived from a structural prediction by Robetta (*14-16*) with disordered loops trimmed in Coot (*50*). A preliminary model was constructed using phenix.AutoBuild (*51*) and refined using phenix.refine (*52, 53*) and model building in Coot to yield a model with R_{free} = 0.22. LigandFit (*54, 55*) analysis in PHENIX (*56*) was used to model 1-OH-PHZ into the active site of $PodA_{30-162}$ with refinement restraints generated using elBOW (simple optimization method) (*57*). The model was modified in Coot to trim side chains with poor electron density coverage. A highly coordinated water molecule was identified by phenix.refine as a potential calcium atom, presumably originating from the inclusion of 100 mM $CaCl_2$ during the final protein purification step. Analysis of the anomalous difference map from a low-energy dataset supported this identification (Fig. S5) and so the corresponding water molecules were replaced with calcium atoms and metal-coordination restraints were generated with phenix.metal_coordination via ReadySet!. The final rounds of refinement were performed using TLS groups (*58*) generated by phenix.refine and hydrogen atoms set in their riding positions to yield a final model of R_{free} = 0.195. Figures were rendered with PYMOL version 1.7.2.1, Schrödinger, LLC.

Biofilm experiments

For all experiments involving inactivated PodA, either the E154A mutant or $PodA_{30-162}$ that was subjected to a 1 hour treatment at 98° C was used. To test the ability of $PodA_{30-162}$ to degrade PYO in the presence of DNA, genomic DNA (gDNA) from *P. aeruginosa* PA14 was used in modified versions of previously described assays (*59*). For experiments using DNA pellets, 0.5 mg of gDNA was pelleted in the presence of 300 mM sodium acetate, pH 5.2 and 70% ethanol. Pellets were

washed with 70% ethanol and dried. 200 µL of 800 µM PYO was added to the gDNA pellet without mixing and left to sit at room temperature for 6 hours to allow for diffusion of PYO into the gDNA pellet. The pellet was washed once with 70% EtOH, and submerged in a solution containing 10 mM Tris, pH 7.0 and 40% isopropanol. The pellet remained blue, consistent with an association of PYO with DNA. $PodA_{30\text{-}162}$ was added to the isopropanol solution to a final concentration of 2 µg mL^{-1} and left to sit for 3 hours to allow for the reaction to proceed. Tubes were imaged before and after $PodA_{30\text{-}162}$ treatment. For experiments using solubilized gDNA, a 400 µg mL^{-1} solution of gDNA was mixed with PYO and allowed to equilibrate for 6 hours. The PYO gDNA mixture was amended with 1 µg mL^{-1} $PodA_{30\text{-}162}$ and loss of PYO was monitored on a BioTek Synergy 4 microplate reader (BioTek) plate reader at 690 nm. Standards were included to quantify PYO loss over time.

To assess biofilm formation in the presence of $PodA_{30\text{-}162}$, biofilms were grown in Nunc Lab-Tek chambered coverglass slides (8-well, 0.8 cm^2 area, supplier #155411) using a modified protocol (*22*). PA14 was inoculated into succinate minimal medium and grown overnight to stationary phase. Cells were resuspended in fresh medium and diluted to a starting OD_{500} of 0.5 in succinate minimal medium. $PodA_{30\text{-}162}$ (2 µg mL^{-1}, final concentration) or DNase (20 µg mL^{-1}) (*22*) was added and 250 µL was added to each well of the 8-well chambered coverglass. Cultures were grown for 5 hours at 37 °C and 100 rpm (Innova 44 shaking incubator, New Brunswick) in a humidified chamber. After incubation, liquid was removed from each well by drawing with a pipet tip placed in the corner of each well and chambers were washed twice with 400 µL of biofilm wash (Tris buffer, pH 7.6 and 100 mM NaCl) to remove planktonic and loosely bound cells. Attached biomass was stained by adding 450 µL biofilm wash containing 10 µg mL^{-1} DAPI (4',6-diamidino-2-phenylindole) (Santa Cruz Biotechnology). Surface associated biomass was imaged on a Leica TCS SPE confocal microscope with a ACS APO 40x/1.15 oil immersion objective. A 405 nm solid-state laser was used for excitation, and data was collected from 420-500 nm. Images were

collected from the same relative position in each well along the mid-point of the outer edge on the opposite edge from where the washing pipet was placed. Images were collected as 10 μm Z-stacks (10 slices) to image the biofilm in its entirety over a surface area of 40,000 μm^2. All Z-stacks were collected in 8-bit mode with 1024x1024 scan format and a line averaging of 2. A sum intensity projection was produced from each Z-stack using ImageJ software (*60*). Images were then thresholded to include pixels with a maximum intensity value >0.15x the maximum possible intensity, and thresholded images were used to determine surface coverage of each biofilm. Data were collected from 12 biological replicates.

Biofilm aggregate experiments

To test the effect of oxygen limitation in the presence of $PodA_{30\text{-}162}$, biofilm aggregates were grown embedded in 0.5% noble agar blocks containing succinate minimal medium. Cultures were grown overnight to stationary phase in LB, washed once with succinate minimal medium, and resuspended to OD_{600} 1.0. Samples were diluted 1:100 in agar at 44°C and 175 μL was transferred to Nunc Lab-Tek chambered coverglass slides (8-well, 0.7 cm^2 area, supplier #155409). After the agar solidified, aggregates were grown for 22 hours in a humidified chamber at 37°C before $PodA_{30\text{-}162}$ (2 μg mL^{-1}, final concentration) was added to the top of the agar for an additional 5 hours at 37°C. After treatment, 1 μL of stain from ThermoFisher LIVE/DEAD BacLight Bacterial Viability Kit in 50 μL ddH_2O was added to the top of the agar for 12 minutes before microscopic analysis. SYTO-9 from the LIVE/DEAD stain kit was used in place of DAPI to minimize background fluorescence. Biomass was imaged with a Leica TCS SPE confocal microscope with a ACS APO 10x/0.30 objective. A 488 nm solid-state laser was used for excitation, and data was collected from 510-550 nm. Images were collected across a 500 μm Z-stack with a 10 μm step size. All Z-stacks were collected in 8-bit mode with 512x512 scan format and a line averaging of 2. Biomass was quantified in ImageJ software (*60*) by identifying the Z-slice with the highest average fluorescent intensity (generally ~200 μm below the agar surface), and setting the pixel threshold

using the default ImageJ thresholding parameters at the Z-slice equivalent to the 100 μm depth. The number of particles in each slice of the Z-stack was determined using this threshold value and counting particles >10 μm^2 in area. To compare biofilm aggregate biomass from different experiments, all Z-stacks were normalized by depth so that the Z-slice with the highest average staining intensity was considered the mid-point of the 3D reconstruction. This processing allowed for comparison of datasets collected on different days with slightly different staining intensities and different Z-plane starting coordinates. Particle numbers for each slice were averaged between independent experiments and plotted against depth to quantify biofilm aggregates. Only experiments with between 400 and 600 aggregates at the plane of peak stain intensity were used for averaging and statistical analysis; this ensured equivalent biomass was present in each experiment.

Oxygen diffusion modeling

To model oxygen diffusion into agar blocks embedded with *P. aeruginosa* aggregates, we utilized the oxygen diffusion model from (*29*). Cell numbers were estimated by determining the average number of aggregates present and calculating the average volume of a given particle with the ImageJ 3D-object counter plug-in (*61*). Given these values, average cell number per mL was estimated by dividing the volume of total detected biofilm aggregates by the average volume of a *P. aeruginosa* cell (*62*) yielding a cell density estimate of 5×10^8. This cell density value is consistent with the overnight growth of *P. aeruginosa* in succinate minimal medium. Oxygen diffusion was modeled using this value and 2-fold higher and lower densities to encompass a plausible range.

Figures

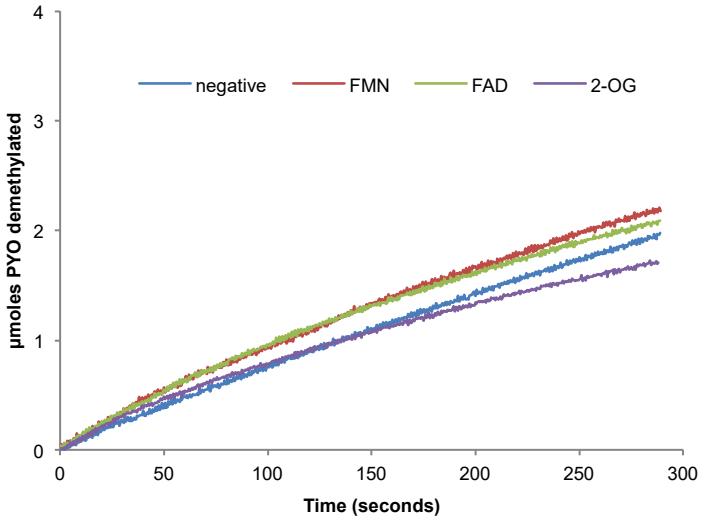

Fig. S1. $PodA_{30\text{-}162}$ activity is not stimulated by the presence of flavins or 2-oxoglutarate (25 µM) in a reaction containing 15 nM $PodA_{30\text{-}162}$. Flavins are known cofactors for many demethylases, whereas several others can utilize 2-oxoglutarate as an electron acceptor.

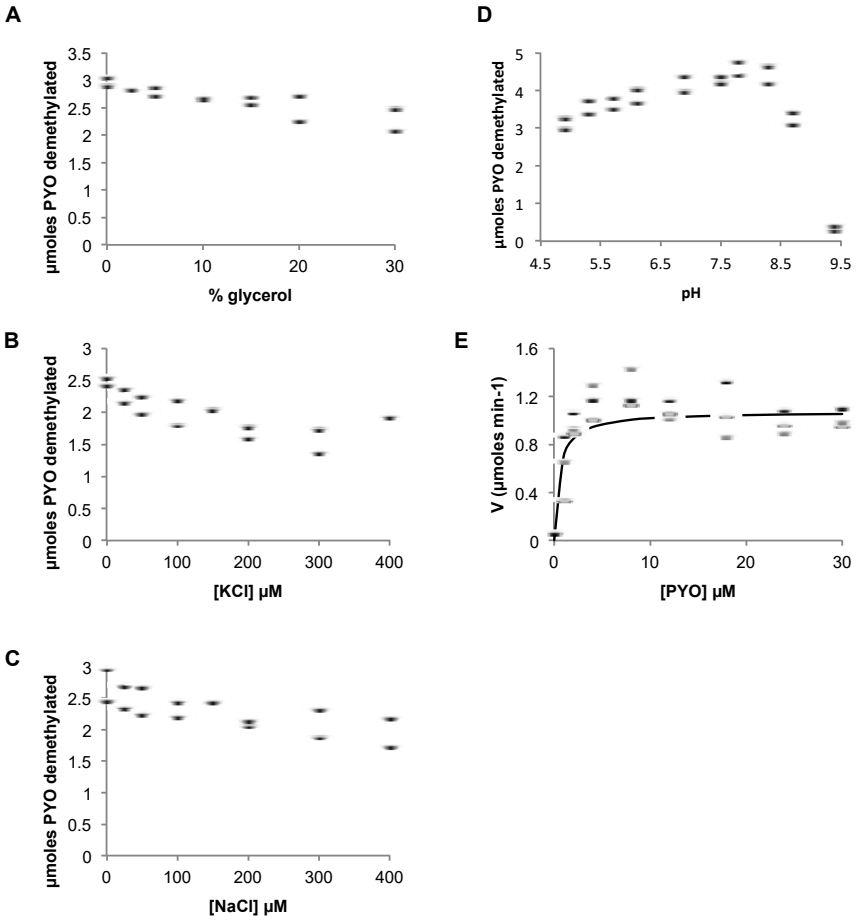

Fig. S2. PodA$_{30\text{-}162}$ activity is minimally inhibited by the presence of glycerol (**A**) or salt (**B,C**). (**D**) PodA is active over a wide pH range, but loses activity at pH above ~9. Data are from duplicate measurements and data was collected for 5 minutes in a reaction mixture containing 20 µM PYO and 15 nM PodA$_{30\text{-}162}$. (**E**) Analysis of PodA$_{30\text{-}162}$ reaction rate, V, across a range of PYO concentrations in a reaction containing 15 nM PodA$_{30\text{-}162}$. Reaction rates are from data collected during the first 10 seconds after enzyme addition. The detection limit of PYO was 0.5 µM; therefore, PYO concentrations below the K_m of the enzyme were not tested. However, based on the shape of the curve of a best fit to an ideal Michaelis-Menten plot, the apparent K_m is below 1 µM. Data are from three independent protein preparations. Each color represents data from a different protein preparation.

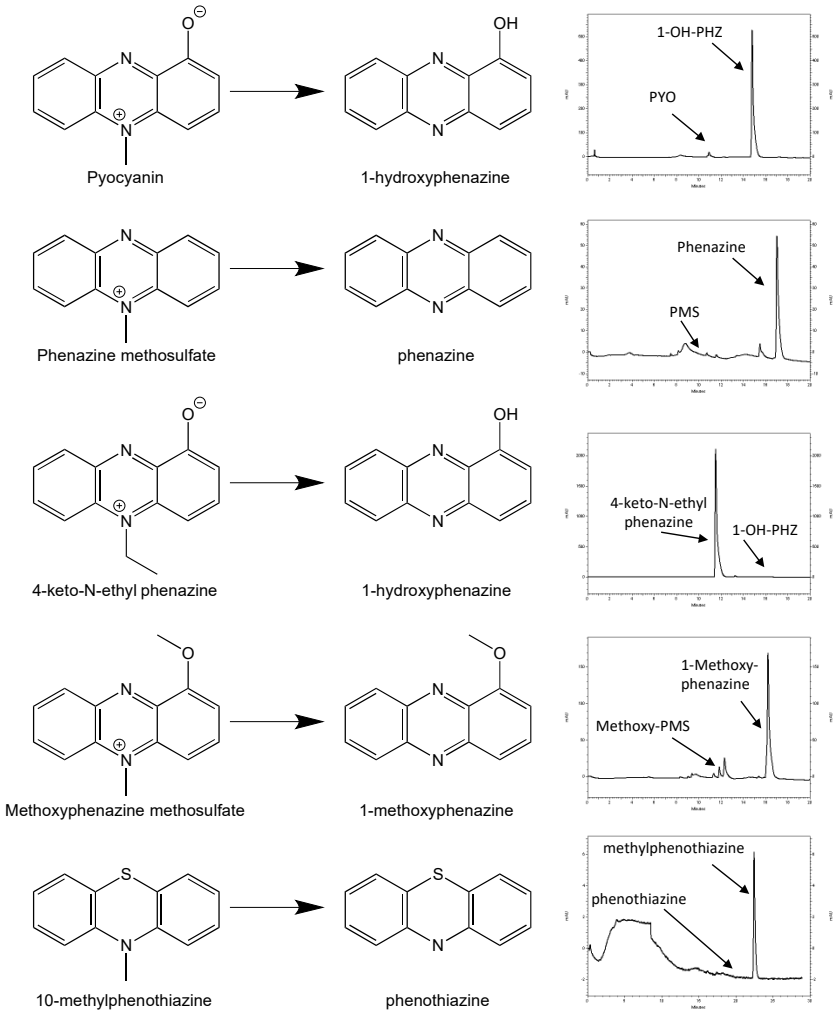

Fig. S3. Alternative substrate utilization by PodA. Methylated substrates and their predicted demethylated products are shown. Mixtures were analyzed by HPLC (right graphs) after 4 hours to determine the resulting products of each reaction. Standards for each product were run to determine retention times (indicated for each molecule with arrows). Only *N*-methylated phenazines were altered by incubation with $PodA_{30\text{-}162}$. 4-keto-N-ethylphenazine and 10-methylphenothiazine were not demethylated or de-ethylated. PMS, phenazine methosulfate.

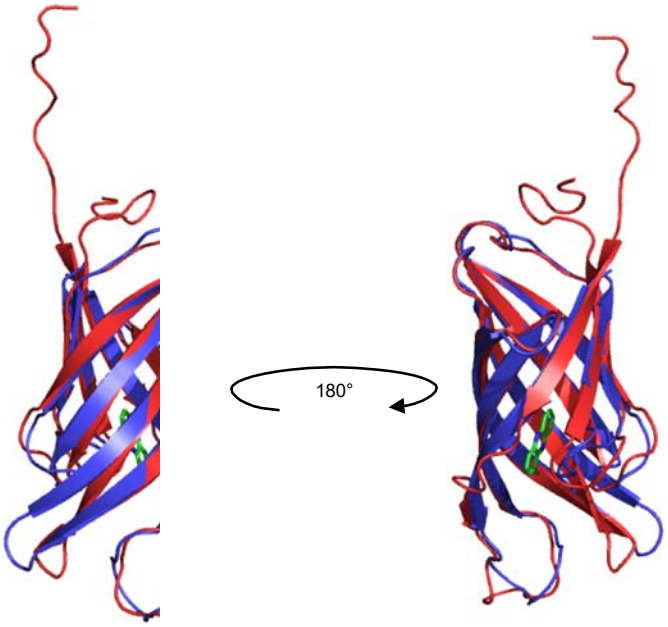

Fig. S4. Overlay of the Robetta structure prediction model (red) with the initial, solved structure of $PodA_{30\text{-}162}$ (R_{free} = 0.22 structure described in the methods) (blue). While $PodA_{30\text{-}162}$ crystallized as a trimer in the asymmetric unit, only the A chain monomer is shown here. RMSD of the C-alpha backbone: 2.23 Å vs. Robetta prediction. A version of the Robetta prediction model with trimmed loops was used to as the search model for molecular replacement (RMSD: 2.11). The N and C terminal extensions on the Robetta prediction were not resolved in the electron density of the solved structure.

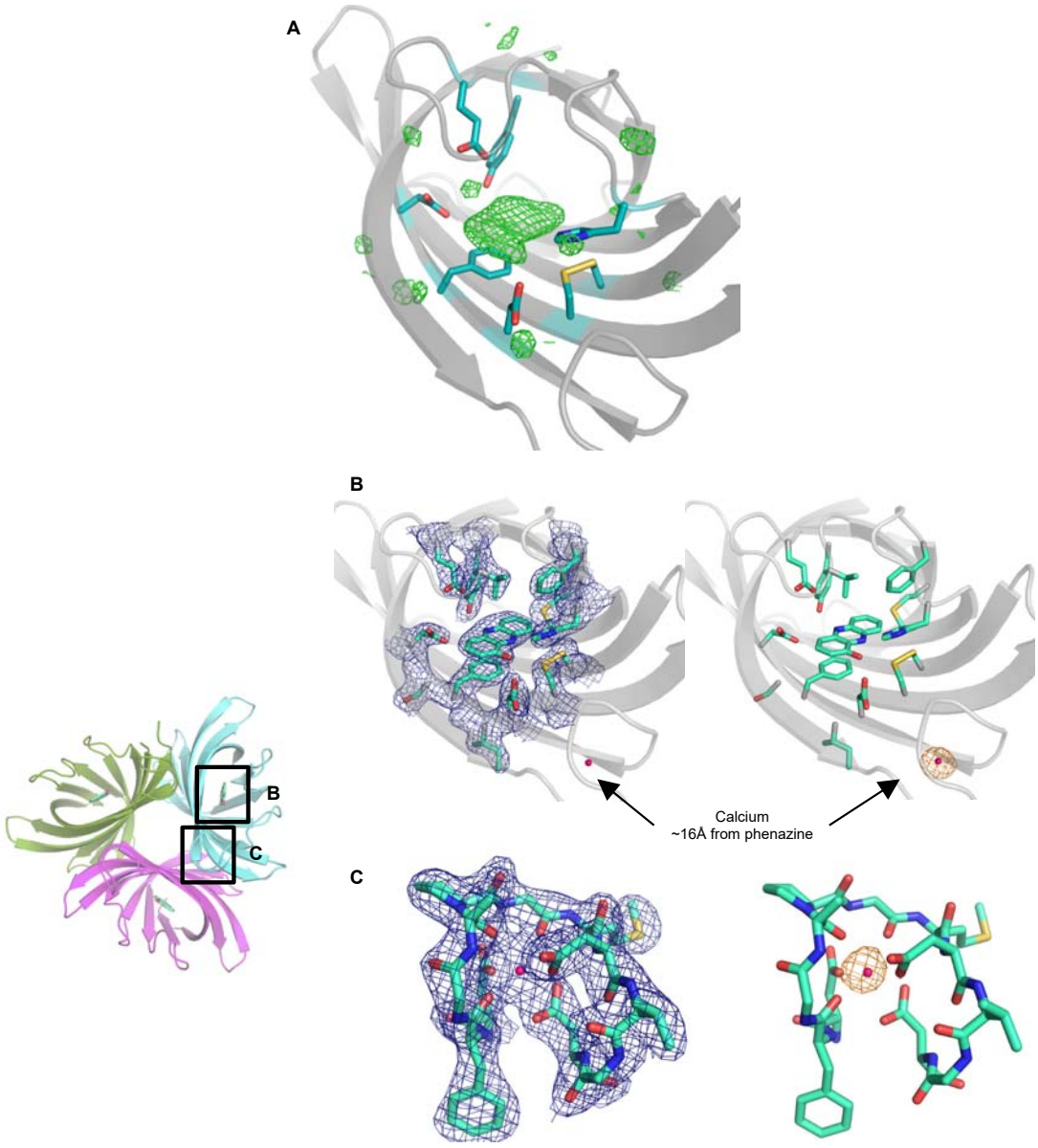

Fig. S5. Electron density maps of the PodA active site and coordinated calcium ion. (**A**) Fo-Fc map of the missing density for 1-OH-PHZ before ligand modeling and refinement (contoured at 3.0 sigma). Only the density within 5 Å of the active site residues is shown to highlight the missing ligand density. (**B**) Zoomed in view of the density around select residues in the active site (2Fo-Fc map, blue – contoured at 1.0 sigma). The anomalous difference map for the entire monomer is shown (orange map – contoured at 5.0 sigma), but density is only apparent around a calcium ion located ~16Å from the bound phenazine. Density for the bound 1-OH-PHZ molecules was apparent in each of the three subunits. Only the active site of the A chain monomer is shown here. There is no apparent density to support the presence of additional cofactors or metal atoms. (**C**) Zoomed in view of the loop containing the coordinated calcium ion.

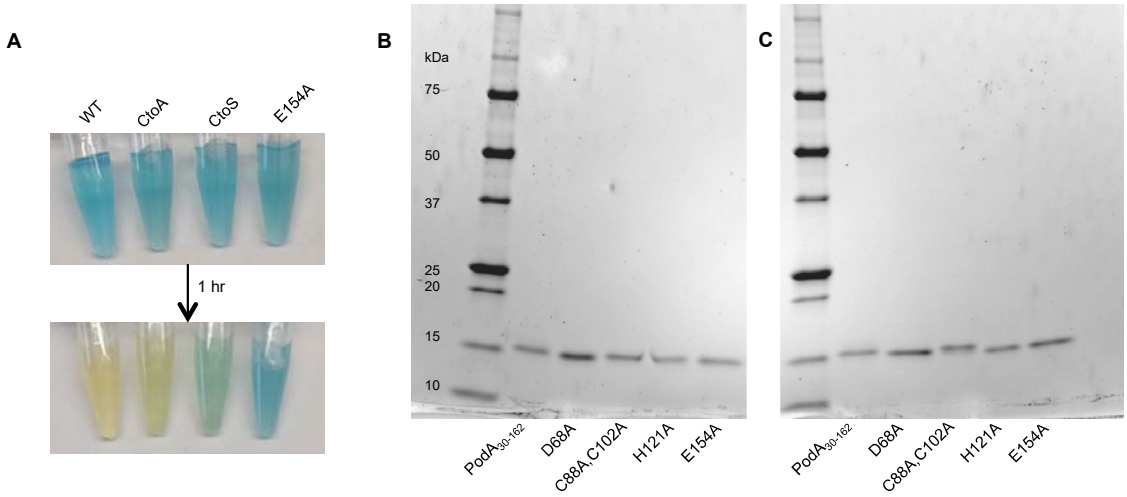

Fig. S6. (**A**) Both the C to A (C88A, C102A) and a C to S (C88S, C102S) double mutants show activity in cell-free lysates of *E. coli* BL21(DE3) expressing the protein of interest. While activity was always apparent in cell-free lysates, it was unstable and often lost upon further purification. (Note: the data for the C to A mutation in panels A-D of Figure 3 are from a rare preparation where protein remained active throughout purification.) C to S has less apparent activity than C to A, but serves as an independent confirmation of the phenotype. Cell lysates of the E154A mutant show that the loss of PYO is not due to an activity inherent to *E. coli*; furthermore, the accumulation of 1-OH-PHZ by both C to A and C to S lysates was confirmed by HPLC. (**B**) Reducing and (**C**) non-reducing SDS-PAGE of mutant $PodA_{30\text{-}162}$ proteins. Under reducing conditions, $PodA_{30\text{-}162}$ and mutant proteins all have similar migration through SDS-PAGE. Under non-reducing conditions, the presence of a disulfide bond leads to slightly faster migration through SDS-PAGE for all proteins except the C to A double mutant.

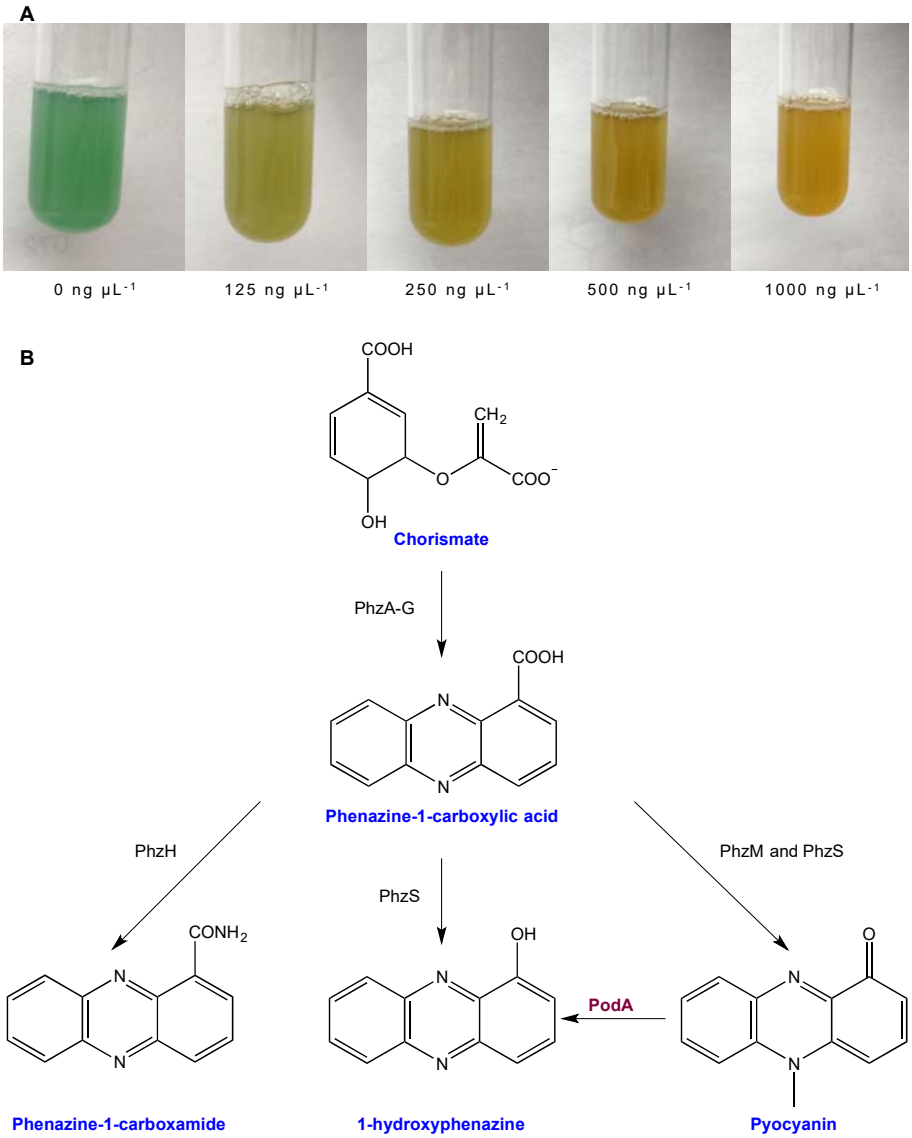

Fig. S7. (**A**) Dose dependence of PodA$_{30\text{-}162}$ activity in overnight cultures grown in TSB in the presence of the indicated amount of enzyme. Enzyme was added at the start of the culture and remained stable throughout the incubation period. (**B**) The phenazine biosynthetic pathways of *P. aeruginosa* (*40*). There is no known direct route for conversion of PYO or 1-OH-PHZ to PCA or PCN. Therefore, the response of *P. aeruginosa* to PodA$_{30\text{-}162}$ addition in Fig. S8 must be due to active regulatory control of the overall distribution of phenazines.

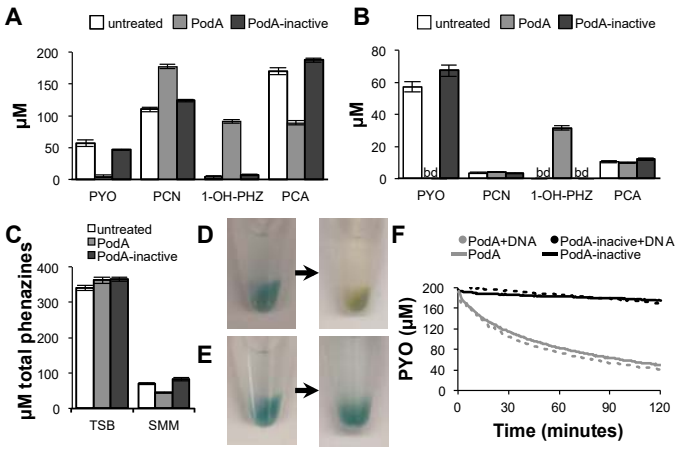

Fig. S8. PodA$_{30\text{-}162}$ alters phenazines in *P. aeruginosa* culture. PodA$_{30\text{-}162}$ alters phenazine concentrations in both TSB (**A**) and succinate minimal medium (SMM) (**B**). Data are averages from quadruplicate measurements and error bars represent one standard deviation around the mean. bd, below detection (< 0.5 µM). (**C**) Total phenazine concentrations in TSB and SSM as summed from panels A and B. While the distribution of phenazines is altered by PodA$_{30\text{-}162}$ in TSB, total concentrations remain constant. (**D**) PYO associated with precipitated DNA is not protected from PodA$_{30\text{-}162}$. (**E**) Inactivated PodA$_{30\text{-}162}$ does not demethylate PYO. (**F**) Solubilized DNA does not block PodA$_{30\text{-}162}$ activity. 200 µM PYO was incubated in the presence or absence of 400 µg mL^{-1} DNA (a stoichiometric excess). While these data do not preclude the possibility that PYO is loosely associated with DNA and may freely dissociate, and PodA may act on this solubilized PYO, they do confirm that DNA does not protect PYO from PodA$_{30\text{-}162}$ activity.

Tables

Table S1. Data collection and refinement statistics for PodA$_{30-162}$

Space group	P21 21 21
Cell dimensions	
a, *b*, *c* (Å)	65.33, 72.98, 79.7
α, β, γ (°)	90, 90, 90
Resolution (Å)	34.98–1.8 (1.864–1.8)
R_{merge}	0.177 (1.98)
R_{meas}	0.180 (2.01)
R_{pim}	0.036 (0.391)
CC1/2	0.999 (0.827)
$I/s(I)$	13.3 (2.3)
Wilson B-factor	24.8
Completeness	1.00 (1.00)
Multiplicity	25.9 (26.1)
No. reflections used in refinement	35987 (3544)
R_{work} / R_{free}	0.168(0.271) / 0.195(0.283)
No. non-hydrogen atoms	2905
Macromolecules	2644
Ligands	48
Average *B* factor	36.5
Macromolecules	36.1
Ligands	36.4
Solvent	42.0
R.m.s. deviations	
Bond lengths (Å)	0.007
Bond angles (°)	0.94
Ramachandran plot statistics (%)	
Favored	98
Allowed	2.5
Outliers	0

Two crystals were used for data collection.

Values in parentheses are for highest-resolution shell.

Table S2. Strains, primers and plasmids used in this study.

Strain	Reference
Pseudomonas aeruginosa PA14	(32)
P. aeruginosa Δ*phz*	(31)
Escherichia coli BL21(DE3)	(33)

Plasmid	Description
pET20b(+)-podA30-162	$podA_{30\text{-}162}$ expressed from the IPTG inducible promoter of pET-20b(+)
pET20b(+)-podA30-162, D68A	D68A mutant $podA_{30\text{-}162}$ expressed from the IPTG inducible promoter of pET-20b(+)
pET20b(+)-podA30-162, D72N	D72N mutant $podA_{30\text{-}162}$ expressed from the IPTG inducible promoter of pET-20b(+)
pET20b(+)-podA30-162, C88A,C102A	C88A,C102A double mutant $podA_{30\text{-}162}$ expressed from the IPTG inducible promoter of pET-20b(+)
pET20b(+)-podA30-162, C88S,C102S	C88S,C102S double mutant $podA_{30\text{-}162}$ expressed from the IPTG inducible promoter of pET-20b(+)
pET20b(+)-podA30-162, H121A	H121A mutant $podA_{30\text{-}162}$ expressed from the IPTG inducible promoter of pET-20b(+)
pET20b(+)-podA30-162, E154A	E154A mutant $podA_{30\text{-}162}$ expressed from the IPTG inducible promoter of pET-20b(+)
pET20b(+)-podA30-162, Y156F	Y156F mutant $podA_{30\text{-}162}$ expressed from the IPTG inducible promoter of pET-20b(+)

Primer	Sequence
podA30-162-NdeI-F	AAAACATATGGACGGTCGCGGCGGCCGGAGTA
podA30-162-TEV-Pst-R	AAAACTGCAGTCAATGGTGATGGTGATGGTGGCTCTGGAAGTACAGGTTTTCGGCTTT CGTCAGTTTCAATTCGTACTTCTCA
podA30-162-pET20b-F-NdeI	AAAACATATGGACGGTCGCGGCGGCCGGAGTACA
podA30-162-pET20b-R-NotI	TTTTGCGGCCGCTCAATGGTGATGGTGATGGTGGCT
CtoS-F	GATAATCCAATGACCTATTCCGAACTGACCATTCACCTCGATGCAGGTGA
CtoS-R	CGGCGTCACATTGGTGAAAAAGGACGCGCCGCCGTCATATCCGACCTGCTTACCGT
CtoA-F	GGATAATCCAATGACCTATGCCGAACTGACCATTCACCTCGATGCAGGTGA
CtoA-R	GGCGTCACATTGGTGAAAAAGGCCGCGCCGCCGTCATATCCGACCTGCTTACCGTCT
D68A-F	GCCATCTTCTCCGACATCCTCTCGGTAGA
D68A-R	CATGTCTCCGACATCCATACCCGGT
H121A-F	GCCACACTCGCACCTTTCACCATGGCCA
H121A-R	CGGGGTGAGGCTACGGGCAAAGATCTCA
E154A-F	GCGAAGTACGAATTGAAACTGACGAAAGC
E154A-R	ATCGGGAGTCGCAACACCGGATACGGT

Supplementary References

31. L. E. Dietrich, A. Price-Whelan, A. Petersen, M. Whiteley, D. K. Newman, The phenazine pyocyanin is a terminal signalling factor in the quorum sensing network of *Pseudomonas aeruginosa*. *Mol Microbiol* **61**, 1308-1321 (2006).
32. L. G. Rahme *et al.*, Common virulence factors for bacterial pathogenicity in plants and animals. *Science* **268**, 1899-1902 (1995).
33. F. W. Studier, B. A. Moffatt, Use of bacteriophage T7 RNA polymerase to direct selective high-level expression of cloned genes. *J Mol Biol* **189**, 113-130 (1986).
34. S. K. DasGupta, S. Jain, D. Kaushal, A. K. Tyagi, Expression systems for study of mycobacterial gene regulation and development of recombinant BCG vaccines. *Biochem Biophys Res Commun* **246**, 797-804 (1998).
35. Y. P. Shih, H. C. Wu, S. M. Hu, T. F. Wang, A. H. Wang, Self-cleavage of fusion protein in vivo using TEV protease to yield native protein. *Protein Sci* **14**, 936-941 (2005).
36. M. M. Bradford, A rapid and sensitive method for the quantitation of microgram quantities of protein utilizing the principle of protein-dye binding. *Anal Biochem* **72**, 248-254 (1976).
37. T. Nash, The colorimetric estimation of formaldehyde by means of the Hantzsch reaction. *Biochem J* **55**, 416-421 (1953).
38. S. B. Jones, C. M. Terry, T. E. Lister, D. C. Johnson, Determination of submicromolar concentrations of formaldehyde by liquid chromatography. *Anal. Chem.* **71**, 4030-4033 (1999).
39. N. L. Sullivan, D. S. Tzeranis, Y. Wang, P. T. So, D. Newman, Quantifying the dynamics of bacterial secondary metabolites by spectral multiphoton microscopy. *ACS Chem Biol* **6**, 893-899 (2011).
40. D. V. Mavrodi *et al.*, Functional analysis of genes for biosynthesis of pyocyanin and phenazine-1-carboxamide from *Pseudomonas aeruginosa* PAO1. *J Bacteriol* **183**, 6454-6465 (2001).
41. G. Kemmer, S. Keller, Nonlinear least-squares data fitting in Excel spreadsheets. *Nat Protoc* **5**, 267-281 (2010).
42. H. McIlwain, The phenazine series. Part IV. Reactionsof alkyl phenazonium salts; the phenazyls. *J Chem Soc*, 1704-1711 (1937).
43. W. Kabsch, Xds. *Acta Crystallogr D Biol Crystallogr* **66**, 125-132 (2010).
44. W. Kabsch, Integration, scaling, space-group assignment and post-refinement. *Acta Crystallogr D Biol Crystallogr* **66**, 133-144 (2010).
45. P. Evans, Scaling and assessment of data quality. *Acta Crystallogr D Biol Crystallogr* **62**, 72-82 (2006).
46. P. R. Evans, G. N. Murshudov, How good are my data and what is the resolution? *Acta Crystallogr D Biol Crystallogr* **69**, 1204-1214 (2013).
47. J. E. Padilla, T. O. Yeates, A statistic for local intensity differences: robustness to anisotropy and pseudo-centering and utility for detecting twinning. *Acta Crystallogr D Biol Crystallogr* **59**, 1124-1130 (2003).
48. M. D. Winn *et al.*, Overview of the CCP4 suite and current developments. *Acta Crystallogr D Biol Crystallogr* **67**, 235-242 (2011).
49. A. J. McCoy *et al.*, Phaser crystallographic software. *J Appl Crystallogr* **40**, 658-674 (2007).

50. P. Emsley, B. Lohkamp, W. G. Scott, K. Cowtan, Features and development of Coot. *Acta Crystallogr D Biol Crystallogr* **66**, 486-501 (2010).
51. T. C. Terwilliger *et al.*, Iterative model building, structure refinement and density modification with the PHENIX AutoBuild wizard. *Acta Crystallogr D Biol Crystallogr* **64**, 61-69 (2008).
52. J. J. Headd *et al.*, Use of knowledge-based restraints in phenix.refine to improve macromolecular refinement at low resolution. *Acta Crystallogr D Biol Crystallogr* **68**, 381-390 (2012).
53. P. V. Afonine *et al.*, Towards automated crystallographic structure refinement with phenix.refine. *Acta Crystallogr D Biol Crystallogr* **68**, 352-367 (2012).
54. T. C. Terwilliger, P. D. Adams, N. W. Moriarty, J. D. Cohn, Ligand identification using electron-density map correlations. *Acta Crystallogr D Biol Crystallogr* **63**, 101-107 (2007).
55. T. C. Terwilliger, H. Klei, P. D. Adams, N. W. Moriarty, J. D. Cohn, Automated ligand fitting by core-fragment fitting and extension into density. *Acta Crystallogr D Biol Crystallogr* **62**, 915-922 (2006).
56. P. D. Adams *et al.*, PHENIX: a comprehensive Python-based system for macromolecular structure solution. *Acta Crystallogr D Biol Crystallogr* **66**, 213-221 (2010).
57. N. W. Moriarty, R. W. Grosse-Kunstleve, P. D. Adams, electronic Ligand Builder and Optimization Workbench (eLBOW): a tool for ligand coordinate and restraint generation. *Acta Crystallogr D Biol Crystallogr* **65**, 1074-1080 (2009).
58. M. D. Winn, M. N. Isupov, G. N. Murshudov, Use of TLS parameters to model anisotropic displacements in macromolecular refinement. *Acta Crystallogr D Biol Crystallogr* **57**, 122-133 (2001).
59. T. Das, S. K. Kutty, N. Kumar, M. Manefield, Pyocyanin facilitates extracellular DNA binding to *Pseudomonas aeruginosa* influencing cell surface properties and aggregation. *PLoS One* **8**, e58299 (2013).
60. C. A. Schneider, W. S. Rasband, K. W. Eliceiri, NIH Image to ImageJ: 25 years of image analysis. *Nat Methods* **9**, 671-675 (2012).
61. S. Bolte, F. P. Cordelieres, A guided tour into subcellular colocalization analysis in light microscopy. *J Microsc* **224**, 213-232 (2006).
62. D. Cohen *et al.*, Oligoribonuclease is a central feature of cyclic diguanylate signaling in *Pseudomonas aeruginosa*. *Proc Natl Acad Sci U S A* **112**, 11359-11364 (2015).

Chapter 7

CONCLUSIONS

Summary

This thesis presents mechanistic insight into how phenazines promote anaerobic survival in *Pseudomonas aeruginosa*. From a physiological perspective, phenazines support redox homeostasis by coupling metabolism to an extracellular oxidant. While the rate of electron transfer may be orders of magnitude lower than when the electron transport chain is used directly, it is still sufficient to support survival. By dissipating reducing equivalents, phenazines enable *P. aeruginosa* to oxidize otherwise unusable substrates with concomitant ATP synthesis. In the case of pyruvate and glucose metabolism, the pyruvate dehydrogenase complex, through the subunit dihydrolipoamide dehydrogenase, can use phenazines as a direct substitute for NAD^+. Other enzymes may also catalyze NADH oxidation using phenazines as an electron acceptor. The ATP is used partly to maintain a membrane potential through the reverse action of the ATP synthase complex. The efflux of reduced phenazines might also drive proton translocation to support a membrane potential. As revealed by metabolite measurements, redox homeostasis by phenazines might also lead to changes in the fatty acid pool, which could have indirect effects through the action of quinolone signaling. In the natural environment, other organisms, such as *Mycobacteria*, likely consume or modify phenazines to produce complex inter-species interactions that we are only beginning to discover.

Future Directions

Pyocyanin and pyruvate secretion

My motivation for revisiting pyruvate secretion in *P. aeruginosa* was to employ it as a probe for intracellular metabolism. While it was previously reported that pyocyanin stimulates pyruvate

secretion, this phenotype appears to be highly dependent on the culture conditions. In my hands, I observed pyruvate secretion more consistently in the *absence* of pyocyanin. Together with my findings in Chapters 3 and 4, which suggest a deep connection with the pyruvate dehydrogenase complex, I suspect that elucidating the relationship between pyocyanin and pyruvate secretion will yield new insights into how phenazines shape metabolism.

As previously hypothesized, my data in Chapter 4 indicate that pyocyanin might inhibit pyruvate dehydrogenase. This interpretation comes from a comparison of phenazine reduction rates between pyruvate dehydrogenase and α-ketoglutarate dehydrogenase. Both reduced phenazine-1-carboxylate at about the same rate, yet pyruvate dehydrogenase reduces pyocyanin more slowly than α-ketoglutarate dehydrogenase. As pyocyanin reduction does not appear to be the rate-limiting step in these complexes, it is possible that pyocyanin inhibits a subunit upstream of dihydrolipoamide dehydrogenase, for example by allosteric regulation or competitive inhibition with thiamine pyrophosphate. Revisiting these kinetic assays might be informative once specific conditions are defined where *P. aeruginosa* consistently secretes pyruvate.

Fatty acid metabolism

I have noticed a great deal of circumstantial evidence suggesting that pyocyanin affects fatty acid metabolism in *P. aeruginosa*. This hypothesis was even foreshadowed by Friedheim himself, who wrote, "The pyocyanine catalysis is not indiscriminately effective in all oxidations, but only in the oxidation of certain substances closely associated with the bacterial body" (The Journal of Experimental Medicine, 1931). In addition to some of Friedheim's pioneering results, two noteworthy pieces of evidence are as follows.

First, I observed an excess of acetate production in *P. aeruginosa* surviving anaerobically with pyruvate. Instead of the expected 1:1 ratio of acetate to lactate, I observed closer to 40–45% acetate and 55–60% lactate. Where do the excess reducing equivalents come from? I also observed

acetate secretion even in the Δ*ackA* mutants. Where does the extra acetate come from? Moreover, Δ*ackA-pta* mutants survived worse than Δ*ackA* mutants. Why is *pta* important? All these questions are readily answered if β-oxidation, which produces acetyl-CoA and a large excess of reducing equivalents, is important for long-term survival in *P. aeruginosa*. Tantalizingly, two independent TnSeq experiments in separate anaerobic conditions, one with phenazines and one with pyruvate, both identified certain β-oxidation genes as essential for long-term survival (David Basta and Scott Saunders, personal communication). Phenazines may be instrumental for dissipating the excess reducing equivalents generated by β-oxidation.

Second, while developing my metabolomics methods, I noticed numerous glycerophospholipids in culture supernatants, and some of these appeared differentially regulated by phenazines. Identifying the precise chain lengths and desaturation patterns of these lipids will require a more concerted effort. I also observed that pyocyanin leads to a reduction in the overall chain length of quinolone signals, suggesting a connection to fatty acid metabolism that is consistent with the known redox effects of phenazines.

Phenazine reductases and transporters

What are the relevant phenazine reductases *in vivo*? My results implicate flavoproteins as non-specific reductases, but it is possible that a small subset of enzymes account for most of the activity. Metabolic flux measurements might identify these enzymes. If phenazines stimulate flux through specific pathways, such as glucose oxidation, possibly only under oxidant-limiting conditions, then one or more enzymes in that pathway might use phenazines as an electron acceptor. Even if the results are not so readily interpretable, compared to testing specific enzymes *in vitro* or mutants with pleiotropic effects, metabolomics has the potential to provide a more direct view of the metabolic effects of phenazines.

A related unknown is the subcellular localization of phenazines. It is surprisingly difficult to remove pyocyanin from a culture by centrifuging cells and washing the pellet. Other students and I have noticed that *P. aeruginosa* retains the reduced form of pyocyanin. This might be simply because the reduced form is more hydrophobic and sticks preferentially to membranes, or it could arise from a selective mechanism of transport. Where phenazines partition into the cell dictates the relevant *in vivo* reductases. For example, if phenazines accumulate mostly in the periplasm, then pyruvate dehydrogenase might not be particularly significant, but if *P. aeruginosa* actively concentrates phenazines in the cytoplasm, then pyruvate dehydrogenase could be highly relevant.

Diffusion and retention

A common question that arises when discussing phenazine redox cycling is whether diffusion alone is sufficient to explain the electron transfer rates we observed. A simple model of diffusion at steady-state, the best-case scenario, shows that it is. This model can be extended to include losses to diffusion or degradation and production over time. The equations quickly become intractable to solve for exact solutions, but they are approachable through numerical methods. Additional laboratory measurements of diffusion and electron-transfer rates in biofilms will help to constrain the equations and produce physically meaningful results. It might be that phenazines *in situ* cycle faster than can be explained by diffusion, possibly because they are embedded in a conductive matrix such as DNA or humic substances.

Environmental relevance

Depending where and how one looks, phenazines exert phenotypic effects in just about any assay. Which of these effects are environmentally relevant, and which are simply artifacts of the laboratory? Despite over 150 years of research, a definitive "purpose" of phenazines—by which I mean the selective pressures that drove the original evolution of phenazines biosynthesis, and the broad dissemination by horizontal transfer of the phenazine biosynthesis gene clusters—remains

elusive. As we learn more about how phenazines shape microbial communities, we may recognize certain patterns or molecular markers, such as correlations between phenazines and ferrous iron, that indicate specific functions are especially important in the environment.